STRUCTURAL INTEGRITY ASSESSMENT OF CORRODED REINFORCED CONCRETE SLAB-COLUMN CONNECTIONS

by

© Mahmoud Essam Said, B.Sc., M.Sc.

A thesis submitted to the

School of Graduate Studies

in partial fulfillment of the requirements for the degree of

Doctor of Philosophy (Civil Engineering)

Faculty of Engineering and Applied Science

Memorial University of Newfoundland

January 2019

St. John’s, Newfoundland, Canada

ABSTRACT

Reinforced concrete (RC) is widely used in structures, e.g. residential buildings, bridges, marine structures, and offshore structures. Some RC structures are constructed in harsh environmental conditions, which increase the probability of their deterioration. Corrosion is one of the main causes of deterioration in concrete structures. Consequently, further research is needed to better understand the effect of corrosion on different RC structural elements and materials.

In this thesis, the punching shear behaviour of RC two-way slabs was investigated under different levels of corrosion. In addition, different corroded areas were also investigated. Accelerated corrosion techniques were used to achieve the targeted corrosion levels and areas. The objective of this study is to provide experimental information and assessments of the structural performance and behaviour of corroded RC two-way slabs under loading. The objectives were achieved by evaluating the effect of three different levels of corrosion on the punching shear of two-way RC slabs; mild corrosion (15% mass loss); moderate corrosion (25% mass loss); severe corrosion (50% mass loss). In addition, three different delaminated corroded areas will be considered: small corroded area; a large corroded area *with* enough reinforcement development length; large corroded area *without* enough reinforcement development length. The experimental program was designed based on statistical methodology in order to do a regression analysis at the end of the test period for the obtained results. The regression analysis used to construct predicted equations that calculate the residual carrying load capacity for corroded RC two-way slabs.

The concrete mixture used to pour those elements was designed to conquer the exposure requirements for horizontal elements against de-icing agents according to ACI. For ensuring the poured concrete had an acceptable quality against chloride ions penetrations, rapid chloride penetration test and chloride diffusion were measured for standard cylinder specimens taken during the pouring. The corrosion performance was monitored for all tested slabs by measuring and tracking current measurement, corrosion cracks widths propagation, half-cell potential measurements, natural frequency measurements, chloride content measurements, and mass loss. In addition, the structural behaviour of the corroded slabs was evaluated based on cracking patterns, deflection capacities, deflection profiles, slab rotations, energy absorptions, and ductility indices. Moreover, the actual capacity for each corroded slab was compared with the predictions of punching capacities according to the yield line theory and four different: the Canadian Code (CSA 23.3-14), the American Code (ACI 318-11), the British Standard (BS 8110-97), and the European Code (EC2). Furthermore, this thesis showed a proposed technique to predict roughly the capacity of the different corroded area in the two-way reinforced concrete slabs using current codes. Finally, equations were proposed based on the analysis of variance for the experimental results that could be used by practicing engineers to determine the residual capacities for existing reinforced concrete two-way slabs suffer from corrosion.

The experimental results will create a database for corroded slabs under real conditions. The database can then be used to verify future analytical studies of corroded RC structures. Thus, the thesis outcomes will help structural engineers to evaluate the strength degradation and load responses of such structures.

ACKNOWLEDGEMENTS

After thanking Almighty "ALLAH" for his numerous blessings and for giving me the strength in life, I want to express my great gratitude to my thesis advisor Dr. Amgad Hussein for offering this great chance and being a real father for me. I really express my gratitude to his support and endlessly fatherly guidance. Finally I would like to thank my supervisory committee members Dr. Ashutosh Dhar and Dr. John Shirokoff for agreeing to be in my thesis supervisory committee.

Many thanks are due to Mr. Shawn Organ, Mr. Matt Curtis, and Mr. Jason Murphy for their constant support and assistance in lab work during my PhD program. The funding provided by Dr. Amgad Hussein, School of Graduate Studies, Mitacs- Accelerate Internship Program, and the Chevron Canada Limited Rising Star Award is greatly acknowledged.

I would like to express my gratitude to Mohamed Essam Said for his support and helping me in all stages for the experimental work.

Nothing can express my gratitude to the support and encouragement provided by my parents, and my brothers during my studies. Finally, I would embrace this opportunity to thank all my friends for encouraging me to finish this PhD degree.

Table of Contents

List of Tables

List of Figures

List of Symbols, Nomenclature or Abbreviations

10M	Bar with dimeter of 10 mm
15M	Bar with dimeter of 16 mm
20M	Bar with dimeter of 19.5 mm
a	Side dimension between supports of a square slab (1830 mm)
A	Ampere (current unit)
A:	Mass loss level parameter
A_{u-p}	Agreement between the experimental and the predicted slab capacity based on ANOVA
ACI 318-14	American code provision
ASTM	American Society for Testing and Materials
b	Side dimension (mm)
b_o	Perimeter for the critical punching shear section
B:	Corroded area parameter
BS8110-97	British code provision
c	Side dimension of the square column stub (250 mm)
cm	Centimeter

cm^2	Centimeter square (area unit)
C	Coulomb (electron charge unit)
C:	Maximum crack width parameter
C_i	Initial chloride ion content
C_s	Surface chloride concentration
$C(x,t)$	Chloride ion at each depth level (x) at exposure time (t_e)
C.A.	Coarse aggregate
CA	Corroded area
C/F	Coarse to fine ratio
Cl^-	Chloride ion
Cl^-_c	Chloride content (%)
C/mol	Coulombs per mole (Faraday's constant unit)
CMT	Cement
CSA 23.3-14	Canadian code provision
d	Effective slab depth (mm)
d_b	Nominal diameter of the reinforcing bars

df	Degree of freedom
D:	Normalized natural frequency parameter
D_a	Chloride diffusion coefficient
DC	Direct current
e^-	Electron
erf(z)	Error function
EC2	European code provision
Eq	Equation
f_c'	Concrete compressive strength
f_r	Modulus of rupture
f_y	Yield strength
F	Faraday's constant
F3	Exposure class condition at ACI 318-14
F.A.	Fine aggregate
Fe	Iron (chemical symbol)
Fe^{2+}	Iron ion shares two of its electrons

$FeCl_2$	Ferrous chloride
$Fe(OH)_2$	Ferrous hydroxide
$Fe(OH)_3$	Ferric hydroxide
$Fe_2O_3H_2O$	Ferric oxide hydrate
FI	Factor interaction
gm	gram
g/mol	Gram per mole (atomic weight unit)
h	Height dimension (mm)
hrs	Hours (time unit)
H_2O	Water (moisture)
HCl	Hydrochloric acid
Hz	Hertz (frequency unit)
I	Current passed in Amperes
k	Size effect according to EC2
k_1	Bond location factor
k_2	Coating factor

k_3	Concrete density factor
k_4	Bar size factor
kN	Kilo-Newton
l	Litre (Volume unit)
L	Length (mm)
L_d	Development length
LVDT	Linear variable differential transformer
m	Meter (length unit)
mA	Milli-ampere (current unit)
mA/cm^2	Milli-ampere per centimeter square (Current intensity unit)
mA/mm^2	Milli-ampere per millimeter square (Current intensity unit)
mm	Millimeter (length unit)
mm^2	millimeter square (area unit)
mol	Mole, unit of atomic weight substance like atom, ion, and electron
mV	Millivolt
M	Atomic weight

M_n	Nominal flexure capacity for the slab section in flexural
MPa	Mega-Pascal
N	Normality (describes a solution that contains 1 gm equivalent weight per litre solution)
NaCl	Sodium Chloride
O_2	Oxygen
OH^-	Hydroxyl ion
P_{code}	Code predicted punching shear resistance
$P_{flexural}$	flexural slab capacity based on line yield theory
P_{SL}	Service load for the un-corroded slab S0
P_p	Predicted slab capacity based on ANOVA
P_u	Experimental punching shear capacity
Ph.D.	Doctor of philosophy
Prob	Probability
R^2	R-squared, the coefficient of determination for regression
R^2_{adj}	Adjusted R-squared

R^2_{Pred}	Predicted R-squared
RC	Reinforced concrete
RCPT	Rapid Chloride Penetration Test
RSM	Response surface method
s	Side dimension of the slab (1900 mm)
S-D1	Slab corroded over reinforcement bandwidth area
S-D2	Slab corroded except the development length
S-D3	Slab corroded and exceeded the development length
S0	Un-corroded slab
S15-D1	Slab corroded till 15% mass loss over reinforcement bandwidth area
S15-D2	Slab corroded till 15% mass loss except the development length
S15-D3	Slab corroded till 15% mass loss and exceeded the development length
S25-D1	Slab corroded till 25% mass loss over reinforcement bandwidth area
S25-D2	Slab corroded till 25% mass loss except the development length
S25-D3	Slab corroded till 25% mass loss and exceeded the development length
S50-D1	Slab corroded till 50% mass loss over reinforcement bandwidth area
S50-D2	Slab corroded till 50% mass loss except the development length

S50-D3	Slab corroded till 50% mass loss and exceeded the development length
SC	Slab corroded till 25% mass loss using constant current
SV	Slab corroded till 25% mass loss using constant voltage
t	Time passed in seconds
t_e	Exposure time for chloride ions
$T_{u\text{-}p}$	Tolerance between the experimental and the predicted slab capacity based on ANOVA
TA	Total slab area
V	Voltage (unit of electrical potential)
w/c	Water to cement ratio
w_c	Maximum corrosion crack width
w_{max}	Maximum crack width at the ultimate load
w_{SL}	Maximum crack width at the service load
x	Depth of the collected dust powder
z	Ion charge (two moles of electron)
μ	Micro (10^{-6})

$\mu A/cm^2$	Micro-ampere per centimeter square (Current intensity unit)
ρ	Reinforcement ratio
ρ_l	Reinforcement ratio according to EC2
ρ_{ly}	Reinforcement ratio in y-direction according to EC2
ρ_{lz}	Reinforcement ratio in z-direction according to EC2
ε_y	Yield strain
$\mu\varepsilon$	Micro-starin
Δ_{SL}	Deflection at the service load
Δ_u	Deflection at the experimental punching shear capacity
φ_c	Concrete resistance factors is taken as unity
φ_s	Steel resistance factors is taken as unity
α_1	Stress-block parameter
α_s	Adjusting factor
λ	Concrete density factor
v_c	Shear stress resistance

v_r	Factored shear resistance
β_c	Ratio of long side to short side of the column
ω	Natural frequency
ω_f	Natural frequency – free-free condition
ω_r	Natural frequency for the reference slab
ω_c	Natural frequency for the corroded slab

Co-Authorship Statement

I, Mahmoud E Said, hold a principle author status for all the manuscript chapters (Chapter 2 - 7) in this dissertation. However, each manuscript is co-authored by my supervisor and co-researchers, whose contributions have facilitated the development of this work as described below.

- Paper 1 in Chapter 2: Mahmoud E. Said, and Amgad Hussein, "Induced Corrosion Techniques for Two-way Slabs".

I was the primary author, with authors 2 - 3 contributing to the idea, its formulation and development, and refinement of the presentation.

- Paper 2 in Chapter 3: Mahmoud E. Said, and Amgad Hussein, "Monitoring of Corrosion Process in Two-Way Reinforced Concrete Slabs".

  I was the primary author, with the second author contributing to the idea, its formulation and development, and refinement of the presentation.

- Paper 3 in Chapter 4: Mahmoud E. Said, and Amgad Hussein, "Effect of Bandwidth Reinforcement Corrosion on the Response of Two Way Slabs".

I was the primary author, with the second author contributing to the idea, its formulation and development, and refinement of the presentation.

- Paper 4 in Chapter 5: Mahmoud E. Said, and Amgad Hussein, "The Response of Two-Way Slabs due to Corrosion of Large Reinforcement Area".

  I was the primary author, with the second author contributing to the idea, its formulation and development, and refinement of the presentation.

- Paper 5 in Chapter 6: Mahmoud E. Said, and Amgad Hussein, "Corroded two-way Slabs with Insufficient Development Length".

I was the primary author, with the second author contributing to the idea, its formulation and development, and refinement of the presentation.

- Paper 6 in Chapter 7: Mahmoud E. Said, Mohamed Essam Said, and Amgad Hussein, "Probabilistic Analysis of Strength Degradation for Two-Way Reinforced Concrete Slabs".

I was the primary author, with authors 2 - 3 contributing to the idea, its formulation and development, and refinement of the presentation.

Mahmoud E Said	Date

Chapter 1 Introduction and Overview

1.1. Background and Research Motivation

Deterioration of reinforced concrete (RC) structures could lead to catastrophic problems. Corrosion of the embedded reinforcement inside the different concrete elements is one of the main reasons for the deterioration of RC structures. RC is commonly used in North America in the construction of residential buildings, bridges, tunnels, parking garages, and offshore structures. North America has a harsh environmental weather that generates favourable conditions, which lead to an increase in the probability of corrosion occurrence (Aoude et al. 2014). Corrosion is a worldwide problem, which also occurs in many structures in industrialized countries in Europe and Asia, and in developing countries (Chung et al. 2008).

Corrosion of the steel reinforcement causes deterioration in RC structures, which could lead to severe damage to them. Concrete has an alkaline nature. As a result of this alkalinity, a protective film is formed around reinforcing steel bar; this film acts as a protection against corrosion as shown in Fig. 1.1. Hence, the instability of this protection film increases the probability of corrosion. Concrete could lose the stability of this film through several processes such as chloride penetration, sulphate attack, and carbonation ingress (Neville 2011). Marine and offshore structures are susceptible to chloride penetration. This is due to the presence of chloride ions in seawater, that through chemical reactions, lead to long-term corrosion of concrete (Neville 2011).

Figure 1-1 The passivation layer around the rebar

Corrosion of steel produces a corrosive product (rust) that has a larger volume than a steel rebar. This increase in volume creates radial tensile stress around the steel rebar, when the stresses exceed the concrete tensile strength, cracks induce in the concrete surface (Neville 2011). Hence, the deterioration due to corrosion appears as a loss in the steel rebar cross-sectional area, cracking of concrete, and spalling or delamination as shown in Fig. 1.2. Moreover, corrosion weakens the bond between the steel bar and concrete; consequently, the overall strength of RC structures is reduced (Neville 2011). Various experimental and numerical studies have concluded that the bond strength of RC structures decreases when the corrosion occurs in the reinforcement steel. Corrosion has two main harmful effects on the steel reinforcement, which decrease the overall strength and serviceability of RC structures. The first effect of corrosion is the reduction of the steel bar diameter while the second is the weakening of the bond between the steel bar and concrete cover (Yubun Auyeung et al. 2000).

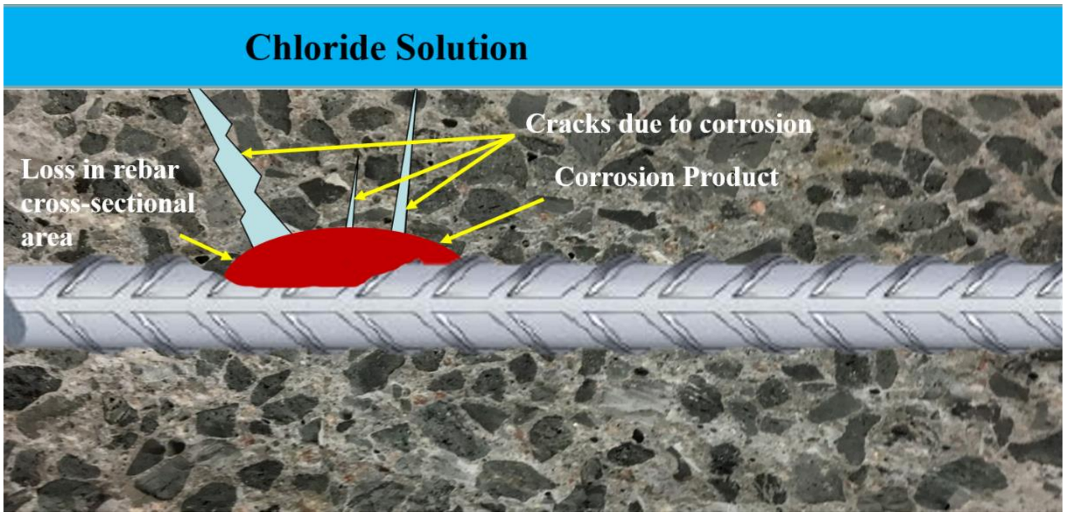

Figure 1-2 The effect on corrrosion in RC element

Many efforts have been made to study the corrosion from various aspects. Some of the investigations were conducted to have a better understanding of the corrosion process (Raupach 1996; Carnot et al. 2003; Chitty et al. 2005). Others were carried out to examine the effect of corrosion on the RC structural elements (El-Maaddawy & Soudki 2003). In addition, monitoring the corrosion rate was investigated (Andrade & Alonso 1996; Andrade & Alonso 2001; Ahmad 2003). Some researchers developed models to predict the structural behaviour of the corroded elements. The models were verified using experimental results (Dodd & Restrepo-Posada 1995; Berto et al. 2008; Coronelli & Gambarova 2004). Repair and rehabilitation of corroded structures were also investigated (Bertolini et al. 2013; Miyagawa 1991; Fedrizzi et al. 2005; Broomfield 2002). Nonetheless, there are very limited investigations on the effect of corrosion when it comes to two-way RC slabs or slab-column connections structural elements. Therefore, the objective of the current study is to focus on developing a better understanding of the behaviour of corroded RC slab-column connections structural elements.

1.2. Background and Literature Review

The corrosion mechanism and its effect on reinforced concrete are presented and the corrosion acceleration technique is discussed. The second part covers a literature survey of the previous research on the effect of corrosion of RC two-way slabs. The discussed subjects are intended to familiarize the reader with the type of research conducted in the present study.

1.2.1. Corrosion Mechanism

Corrosion occurs due to an electrochemical reaction between metal (such as steel) and its surrounding environment (such as air, water, or moisture). This reaction causes changes in the properties of the metal, which lead to strength capacity loss of the metal. For RC structural elements, when corrosion reaches the steel bars, a reduction in strength and ductility takes place. Thus, the safety and serviceability of RC structures are reduced (Neville 2011).

1.2.2. Corrosion of reinforcement in Concrete

The reaction of the corrosion process occurs due to the difference in the electrical potential along the steel bar inside concrete. This reaction can be separated into two partial reactions: first, is the oxidation reaction. In this reaction, the iron atoms of steel convert from the metallic state to the ionic state, in which the electrons and ions are released from the bar as shown in Fig. 1.3. This active part of the bar is known as an anode. This reaction process is also called the half-cell oxidation reaction, or the anodic reaction, which can be represented by

$$Fe \longrightarrow Fe^{2+} + 2e^{-}$$

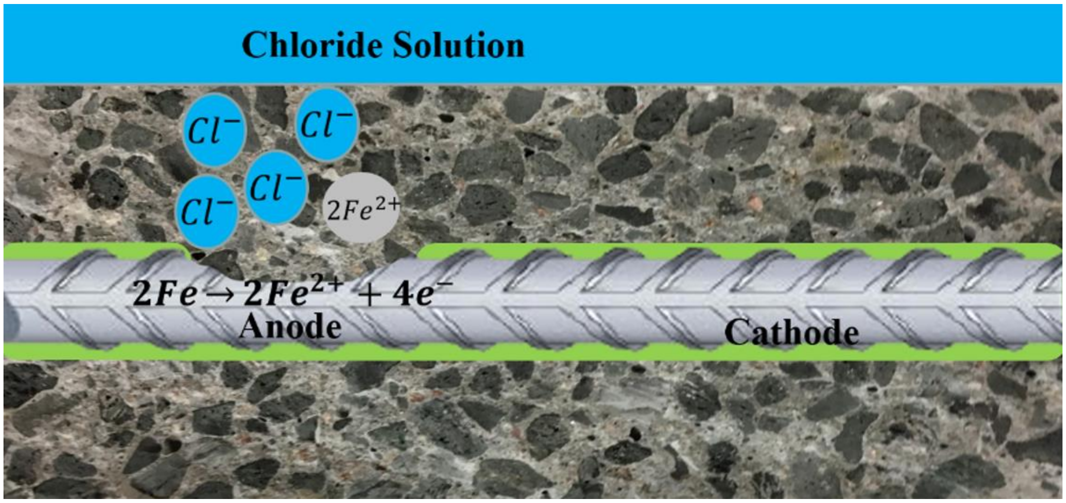

Figure 1-3 Oxidation reaction at the anode

The second reaction is called the reduction reaction. This reaction occurs at the cathode as shown in Fig 1.4, which is a part of the bar where electrons flow to. The electrons that are released during the oxidation reaction travel through the bar to the cathodic part in the existence of an electrolyte solution. In the cathodic part, the negative electrons convert to hydroxyl ions (OH^{-}) (oxidizing agent) in the presence of moisture and oxygen as

$$O_2 + 2H_2O + 4e^{-} \longrightarrow 4OH^{-}$$

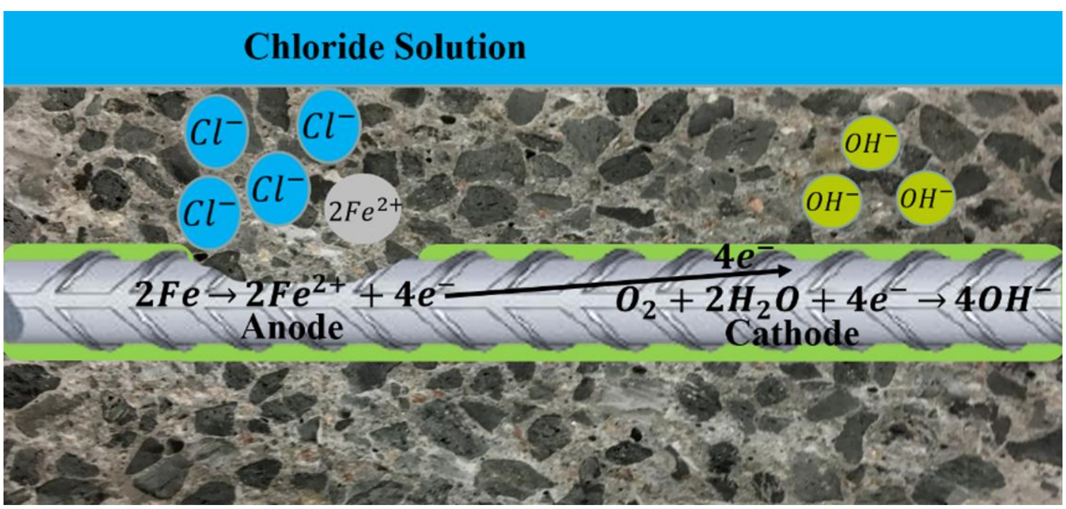

Figure 1-4 Reduction reaction at the cathode

These hydroxyl ions travel through the electrolyte solution (concrete pore water) and combine with the ferrous ions to form iron hydroxides $(Fe(OH)_2)$ as shown in Fig. 1.5. In the presence of oxygen and moisture, the ferrous hydroxide $(2\,Fe(OH)_2)$ converts to ferric oxide $(Fe_2O_3H_2O)$ as shown in Fig. 1.6, i.e. rust (Neville 2011).

$$Fe^{2+} + 2\,OH^{-} \longrightarrow Fe(OH)_2 \qquad \text{(Ferrous hydroxide)}$$

$$4\,Fe(OH)_2 + 2H_2O + O_2 \longrightarrow 4\,Fe(OH)_3 \qquad \text{(Ferric hydroxide)}$$

It is concluded that corrosion needs three elements to exist: a chemical potential difference between the two sides of the steel bar; an electrolyte solution to provide conductivity; and an electron path through the metal to allow the flow of electrons.

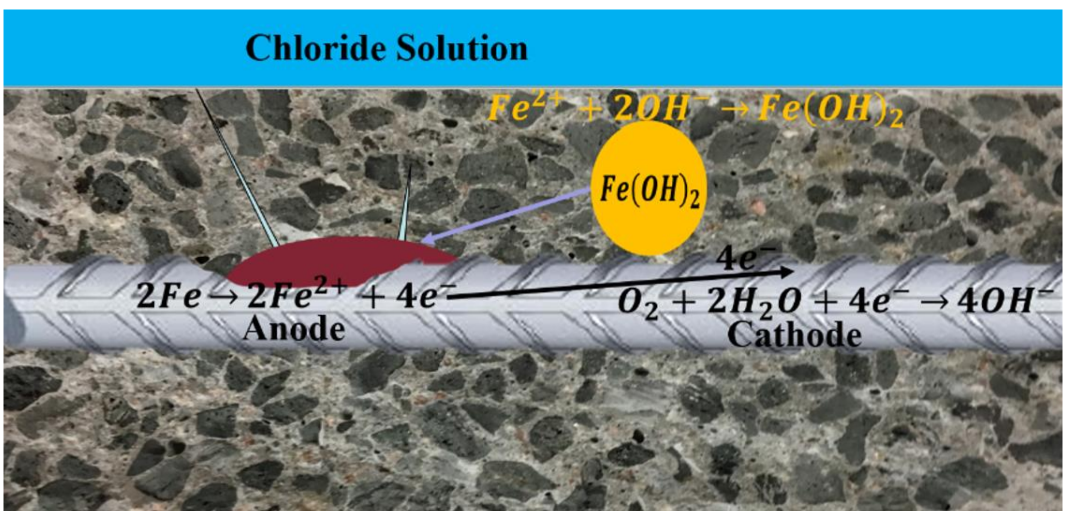

Figure 1-5 The formation of ferrous hydroxide (black rust)

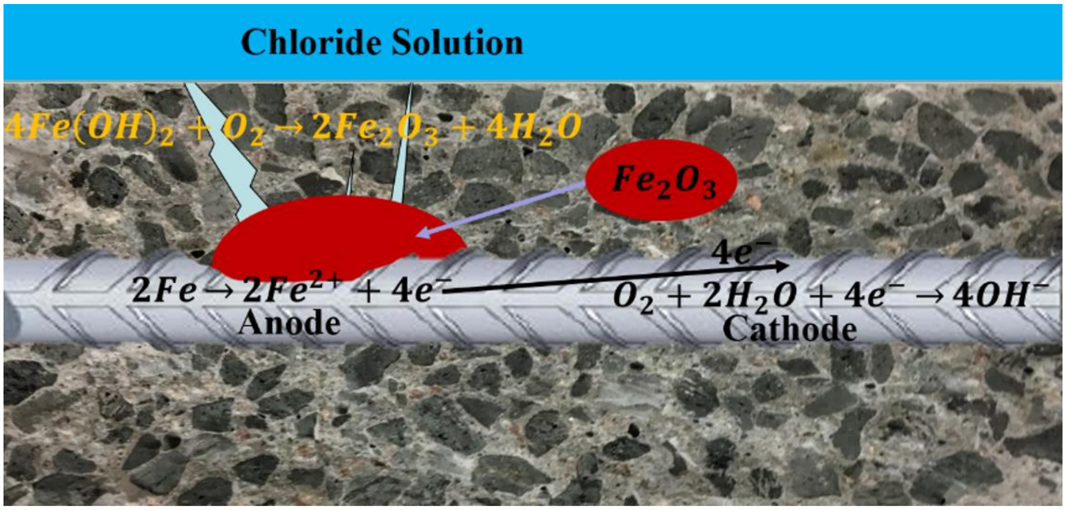

Figure 1-6 The formation of ferric oxide (red rust)

Concrete has an alkaline nature, which provides a thin oxide protection layer that surrounds the steel bar and protects it from corrosion. This layer is called the passivation layer. To initiate the corrosion process, the passivation layer needs to be weakened. This happens by decreasing the alkalinity of the concrete as in carbonation or when chloride ions penetrate the concrete cover towards the steel bar. Therefore, chlorides create an active environment, which converts the surface of steel bar to an anode. The rest passivated surface of steel bar works as a cathode as shown in Fig. 1.7. The reaction of chlorides is (Neville 2011):

$$Fe^{2+} + 2Cl^- \longrightarrow FeCl_2$$

$$FeCl_2 + 2H_2O \longrightarrow Fe(OH)_2 + 2HCl$$

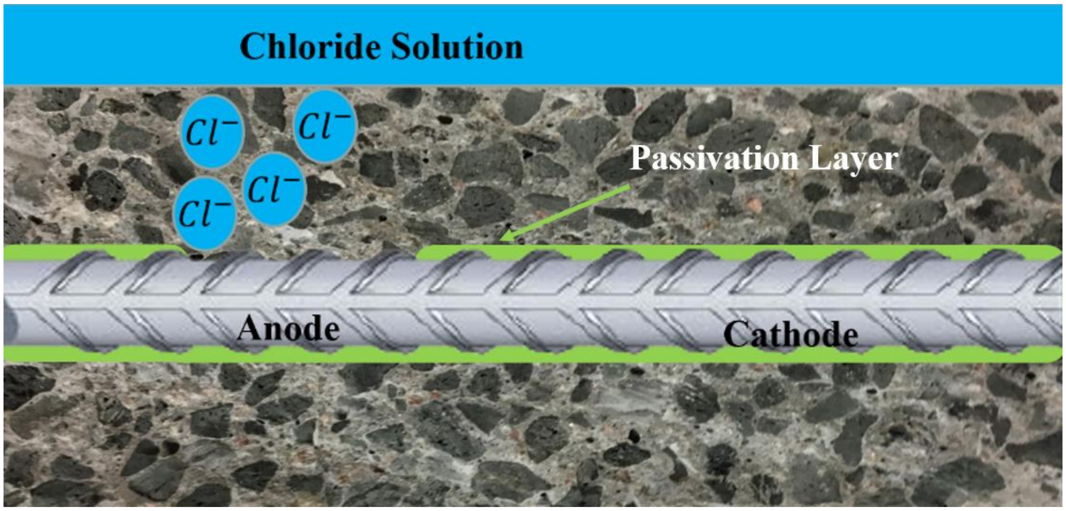

Figure 1-7 Chloride ion penetration concrete cover causing weaken to passivation layer

1.2.3. Accelerated Corrosion Technique

The corrosion process naturally takes a long period to occur. Therefore, researchers use accelerated corrosion techniques to speed up corrosion process under laboratory conditions to save time and money. Accelerated corrosion tests are used in investigating the behaviour of corroded structural elements. The objective of the researchers is to create a bridge between the accelerated corroded laboratory results and the real corrosion that occurs to the structures during their service life (Davis 2000). The mechanism used in the accelerated electro-chemical corrosion technique is to provide a salinity environment (such as sodium chloride solution) to ensure the transfer of ions through this environment.

Faraday's law uses to calculate the mass loss of the corroded rebar depends on the amount of direct electrical current and its passing time through the rebar (Toongoenthong & Maekawa 2004). There are two accelerated techniques in literature, the test setup in both techniques is the same, where an electrochemical potential is applied between the anode and the cathode. The embedded rebar works as an anode in the presence of a cathode that could be internal or external. The internal cathode could be made from a stainless bar while the external one could be made from copper or stainless steel mesh. An electrolyte solution is used to activate the corrosion process. This solution always is prepared from chloride slats solution that could be added during the concrete mixture or submerged the RC element inside the solution after days from casting it (El-Maaddawy & Soudki 2003). The electrochemical potential difference is induced using a direct current from a power supply.

A technique keeps the voltage constant and the current varies during the accelerated test, this method called constant voltage technique (Pellegrini-Cervantes et al. 2013; Al-Swaidani & Aliyan 2015; Kumar et al. 2012; Lee et al. 2000; Deb & Pradhan 2013; Amleh 2000; Ahwazi 2001; Yoon et al. 2001; Xia et al. 2012). The constant voltage was varying between 5 V to 30 V in the previous studies. The current needs in this technique to be monitored all the time using a computer-controlled data acquisition system.

Another technique keeps the direct current constant during the corrosion test and this accelerated method called constant or implied current technique (El-Maaddawy & Soudki 2003; El-Maaddawy et al. 2005a; Kashani et al. 2013; Pritzl et al. 2014; Talakokula et al. 2014; Altoubat et al. 2016; Almusallam et al. 1996; Bonacci et al. 1998). Faraday's mass loss equation is easily applying in this technique because there is no need to monitor the current during the test because it's always constant. The impressed current technique reaches the targeted corrosion level within a reasonable amount of time (El-Maaddawy & Soudki 2003). The impressed current density in the previous studies varies between $45\,\mu A/cm^2$ and $10400\,\mu A/cm^2$. There was a previous study done by El-Maaddawy & Soudki (2003) about the effect of different current intensities on the corrosion behavior of corroded elements. They recommended first to keep the current intensity constant for all test specimen to avoid any misinterpretation for the test results. However, they did not notice any effect on the percentage of mass loss that was calculated based on Faraday's law. Secondly, they recommended not to exceed the current intensity above $200\,\mu A/cm^2$ to avoid unrealistic damage behavior due to the significant increase in crack width and strain response due to the high current intensities.

There is a previous comparison study done by Altoubat et al. (2016) between constant voltage and constant current techniques. They applied those techniques on a small column specimen and they reached a maximum mass loss of 8%. The mass loss for both techniques was the same, but they noticed that constant current technique caused more damage than constant voltage. They recommended using constant current as an accelerated corrosion technique to simulate corrosion damage, especially constant current reaches the targeted corrosion level within a reasonable amount of time.

1.2.4. Effect of Corrosion on the Structural Performance of RC Elements

1.2.4.1. Effect on Corrosion on RC Beams

Several researchers investigated the structural performance of corroded RC beams. Three parameter were examined. First, cracking and spalling of the concrete cover, which cause loss in the concrete cross-sectional effective area. Second, the reduction of the steel reinforcement area, which reduces the mechanical properties of the steel reinforcement. Finally, the bond deterioration due to corrosion product between steel reinforcement and concrete (Wang & Liu 2006; Fang et al. 2004). several studies have been carried out in an attempt to understand and assess the corrosion effects on RC beams. The effect of corrosion on bond, flexural, and shear that was reported by different researches is presented in the following sections.

1.2.4.1.1. Effect of Corrosion on Bond Strength of RC Beams

The bond strength is affected by bar geometry, bar surface condition, confinement condition around the bar, and concrete properties (Macgregor, James G. Wight 2009). Bond Strength between steel reinforcement and concrete has a significant effect on the behavior of any RC element. Corrosion of steel reinforcement is a form of deterioration that causes loss of bond between steel and concrete (Fang et al. 2004; Fu & Chung 1997). The product of corrosion accumulates around the reinforcement, which causes an interface layer between reinforcement and concrete. This interface layer causes bond degradation, which reduces the service life of the structural element (Fang et al. 2004). Many researchers investigated the effect of corrosion on the bond strength of RC concrete elements. Most of the studies reported that the bond strength at the initiation of corrosion increases until the concrete start to crack, after that the bond strength decreases with the increase in the level of corrosion (Almusallam et al. 1996; Al-Sulaimani et al. 1990; Bhargava et al. 2007; Ouglova et al. 2007).

Cabrera (Cabrera 1996) studied the relation between the rate of corrosion and the loss of serviceability by measuring bond strength, cracks, and deflections. The effect of using fly ash on the rate of corrosion was also examined. An accelerated corrosion technique was used through the application of constant volt; 3V. The experimental program was divided into three stages: the first stage was designed to study the effect of cement type, bar diameter, and cover thickness on the corrosion. The tested specimen used in this stage had dimensions of 100 mm × 200 mm × 300 mm. The second stage investigated the bond strength by conducting pullout tests using concrete cubes. The cubes had dimensions of 150 mm × 150 mm × 150 mm with 12 mm steel bar embedded in the middle of the cube. The final stage examined the effect of two different embedded lengths and shear span for two groups of RC beams with cross-sectional area of 125 mm × 160 mm. One group of beams was designed to fail due to flexure and the second group to fail due to bond slip. The results indicated that increasing the level of corrosion had a significant effect on increasing crack intensities, reducing bond strength, and increasing mid span deflection. In addition, the level of corrosion was affected by the concrete cover in a vice versa relationship. Eventually, the author indicated that using fly ash increased the resistivity of concrete against corrosion.

Almusallam et al. (Almusallam et al. 1996) investigated the effect of corrosion on the bond strength. In addition, the effect of rib profile on crack widths was studied. An impressed current of 0.4 A was used to accelerate the corrosion process in the specimen. The results indicated that the initial ultimate bond strength increased with the increasing the level of corrosion. Afterwards, the bond strength decreased until 6% of rebar corrosion was reached. There was no significant variation of the ultimate bond strength after 6% of corrosion. Finally, the authors found that the rib profile had no effect on bond strength degradation.

Jin and Zhao (Wei-liang & Yu-xi 2001) carried out pullout and bending tests to investigate the effect of corrosion on the bond behavior and bending strength. An impressed current accelerated technique was used to accelerate the corrosion process. The pullout test specimens had a side dimension 100 mm and a steel bar of diameter 12 mm that was embedded 80 mm in the middle of each cubic specimen. Two types of steel bars were used: plain, and deformed. The results revealed that when corrosion increased the bond strength between plain bars and concrete initially increased then decreased due to cracks forming in concrete cover. On the contrary, in deformed bars, the cracks of concrete cover had no effect on the bond strength. However, the bond strength increased then decreased with the increase of corrosion level. The authors recommended to use a bond strength coefficient to develop a bond stress-slip relationship between corroded reinforcement and concrete cover.

Fang et al. (Fang et al. 2004) carried out pullout tests to investigate the influence of corrosion on bond strength. The effect of bar surface and confinement condition on bond strength in corroded specimen were also studied. An accelerated corrosion technique was used to accelerate the corrosion process by applying a constant direct current to the corroded specimen. The results indicated that corrosion of deformed bars had no significant effect on the bond strength in specimen with confinement. On the contrary, the bond strength for non-confinement specimen decreased with the increase of corrosion level. Moreover, for smooth bars without confinement, the bond strength initially increased with corrosion until certain level then deceased with increasing corrosion level. On the other hand, the bond strength increased with the increasing of corrosion for smooth bars with confinement.

Wang et al. (Wang & Liu 2006) developed a theoretical model to predict the bond splitting failure strength of corroded specimen without stirrups. The model takes into consideration some parameters that affect the bond strength due corrosion such as: confinement, concrete strength, pressure due to corrosion, ratio between rust and uncorroded steel bar, geometry of ribbed bar, and rib profile reduction.

1.2.4.1.2. Effect of Corrosion on Flexural Strength of RC Beams

Several studies have been conducted to investigate the corrosion of RC beams under flexure. The objective of most of these studies are to determine the degradation in the flexural capacity and to relate it with either the mass loss of corroded reinforcement or the depth of corrosion penetration.

Rodriguez et al. (Rodriguez et al. 1997) examined the effect of corrosion on both bending and shear. A total of six beams were tested, five beams had dimensions of 150 mm × 200 mm × 2300 mm and one beam had dimension of 150 mm × 200 mm × 2050 mm. The reinforcement was corroded through adding calcium chloride to the mixing water. After 28 days of curing, an impressed current with a current density of 100 μA/cm^2 was applied to accelerate the corrosion. The experimental parameters were the tensile reinforcement ratio, compression reinforcement ratio, shear reinforcement spacing, and reinforcement anchorage length. The results indicated that corrosion at service load led to an increase in the deflection and crack widths, whereas corrosion at ultimate load decreased the capacity.

Mangat and Elgarf (P. S. Mangat & Elgarf 1999) studied the flexural performance of under-reinforced RC beams with different levels of corrosion. A total of 111 beams were tested. The beams had dimension of 100 mm × 150 mm × 910 mm. Corrosion was induced by using impressed current accelerated corrosion technique. Beams were corroded with different levels ranging from 1.25% to 10 %, with corrosion rates 1 mA/cm^2, 2 mA/cm^2, 3 mA/cm^2, and 4 mA/cm^2. The results demonstrated that corrosion of reinforcement had a significant effect on both the flexural load capacity and deflection of the corroded beams.

Castel et al. (A. Castel et al. 2000; A Castel et al. 2000) investigated the effect of corrosion on the behavior of RC beams under service and ultimate states. This experimental work was a part of a long-term program. During fourteen years, the corroded specimens were exposed to a saline environment and the specimens were under loading to consider the effect of load, service cracks, and micro-cracks. The corroded specimens had cross-section dimension of 150 mm × 280 mm with a length of 3000 mm. The results showed that under service load, significant behavior degradation, at the tension zone, was observed. This degradation was as a result of the loss in the bending stiffness of the corroded beams. In addition, at the ultimate load, the loss in capacity and ductility occurred due to the reduction in steel cross-section. Finally, the behavior of the corroded beams was adversely affected by the reduction of stress transmitted between concrete and reinforcement.

Yoon et al. (Yoon et al. 2001) investigated the interaction between the loading level, corrosion rate, deflection, and residual strength of reinforced concrete beams. A total of ten beams with dimension of 100 mm × 150 mm × 1170 mm were cast. A constant volt accelerated corrosion technique was used. The starting volt value was 10 V then increased incrementally up to 27 V and was kept on this value; the purpose of the increased incremental volt was to simulate a desirable corrosion propagation rate. Some of the beams were corroded under sustained load. The results indicated that loading history and loading level have a significant impact on both the corrosion initiation and corrosion rate. Moreover, the failure mode was affected by the level of corrosion; when corrosion increased, the failure mode changed from shear to bond splitting. Furthermore, the increase in mass loss led to a decrease in the loading capacity of the beams. The authors suggested to take into consideration the service life load with the combination of both environmental conditions and mixture proportions to creating models to predict the service life of the concert structures.

Ballim et al. (Ballim et al. 2001) carried out an experimental investigation to determine the deflections, in both service limit and ultimate limit states, of corroded RC beams under static load. An impressed current technique was used to accelerate the corrosion process by applying constant current of 300 mA. A total of twelve beams of dimensions 100 mm × 160 mm × 1550 mm were cast. The results demonstrated that the deflection increases as the corrosion increases. Moreover, the deflection of corroded beams increased under sustained loads.

Jin and Zhao (Wei-liang & Yu-xi 2001) carried out pullout and bending tests to investigate the effect of reinforcement corrosion on the bond behavior and flexural strength. An impressed current accelerated technique was used to accelerate the corrosion process. The flexural tests were carried out on beams of dimensions 150 mm × 150 mm × 1140 mm. The results demonstrated that the flexural strength decreases with the increasing of corrosion due to the reduction in steel bar diameter, yield strength, and bond capacity.

Ballim and Reid (Ballim & Reid 2003) studied the effect of corrosion on the serviceability of RC beams. An impressed current (300 mA) accelerated corrosion technique was applied.

The corroded beams were under sustained load. The authors recommended to assess the performance of corroded beams under sustained load condition to simulate situ condition.

El Maaddawy et al. (El-Maaddawy et al. 2006) investigated the effect of corrosion under sustained loads on the structural performance of RC beams. A total of nine beams with dimensions of 152 mm × 254 mm × 3200 mm were cast. An impressed current technique was applied to accelerate the corrosion process. The results showed that the combination of corrosion with sustained load accelerate the formation of cracks and widen the crack widths. In addition, the mass loss rate at the beginning of the corrosion process had an effect on the formation of flexural cracks and the reduction of beam strength. On the contrary, there was no relationship observed at high level of corrosion between the presence of flexural cracks and the reduction in beam strength.

Azad et al. (Azad et al. 2007) studied the influence of corrosion on the flexural behaviour of RC beams. A total of 56 beams with dimensions of 150 mm × 150 × mm × 1100 mm were cast. An impressed current (2 and 3 mA/cm^2) accelerated corrosion technique was used. The experimental data was used to develop a model to predict the residual flexural strength. The predication method depends on mass loss and a correction factor to compensate the loss in the bond. This correction factor take into consideration the effect of corrosion current density, corrosion time, and the reinforcing bar diameter. The results showed that the mass loss in big diameter bars is less than those in small diameter. In addition, the deflection increased in corroded beams due to the degradation in the flexural stiffness.

Torres-Acosta et al. (Torres-Acosta et al. 2007) investigated the effect of corrosion on the residual flexural capacity of RC beams. Beams with dimension 100 mm × 100 mm × 1500 mm were tested. An impressed current (80 µA/cm^2) was applied to accelerate the corrosion process. Chloride ions were added to the mixing water. The results showed that dry corrosion environment created more cracks than wet corrosion environment. This was attributed to the more presence of the corrosion product under concrete cover in dry environment than wet environment. This led to an increase in the internal pressure and an increase in the probability of creating more cracks.

Xia et al. (Xia et al. 2012) studied the effect of corrosion on the flexural strength of RC beams. Beams with dimensions 150 mm × 200 mm × 1500 mm were cast. A constant volt (30 V) accelerated corrosion technique was applied. The results demonstrated that maximum and average crack widths increased with the increase of corrosion, whereas both deflection and stiffness decreased. In addition, an average crack width was recommended to predict the flexural strength instead of maximum crack width. This was suggested due to the better correlation found between the average crack width and flexural capacity. Moreover, the increase of corrosion lead to change the failure mode from ductile to brittle one.

1.2.4.1.3. Effect of Corrosion on Shear Behavior of RC Beams

Failure of reinforced concrete (RC) members due to shear could be catastrophic collapse (Bentz et al. 2006). Shear deficiencies may occur in RC members due to several reasons: excessive service loads, insufficient shear reinforcement, design/construction defects, and reduction in steel area due to corrosion. Corrosion of steel reinforcement has a significant effect on structural capacity, and safety of RC structures (Makki 2014).

Many efforts have been exerted in studying the corrosion of both longitudinal and transverse reinforcement in beams (El-Maaddawy et al. 2005b; Azad et al. 2007). Moderate and severe level of corrosion affect both the ultimate shear strength and ductility (Juarez et al. 2011). Transverse reinforcement (stirrups) may be less protected than longitudinal reinforcement due to the possibility of having thinner concrete cover and the smaller diameter has used as stirrups (Juarez et al. 2011). Corroded shear reinforcement decreases shear strength (Val 2007). More studies are needed to develop a better understanding of the effect of corrosion on the structural shear behavior.

1.2.4.1.3.1. Effect of Corrosion on Longitudinal Shear Reinforcement on RC Beams

Toongoenthong and Maekawa (Toongoenthong & Maekawa 2004) investigated the effect of corrosion on the diagonal shear in RC beams with no stirrups. The beams were with dimension of 250 mm × 350 mm × 2400 mm. Accelerated corrosion technique was applied to the longitudinal reinforcement. A three-point load test was applied on the beams. The results indicated that cracks due to corrosion around mid-span showed no effect on the diagonal shear cracks, whereas cracks due to corrosion at the shear span met the diagonal shear cracks. It was indicated that reducing the cracks due to corrosion in shear span enhance the function of the compression strut in the beams, which lead to increase the shear capacity.

Azam (2010) investigated the effect of three different level of corrosions (2.5%, 5%, and 7.5%) of the longitudinal steel reinforcement on the shear behavior of RC beams. Two types of beams were tested: deep beams (shear to span depth a/d = 1.63, 150 mm × 350 mm × 1400 mm) and slender beams (a/d = 3.25, 150 mm × 350 mm × 2400 mm). An accelerated corrosion technique of constant current 150 μA/cm^2 was applied. The full specimen's length was corroded except 400 mm from each edge. The results showed that the load transfer mechanism of the slender beams changed from pure beam action in the uncorroded beams to pure arch action in the corroded ones. On the other hand, the load transfer mechanism of deep beams changed from a combination of beam and arch action in the uncorroded beams to pure arch action in the corroded ones. Moreover, inclined shear cracks appeared in the uncorroded specimens, whereas these inclined cracks did not appear in the corroded ones. This was attributed to the transfer of load directly from the loaded point to the support (arch action). Furthermore, the stirrups in the uncorroded deep beams enhanced the deflection and ultimate load, whereas stirrups in the corroded deep beams showed no significant effect. On the contrary, the stirrups in the uncorroded slender beams showed no significant effect, whereas stirrups in the corroded slender beams changed the failure mode. Hence, corroded slender beams without stirrups failed due to an anchorage failure, while slender beams with stirrups were failed due to yielding of the longitudinal reinforcement. The author concluded that the structural performance of slender beams with stirrups are better than those without stirrups.

Sahmaran et al. (2015) studied the effect of different levels of corrosion on the shear performance of engineered cementitious composite (ECC) beams. A total of ten beams with dimension of 150 mm × 220 mm × 1400 mm were cast. All beams designed with span to depth ratio equal to 2.5. Accelerated corrosion technique of constant current 1 A was used. Four levels of corrosion were reached: 5%, 10%, 15%, and 20%. The results showed that the performance of ECC beams under corrosion was better than the performance of NC with regard to capacity, stiffness, strength, and energy absorption. This was attributed to the high ductility and deformability showed by ECC beams. On the contrary, the shear displacement of NC beams was higher than those of ECC ones; however, the difference in shear displacement between both beams decreased when corrosion level increased.

1.2.4.1.3.2. Effect of Corrosion on Transverse Shear Reinforcement on RC Beams

Stirrups carry the shear force directly and improve the load carrying capacity of the RC beams. Stirrups restrain the propagation of cracks and limit their widths. In addition, stirrups arrest the horizontal splitting cracks at the level of main reinforcement, which improve the dowel action strength to enhance the shear capacity. Stirrups are the most vulnerable part in beams that could suffer from corrosion because they may have smaller concrete cover compared to the main reinforcement, and their diameter is usually smaller than main reinforcement; therefore, their mass loss could be faster than main reinforcement (Xia et al. 2011).

Juarez et al. (2011) investigated the effect of corroded stirrups on the shear strength in normal weight RC beams. The effect of stirrups spacing was studied. A total of eight beams of dimensions 200 mm × 350 mm × 2000 mm with shear span to depth ratio (a/d) equal 2. A constant current of 100 μA/cm^2 was applied to accelerate the corrosion process. The results showed that moderate and severe level of corrosion affect both the ultimate shear strength and ductility due to the loss of bond between the corroded stirrups and the concrete cover. The failure of the corroded beams was sudden and brittle.

Wang et al. (2015) investigated the effect of corroded transverse reinforcement (stirrups and inclined bars) on the shear behavior of normal weight RC beams. A total of fourteen RC beams of dimension 250 mm × 500 mm × 3600 mm with low a/d = 1.75 were tested. The corroded specimen were divided into two groups: one group examined the corrosion of the stirrups, while the second group was tested to investigate the effect of corrosion on both stirrups and inclined reinforcement. A constant current with a current density of 0.0183 mA/mm^2 was applied. The results showed no change in the compression failure mode due to the corrosion of stirrups and inclined bars. However, the severe corrosion in the beams led to an early transverse reinforcement rupture and reduced the cracks number.

Imam & Azad (2016) studied the effect of corroded stirrups on the shear behavior of RC beams. The tested beams had a length of 1150 mm and two different cross sectional areas: 140 mm × 220 mm and 150 mm × 240 mm. An impressed current with a current density of 2 mA/cm^2 was applied. The results showed that a reduction in shear strength of the corroded beam occurred. The authors attributed that to two reasons: the reduction of the stirrups cross-sectional area, and the cracks, due to corrosion, in the concrete cover.

1.2.4.2. Effect of Corrosion on the Structural Performance of Two-way Slabs

Reinforced concrete (RC) two-way slabs are commonly used in many structures such as parking garage, bridges, and residential buildings. Parking and bridge structures are ones of the most structures that are exposed directly to harsh environmental conditions, especially in cold climates such as Canada. These structures are usually exposed to water, snow, ice, and de-icing salts, which increase the probability of corrosion of the top flexural reinforcement. The most vulnerable structural element that can be affected by corrosion in the parking structures is the slab-column connection. The connection could fail due to punching shear if it loses its structural integrity (Reilly et al. 2014). There are some existing structures that collapsed due to punching shear failure such as a parking garage collapse in Bluche, Switzerland, in 1981 (Mirzaei 2008); and a parking garage collapse in Ville St. Laurent, Québec in 2008 (Reilly et al. 2014).

Limited research was carried out to investigate the effect of corrosion on two-way slabs. Rahman (Rahman 1992a) studied the effect of corrosion on the slab-column connection. The author simulated the effect of corrosion by decreasing the number of top flexural bars and using empty sheathes as broken tendons. The researcher concluded that 50% loss in a bar and tendon area reduced the punching shear capacity by 30%. The effect of loss of bond and concrete delamination was also examined. The author simulated the loss of bond by wrapping the reinforcing bars with adhesive plastic tape. The delamination was simulated by placing a polyethylene sheet between the upper and lower layers of the top reinforcing mat. Deflections and crack widths were more noticeable higher due to loss of bond and delamination. However, the punching load capacity in both cases increased slightly, which is obviously in contrast to what might be expected.

Aoude et al. (Aoude et al. 2014) simulated delamination of two-way slab-column connections. The delamination was simulated by placing a plastic sheet under the flexural reinforcement. Four different specimens were tested: a control specimen with no delamination; a specimen simulating a slight delamination by extending this plastic sheet for a short distance around the column; a specimen simulating medium delamination by using the plastic sheet with dimension such that the flexural reinforcement had a remaining embedment length at the edges of the specimen equal to the development length, L_d; and a specimen simulating a large degree of delamination by using a plastic sheet allowing only $0.5L_d$ of the flexural reinforcement to remain bonded. The authors concluded that slight delamination caused a 4% increase in the punching shear capacity; medium delamination caused only a 3% decrease in the punching shear capacity, and severe delamination caused a 12% reduction in punching shear capacity.

Reilly et al. (Reilly et al. 2014) studied the effect of large delamination on the punching and post-punching responses of slab-column connections using the same technique as Aoude et al. (Aoude et al. 2014). The authors concluded that severe delamination of the flexural reinforcement leads to a decrease in the pre-punching stiffness, punching shear capacity, and post-punching shear resistance of the specimens. They also concluded that proper design of structural integrity reinforcement enhanced post-punching shear resisting mechanism, where it caused an increase in the post-punching shear resistances and ultimate deflections.

Nonetheless, there is no investigation on the effect of real corrosion on two-way RC slabs. Hence, there is need to do research on two-way slabs under accelerated corrosion technique. This research would provide better simulation for the behaviour of the bond, the change of steel mechanical properties, and the cracks of the concrete cover under corrosion. Thus, a better understanding of the behaviour of corroded two-way RC slabs would be developed.

1.3. Research Objectives and Significance

Rehabilitation of corrosion-damaged RC structures requires a good understanding of the failure mechanisms and efficient techniques to determine the residual strength of the deteriorated structures. There are four main objectives in this thesis. Firstly, develop and build a test set-up to induce corrosion in the reinforcement of two-way slabs reaching high level of mass loss. Secondly, assess the structural behavior of slab-column connections under realistic corrosion conditions. Thirdly, provide guidelines for engineers to evaluate the strength of corroded slab-column connections or two-way slabs using current codes provisions. Finally, propose design equations, using statistical tools, which could enable the evaluation of deteriorated two-way slabs in existing structures.

Slab-column connections were exposed to different levels of corrosion and different corroded areas. This portion of the study aims at assessing the effect of corrosion on the punching shear behaviour of such slabs. Moreover, the effect of the development length of the corroded bar on the degradation of the concrete strength; loss of serviceability; and crack distributions are studied. The novelty of this study lies in obtaining results based on realistic corrosion processes for full-scale slab-column connections. These results then used to create empirical equations to calculate the residual capacity for two-way corroded slabs. The equation would construct based on analysis of variance for the obtained results.

Moreover, this study proposed another technique to predict the residual capacity based on current codes.

1.4. Thesis Outline

This research proposal consists of eight chapters described as follows:

Chapter 1 describes the research background and motivation, a review of the literature pertaining to the areas of corrosion of reinforcement in concrete, and the reinforcement corrosion of slabs, and the objectives and the significance of the doctoral dissertation.

Chapter 2 illustrates different induced corrosion techniques for two-way slabs.

Chapter 3 demonstrates the monitoring data of corrosion process in two-way RC slabs using constant voltage technique.

Chapter 4 studies the effect of bandwidth reinforcement corrosion on two-way RC slabs.

Chapter 5 studies the response of two-way slabs due to corrosion for a large corroded area with enough development length.

Chapter 6 studies response of two-way slabs due to corrosion for a large corroded area without insufficient development length.

Chapter 7 performs a probabilistic analysis of strength degradation for two-way RC slabs.

Chapter 8 presents the summary and recommendations from the completed research.

1.5. Reference

Ahmad, S. (2003) ‘Reinforcement corrosion in concrete structures, its monitoring and service life prediction - A review’, Cement and Concrete Composites, 25(4–5 SPEC), pp. 459–471. doi: 10.1016/S0958-9465(02)00086-0.

Ahwazi, B. B. N. (2001) A comparative study of deterioration of bond due to corrosion in different concretes. McGill University.

Al-Sulaimani, G. J., Kaleemullah, M., Basunnul, I. A. and Rasheeduzzafar, A. A.-M. (1990) ‘Influence of corrosion and cracking on bond behavior and strength of reinforced concrete members’, ACI Structural Journal, 87(2), pp. 220–231. Available at: http://www.concrete.org/PUBS/JOURNALS/OLJDetails.asp?Home=SJ&ID=2732.

Al-Swaidani, A. M. and Aliyan, S. D. (2015) ‘Effect of adding scoria as cement replacement on durability-related properties’, International Journal of Concrete Structures and Materials. Korea Concrete Institute, 9(2), pp. 241–254. doi: 10.1007/s40069-015-0101-z.

Almusallam, A., Al-Gahtani, A. S., Aziz, A. R. and Rasheeduzzafar, A. (1996) ‘Effects of reinforcement corrosion on bond strength’, Construction and Building Materials, 10(2), pp. 123–129.

Altoubat, S., Maalej, M. and Shaikh, F. U. A. (2016) ‘Laboratory simulation of corrosion damage in reinforced concrete’, International Journal of Concrete Structures and Materials. Korea Concrete Institute, 10(3), pp. 383–391. doi: 10.1007/s40069-016-0138-7.

Amleh, L. (2000) Bond deterioration of reinforcing steel in concrete due to corrosion. McGill University.

Andrade, C. and Alonso, C. (1996) ‘Corrosion rate monitoring in the laboratory and on-site’, Construction and Building Materials, 10(5 SPEC. ISS.), pp. 315–328. doi: 10.1016/0950-0618(95)00044-5.

Andrade, C. and Alonso, C. (2001) ‘On-site measurements of corrosion rate of reinforcements’, Construction and Building Materials, 15(2–3), pp. 141–145. doi: 10.1016/S0950-0618(00)00063-5.

Aoude, H., Cook, W. D. and Mitchell, D. (2014) ‘Effects of simulated corrosion and delamination on response of two-way slabs’, Journal of structural Engineering, 140(1), pp. 1–9. doi: 10.1061/(ASCE)ST.1943-541X.0000775.

Auyeung, Y., Balaguru, P. and Chung, L. (2000) ‘Bond behavior of corroded reinforcement bars’, ACI Structural Journal, 97(2), pp. 214–220. doi: 10.14359/826.

Azad, A. K., Ahmad, S. and Azher, S. a (2007) ‘Residual strength of corrosion-damaged reinforced concrete beams’, ACI Materials Journal, 104(1), pp. 40–47.

Azam, R. (2010) Behaviour of shear critical RC beams with corroded longitudinal steel reinforcement. Waterloo.

Ballim, Y. and Reid, J. C. (2003) ‘Reinforcement corrosion and the deflection of RC beams - An experimental critique of current test methods’, Cement and Concrete Composites, 25(6), pp. 625–632. doi: 10.1016/S0958-9465(02)00076-8.

Ballim, Y., Reid, J. C. and Kemp, A. R. (2001) ‘Deflection of RC beams under simultaneous load and steel corrosion’, Magazine of Concrete Research. Thomas Telford, 53(3), pp. 171–181.

Bentz, E. C., Vecchio, F. J. and Collins, M. P. (2006) ‘Simplified modified compression field theory for calculating shear strength of reinforced concrete elements’, ACI Structural Journal, 103(4), pp. 614–624. doi: 10.14359/16438.

Berto, L., Simioni, P. and Saetta, A. (2008) ‘Numerical modelling of bond behaviour in RC structures affected by reinforcement corrosion’, Engineering Structures. Elsevier, 30(5), pp. 1375–1385.

Bertolini, L., Elsener, B., Pedeferri, P., Redaelli, E. and Polder, R. B. (2013) Corrosion of steel in concrete: prevention, diagnosis, repair. John Wiley & Sons.

Bhargava, K., Ghosh, A. K., Mori, Y. and Ramanujam, S. (2007) ‘Models for corrosion-induced bond strength degradation in reinforced concrete’, ACI Materials Journal, 104(6), pp. 594–603. doi: 10.1016/j.nucengdes.2007.01.010.

Bonacci, J., Thomas, M., Hearn, N., Lee, C. and Maalej, M. (1998) ‘Laboratory simulation of corrosion in reinforced concrete and repair with CFRP wraps’, in Annual Conference of the Canadian Society of Civil Engineering, pp. 653–662.

Broomfield, J. P. (2002) Corrosion of steel in concrete: understanding, investigation and repair. CRC Press.

Cabrera, J. G. (1996) ‘Deterioration of concrete due to reinforcement steel corrosion’, Cement and Concrete Composites, 18(1), pp. 47–59. doi: 10.1016/0958-9465(95)00043-7.

Carnot, A., Frateur, I., Zanna, S., Tribollet, B., Dubois-Brugger, I. and Marcus, P. (2003) ‘Corrosion mechanisms of steel concrete moulds in contact with a demoulding agent studied by EIS and XPS’, Corrosion science. Elsevier, 45(11), pp. 2513–2524.

Castel, A., François, R. and Arliguie, G. (2000) ‘Mechanical behaviour of corroded reinforced concrete beams—Part 1: Experimental study of corroded beams’, Materials and Structures, 33(9), pp. 539–544. doi: 10.1007/BF02480533.

Castel, A., Franfois, R., Arliguie, G. and Mat, L. (2000) ‘Mechanical behaviour of corroded reinforced concrete beams - part 2 : bond and notch effects’, Materials and Structures, 33(9), pp. 545–551.

Chitty, W.-J., Dillmann, P., L’Hostis, V. and Lombard, C. (2005) ‘Long-term corrosion resistance of metallic reinforcements in concrete—a study of corrosion mechanisms based on archaeological artefacts’, Corrosion Science. Elsevier, 47(6), pp. 1555–1581.

Chung, L., Najm, H. and Balaguru, P. (2008) ‘Flexural behavior of concrete slabs with corroded bars’, Cement and Concrete Composites, 30(3), pp. 184–193. doi: 10.1016/j.cemconcomp.2007.08.005.

Coronelli, D. and Gambarova, P. (2004) ‘Structural assessment of corroded reinforced concrete beams: modeling guidelines’, Journal of Structural Engineering. American Society of Civil Engineers, 130(8), pp. 1214–1224.

Davis, J. (2000) Corrosion: understanding the basics. doi: 10.1361/cutb2000p001.

Deb, S. and Pradhan, B. (2013) ‘A study on corrosion performance of steel in concrete under accelerated condition’, in Proceedings of the International Conference on Structural Engineering Construction and Management, Kandy, Sri Lanka. Available at: http://dl.lib.mrt.ac.lk/handle/123/9365.

Dodd, L. L. and Restrepo-Posada, J. I. (1995) ‘Model for predicting cyclic behavior of reinforcing steel’, Journal of Structural Engineering. American Society of Civil Engineers, 121(3), pp. 433–445.

El-Maaddawy, T. and Soudki, K. (2003) ‘Effectiveness of impressed current technique to simulate corrosion of steel reinforcement in concrete’, Journal of Materials in Civil Engineering. American Society of Civil Engineers, 15(1), pp. 41–47. doi: 10.1061/(ASCE)0899-1561(2003)15:1(41).

El-Maaddawy, T., Soudki, K. and Topper, T. (2005a) ‘Analytical model to predict nonlinear flexural behavior of corroded reinforced concrete beams’, ACI Structural Journal, 102(4), pp. 550–559.

El-Maaddawy, T., Soudki, K. and Topper, T. (2005b) 'Long-term performance of corrosion-damaged reinforced concrete beams', ACI Stractural Journal, 102(5), pp. 649–656.

El-Maaddawy, T., Soudki, K. and Topper, T. (2006) 'Long-term performance of corrosion damaged reinforced concrete beams', ACI Structural Journal, 102(5), pp. 649–656.

Fang, C., Lundgren, K., Chen, L. and Zhu, C. (2004) 'Corrosion influence on bond in reinforced concrete', Cement and Concrete Research, 34(11), pp. 2159–2167. doi: 10.1016/j.cemconres.2004.04.006.

Fedrizzi, L., Azzolini, F. and Bonora, P. L. (2005) 'The use of migrating corrosion inhibitors to repair motorways' concrete structures contaminated by chlorides', Cement and concrete research. Elsevier, 35(3), pp. 551–561.

Fu, X. D. D. L. and Chung, D. D. L. (1997) 'Effect of corrosion on the bond between concrete and steel rebar', Cement and Concrete Research, 27(12), pp. 1811–1815.

Imam, A. and Azad, A. K. (2016) 'Prediction of residual shear strength of corroded reinforced concrete beams', International Journal of Advanced Structural Engineering. Springer Berlin Heidelberg, (8), pp. 307–318. doi: 10.1016/j.engstruct.2016.04.018.

Juarez, C. a., Guevara, B., Fajardo, G. and Castro-Borges, P. (2011) 'Ultimate and nominal shear strength in reinforced concrete beams deteriorated by corrosion', Engineering Structures. Elsevier Ltd, 33(12), pp. 3189–3196. doi: 10.1016/j.engstruct.2011.08.014.

Kashani, M. M., Crewe, A. J. and Alexander, N. A. (2013) 'Nonlinear stress-strain behaviour of corrosion-damaged reinforcing bars including inelastic buckling', Engineering Structures, 48, pp. 417–429. doi: 10.1016/j.engstruct.2012.09.034.

Kumar, M. K., Rao, P. S., Swamy, B. L. P. and Chandra Mouli, C. (2012) 'Corrosion resistance performance of fly ash blended cement concrete', Internatioanl Journal of Research in Engineering and Technologi, 1(3), pp. 448–454. doi: 10.1016/0140-6701(95)93047-7.

Lee, C., Bonacci, J. F., Thomas, M. D. a., Maalej, M., Khajehpour, S., Hearn, N., Pantazopoulou, S. and Sheikh, S. (2000) 'Accelerated corrosion and repair of reinforced concrete columns using carbon fibre reinforced polymer sheets', Canadian Journal of Civil Engineering, 27(5), pp. 941–948. doi: 10.1139/cjce-27-5-941.

Macgregor, James G. Wight, J. K. (2009) Reinforced concrete mechanics & design. doi: 10.1017/CBO9781107415324.004.

Makki, R. F. (2014) 'Response of reinforced concrete beams retrofitted by ferrocement', International Journal of Science & Technology Research, 3(9), pp. 27–34.

Mangat, P. S. and Elgarf, M. S. (1999) 'Flexural strength of concrete beams with corroding reinforcement', ACI Structural Journal, (96), pp. 149–158. Available at: http://shura.shu.ac.uk/1042/.

Mirzaei, Y. (2008) 'Post punching behavior of reinforced slab-column connections', in 7th Int. FIB Ph.D. Symp., IWB Universität Stuttgart, Stuttgart., pp. 1–8.

Miyagawa, T. (1991) ‘Durability design and repair of concrete structures: chloride corrosion of reinforcing steel and alkali–aggregate reaction’, Magazine of Concrete Research. Thomas Telford Ltd, 43(156), pp. 155–170.

Neville, A. M. (2011) Properties of concrete (Fifth Edition), Cement and Concrete Research. doi: 10.1016/0008-8846(96)82366-0.

Ouglova, A., Berthaud, Y., Foct, F., François, M., Ragueneau, F. and Petre-Lazar, I. (2007) ‘The influence of corrosion on bond properties between concrete and reinforcement in concrete structures’, Materials and Structures, 41(5), pp. 969–980. doi: 10.1617/s11527-007-9298-x.

Pellegrini-Cervantes, M. J., Almeraya-Calderon, F., Borunda-Terrazas, A., Bautista-Margulis, R. G., Chacón-Nava, J. G., Fajardo-San-Miguel, G., Almaral-Sanchez, J. L., Barrios-Durstewitz, C. P. and Martinez-Villafañe, A. (2013) ‘Corrosion resistance, porosity and strength of blended portland cement mortar containing rice husk ash and nano-SiO2’, International Journal of Electrochemical Science, 8(8), pp. 10697–10710.

Pritzl, M. D., Tabatabai, H. and Ghorbanpoor, A. (2014) ‘Laboratory evaluation of select methods of corrosion prevention in reinforced concrete bridges’, International Journal of Concrete Structures and Materials, 8(3), pp. 201–212. doi: 10.1007/s40069-014-0074-3.

Rahman, A. H. (1992) Effect of steel corrosion on the strength of slab-column connections, National Research Council Canada, Institute for Research in Construction. National Research Council Canada, Institute for Research in Construction.

Raupach, M. (1996) ‘Chloride-induced macrocell corrosion of steel in concrete - Theoretical background and practical consequences’, Construction and Building Materials, 10(5 SPEC. ISS.), pp. 329–338. doi: 10.1016/0950-0618(95)00018-6.

Reilly, J. L., Cook, W. D., Bastien, J. and Mitchell, D. (2014) ‘Effects of delamination on the performance of two-way reinforced concrete slabs’, Journal of Performance of Constructed Facilities, 28(4), pp. 1–8. doi: 10.1061/(ASCE)CF.

Rodriguez, D. J., Ortega, L. and Casal, J. (1997) ‘Load carrying capacity of concrete structures with corroded reinforcement’, Construction and Building Materials, 11(4), pp. 239–248.

Sahmaran, M., Anil, O., Lachemi, M., Yildirim, G., Ashour, A. F. and Acar, F. (2015) ‘Effect of corrosion on shear behavior of reinforced engineered cementitious composite beams’, ACI Structural Journal, 112(6), pp. 771–782. doi: 10.14359/51687749.

Talakokula, V., Bhalla, S. and Gupta, A. (2014) ‘Corrosion assessment of reinforced concrete structures based on equivalent structural parameters using electro-mechanical impedance technique’, Journal of Intelligent Material Systems and Structures, 0(0), pp. 1–16. doi: 10.1177/1045389X13498317.

Toongoenthong, K. and Maekawa, K. (2004) ‘Interaction of pre-induced damages along main reinforcement and diagonal shear in RC members’, Journal of Advanced Concrete Technology, 2(3), pp. 431–443. doi: 10.3151/jact.2.431.

Torres-Acosta, A. a., Navarro-Gutierrez, S. and Terán-Guillén, J. (2007) ‘Residual flexure capacity of corroded reinforced concrete beams’, Engineering Structures, 29(6), pp. 1145–1152. doi: 10.1016/j.engstruct.2006.07.018.

Val, D. V. (2007) ‘Deterioration of strength of RC beams due to corrosion and its influence on beam reliability’, Journal of Structural Engineering, 133(9), pp. 1297–1306. doi: 10.1061/(ASCE)0733-9445(2007)133:9(1297).

Wang, L., Zhang, X., Zhang, J., Ma, Y. and Liu, Y. (2015) ‘Effects of stirrup and inclined bar corrosion on shear behavior of RC beams’, Construction and Building Materials. Elsevier Ltd, 98, pp. 537–546. doi: 10.1016/j.conbuildmat.2015.07.077.

Wang, X. and Liu, X. (2006) ‘Bond strength modeling for corroded reinforcements’, Construction and Building Materials, 20(3), pp. 177–186. doi: 10.1016/j.conbuildmat.2005.01.015.

Wei-liang, J. and Yu-xi, Z. (2001) ‘Effect of corrosion on bond behavior and bending strength of reinforced concrete beams’, Journal of Zhejiang University-Science, (3), pp. 298–308. doi: 10.1007/BF02839464.

Xia, J., Jin, W.-L. and Li, L.-Y. (2012) ‘Effect of chloride-induced reinforcing steel corrosion on the flexural strength of reinforced concrete beams’, Magazine of Concrete Research. Thomas Telford, 64(6), pp. 471–485.

Xia, J., Jin, W. and Li, L. (2011) ‘Shear performance of reinforced concrete beams with corroded stirrups in chloride environment’, Corrosion Science. Elsevier Ltd, 53(5), pp. 1794–1805. doi: 10.1016/j.corsci.2011.01.058.

Yoon, S., Wang, K., Weiss, W. and Shah, S. (2001) ‘Interaction of reinforced between loading, corrosion, and serviceability of reinforced concrete’, ACI Materials Journal, 97(6), pp. 637–644.

Chapter 2 Induced Corrosion Techniques for Two-way Slabs

2.1. Abstract:

Accelerated corrosion techniques are used to assess the structural performance of corroded reinforced concrete elements. This paper aims to illustrate the use of different techniques by showing their advantages and disadvantages. Two different corrosion techniques were investigated; constant voltage and constant current. Each technique was used to corrode a full-scale structural element. Two reinforced concrete two-way slabs were prepared and cast for this purpose. The slabs had identical dimensions of 1900 mm × 1900 mm × 150 mm. Each slab had a column stub with a cross-sectional area of 250 mm × 250 mm and a height of 200 mm. The two slabs were corroded to the same level of 25% mass loss. The setup and procedure for each technique is described in detail showing its appropriateness and difficulties. The corrosion of each corroded slab was evaluated based on the experimental results of current measurement, half-cell potential readings, crack patterns, natural frequency, chloride content, and mass loss. The theoretical mass loss was calculated based on Faraday's equation for both techniques. After the induced corrosion process was completed, the concrete cover was carefully removed and the corroded bars were extracted, cleaned up, and weighed. It was found that the actual mass loss for the corroded bars showed a close agreement with the theoretical mass loss for both techniques. The corrosion causes cracks on the concrete surface, which facilitate the flow of electricity between the anode and the cathode. In case of constant current technique, the cracks do not affect the

current intensity since the current is kept constant under controlled conditions. While in the case of constant voltage technique, the cracks cause fluctuation in the current value. Thus, the current intensity could reach extreme values, which affect the damage that occurs in the corroded element. Hence, constant voltage may cause more damage than what would occur under uniform corrosion conditions when a constant current is used.

Keywords: Accelerated corrosion; constant voltage; constant current; two-way slabs; chloride content; mass loss

2.2. Introduction

Reinforced concrete (RC) structures that are constructed in harsh environmental conditions have a higher probability of deterioration due to the exposure conditions. Bridges and parking garages in cold climate regions are exposed to the corrosive effects of de-icing salts. The chloride ions that exist in the de-icing salts mix with the snow leak through the bridges' joints (Konecný 2007). When vehicles park in indoor garages the attached snow and de-icing salt melt and fall on the garage deck (Reilly et al. 2014; Aoude et al. 2014). Consequently, the chloride ions penetrate the concrete cover and destroy the passivation layer. The corrosion process begins in the presence of moisture and oxygen (Neville 2011). Corrosion of steel produces a corrosive product (rust) that has a larger volume than steel rebar. This increase in volume creates radial tensile stresses around the steel rebar, when the stresses exceed the concrete tensile strength, cracks to the concrete surface will occur (Neville 2011). The deterioration due to corrosion appears as a loss in the steel bar cross-sectional area, cracking of concrete, and spalling or delamination. Federal Highway Administration (FHWA) conducted a study in 2002 which estimated the annual repair costs of corrosion for bridges to be around $8.3 billion/year (Gerhardus H. Koch 2002). The repair cost of the deterioration parking garages in Canada was $1.5 billion estimated by National Research Council (Litvan 1982). Figure 2.1 shows an example of a deteriorated two-way slab garage due to corrosion, built in Canada. Therefore, there is a need to develop a better understanding of the performance and behaviour of corroded slabs.

Corrosion that occurs naturally is a very slow process. Therefore, researchers look for techniques to accelerate the corrosion process under laboratory conditions to save time and money. Corrosion needs three elements to exist: a chemical potential difference between the two sides of the steel reinforcement; an electrolyte solution to provide conductivity; and an electron path through the metal to allow the flow of electrons (Neville 2011). This corrosion mechanism is similar to flashlight battery mechanism. Therefore, accelerated corrosion techniques were created from the idea of flashlight battery in order to simulate the corrosion process in a laboratory under normal environmental conditions (Amleh 2000). The ultimate goal of the researchers is to correlate between the accelerated corrosion results to the real ones that occur in real structures (Davis 2000). Consequently, accelerated tests could be used in investigating the behaviour of corroded structural elements. The mechanism used in the accelerated electro-chemical corrosion technique is to provide a salinity environment (such as sodium chloride solution) to ensure the transfer of ions through this environment.

The corrosion level is controlled by exposing a direct electrical current to the RC element. Here, the mass loss of corroded reinforcement is calculated based on Faraday's law depending on the accumulative electrical current passing through the corroded element

(Toongoenthong & Maekawa 2004). There are two techniques used in accelerated corrosion tests on RC beams; constant voltage technique (Pellegrini-Cervantes et al. 2013; Al-Swaidani & Aliyan 2015; Kumar et al. 2012; Lee et al. 2000; Deb & Pradhan 2013; Amleh 2000; Ahwazi 2001), and constant, or impressed current technique (El-Maaddawy & Soudki 2003; El-Maaddawy et al. 2005a; Kashani et al. 2013; Pritzl et al. 2014; Talakokula et al. 2014; Altoubat et al. 2016). In both techniques, an electrochemical potential is applied to the reinforcement that acts as an anode and an internal or external cathode. A cathode is made of copper or stainless-steel mesh if it is external, while, if internal, it could be made with a stainless-steel bar. Chloride salts are used to activate the corrosion process. Either Chloride salts are added to the concrete mix or the specimens are immersed in Chloride salt solution after 28 days from casting (El-Maaddawy & Soudki 2003).

In constant voltage technique, an electrical power supply provides the potential difference between the anode and the cathode. A constant voltage is applied to the specimen. The constant volt for several studies on RC beams varied from 5V to 30V (Ahwazi 2001; Yoon et al. 2001; Xia et al. 2012). The corrosion is monitored by measuring the current using a computer-controlled data acquisition system. While in constant current technique, an electrical power supply provides the potential difference between the anode and the cathode to reach the required current densities. The impressed current technique reaches the targeted corrosion level within a reasonable amount of time (El-Maaddawy & Soudki 2003).

Altoubat et al. (2016) conducted an experimental study to examine the effect of both accelerated techniques (constant voltage and constant current) on the corrosion process. The authors noticed that the damage created in the concrete by a constant current is more than that created by constant volt. Nonetheless, both techniques caused the same mass loss for the corroded reinforcement. They recommended using constant current as an accelerated corrosion technique to simulate corrosion damage, especially the constant current reaches the targeted corrosion level within a reasonable amount of time.

Several studies used the impressed current techniques with different current densities that range from $45\mu A/cm^2$ as a minimum value to $10400\mu A/cm^2$ as a maximum value (Almusallam et al. 1996; Bonacci et al. 1998). El Maaddawy & Soudki (2003) concluded that the use of different current densities has no effect on the percentage of mass loss that was calculated based on Faraday's law. The corroded specimens in the study reached mass loss up to 7.27%. However, the authors noticed that using current density above $200\mu A/cm^2$ would cause a significant increase in crack width and strain response due to the corrosion. The authors also recommended not to use different current densities for the same amount of time to reach different levels of corrosion. They concluded that changing the current densities to get a different level of corrosion may misguide the analysis of the test results.

The previous studies on accelerated corrosion of reinforced concrete elements were conducted mainly on beams and one-way slabs. In the literature, there are several publications on this topic as shown in Table 2.1. As could be seen from the table, the techniques of inducing the corrosion were used only on small number of bars that served as flexural reinforcement or stirrups. The flexural reinforcement in those beams were placed in one layer.

On the other hand, there are no studies reported in the literature on inducing corrosion in two-way slabs using accelerated techniques. There are several challenges that could be faced while conducting such tests especially when it comes to the equipment and space available in most research labs. The nature of the reinforcement used in two-way slabs is considered one of those challenges where the bars are distributed in several layers. Suitable precautions must be made to avoid any conductivity between the bars during the experiment. In addition, the large number of bars requires many channels of a data acquisition system to record the current during the corrosion process. Most of the data acquisition systems that are commonly available in research labs record voltage rather than current readings. Voltage output is produced by most transducers such as linear variable differential transformer (LVDT), crack gauges, strain gauges, etc. Data acquisition systems that read current are not commonly available and are more expensive. Another important challenge is providing and managing lab-space availability; especially, the corrosion period could reach several months to achieve the targeted corrosion level.

This paper aims to highlight the difficulties that could be faced when using different accelerated corrosion techniques for two-way slabs. The paper also provides proposals to overcome the challenges that could be faced during the accelerated corrosion tests on full-scale two-way slabs.

Table 2-1 Literature review for different accelerated corrosion techniques on beams

Article	Accelerated corrosion type	Dimensions b × h × L (mm)	Parameters
Rodriguez et al. (1997)	Constant current ($100\ \mu A/cm^2$)	150 × 200 × 2300 150 × 200 × 2050	Flexural reinforcement ratio, compression reinforcement ratio, stirrups spacing, anchorage length, and corrosion level.
Mangat & Elgarf (1999)	Constant current ($1\text{-}4\ mA/cm^2$)	100 × 150 × 910	Number of corroded bars, corrosion level, and stirrups presence
Castel et al. (2000)	Long-term corrosion (14 years)	150 × 280 × 3000	Service & ultimate loads, sustained loads, and corrosion level
Yoon et al. (2001)	Constant volt started 10V increased to 27 V	100 × 150 × 1170	Load history & level, sustained load, and corrosion level
Wei-liang & Yu-xi (2001)	Constant current	150 × 150 × 1140	Bar surface (plain or deformed), and corrosion level
Ballim et al. (2001)	Constant current (300 mA)	100 × 160 × 1550	Service & ultimate loads, sustained load, and corrosion level
Ballim & Reid (2003)	Constant current (300 mA)	100 × 160 × 1500	Service load, sustained load, and corrosion level
Maaddawy et al. (2005)	Constant current	152 × 254 × 3200	Sustained load, and corrosion level
Azad et al. (2007)	Constant current ($2\ \&\ 3\ mA/cm^2$)	150 × 150 × 1100	Bar diameter, corrosion time, and corrosion level
Torres-Acosta et al. (2007)	Constant current ($80\ \mu A/cm^2$)	100 × 100 × 1500	Dry & wet corrosion, and corrosion level
Xia et al. (2012)	Constant volt (30 V)	150 × 200 × 150	Stirrups bar diameter, and corrosion level
Azam (2010)	Constant current ($150\ \mu A/cm^2$)	150 × 350 × 1400 150 × 350 × 2400	Beam type (deep, slender), corrosion of flexural steel, and corrosion level
Juarez et al. (2011)	Constant current ($100\ \mu A/cm^2$)	200 × 350 × 2000	Stirrups spacing, corrosion level, and corrosion of stirrups
Lachemi et al. (2014)	Constant volt	150 × 220 × 1400	Concrete type (NC & SCC), corrosion in flexure & stirrups, and corrosion level
Sahmaran et al. (2015)	Constant current (1 A)	150 × 220 × 1400	Concrete type (NC & ECC), corrosion of flexural steel, and corrosion level
Wang et al. (2015)	Constant current ($0.0183 mA/mm^2$)	250 × 500 × 3600	Corrosion of stirrups, corrosion of inclined bars, and corrosion level
Imam & Azad (2016)	Constant current ($2\ mA/cm^2$)	140 × 220 × 1150 150 × 240 × 1150	Corrosion of stirrups, and corrosion level

Figure 2-1 Deteriorated slab in a parking garage. (Photo courtesy of Amgad Hussein)

2.3. Research Significance

This paper presents a novel study on the accelerated techniques of inducing corrosion in the flexural reinforcement of full-scale two-way slabs. It provides practical guidelines that could help and be used by researchers in constructing different accelerated corrosion test-setups for full-scale two-way slabs with equipment that are commonly available in research labs and in a reasonable time which could also help in planning the lab-space availability requirements. The complex interactions that occur between different reinforcement layers during the induced corrosion process need to be simulated in the laboratory in a controlled manner so that their individual and cumulative effects on the structural performance can be quantified and evaluated. The current study, and to the best of the authors' knowledge, is the first on inducing corrosion in full-scale two-way reinforced concrete slabs. In addition, there are currently no studies in the literature that compares constant voltage versus constant current techniques in elements with dense reinforcement meshes that are placed in several layers. Finally, in the current paper, high level of corrosion was reached; 25% mass loss. This targeted high level has its own challenges and they are useful in providing the researchers with a complete picture of the corrosion process at severe levels.

2.4. Experimental Program

Two techniques were used to reach the same level of corrosion, 25% mass loss, for full-scale two-way RC slab. The only difference between the corroded slabs, except the use of different accelerated corrosion techniques, was the targeted corroded area, which is not the focus of this paper. The induced corrosion in the slabs was evaluated based on the results of the current measurement, half-cell potential tests, chloride content, and mass loss. SV is used as an indication for the slab that used constant voltage technique and SC for the slab that used constant current technique.

2.4.1. Details of Test Specimens

Two two-way RC slab specimens were tested. The slabs had identical dimensions of 1900 mm × 1900 mm × 150 mm. The tension reinforcement was 15M bars distributed uniformly at a spacing of 190 mm as shown in Fig. 2.2. The clear cover was 30 mm. The compression reinforcement was 10M bars spaced at 300 mm. The details of the test specimens are shown in Table 2.2. All tension reinforcement were weighed and labelled before casting and pouring the slabs in order to use these values in calculating the mass loss. Special consideration was given to avoid any conductivity between the reinforcement especially between the compression and tension meshes as well as at the intersection points between all tension reinforcement mesh. This was achieved by insulating the contact surfaces between reinforcement by using an electrical tape and plastic ties instead of steel. This insulation provided more control to ensure that each bar was corroded separately which insured uniform corrosion over the targeted area. The bars under corrosion were connected with electrical wire from both ends for use in the corrosion process. Figure 2.3 shows a typical specimen before casting the concrete.

Slab SV was corroded till 25% mass loss was reached using constant voltage. Slab SC reached the same level of corrosion using constant current.

Table 2-2 Details of Slab Specimens

Side dimensions (mm × mm)	h (mm)	c (mm)	d (mm)	f'_c (MPa)	Main reinforcement
1900 × 1900	150	250	104	41.1	Two layers-15M bars (ρ = 1%)

*h is the height; c is column width; d is the effective slab depth; ρ is the reinforcement ratio; and f'_c is the concrete compressive strength.

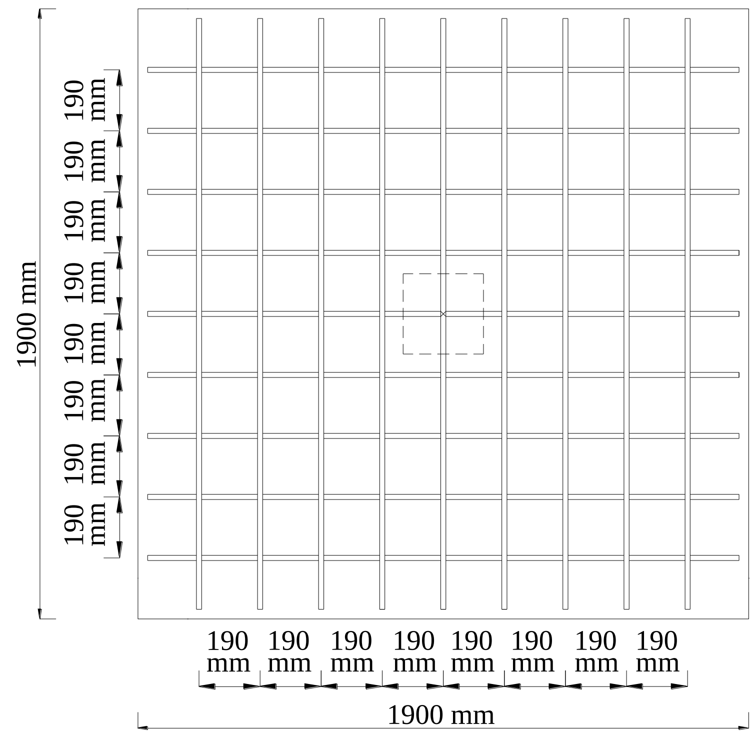

a. Top mat reinforcement 15M @ 190 mm

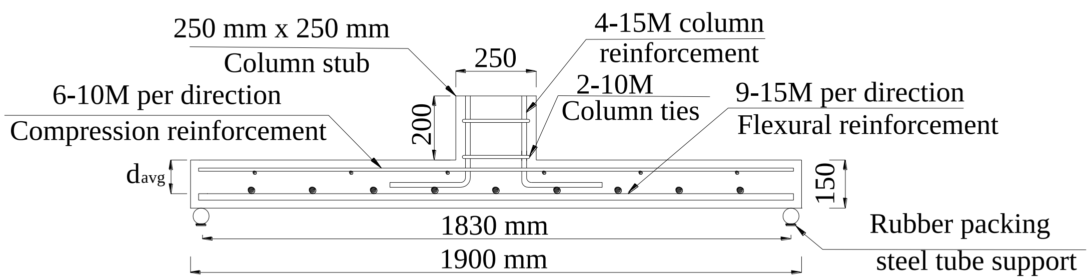

b. Cross-section for the slab

Figure 2-2 Details of a typical slab.

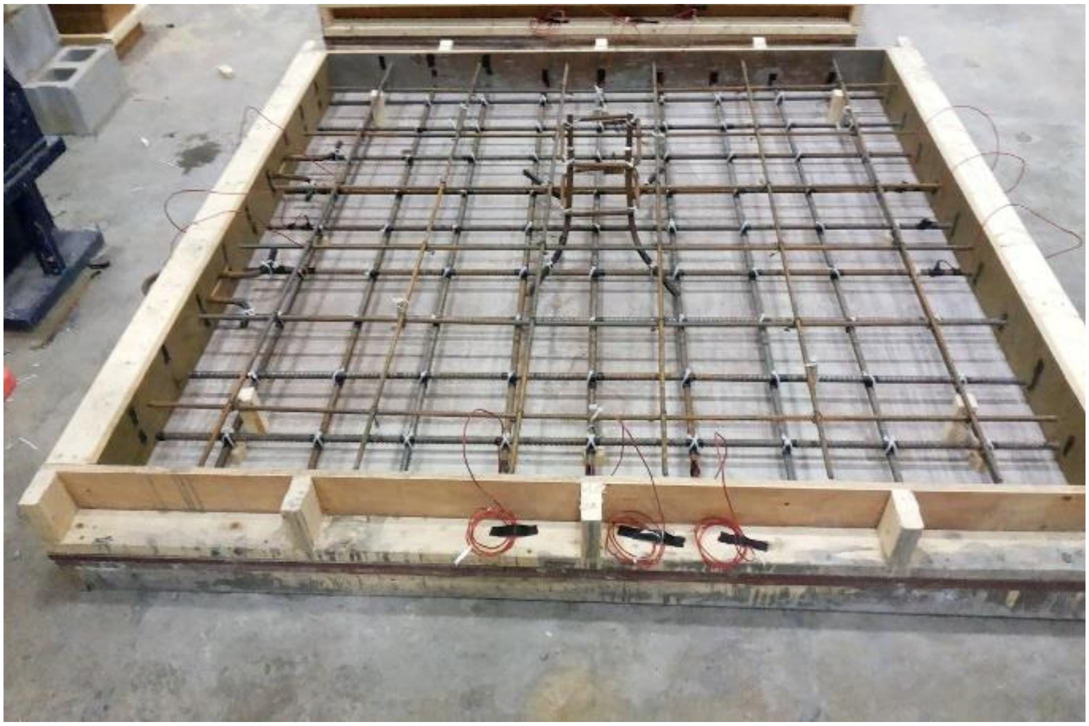

a.

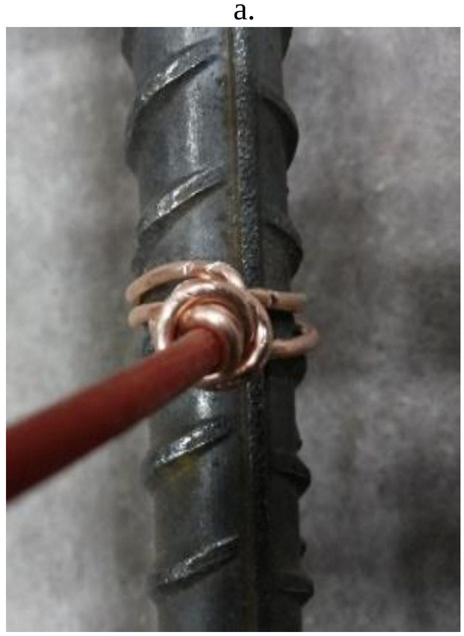

b.

Figure 2-3 Typical slab specimens: (a) reinforcement; (b) Wire-bar connection.

2.4.2. Material Properties

Table 2.3 shows the mixture composition of concrete used in casting the specimen. The targeted compressive strength and water to cement (w/c) ratio was chosen based on the recommendation of American Concrete Institute (ACI) specification regarding concrete horizontal elements exposed to de-icing salts which are classified as class F3 (ACI 318-14 2014). Therefore, the 28-days targeted concrete strength was chosen to be not less than 35 MPa and the w/c ratio was chosen to be not more than 0.4. Table 2.4 illustrates the material properties of the Grade 400 MPa for 15M bars used as flexural reinforcement. Table 2.4 also shows the compressive strength and modulus of rupture of the concrete.

Table 2-3 Mixture Composition of Concrete

cement (kg)	w/c	Water (l)	C/F	C.A. (kg)	F.A. (kg)	Aggregate size (mm)	Fresh density (kg/m3)
350	0.4	140	1.3	1083	833	10	2407

* w/c is the water to cement ratio, C/F is the coarse to fine ratio, C.A. is the coarse aggregate, and F.A. is the fine aggregate

Table 2-4 Steel and Concrete Properties

Designation	Steel properties			Concrete Properties	
	Area (mm^2)	f_y (MPa)	ε_y ($\mu\varepsilon$)	f'_c (MPa)	f_r (MPa)
15M	200	475	2200	41.1	3.82

* f_y is the yield strength, ε_y is the yield strain, f'_c is the compressive strength, and is f_r the modulus of rupture.

Before casting the slabs, the slump was measured, and prisms and cylinders were prepared. The concrete was poured in the prepared formwork and consolidated using an electrical vibrator. After a day of casting the slab, the column stub was cast. The curing process started after one day from casting the concrete by using water curing for four days and then was kept at room temperature until day 28 after casting.

2.4.3. Accelerated Corrosion Setup

The accelerated corrosion setup consisted of a source of direct current, steel mesh used as a cathode, and electrolyte solution (5% Sodium Chloride by weight of water). First, the slab was placed upside-down in a levelled position. A dike was constructed above the slab over the targeted corroded area using foam sheets. A hose with a valve was connected to the lower point of the dike to empty it from the electrolyte solution when needed. The steel mesh was placed in the dike and connected with the negative pole of the power source; hence, this mesh was considered as the cathode. The dike was then filled with the electrolyte solution. To ensure that the concentration of the sodium chloride in the electrolyte solution remained at the desired levels, the solution was changed every week. Concrete cylinders were used as weight above the steel mesh to avoid floating of it and to ensure full contact between the mesh and the concrete surface. A direct current was applied to the bars under the targeted corroded area, which served as anodes. The theoretical mass loss is calculated based on Faraday's equation as

$$\text{Mass loss} = \frac{t\,I\,M}{z\,F} \tag{2.1}$$

Where t is the time passed in seconds, I is the current passed in Amperes, M is atomic weight (for iron $M = 55.847$ g/mol), z is the ion charge (two moles of electrons), and F is Faraday's constant which is the amount of electrical charge in one mole of electron ($F = 96{,}487$ coulombs per mole (C/mol)) (Lachemi et al. 2014).

The current was applied to slab SV through the application of constant voltage and connected to slab SC through the application of constant current.

2.4.3.1. Constant Voltage Technique Setup

The setup for accelerated corrosion technique through the application of constant voltage consisted of a power supply, data acquisition systems, current transducers, electrical board, computer to process the data, electrolyte solution, and steel mesh. Figure 2.4 shows a schematic diagram for constant voltage accelerated corrosion setup.

The slab needed only one power supply with enough load capacity. The power supply was adjusted to produce constant voltage of 15 V. An electrical board was constructed and used to distribute the current from one power supply to several outlet terminals as shown in Fig. 2.4. The electrical board was prepared in a parallel circuit basis to keep the voltage constant across each outlet terminal of the board. The electrical board was connected to the positive terminal of the power supply, and then distributed the current to several outlet terminals. The outlets number was the same as the number of the corroded bars in slab SV. Each outlet terminal from the electrical board was connected to a bar that was required to be corroded. Thus, the output current from the power supply was equal to the summation of the current output from all outlets of the electrical board while keeping the voltage constant. The current passing through each corroded bar was monitored using a computer-controlled data acquisition system. A data acquisition system with enough channels equal to the number of the required corroded bars was used. The data acquisition system transferred the data of the current flow through the bar to a computer and the data was recorded using Lab View software. The data acquisition system used could read only voltage reading as most commercial ones. However, the current reading was the one needed to be recorded to calculate the expected theoretical mass loss based on Faraday's equation. Therefore, a current transducer board was built to convert the current to a voltage. Thereafter, the mass loss was calculated. Each transducer was calibrated manually, and a calibration equation was established for each one separately. This process insured more accuracy during the transformation process of the recorded voltage reading to the current reading. The current transducer board shown in Fig. 2.5(a) consisted of an excitation source of 5 A, current transducers sensors, and fuses. The board had current transducers sensors for each channel of the data acquisition system. Fuses used before each current transducer sensor to protect from any sudden increase in current during the corrosion test. Each sensor had inlet, outlet, and cable data. The inlet was connected to the fuse that was connected to one of the outlet terminals of the electrical board. The outlet was connected directly to the bar under corrosion process. The data cable was connected to the data acquisition system to read the voltage reading and record it on the computer as shown in Fig. 2.4. The data were recorded every four-second interval. Separate files were used every 48 hours the recorded data.

To summarize, the constant voltage accelerated corrosion technique started using 15 V. The negative terminal was connected directly to the steel mesh that served as a cathode. The steel mesh was immersed in the electrolyte solution inside a dike above the corroded targeted area. The positive terminal was connected to the electrical board that distributed the input current into several output terminals with the same constant volt. Each output terminal was connected to the current transducer board. The current transducer converted the current to voltage and sent the data to data acquisition system then to the computer. The outlet from each transducer in the current transducer board was connected to the bars under corrosion process.

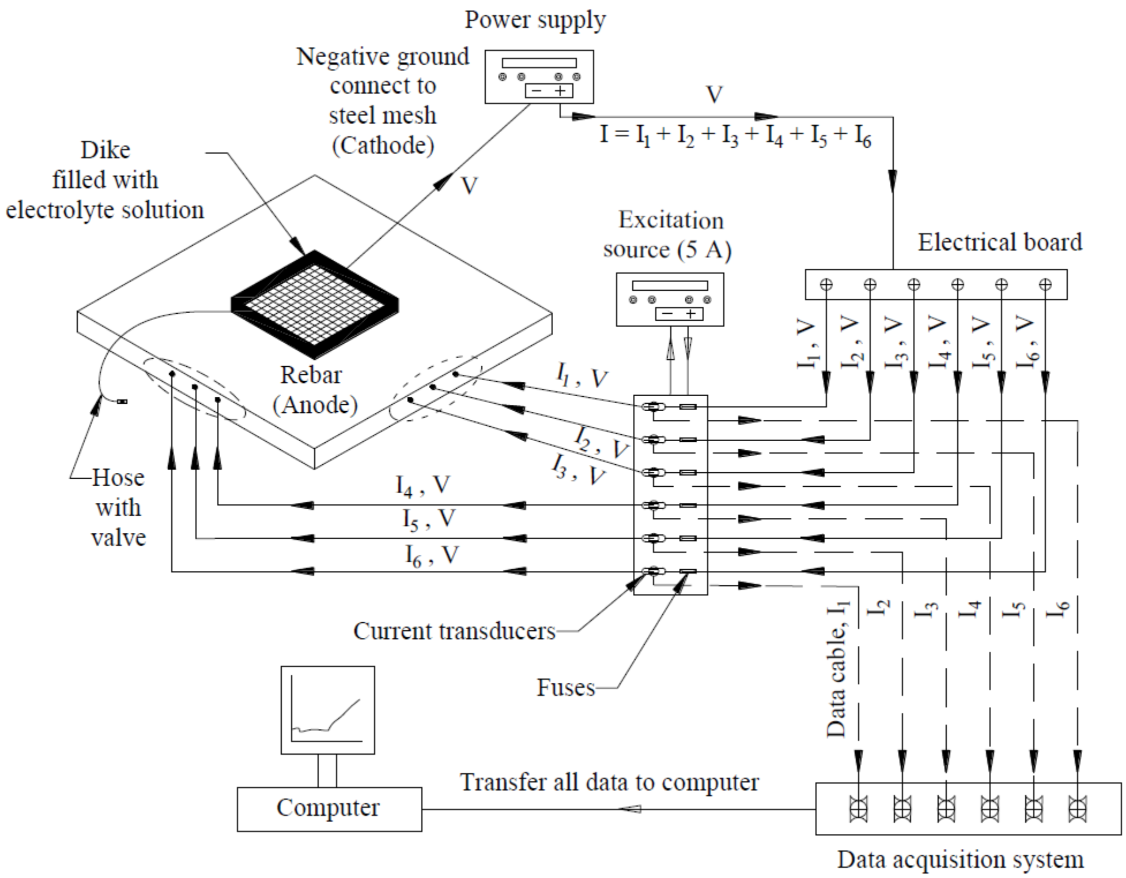

Figure 2-4 Schematic for Constant voltage accelerated corrosion setup.

2.4.3.2. Constant Current Technique Setup

The setup for the application of constant current consisted of power supplies, electrolyte solution, and steel mesh. The corroded slab needed multiple power supplies equal to the number of the corroded bars. Figure 2.6 shows a schematic diagram of the constant current setup. The power supply was adjusted to apply the constant current with a density of $200\mu A/cm^2$. The current density is the current in Amperes divided by the surface area of the corroded bar. This value was chosen according to the recommendations of El Maaddawy & Soudki (2003) not to exceed $200\mu A/cm^2$ to avoid any significant increase in crack width and strain response due to the induced corrosion. Hence, the power supply was

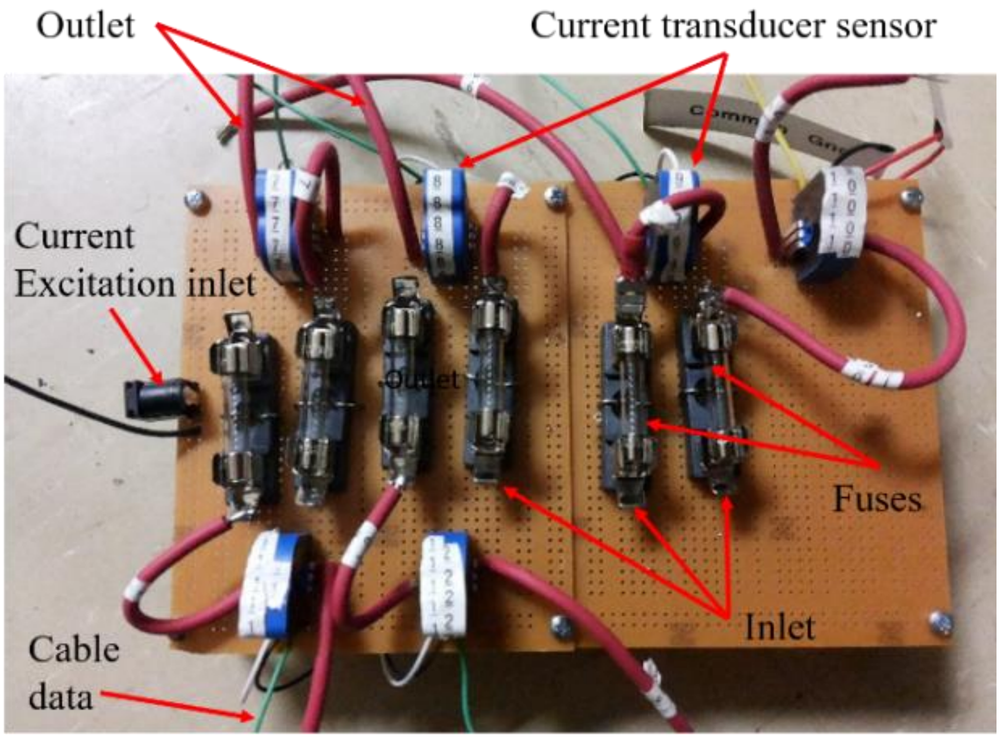

a. Current transducer board

b. Computer-controlled data acquisition system

Figure 2-5 Elements used for constant voltage accelerated corrosion setup.

adjusted to provide a constant current 0.1 A so that a current density of $200 \mu A/cm^2$ was used on each bar with a diameter of 16 mm and corroded length of 1060 mm. The counting of corroded time started after the half-cell potential read more than -350 mV. Thus, the occurrence probability of corrosion was more than 90% according to American Society for Testing and Materials (ASTM) (ASTM C876 2015). Figure 2.7 shows the elements used in the setup for constant current accelerated corrosion.

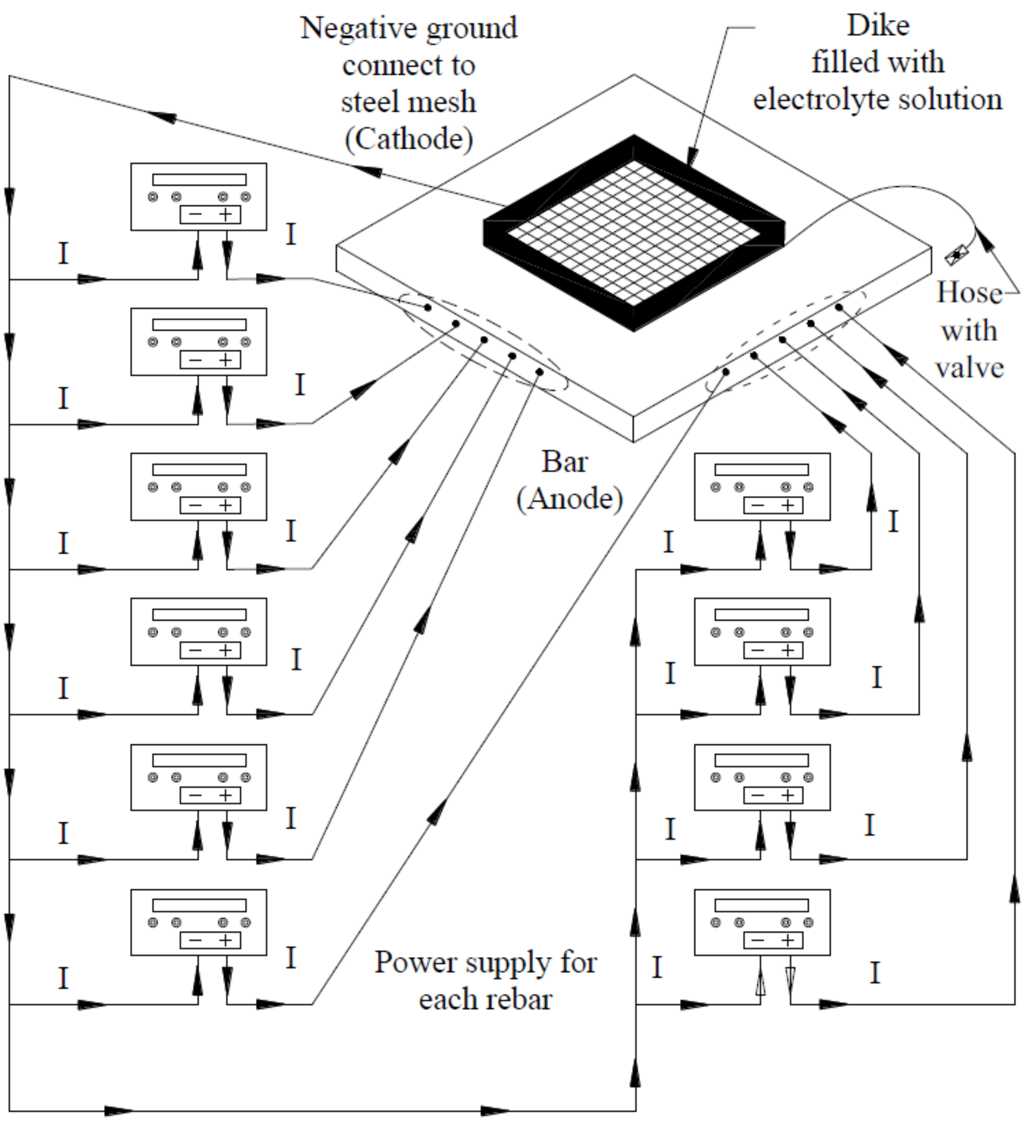

Figure 2-6 Schematic for Constant current accelerated corrosion setup.

Figure 2-7 Constant current accelerated corrosion.

2.4.4. Half-Cell Potential Measurements

ASTM C876-15 standard for half-cell potential technique is used to determine the corrosion activity of the uncoated reinforcement bars. This method measures the electrochemical potential of reinforcement embedded inside concrete against a reference that is placed on the concrete surface. Saturated wetted sponge with an agent (95 mL of liquid household detergent mixed with 19 L of potable water) was placed between the reference electrode (copper / copper - sulphate) and the concrete surface above the location of the embedded reinforcement. The sponge was left in its place at least for 5 min until the voltage reading become stable (±0.02 V). The half-cell potential readings are an indication of the occurrence probability of corrosion. More negative reading values indicate a higher probability of corrosion to occur while less negative or positive readings imply a lower one. All the readings were performed under controlled lab condition.

The readings of the half-cell potential in slab SV were recorded periodically every three days during the induced corrosion process. The readings were taken at twenty-four different points over the corroded area. The readings were recorded after stopping the accelerated test and evacuating the dike from the electrolyte solution and the steel mesh. The corrosion time to reach the targeted mass loss was calculated from the first day of the test. On the other hand, the half-cell potential readings in slab SC were measured at the beginning of the corrosion process until the average reading for all points was equal to -350 mV. After that, the corrosion time started to be counted. Thus, to ensure that the occurrence possibility of corrosion is more than 90% (ASTM C876 2015).

2.4.5. Natural Frequency Measurements

The natural frequency was measured for both slabs under free-free boundary condition. Free boundary condition was performed to avoid any misleading interpretation that could result from structural behaviour due to any kind of boundary conditions (Ahmed & Mohammad 2014). An experimental modal analysis was performed to measure the natural frequency for each slab. An excitation was induced in each slab by using an impact hammer that was attached to a load cell to transfer the magnitude of the force to a corresponding analog electrical signal. Three accelerometers sensors were attached to the slab, two sensors were attached to the far corner of the slab and the third sensor attached to the centre as shown in Fig. 2.8. The accelerometers' data was processed using a computer software (Modal-View) to obtain the natural frequency value for the slab.

2.4.6. Measurement of Chloride Content

The corrosion state was examined through determining the chloride ion content near the bar surface. After the corrosion level was reached, several concrete powder samples were taken directly from the contact surface between corroded reinforcement and the concrete cover using an electric drill. Each concrete powder sample weighted 3 gm and was dissolved in 20 ml chloride extraction liquid inside a small plastic vial. The liquid used had a concentration of acid that was precisely measured. The powder was added slowly inside the extraction liquid vial to avoid any excessive fizzing or interlocking of powder particles. Before drilling to extract the powder, the concrete samples were left until they become completely dry. This was carried out in order to avoid collecting wet dust and to ensure that the weight of water was not included in the calculation. Each sample was left overnight inside the vial before testing. An electrochemical reaction occurred between the chloride ions in the powder sample and the acid in the extracted liquid. The electrochemical reaction was measured using an electrode with an integral temperature sensor. This electrode was calibrated before the test by using five standard samples containing chloride ranging from 0.005% to 0.5% by weight.

2.4.7. Measurement of Mass Loss

After the corrosion process was completed, the concrete cover was removed using a demolition hammer. Then, the flexural corroded bars were extracted from the slab. The corrosion damage products on the bars were removed using a wire brush, then the bars were soaked in an HCl solution according to ASTM G1 2003 standards. After that, the bars were lightly brushed to remove the loose corrosion products. Thereafter, the cleaned bars were weighted using a sensitive scale and compared with their original weight before the corrosion process. All bars were weighted and labelled before casting and pouring the concrete. The percentage mass loss for each bar was calculated as:

$$\%\ \text{mass loss} = \frac{(\text{initial weight-final weight})}{\text{initial weight}} \qquad 2.2$$

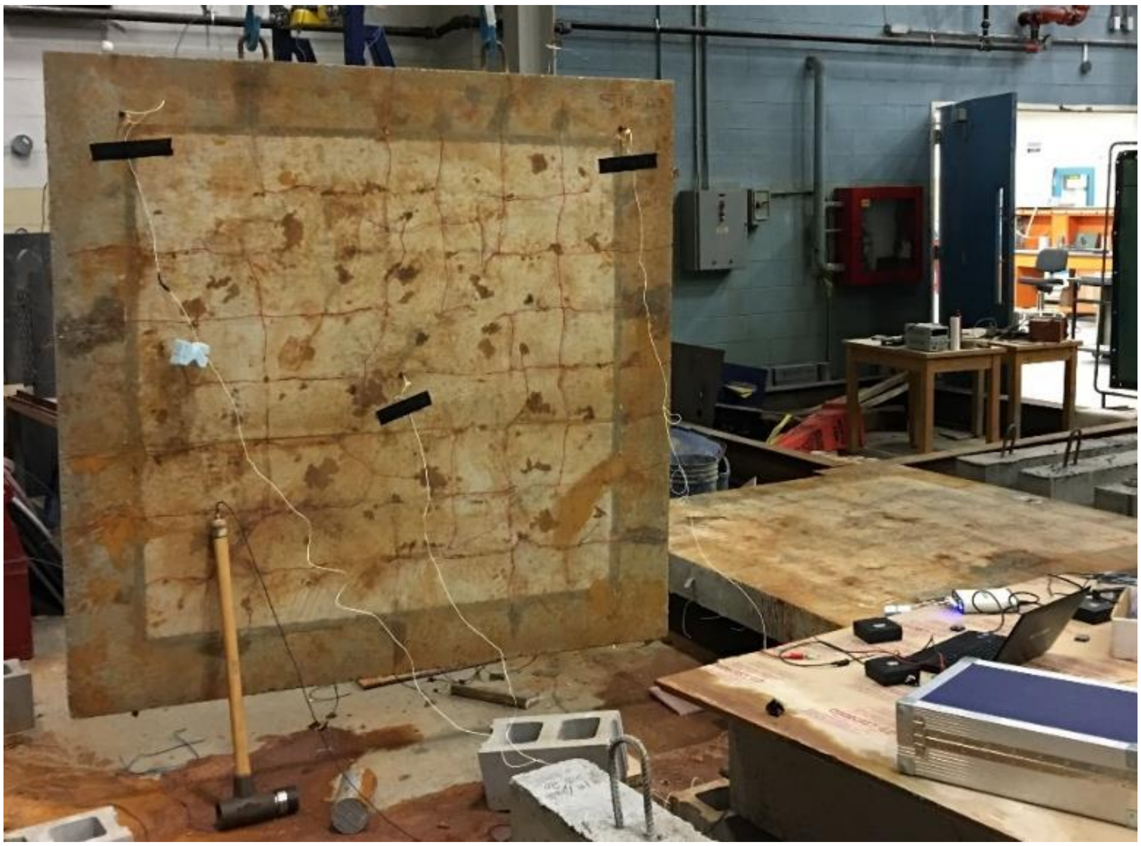

Figure 2-8 Accelerometers location for natural frequency measurement.

2.5. Experimental Results and Analysis

2.5.1. Time-dependent Corrosion Tests Results

2.5.1.1. Current Results

Slab SC was corroded under constant current accelerated technique. The current intensity applied was $200\,\mu A/cm^2$ for the 16 mm bars with corroded length equal to 1060 mm and the current applied was 0.1 A. This current was constant all over the period of the corrosion process that was 146 days. The time was counted after the half-cell potential read more than -350 mV in most of the targeted area. One of the main benefits of this technique is the ability to determine how long the corrosion test would take to reach the targeted corrosion level. On the other hand, Slab SV was corroded under constant voltage of 15 V. The current fluctuated all over the period of the corrosion test. The current was monitored and recorded using a computer-controlled data acquisition system. Corrosion was induced in six bars in slab SV. The current in each bar was separately recorded. Three bars were positioned at the upper layer near the concrete cover and the other three were placed in the lower layer that was farther from concrete cover. Figure 2.9 shows the relation between the current and the immersion time for each corroded bar. It was noticed that the current in all bars initially dropped followed by slight increase then gradually increased till the targeted level of corrosion 25% of mass loss was reached. The drop in the current at the initiation process of corrosion could be attributed to the presence of the passive film layer around each bar that protected it against corrosion. When the current weakened this layer due to chloride ingress, the corrosion started and its rate increased progressively. The sudden jump in the current could be ascribed to the bond loss between the corroded bar and the concrete cover in which spalling of concrete covers started to occur.

Figure 2.10 shows the mass loss rate versus time for each corroded bar. It can be seen that the mass loss rate increased with increasing the current rate, which is associated with an increase in the rate of corrosion. Each bar had its time period to reach its targeted level of corrosion. This time could not be determined because Faraday's equation depends on current, where the current rate changed all over the duration of the experiment. Table 2.5

shows the corrosion duration for each bar and the maximum current that bar reached at the end of the corrosion process. The current intensity was calculated based on 16 mm bar that was corroded over a length of 700 mm. The current intensity at the end of corrosion process for all bars was found to be more than $200 \mu A/cm^2$, which exceeded the recommended values by El Maaddawy & Soudki (2003). This would cause a significant increase in crack width and strain response due to the corrosion.

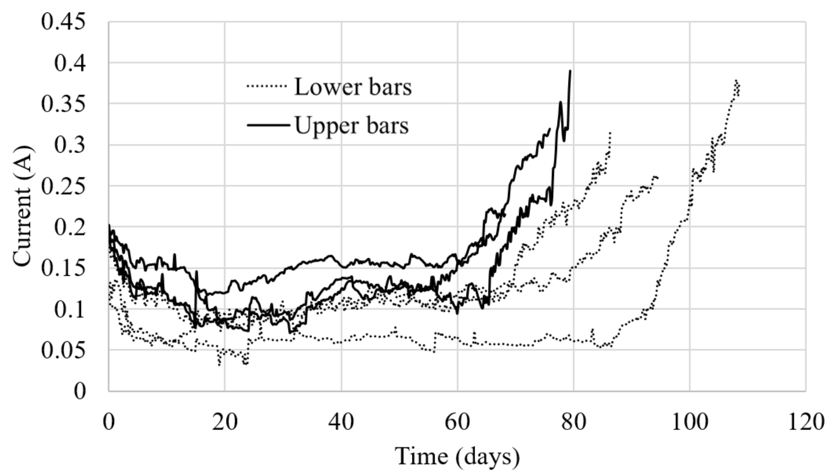

Figure 2-9 Current time history for SV specimen.

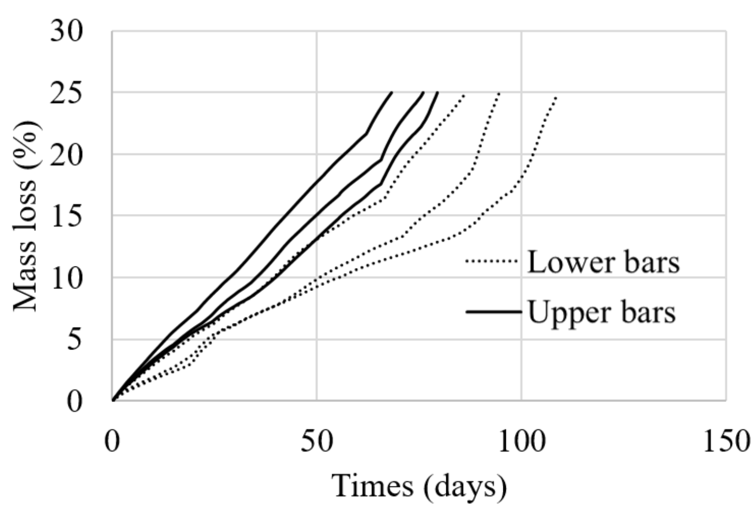

Figure 2-10 Mass loss rate with time.

Table 2-5 Details of Constant Voltage Technique

bar #	Corrosion period (Days)	Current (A)	Current intensity ($\mu A/cm^2$)
1 (Lower layer)	109	0.37	1051.6
2 (Lower layer)	95	0.27	767.4
3 (Lower layer)	87	0.32	909.5
4 (Upper layer)	80	0.39	1108.4
5 (Upper layer)	76	0.31	881.0
6 (Upper layer)	69	0.22	625.3

2.5.1.2. Half-Cell Potential Measurements

The half-cell potential was used only in slab SC to specify the starting time that could be used to calculate the duration required to achieve the targeted level of corrosion based on Faraday's equation. When the half-cell potential readings at most corroded points read more than -350 mV, the corrosion time started to be counted. The half-cell was used to evaluate the corrosion performance of slab SV during the test. When the reading of half-cell potential gave more negative values, it was an indication of the higher probability of corrosion. Table 6 shows the average half-cell reading and the corresponding mass loss at 3, 9, 36, and 75 days. Figure 2.11 shows the reading variation of the average half-cell reading with time over the corroded area. The potential reading was measured above each corroded bar of the reinforcement mesh in both directions. Figure 2.12 shows the reading variation of the average half-cell reading versus the average level of corrosion for all corroded bars. It is clear from the table and both figures that the corroded bars in the upper layer of the mesh had more negative values than the lower layer. This could be attributed to the clear concrete cover that was 30 mm for the upper layer while it was 46 mm for the lower layer. Hence, the upper layer was exposed to more chlorides ingress than the lower one. This result was observed in previous studies that the concrete cover has a significant effect on the readings of the half-cell potential values for in-situ tests (Klinghoffer 1995). Both figures also show that there was no variation in the reading of the half-cell when the corrosion started. Therefore, this test was used only as an indication of the occurrence probability of corrosion for un-corroded members.

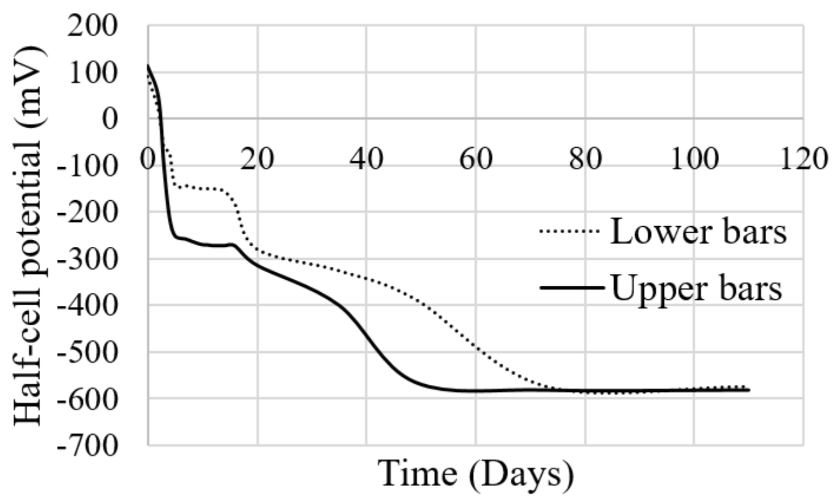

Figure 2-11 Half-cell potential values vs. time for slab SV.

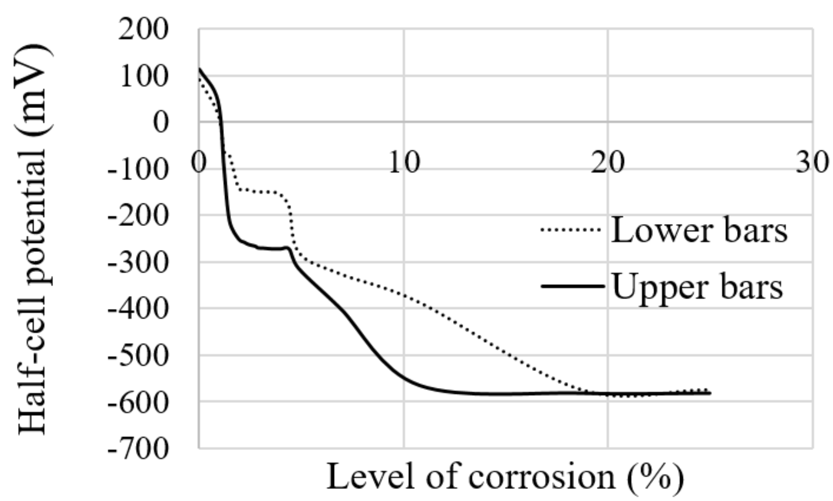

Figure 2-12 Half-cell potential values vs. corrosion level for slab SV.

2.5.2. Test Results after Corrosion

2.5.2.1. Crack Pattern Behaviour

Figure 2.13 shows the crack pattern for both slabs SV and SC. It was noticed that all cracks in slab SC appeared above the corroded bars. SC had ten corroded bars, each bar created a longitudinal crack above it due to the presence of the corrosive products. The stars in Fig. 2.13 represent the cracks, and the total number of stars represent the total number of induced cracks. The crack intensity was equal to one, which was calculated as the number of cracks over the total number of corroded bars. On the other hand, Slab SV had random crack pattern. Moreover, the crack intensity was equal to 1.83, where Slab SV had six corroded bars only. It can be concluded from the cracks pattern that the constant voltage technique did not provide a realistic crack behaviour that was expected in a real corroded slab. As noticed from Fig. 2.1, the cracks in a real slab develop parallel to the corroded bars. This could be attributed to the fluctuation in the current value that occurred in constant voltage when the cracks occurred. These fluctuations happened because cracks facilitate the flow of current between the anode and the cathode, which cause current to reach extreme values leading to extreme damage. Therefore, a constant current is preferred to be used to provide better representation for the crack pattern.

2.5.2.2. Natural Frequency Measurements

The natural frequency for the un-corroded slab was found to be 134 Hz which was in close agreement with the analytical value that was calculated by Ahmed & Mohammad (2014). The natural frequency for slabs SV and SC was 64Hz and 35 Hz, respectively. The difference between both natural frequencies could be attributed to the difference in the corroded area, which means that the accumulation of the corrosive products under slab SC was more than that on slab SV. The corrosive products caused a damping to the excited vibration that was reflected on reducing the natural frequency. More extensive studies are needed to further investigate the response of corroded two-way slabs with different corrosion levels and to enhance the reliability of measuring the natural frequency.

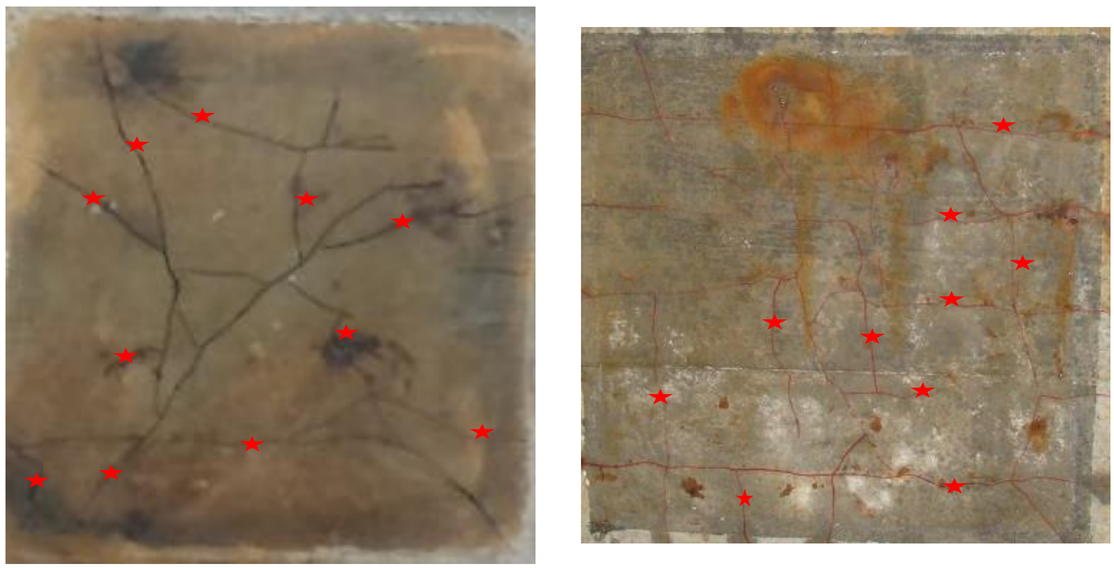

SV SC

Figure 2-13 Crack pattern for the corroded slabs.

2.5.2.3. Chloride content

Different samples were extracted from each slab at eight locations and two different depths to determine the chloride content. The samples were extracted from one quarter of the targeted corroded area to obtain the chloride content. Four samples where extracted directly from the contact surface between the upper layer and the concrete cover at a depth of 30 mm. The other four samples were extracted at a depth of 46 mm at the contact surface between the lower layer and the concrete cover. Figure 2.14 shows the chloride content that was determined for both upper and lower layers of each slab. In general, the chloride ion content near the bar surface at all the locations on both slabs showed a close agreement

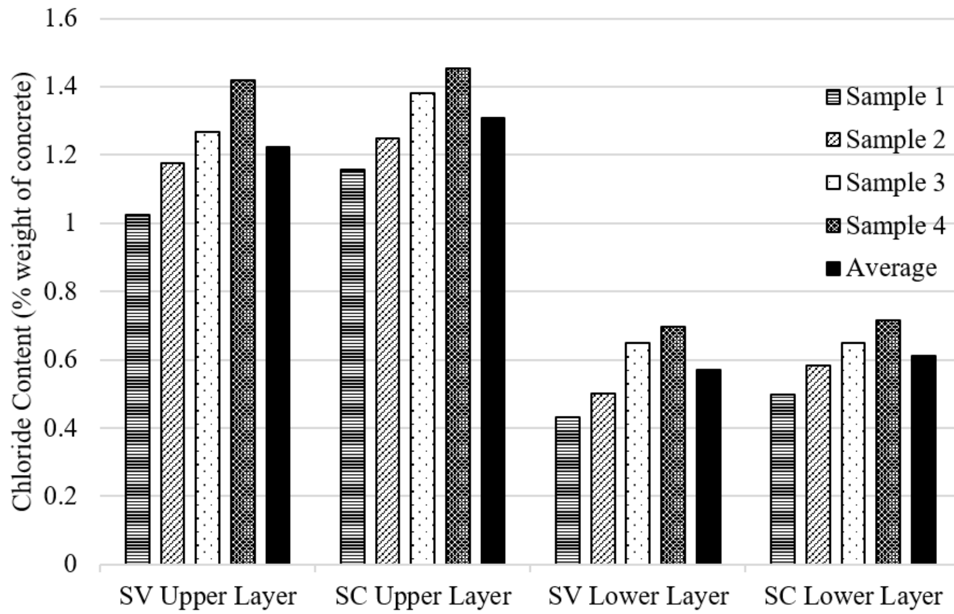

Figure 2-14 Chloride content % above upper and lower steel mesh layer for each slab.

with each other. The average chloride content for the four randomly selected points above the upper reinforcement layer of slab SV was 1.22 and 1.31 for slab SC; there was only 7% difference between both techniques. In addition, the average chloride content for the other four points near the lower layer for slabs SV and SC was 0.570 and 0.611, respectively. The difference in the lower layer values for both techniques was 7%. The results confirmed that both techniques approximately reached the same level of chloride ions content for the same level of corrosion. The increase in the average chloride content in slab SC could be attributed to the large duration of the corrosion process of that specimen as slab SC was corroded for 37 days more than slab SV. The average chloride content for the upper layer of the reinforcement mesh was higher than that of the lower layer. This could be attributed to the thickness of the concrete cover above each layer, where the chloride content decrease with increasing the concrete cover. This reason also explains why the difference in chloride content between both slabs for lower layer was less than the upper layer.

2.5.2.4. Mass Loss

Figure 2.15 shows the corroded reinforcement for both slabs after removing the concrete cover. Faraday's Equation was used to calculate the theoretical mass loss in both slabs SV and SC. After reaching the targeted corrosion level in each slab, the current was stopped and hence its flow across the corroded bar was ended. After conducting the test, the concrete cover was removed to extract the corroded bars. The bars were then weighed after cleaning all attached corrosive products in accordance with ASTM G1-03 (2003).

a. Slab SV

b. Slab SC

Figure 2-15 Corroded bars after demolition process.

Figure 2.16 shows the actual mass loss for each corroded bar in both slabs and Fig. 2.17 shows the error between the actual mass loss and the theoretical values. Both slabs had actual mass loss in close agreement with the theoretical mass loss. The maximum mass loss error in slab SV was 4.27% while in slab SC it was 4.41%; which was a small error between each other. The average error in mass loss was 2.44% and 2.65% for SV and SC, respectively. The small discrepancy in slab SC was attributed to the corroded length which was longer than that in slab SV. Both accelerated corrosion techniques had actual mass loss less than the theoretical ones. This was observed by several researchers (Spainhour & Wootton 2008; YuBun Auyeung et al. 2000). This mean that some other process rather than the ionization of iron could have taken place. A kind of this process could be the decomposing that happens to the water due to passing the current through it. The current causing oxidation-reduction reactions which releases oxygen ions as a results of this reaction. During the acceleration process, bubbles were observed during the acceleration process and the previous reason could explain that bubbles (Chen & Luckham 1994). on concrete beams. Faraday's equation depends on the amount of the current passing through a bar suspended in salt solution regardless the voltage value. Eventually, Faraday's equation provides a good prediction of the mass loss regardless of the accelerated corrosion technique used. In order to isolate the upper bars from the lower ones and to avoid any

conductivity between them, electric tape was used as insulation at those locations. This precaution was necessary and unavoidable, but it had some effects on the corrosion profile of the bars. At the intersection points, the tape prevented the occurrence of corrosion at the intersection points. Therefore, the corrosion was mostly uniform except at those locations.

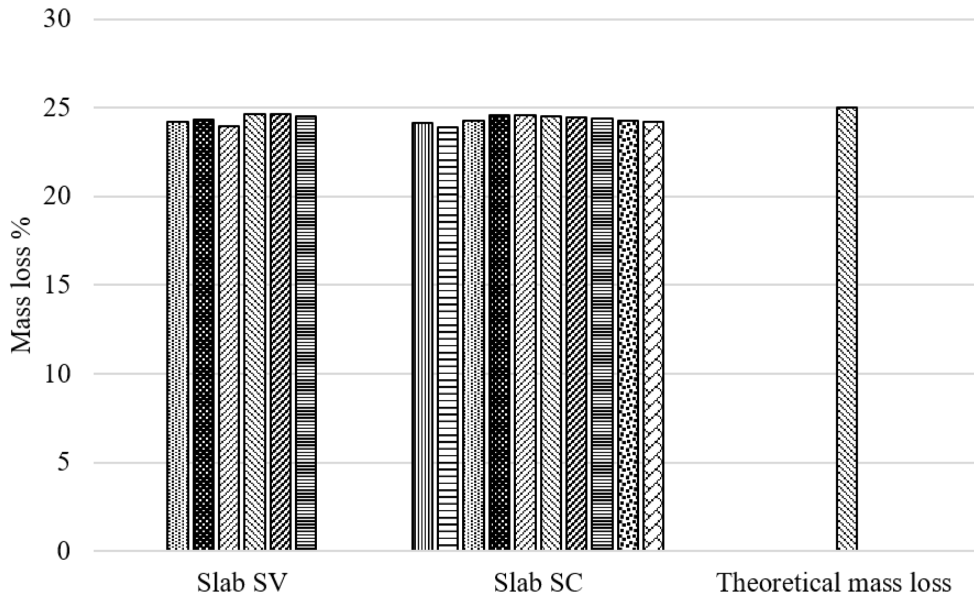

Figure 2-16 Mass loss % for all corroded bars in each slab.

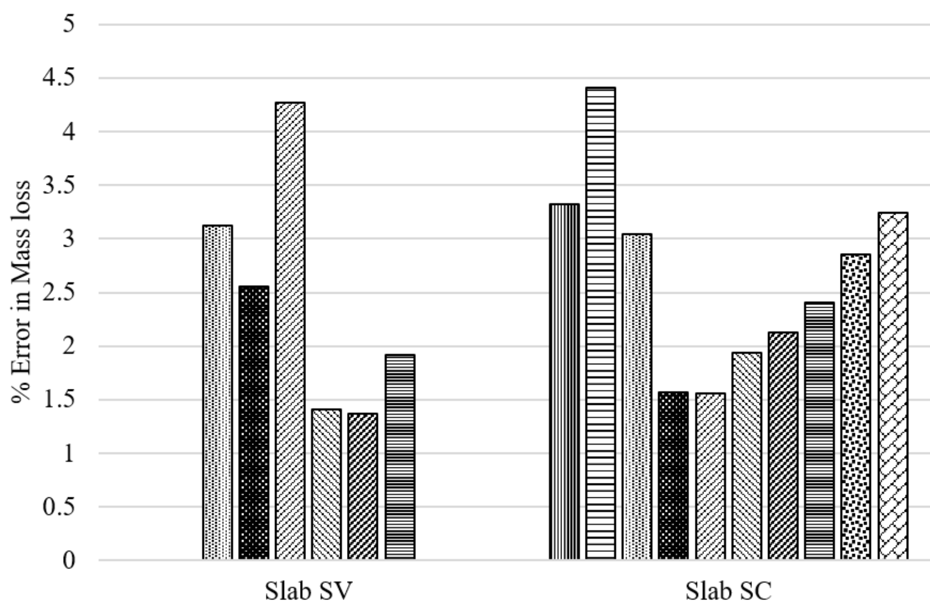

Figure 2-17 The error in mass loss % for all corroded bars in each slab.

2.6. Conclusion

Two different accelerated techniques were used to corrode the reinforcement of two RC two-way slabs. The purpose of this study was to determine the most suitable technique to simulate a real corrosion process. Based on the performance of each corroded technique, the following conclusions were reached.

- Both techniques show a close agreement between the actual mass loss and the theoretical one. Subsequently, Faraday's equation could be used to estimate the actual mass loss regardless of the accelerated corrosion technique. For all corroded bars, it was found that the theoretical mass loss overestimated the actual mass loss. Hence, the theoretical mass loss estimation could be used to determine the effect of corrosion over time using both constant current and constant voltage accelerated corrosion techniques.
- The amount of raw data that needed to be processed in constant voltage technique, to calculate the theoretical mass loss, is large compared with a constant current. This requires more time and effort to track the theoretical mass loss daily to determine the exact time to stop the test.
- Regarding time limits and management, the constant current technique is better. Faraday's equation that is used to predict the expected mass loss and how much time is needed to reach the targeted level of corrosion depends on the amount of current that pass through the bars. In the constant current technique, the current is always known and constant; therefore, the time can be exactly determined. On the other hand, the current varies during the constant voltage technique experiment,

therefore; it cannot be used to calculate how long the test should proceed to reach the targeted corroded level.

- The setup cost of the constant voltage accelerated corrosion technique is high compared to that of constant current. More number of components is required to set up constant voltage technique. The components that are required to provide constant voltage are one high load power supply, current transducers sensors, data acquisition system with several channels, and a computer unit. The number of current transducers and free channels in data acquisition system must be equal to the number of corroded bars. Therefore, when the corroded area increase, the number of bars increase which will lead to higher cost of conducting the experiment. On the other hand, the only component that is required to provide the constant current is the power supplies which should be equal to the number of corroded bars. In the constant current, the power supplies do not need to provide high load because the current intensity not exceed $200\,\mu A/cm^2$.
- The resistivity of concrete increases with time. Therefore, using constant voltage 15 V need time to overcome the concrete resistivity and to successfully pass a current through the cover to reach the steel bars. Whereas in constant current technique, the resistivity does not play an important role because increasing the voltage can overcome the concrete resistivity. Thus, in constant voltage, the induced corrosion should start earlier to avoid increasing the resistivity.
- There is no limitation on the maximum current intensity in constant voltage technique. Therefore, when cracks occur while keeping the voltage constant, the

current flow is facilitated from anode to cathode. Thus, the current intensity increases and could exceed the limitation of 200 μA/cm^2 according to the recommendation of El Maaddawy & Soudki (2003). Therefore, the constant voltage could cause more damage than real corrosion and may not realistically simulate the performance of the corroded element.

According to these observations, the authors believe that using constant current for two-way slabs induced corrosion tests is better with regard to cost and time. Moreover, for severe levels of corrosion, constant current could be more appropriate to simulate the performance of real corrosion compared to a constant voltage.

2.7. References

ACI 318 (2014) Building code requirement for structural concrete (ACI 318M-14) and commentary (ACI 318RM-14), Building Code Requirements for Structural Concrete.

Ahmed, M. S. and Mohammad, F. A. (2014) 'Theoretical modal analysis of freely and simply supported RC slabs', International Journal of Mechanical, Aerospace, Industrial, Mechatronic and Manufacturing Engineering, 8(12), pp. 2026–2030.

Ahwazi, B. B. N. (2001) A comparative study of deterioration of bond due to corrosion in different concretes. McGill University.

Al-Swaidani, A. M. and Aliyan, S. D. (2015) 'Effect of adding scoria as cement replacement on durability-related properties', International Journal of Concrete Structures and Materials. Korea Concrete Institute, 9(2), pp. 241–254. doi: 10.1007/s40069-015-0101-z.

Almusallam, A., Al-Gahtani, A. S., Aziz, A. R. and Rasheeduzzafar, A. (1996) 'Effects of reinforcement corrosion on bond strength', Construction and Building Materials, 10(2), pp. 123–129.

Altoubat, S., Maalej, M. and Shaikh, F. U. A. (2016) 'Laboratory simulation of corrosion damage in reinforced concrete', International Journal of Concrete Structures and Materials. Korea Concrete Institute, 10(3), pp. 383–391. doi: 10.1007/s40069-016-0138-7.

Amleh, L. (2000) Bond deterioration of reinforcing steel in concrete due to corrosion. McGill University.

Aoude, H., Cook, W. D. and Mitchell, D. (2014) 'Effects of simulated corrosion and delamination on response of two-way slabs', Journal of structural Engineering, 140(1), pp. 1–9. doi: 10.1061/(ASCE)ST.1943-541X.0000775.

ASTM C876 (2015) 'Standard test method for corrosion potentials of uncoated reinforcing steel in concrete', p. 8. doi: 10.1520/C0876-09.2.

ASTM G1 (2003) Standard practice for preparing, cleaning, and evaluation corrosion test specimens.

Auyeung, Y., Balaguru, P. and Chung, L. (2000) 'Bond behavior of corroded reinforcement bars', Materials Journal, 97(2), pp. 214–220.

Azad, A. K., Ahmad, S. and Azher, S. a (2007) 'Residual strength of corrosion-damaged reinforced concrete beams', ACI Materials Journal, 104(1), pp. 40–47.

Azam, R. (2010) Behaviour of shear critical RC beams with corroded longitudinal steel reinforcement. Waterloo.

Ballim, Y. and Reid, J. C. (2003) ‘Reinforcement corrosion and the deflection of RC beams - An experimental critique of current test methods’, Cement and Concrete Composites, 25(6), pp. 625–632. doi: 10.1016/S0958-9465(02)00076-8.

Ballim, Y., Reid, J. C. and Kemp, A. R. (2001) ‘Deflection of RC beams under simultaneous load and steel corrosion’, Magazine of Concrete Research. Thomas Telford, 53(3), pp. 171–181.

Bonacci, J., Thomas, M., Hearn, N., Lee, C. and Maalej, M. (1998) ‘Laboratory simulation of corrosion in reinforced concrete and repair with CFRP wraps’, in Annual Conference of the Canadian Society of Civil Engineering, pp. 653–662.

Castel, A., Franfois, R., Arliguie, G. and Mat, L. (2000) ‘Mechanical behaviour of corroded reinforced concrete beams - part 2 : bond and notch effects’, Materials and Structures, 33(9), pp. 545–551.

Chen, T. Y. and Luckham, P. F. (1994) ‘A study of the electrical current passing through water-activated electro-rheological fluids’, Jpournal pf Physics D: Applied Physics, 27(7), p. 1556.

Davis, J. (2000) Corrosion: understanding the basics. doi: 10.1361/cutb2000p001.

Deb, S. and Pradhan, B. (2013) ‘A study on corrosion performance of steel in concrete under accelerated condition’, in Proceedings of the International Conference on Structural

Engineering Construction and Management, Kandy, Sri Lanka. Available at: http://dl.lib.mrt.ac.lk/handle/123/9365.

El_Maaddawy, T., Soudki, K. and Topper, T. (2005) ‘Long-term performance of corrosion-damaged reinforced concrete beams’, ACI Stractural Journal, 102(5), pp. 649–656.

El-Maaddawy, T. and Soudki, K. (2003) ‘Effectiveness of impressed current technique to simulate corrosion of steel reinforcement in concrete’, Journal of Materials in Civil Engineering. American Society of Civil Engineers, 15(1), pp. 41–47. doi: 10.1061/(ASCE)0899-1561(2003)15:1(41).

El-Maaddawy, T., Soudki, K. and Topper, T. (2005) ‘Analytical model to predict nonlinear flexural behavior of corroded reinforced concrete beams’, ACI Structural Journal, 102(4), pp. 550–559.

Gerhardus H. Koch, M. P. H. B. (2002) Corrosion costs and preventive strategies in the United States, Nace International.

Imam, A. and Azad, A. K. (2016) ‘Prediction of residual shear strength of corroded reinforced concrete beams’, International Journal of Advanced Structural Engineering. Springer Berlin Heidelberg, (8), pp. 307–318. doi: 10.1016/j.engstruct.2016.04.018.

Juarez, C. a., Guevara, B., Fajardo, G. and Castro-Borges, P. (2011) ‘Ultimate and nominal shear strength in reinforced concrete beams deteriorated by corrosion’, Engineering Structures. Elsevier Ltd, 33(12), pp. 3189–3196. doi: 10.1016/j.engstruct.2011.08.014.

Kashani, M. M., Crewe, A. J. and Alexander, N. A. (2013) 'Nonlinear stress-strain behaviour of corrosion-damaged reinforcing bars including inelastic buckling', Engineering Structures, 48, pp. 417–429. doi: 10.1016/j.engstruct.2012.09.034.

Klinghoffer, O. (1995) 'In situ monitoring of reinforcement corrosion by means of electrochemical methods', Nordic Concrete Research, 95(1), pp. 1–13. Available at: http://www.germann.org/Publications/GalvaPulse/2. Klinghofer, O., In Situ Monitoring of Reinforcement Corrosion by means of Electrochemical Methods, Nordic Concrete Research 95 1.pdf.

Konecný, P. (2007) Reliability of reinforced Concrete bridge decks with respect To ingress of chlorides, Department of Structural Mechanics\Faculty of Civil Engineering\ University of Ostrava. doi: 10.13140/RG.2.1.3729.4165.

Kumar, M. K., Rao, P. S., Swamy, B. L. P. and Chandra Mouli, C. (2012) 'Corrosion resistance performance of fly ash blended cement concrete', Internatioanl Journal of Research in Engineering and Technologi, 1(3), pp. 448–454. doi: 10.1016/0140-6701(95)93047-7.

Lachemi, M., Al-Bayati, N., Sahmaran, M. and Anil, O. (2014) 'The effect of corrosion on shear behavior of reinforced self-consolidating concrete beams', Engineering Structures. Elsevier Ltd, 79, pp. 1–12. doi: 10.1016/j.engstruct.2014.07.044.

Lee, C., Bonacci, J. F., Thomas, M. D. a., Maalej, M., Khajehpour, S., Hearn, N., Pantazopoulou, S. and Sheikh, S. (2000) 'Accelerated corrosion and repair of reinforced concrete columns using carbon fibre reinforced polymer sheets', Canadian Journal of Civil Engineering, 27(5), pp. 941–948. doi: 10.1139/cjce-27-5-941.

Litvan, G. G. (1982) 'Evaluation and repair of deteriorated garage floors', Canadian Building Digest, Division of Building Research, p. 4.

Mangat, P. S. and Elgarf, M. S. (1999) 'Flexural strength of concrete beams with corroding reinforcement', ACI Structural Journal, 96(1), pp. 149–158.

Neville, A. M. (2011) Properties of concrete (Fifth Edition), Cement and Concrete Research. doi: 10.1016/0008-8846(96)82366-0.

Pellegrini-Cervantes, M. J., Almeraya-Calderon, F., Borunda-Terrazas, A., Bautista-Margulis, R. G., Chacón-Nava, J. G., Fajardo-San-Miguel, G., Almaral-Sanchez, J. L., Barrios-Durstewitz, C. P. and Martinez-Villafañe, A. (2013) 'Corrosion resistance, porosity and strength of blended portland cement mortar containing rice husk ash and nano-SiO2', International Journal of Electrochemical Science, 8(8), pp. 10697–10710.

Pritzl, M. D., Tabatabai, H. and Ghorbanpoor, A. (2014) 'Laboratory evaluation of select methods of corrosion prevention in reinforced concrete bridges', International Journal of Concrete Structures and Materials, 8(3), pp. 201–212. doi: 10.1007/s40069-014-0074-3.

Reilly, J. L., Cook, W. D., Bastien, J. and Mitchell, D. (2014) 'Effects of delamination on the performance of two-way reinforced concrete slabs', Journal of Performance of Constructed Facilities, 28(4), pp. 1–8. doi: 10.1061/(ASCE)CF.

Rodriguez, D. J., Ortega, L. and Casal, J. (1997) ‘Load carrying capacity of concrete structures with corroded reinforcement’, Construction and Building Materials, 11(4), pp. 239–248.

Sahmaran, M., Anil, O., Lachemi, M., Yildirim, G., Ashour, A. F. and Acar, F. (2015) ‘Effect of corrosion on shear behavior of reinforced engineered cementitious composite beams’, ACI Structural Journal, 112(6), pp. 771–782. doi: 10.14359/51687749.

Spainhour, L. K. and Wootton, I. A. (2008) ‘Corrosion process and abatement in reinforced concrete wrapped by fiber reinforced polymer’, Cement and Concrete Composites. Elsevier, 30(6), pp. 535–543.

Talakokula, V., Bhalla, S. and Gupta, A. (2014) ‘Corrosion assessment of reinforced concrete structures based on equivalent structural parameters using electro-mechanical impedance technique’, Journal of Intelligent Material Systems and Structures, 0(0), pp. 1–16. doi: 10.1177/1045389X13498317.

Toongoenthong, K. and Maekawa, K. (2004) ‘Interaction of pre-induced damages along main reinforcement and diagonal shear in RC members’, Journal of Advanced Concrete Technology, 2(3), pp. 431–443. doi: 10.3151/jact.2.431.

Torres-Acosta, A. a., Navarro-Gutierrez, S. and Terán-Guillén, J. (2007) ‘Residual flexure capacity of corroded reinforced concrete beams’, Engineering Structures, 29(6), pp. 1145–1152. doi: 10.1016/j.engstruct.2006.07.018.

Wang, L., Zhang, X., Zhang, J., Ma, Y. and Liu, Y. (2015) 'Effects of stirrup and inclined bar corrosion on shear behavior of RC beams', Construction and Building Materials. Elsevier Ltd, 98, pp. 537–546. doi: 10.1016/j.conbuildmat.2015.07.077.

Wei-liang, J. and Yu-xi, Z. (2001) 'Effect of corrosion on bond behavior and bending strength of reinforced concrete beams', Journal of Zhejiang University-Science, (3), pp. 298–308. doi: 10.1007/BF02839464.

Xia, J., Jin, W.-L. and Li, L.-Y. (2012) 'Effect of chloride-induced reinforcing steel corrosion on the flexural strength of reinforced concrete beams', Magazine of Concrete Research. Thomas Telford, 64(6), pp. 471–485.

Yoon, S., Wang, K., Weiss, W. and Shah, S. (2001) 'Interaction of reinforced between loading, corrosion, and serviceability of reinforced concrete', ACI Materials Journal, 97(6), pp. 637–644.

Chapter 3 Monitoring of Corrosion Process in Two-Way Reinforced Concrete Slabs

3.1. Abstract

The corrosion performance of reinforced concrete two-way slabs was monitored in this study. Three different level of corrosion has been reached: mild (15% mass loss), moderate (25% mass loss), and severe (50% mass loss). Accelerated corrosion technique used to corrode the slabs through the application of constant voltage. Four identical full-scale slabs were cast for this purpose with dimensions of 1900 mm × 1900 mm × 150 mm. The concrete mixture was designed to attain the requirements of exposure conditions for horizontal elements according to ACI. The rapid chloride penetration test and chloride diffusion were measured to ensure that the concrete has acceptable quality against chloride ions penetrations. The corrosion performance was evaluated based on the results of the current measurement, corrosion cracks widths propagation, half-cell potential measurements, natural frequency measurements, chloride content measurements, and mass loss. The test results show that the increase in mass loss causing an increase in crack widths and chloride content while causing a decrease in the natural frequency.

Keywords: Two-way slabs; mass loss; accelerated corrosion; permeability; natural frequency

3.2. Introduction

Reinforcement corrosion is one of the major durability problems (Roberge & Pierre 1999). Corrosion of the embedded reinforcement inside the concrete is an electrochemical process.

A portion of the embedded bar exhibits as an anode and a portion as a cathode, in which an electrical potential difference occurred along the bar. At the anode, an anodic reaction (oxidation process) takes place, which the bar loss some of its mass due to releasing electrons that travel through the electrolyte solution to the cathodic part in the bar. The concrete pore water considers as the electrolyte solution. At the cathodic portion, a cathodic reaction (reduction process) takes place, which the released negative electrons, in the presence of moisture and oxygen, converts to hydroxyl ions (OH^-). The hydroxyl ions travel through the electrolyte solution to the anode and combine with the ferrous ions (Fe^{2+}) form ferric hydroxide $(2Fe(OH)_2)$ that concerts to ferric oxide $(Fe_2O_3H_2O)$ in the presence of oxygen and moisture, which consider the rust (corrosive products). The corrosive products create radial tensile stresses around the steel bar. When these stresses exceed the concrete tensile strength, the concrete cover cracks (Neville 2011).

Concrete considers a protection for the embedded reinforcement from corrosion. The concrete distinguishes that it has high alkalinity (pH > 13.5), which provides a passivation film around the embedded reinforcement that prevents it from corrosion. The concrete has to be contained low water/cement (w/c) ratio, perfectly consolidated, and well cured in order to enhance the concrete quality against the penetration of corrosion inducing agents such as chloride ions, carbonation, and moisture. Moreover, the cover thickness and the surface cracks have a significant effect on the concrete quality. In addition, the strength of concrete enhances the electrical resistivity which reduces the electrical flow between the anode and cathode causing restrictions on increasing corrosion rate (Ahmad 2003).

The research on corrosion split into several areas. Some researchers tried to understand the corrosion process itself (Raupach 1996; Carnot et al. 2003; Chitty et al. 2005). Other monitored the corrosion performance of Reinforced concrete (RC) beams (Andrade & Alonso 1996; Andrade & Alonso 2001; Ahmad 2003). Other studied the structural behaviour of corroded beams and compared it with a control specimen (El-Maaddawy & Soudki 2003). Other constructed numerical models to simulate the corrosion on beams (Dodd & Restrepo-Posada 1995; Berto et al. 2008; Coronelli & Gambarova 2004). Other focused of rehabilitation techniques for corroded beams (Bertolini et al. 2013; Miyagawa 1991; Fedrizzi et al. 2005; Broomfield 2006). Even though, there is a huge lack in studying the corrosion behaviour of two-way slabs, which exist in most of the bridges and parking garages. RC bridges and parking garages suffer from severe corrosion conditions, especially in the cold climate regions. Most of the roads spray de-icing agents that contain chloride ions. The chloride ions mix with the snow that attaches to the vehicles' tires, which melts on decks of indoor parking garages (Reilly et al. 2014; Aoude et al. 2014). In addition, the snow leaks through the bridge joints (Konecný 2007). Subsequently, the chloride ions penetrate the concrete covers and induce the corrosion. The annual cost spent in 2002 to repair bridges that deteriorated from corrosion in the United States was around $8.3 billion/year based on a study conducted by Federal Highway Administration (FHWA) (Gerhardus H. Koch 2002). The repair cost for parking garages in Canada, based on National Research Council, was $1.5 billion (Litvan 1982). Therefore, there is a need to study the corrosion performance of two-way RC slabs.

3.3. Research Significance

This paper proposed an accelerated corrosion setup for a full-scale RC two-way slab. To best of authors' knowledge, there is no previous experimental study occurred before on using the accelerated technique to corrode two-way slabs. The corrosion of two-way slabs is very challenging for several reasons. First, the time consuming to reach the targeted corrosion levels especially the severe one. In addition, the duration time for corrosion period is not applicable to be predicted according to Faraday's equation, which depends on the current value that changes every day during the test period. Moreover, the availability of data acquisition system with enough free channels to record the data consider another challenge, especially the corroded flexural bars in two-way slabs are more than that in beams. Furthermore, the space availability in the laboratory especially with the long corrosion test periods. Therefore, this paper aimed to cover some lack of information about the real corrosion of two-way slabs. This paper evaluated the corrosion performance of RC two-way slabs, which consider a novelty study on two-way slabs. Moreover, the natural frequency was measured for the tested slabs and this study proposed to use it as a non-destructive test to be an indication for the corrosion.

3.4. Experimental Program

The experimental program designed to study the corrosion damage in full-scale two-way slabs subjected to an accelerated corrosion test. The corrosion levels were tracked by recording the current passing through the tested slabs with time. The corrosion characteristic was examined periodically during the test by measuring the potential using the half-cell at a different location along the tested slabs. In addition to examining the corrosion characteristic after the test by measuring the chloride ion content near the bar surface, crack patterns and widths, and mass loss of bar. This program measured experimentally the rapid chloride permeability test (RCPT) for the concrete mixture that used in pouring the tested slabs. Four slabs were under investigation with different levels of corrosion: non-corroded one represent the reference slab (S0), mild corrosion; 15% mass loss (S15-D1-D1), moderate corrosion; 25% mass loss (S25-D1-D1), severe corrosion; 50% mass loss (S50-D1-D1). These levels were chosen to assess the variation of corrosion performance and their effect in inducing cracking along full-scale two-way RC slabs. The total number of the tested specimen is only four, which consider limited, because of two dependent main reasons: first the long test periods to reach the desired corrosion level, and the space-availability in the laboratory, especially with this large specimen size. These reasons were challenging to do replication in the specimen to improve the reliability of the obtained results. Therefore, an additional number of samples are recommended to be tested to confirm the outcome of this study, and to cover more corrosion levels and different concrete types.

3.4.1. Mixture Proportions and Material Properties

RC two-way slabs were cast using a normal strength concrete mixture. The mixture composition used shown in Table 3.1. The concrete mixture used Normal Portland cement similar to Type I (ASTM C150/C150M 2017), with a specific gravity of 3.15, for all tested specimen. The chemical and physical properties of this cement are shown in Table 3.2. A maximum aggregate size of 10 mm and natural sand, which have a specific gravity of 2.6, were used as coarse and fine aggregates, respectively (see Table 3.3). The water to cement (w/c) ratio and the targeted compressive strength were chosen to specify the exposure fulfillment requirement of class F3 in ACI specification regarding concrete horizontal elements exposed to de-icing salts. Therefore, the w/c ratio was chosen to be 0.4 and the targeted concrete strength was chosen to be 40 MPa after 28-days. 15M bars with a Grade 400 MPa was used as a flexural reinforcement for the tested slabs (see Table 3.4). The compressive strength and modulus of rupture of the concrete were shown in Table 3.4. The mixture ingredients were blended in a concrete mixture truck at a batch plant. After arriving the mixture truck to the concrete laboratory, the slump test was measured for the fresh concrete according to (ASTM C143/C143M-15a 2015). The targeted workability was reached by adding sufficient amounts of superplasticizer to achieve the desired slump of 50 ± 10 mm. After completing the slump test, the slabs were cast and consolidated using an electrical vibrator; in addition, a suitable number of concrete cylinders and prisms were prepared for the chloride permeability and hardened strength tests. The column-stub was then cast after a day after pouring the slabs. The water curing process started after 24 hrs from casting the slabs for four days and then was followed by the air-curing process by keeping the cast slabs at room temperature till day 28 after casting.

Table 3-1 Mix Composition of Concrete Mixture

CMT (kg)	w/c	Water (l)	C/F	C.A. (kg)	F.A. (kg)	Aggregate size (mm)	Fresh density (kg/m3)
350	0.4	140	1.3	1083	833	10	2407

*CMT is the cement, w/c is the water to cement ratio, C/F is the coarse to fine ratio, C.A. is the coarse aggregate, and F.A. is the fine aggregate

Table 3-2 Chemical and Physical Properties of Cement

Chemical analysis (%)		Physical analysis	
SiO_2	19.64	Residue 45 μm (%)	8.42
Al_2O_3	5.48	Blaine fineness (m^2/kg)	410
Fe_2O_3	2.38	Air content (%)	7.78
CaO	62.44	Initial Set (min)	103
MgO	2.48	Auto. expansion (%)	0.14
SO_3	4.32	Sulf. expansion (%) (prev. month)	0.013
Total alkali	0.97	-	-
Free lime	1.03	Compressive strength (MPa)	-
LOI	2.05	1 day	19.23
C_3S	52.34	3 days	29.12
C_2S	16.83	7 days	33.82
C_3A	10.50	28 days	41.45
C_4AF	7.24	-	-

Table 3-3 Sieve analysis

Sieve Size	10 mm C.A. (% passing)	Sieve size	F.A. (% passing)
14	100	10	100
10	95.8	5	99.4
5	21	2.5	79.4
2.5	2.9	1.25	55.4
1.25	0	0.63	35.2
0.63	-	0.32	18.6
0.32	-	0.16	7.3
0.16	-	0.08	2.2

*C.A. coarse aggregate, and F.A. fine aggregate.

Table 3-4 Steel and Concrete Properties

Designation	Steel properties			Concrete Properties	
	Area (mm^2)	f_y (MPa)	ε_y (με)	f'_c (MPa)	f_r (MPa)
15M	200	475	2200	41.1	3.82

* f_y is the yield strength, ε_y is the yield strain, f'_c is the compressive strength, and is f_r the modulus of rupture.

3.4.2. Rapid Chloride Penetration and Diffusion test

Rapid Chloride Penetration Test (RCPT) is ASTM standard test indicate the ability of concrete to resist chloride ion penetration by determining the concrete's electrical conductivity (ASTM C1202-17a 2017). This test used to evaluate the material proportion that used in the concrete mixture in order to ensure an acceptable quality control for the cast slabs against chloride penetration. After curing time for the cast cylinders, a cylinder of a diameter 100 mm cut to slices by using a water-cooled diamond saw, each slice had a thickness of 50 mm ± 3 mm. A belt sander has been used to remove any burrs attached to the slices. Then, the slices placed in a vacuum desiccator as shown in Fig. 3.1. A vacuum pump kept the desiccator vacuumed for three hours. After that, the water allowed covering all slices with maintaining the vacuum pump to work another one additional hour. The specimen kept soaked under water for 20 hrs. The 50 mm slices have been placed inside each RCPT cell, to monitor the amount of electrical charge passed through the slices in Coulombs during a period of six hours. The potential difference, which applied through a DC, between each cell's sides was 60 V, one side of cells was filled with a sodium chloride solution (3% by mass in distilled water) and connected to the negative terminal of the power supply. The other side of the cell filled with a sodium hydroxide solution (0.3 N in distilled water) and connected to the positive terminal of the power supply as shown in Fig. 3.1. Each slice inside RCPT specimen-cell was efficiency sealed by using silicone greases and rubber gaskets. RCPT related to the amount of electrical charge and the resistance of the concrete slice to the chloride ion penetration. The interpretation of RCPT values as per ASTM (C1202-17a 2017) is illustrated in Table 3.5.

a. b.

Figure 3-1 RCPT instruments.

Table 3-5 Interpretation of RCPT values as per ASTM (C1202-17a 2017)

Charge passed (Coulombs)	Chloride ion penetrability
> 4,000	High
2,000-4,000	Moderate
1,000-2,000	Low
100-1,000	Very Low
< 100	Negligible

The corrosion service life of any concrete structure divided into three stages: diffusion, corrosion, and damage (Bazant 1979; Cady & Weyers 1984). The diffusion is the time required from chlorides ions to penetrate through concrete cover till reaching the threshold value at the reinforcement bars. Diffusion used as an indicator for the concrete quality beside the permeability test. The diffusion determined by using bulk chloride diffusion test (Andrade 1993). According to ASTM (C1556-11a 2016), the initial chloride ion content (C_i) was determined as a first step by crushing a 20 mm slice into powder. Then, a concrete cylinder cut to two slices each slice had a thickness of 75 mm. Each slice sealed from all sides except the top surface, the seal was done carefully to avoid any voids or cracks on the seal. The slice weighted then immersed in a saturated calcium hydroxide (limewater) water bath to prevent initial sorption effect when chloride solution is introduced. The slices weighed with a surface dry condition every day until the weight became constant without any changes. The slices kept immersed for 30 days in the calcium hydroxide water bath. The slices removed from this bath and rinsed then exposed to sodium chloride solution for 40 days. The slices then removed from the exposure liquid and dried at room temperature for 24 hrs, then each slice ground for eight different depths as recommended depth intervals in (ASTM C1556-11a 2016). At each depth (x) the dust powder collected and kept in a plastic bag. The chloride ion $(C(x,t))$ at each depth level (x) at exposure time (t_e) were measured using a chloride meter device after storing the powder in a bottle of a specific extraction liquid for 24 hours. After that, the chloride content profile was plotted and used to determine the surface chloride concentration (C_s) and the chloride diffusion coefficient (D_a). The D_a was calculated by using the error function $(\mathrm{erf}(z))$ solution to Fick's second law of diffusion:

$$C(x,t) = C_s - (C_s - C_i) \, . \, \mathrm{erf}\left(\frac{x}{\sqrt{4 D_a t_e}}\right) \qquad 3.1$$

3.4.3. Details of Test Specimen

A total number of four identical two-way slabs was prepared for this study. Each slab had dimensions 1900 mm × 1900 mm × 150 mm with a concrete cover of 30 mm. All slabs had a square column stub 250 mm × 250 mm extended to 300 mm from the compression side.

The slabs used 15M bars spaced every 190 mm, and 10M bars spaced every 300 mm as flexural reinforcement, and compression reinforcement, respectively. The flexural reinforcement isolated at the mesh intersection points to avoid any conductivity between the bars. Thus, this provides a possibility to control separately the corrosion for each bar to reach uniform corrosion. A wire connected to each bar under the targeted corroded area before pouring the concrete, in order to use it in the accelerated corrosion process as shown in Fig. 3.2. The details of slab specimens specified in Table 3.6. Figure 3.3 showed a sketch of the slab detailing. The corroded area was chosen as the reinforcement bandwidth of c + 3h (700 mm × 700 mm), where c is the column dimension and h is the slab thickness, as defined in CSA A23.3-14 (2014). The targeted corroded area was chosen as shown in Fig. 3.4.

Figure 3-2 Setup of wires that connected to the bars under corrosion.

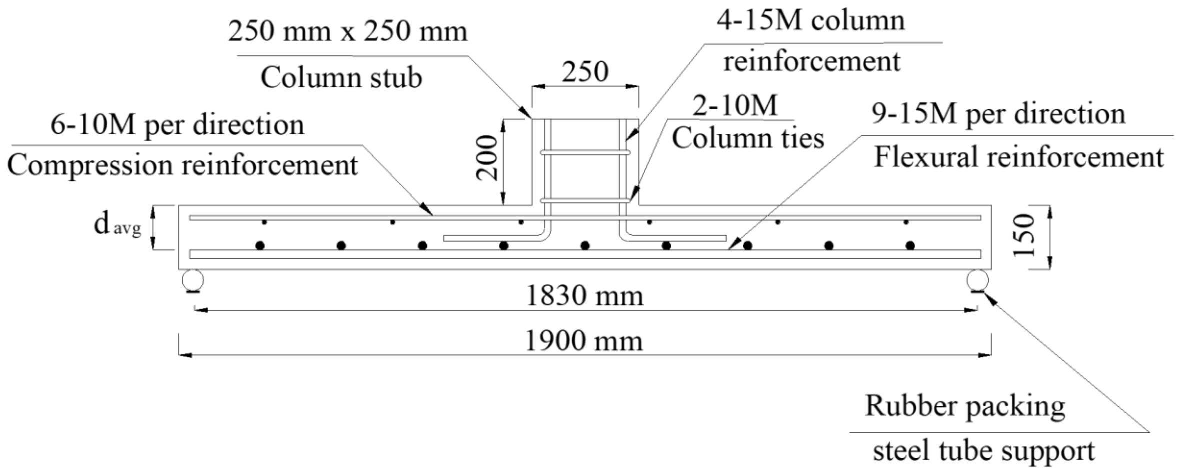

Figure 3-3 Details of a typical slab.

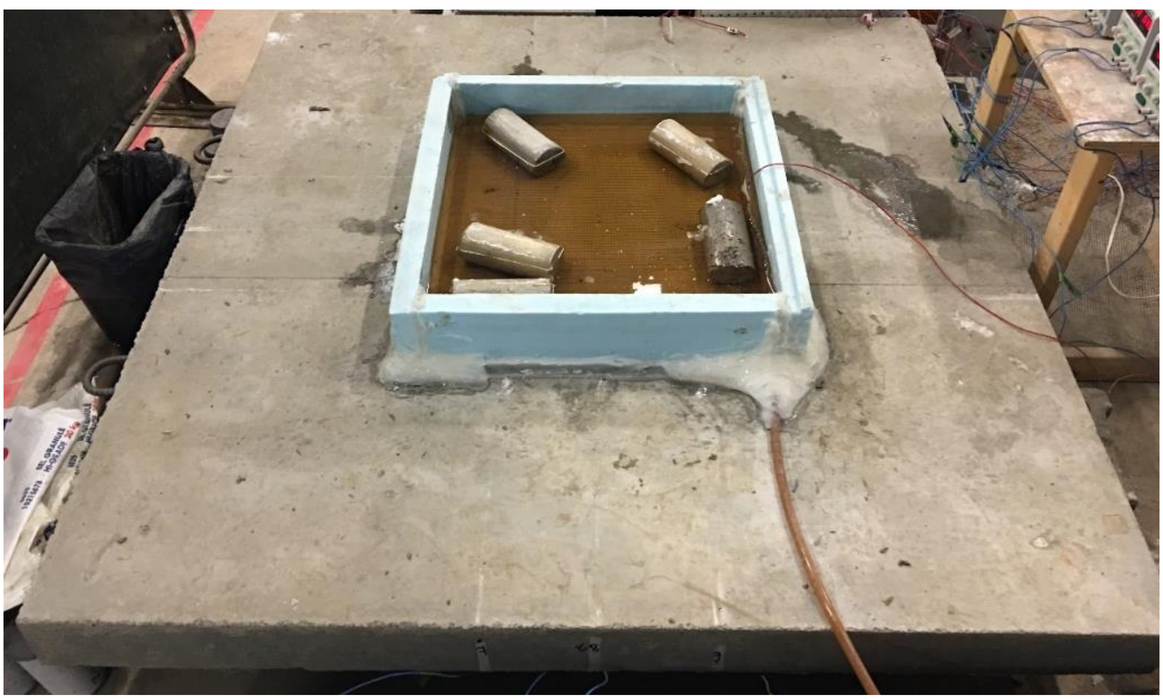

Figure 3-4 The targeted corroded area.

Table 3-6 Detailed of Slab Specimens

Side dimensions (mm × mm)	h (mm)	c (mm)	d (mm)	f'_c (MPa)	Main reinforcement
1900 × 1900	150	250	104	41.1	Two layers-15M bars (ρ = 1%)

*h is the height; c is column width; d is the effective slab depth; ρ is the reinforcement ratio; and f'_c is the concrete compressive strength.

3.4.4. Accelerated Corrosion Setup

An accelerated corrosion technique based on the application of constant voltage was used to corrode the tested slabs. The setup consisted of a power supply, data acquisition systems, current transducers, electrical distribution board, computer to process the data, electrolyte solution, foam sheets, and steel mesh. Figure 3.5 shows a schematic diagram for accelerated corrosion setup. First, each slab placed in a levelled inverted position, where the column stub was on the bottom. A dike was constructed around the perimeter of the reinforcement bandwidth, the corroded area under investigation. An electrolyte solution (5% Sodium Chloride by weight of water) filled the dike. A hose with a valve was attached to the lowered levelled point of the dike to facilitate the evacuation process of the dike in case of need. A regulator power supply used to provide a source of a direct current, which acted to keep the output voltage constant; 15 V. The positive terminal was connected to an electrical distribution board, which was connected as a parallel circuit in order to split the input current to six output terminal with keeping the voltage constant. Each positive terminal from the board was connected to a targeted embedded bar inside concrete that was required to be corroded, these bars considered as an anode. The negative terminal attached to a steel mesh that placed inside the dike and covered all targeted corroded area, the steel mesh considered as a cathode. The theoretical mass loss is calculated based on Faraday's equation as

$$\text{Mass loss} = \frac{t\,I\,M}{z\,F} \qquad 3.2$$

Where t is the time passed in seconds, I is the current passed in Amperes, M is atomic weight (for iron $M = 55.847$ g/mol), z is the ion charge (two moles of electrons), and F is Faraday's constant which is the amount of electrical charge in one mole of electron ($F = 96{,}487$ coulombs per mole (C/mol)) (Lachemi et al. 2014).

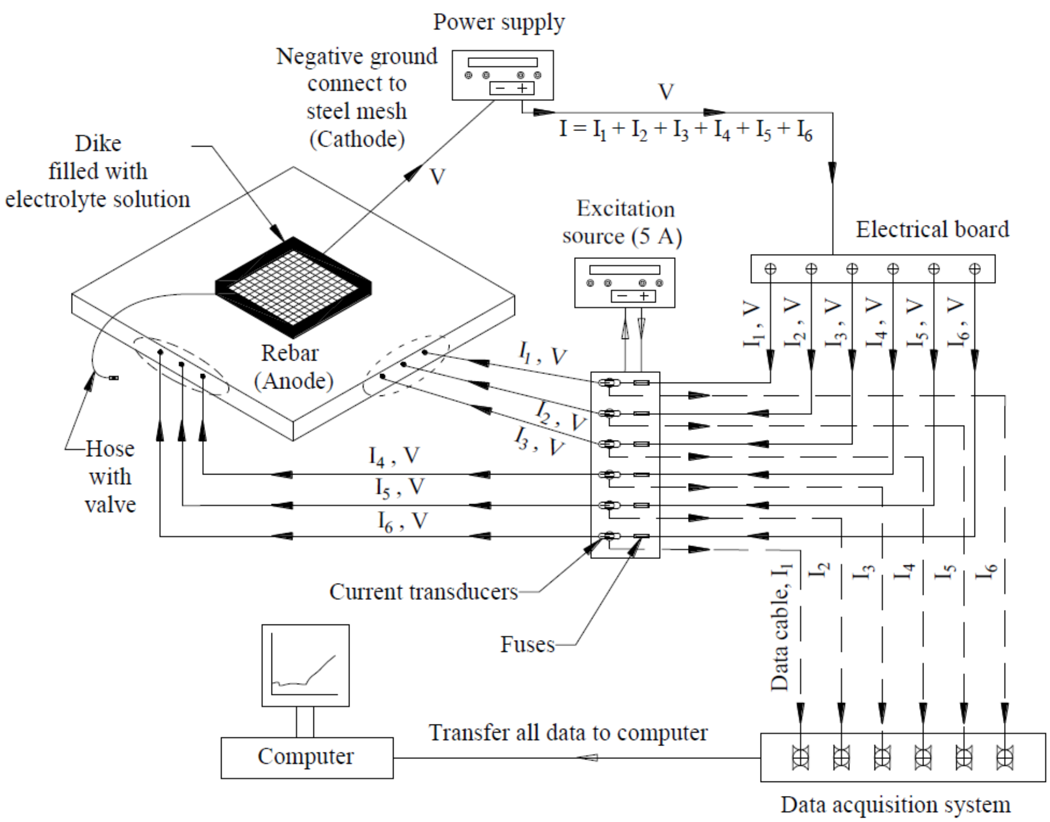

Figure 3-5 Schematic for Constant voltage accelerated corrosion setup.

According to Faraday's equation, the current passed through each corroded bar was required to be recorded to be able to use this equation. Unfortunately, the data acquisition system that was available at the laboratory reads only voltage. Therefore, current transducer sensors used to convert the current passed through each bar into a corresponding voltage reading, then sent it to the data acquisition system to read it and record it on a desktop computer. The recorded voltage reading reconverted to a current reading again using a calibration equation for each current transducer used to calculate the theoretical mass loss.

3.4.5. Half-cell Potential Measurement

The half-cell potential is a technical standard test verified by the American Society for Testing and Materials (ASTM C876 2015). This method measured the electrochemical potential of RC elements, at different points over a certain area, against a reference electrode (copper/ copper-sulphate - Cu/CuSO4). This technique provided the specialists with a qualitative index that if the corrosion has occurred or not. ASTM (C876 2015) performed a correlation between the half-cell potential readings and the chance for corrosion occurrence as shown in Table 3.7. It has been illustrated from the table that more negative values indicated a higher chance of corrosion occurrence and vice-versa. The reading of the half-cell recorded on different twenty-four location over the corroded area. Twelve location above the upper layer and the other twelve above the lower layer of flexural reinforcement, the reference was connected to each layer when the reading was recorded. Figure 3.6 shows the typical layout for the tested location points on each slab. The reading was measured periodically every three days during the induced corrosion process. When the half-cell potential reading was recorded, the accelerated test was not working and the dike was empty from the electrolyte solution. The steel mesh that was used as a cathode also removed from the dike. After that, the reference electrode was placed on the concrete surface after putting a wet sponge to do conductivity between the reference and the embedded rebar to measure the potential. The readings of the half-cell get affected by various factors such as the moisture condition of the concrete surface and its uncleanness, especially if it exposed to chlorides or carbonations. The wet surface and the surface contaminated with chlorides affected the potential readings and show more negative values (Klinghoffer 1995). Therefore, the potential readings were recorded after doing two precaution steps in order to guarantee a fair comparison between all tested slabs. The first precaution cleaned the corroded surface directly after draining the electrolyte solution using a brush and rinse it with a fresh water. Second precaution, the potential readings recorded after six hours of draining the electrolyte solution from the dike to ensure obtaining a dry surface.

Table 3-7 Interpretation of half-cell potential values as per ASTM (C876 2015)

Half-cell potential (mV) relative to Cu/CuSO4 reference electrode	Percentage chance of active corrosion
<-350	90
-250 to -350	50
>-200	10

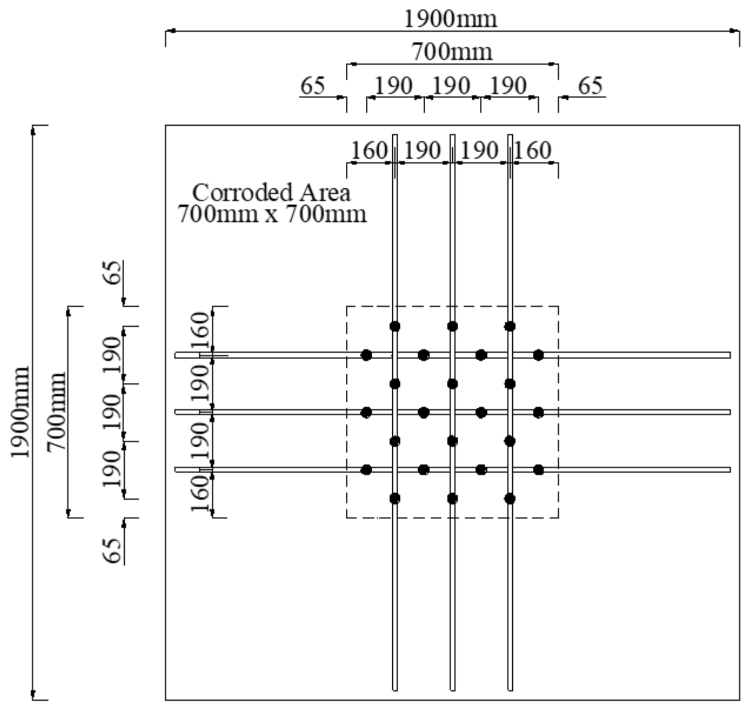

Figure 3-6 Typical layout of the tested points along the corroded area of the slab.

3.4.6. Natural Frequency Measurements

A study suggested measuring the natural frequency for RC slabs under free-free boundary condition. This boundary condition reflects the actual properties of the structure without the destruction and the influence of supports that could misinterpret the structural behaviour (Ahmed & Mohammad 2014). Therefore, the natural frequency for the tested slabs was measured under free-free boundary condition as shown in Fig 3.7.

The natural frequencies for the tested slabs were obtained from an experimental modal analysis. A dynamic vibration happened by a source of known excitation, then the response transferred through a function spectrum that analyzed to get the natural frequency value. The needed components to measure the natural frequency were: impact hammer, three accelerometers sensors, data acquisition system, and a computer. The impact hammer used to induce an excitation. A load cell was attached to the hammer face which transfers the magnitude of the force to a corresponding analog electrical signal. The accelerometers sensors attached to the structural element, which two distributed around the far corner of the tested slab and one in the middle as shown in Fig 3.7. The accelerometers sensors captured the dynamic response in a form of analog electrical signal. The data acquisition system collected all analog signals, filtered, amplified them, and then streamed all data to be digital processing by using a computer software (Modal-View) that provided the natural frequency value for the tested element.

Figure 3-7 Accelerometers location for natural frequency measurement.

3.4.7. Chloride Content Measurements

The chloride ion content near concrete bars was determined in order to examine the corrosion state. Eight concrete powder samples were extracted from each tested slab using an electric drill. The drilling process happened after ensuring that the concrete surface became totally dry, in order to avoid collecting wet powder because the weight of water in wet powder could affect the calculation of chloride ion content. The powder samples extracted from the contact surface between the concrete cover and the flexural reinforcement mesh. Four samples extracted directly from the contact surface above the upper layer of flexural reinforcement mesh, which was at depth of 30 mm. The other four samples extracted from the depth of 46 mm, which consider the lower layer of flexural mesh. The four samples from each mesh were extracted from different four locations on the same one-quarter of the corroded area. Each powder sample with the weight of 3 gm added slowly to a vail contained 20 ml chloride extraction liquid, which had a precise acid concentration, to avoid any interlocking between powder particles. Then the sample left for 24 hrs inside the vail before conducting the test. A calibrated high impedance electrometer used to measure the chloride content for powder sample inside the vail. A calibration process happened to the electrometer before measuring chloride content by using five standard samples containing different five chloride range: 0.005%, 0.01%, 0.05%, 0.1%, and 0.3% by weight. After calibration, the electrometer was lowered gently inside each vail with avoiding touch the dust at the bottom of the vail. Then the electrometer measured the chloride content as a percentage of concrete mass.

3.4.8. Mass Loss Measurements

The theoretical mass loss calculated based on Faraday's equation. After the slabs reached the theoretical mass loss, the corrosion process stopped. After finishing the test of the corroded slabs and recording all requirement measurements, the concrete cover was cut off using a demolition hammer to extract the flexural reinforcement as shown in Fig. 3.8.

a. During demolition

b. After Demolition

Figure 3-8 The extraction process of corroded bars.

The corroded bars were cleaned by removing all free corrosion products using a wire brush, then soaked the bars in a hydrochloric acid solution and brush them lightly to remove the rest corroded products (ASTM G1 2003). After that, the cleaned bars were weighed and the mass loss was calculated from the following Equation:

$$\%\text{ mass loss} = \frac{\text{initial weight - final weight}}{\text{initial weight}} \qquad 3.3$$

3.5. Test Results and Discussion

3.5.1. Rapid Chloride Penetration Test

The electrical charged passed through different four slices were 1323, 1356, 1428, and 1473 Coulombs. All tested slices lied on the low range of RCPT, which was between 1000 to 2000 Coulombs. CSA A23.1-14 recommended RCPT has to be less than 1500 Coulombs for structural RC elements exposed to chlorides with or without freezing condition. Therefore, the results from the RCPT indicated that the cast slabs had a good quality according to their compressive strength to resist chloride ion penetration.

3.5.2. Diffusion Test

A chloride content profile was plotted as shown in Fig 3.9. After collecting the experimental results, a statistical analysis was performed on the data and prediction models were established. As shown in Fig. 3.9 that the coefficient of multiple determination $\left(R^2\right)$ equal to 0.997 which indicated the goodness of curve fitting. The chloride ion diffusion coefficient equal to $4.54\text{E-}12\ \mathrm{m}^2/\mathrm{Sec}$, this value is a close to a value obtained before by (Moreno et al. 2015; Park et al. 2016). This value indicated that the mixture composition was reasonable and suitable with the obtained compressive strength to resist chloride ion penetration. The bulk chloride diffusion test confirmed the results of RCPT that this concrete mixture was good to resist chloride ion penetration.

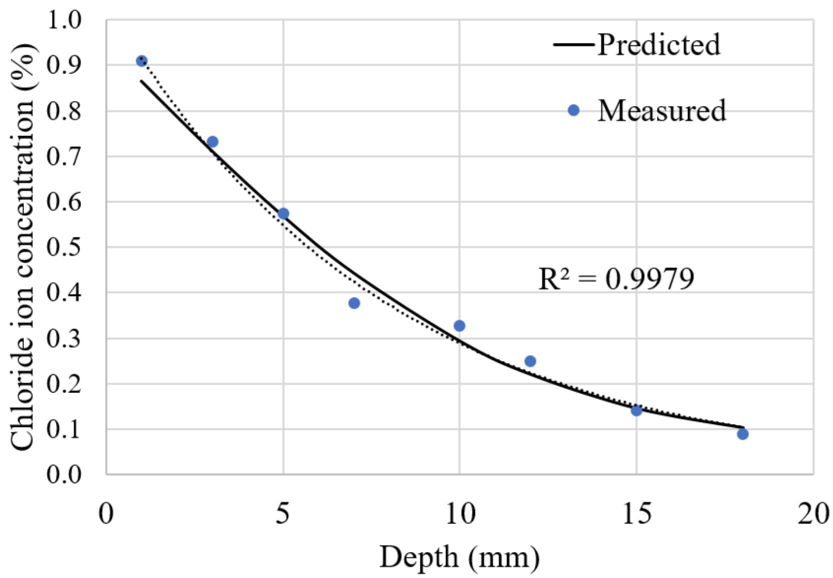

Figure 3-9 Chloride ion concentration vs depth.

3.5.3. Current Results

The current passed through each corroded bar was separately recorded. Figure 3.10 shows the relation between the current and the elapsed time to reach the targeted corrosion level. The first stationary point in the curve is a sign of the corrosion initiation, and the increase of the slope is an indication of the rate of corrosion. It was noticed for all tested slabs that the current at initial stages of corrosion decreased then followed by a gradual increase in the current. This initial decrease in current could be an indication to the formation of the passivation layer around the bar that protects it from corrosion. Corrosion started when the de-passivation occurred, then the rate of corrosion started to increase (Cornet et al. 1968).

The final current values in most of the corroded bars in slab S15-D1 did not exceed the initial current value except for two bars. The initial current values for these two bars were the lowest among the other bars. Moreover, the current values in most of test period were the lowest for these two bars, which meant that they had the lowest rate of corrosion. Based on Faraday's equation that depends on the current intensity, the others bars reached the targeted corrosion level in a period less than these two bars. When the de-passivation occurred on these two bars, the rate of corrosion increased significantly until reached the targeted corrosion level.

S25-D1 demonstrated high current values at the end of the test period for all corroded bars, which represented high corrosion rate. The corroded bars in S50-D1 provided a complete scope of the relation between the current intensity and the time. It has been noticed that there was two sudden jump, each followed by a sudden drop in the slope. The first sudden jump in the slope happened directly after the current overcome the passivation layer and concrete resistivity against the ingress of chlorides. In addition, the bond between the corroded bar and the concrete covers started to occur. Then, the slope significantly dropped, which was attributed to the formation of the corrosive products that locked the cracks and obstructed the current to reach the corroded bar. The current then remained constant. Some bars reached the targeted corrosion level and some bars suffered from a second suddenly jump. This second jump could be attributed to that the current fastened the crack widths from some of the corrosive products and reached the corroded bar. The second drop happened because of the same reason, the increased volume of the corrosive products. Figure 3.11 demonstrates the rate of mass loss versus time. The mass loss rate increased with the increase of current rate based on Faraday's equation.

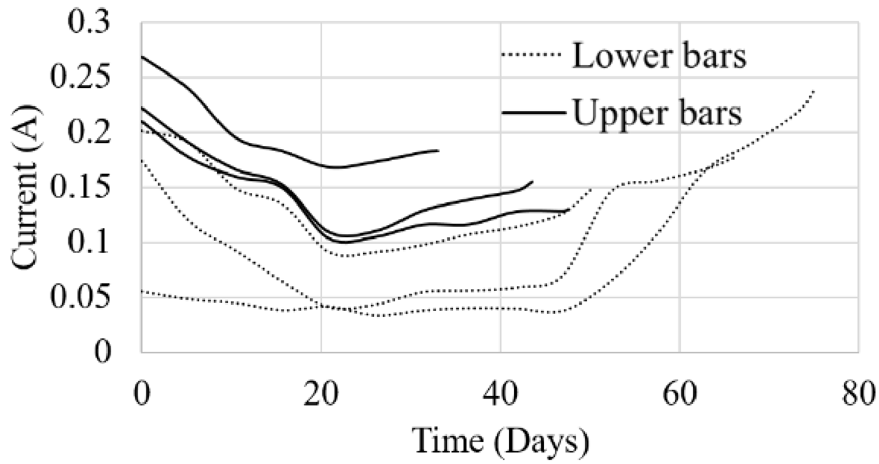

a. Mild corrosion level - S15-D1

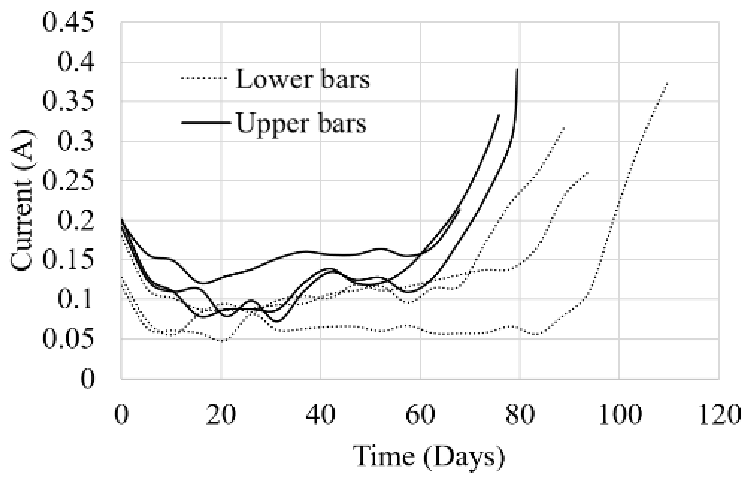

b. Moderate corrosion level - S25-D1

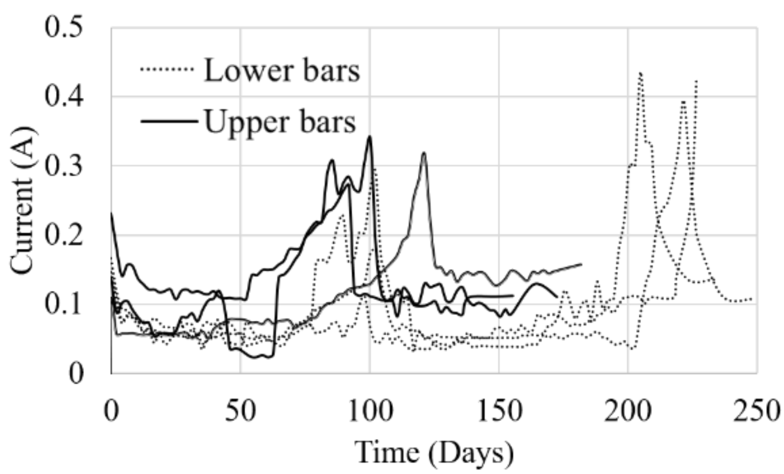

c. Severe corrosion level - S50-D1

Figure 3-10 Current time history for the tested slabs.

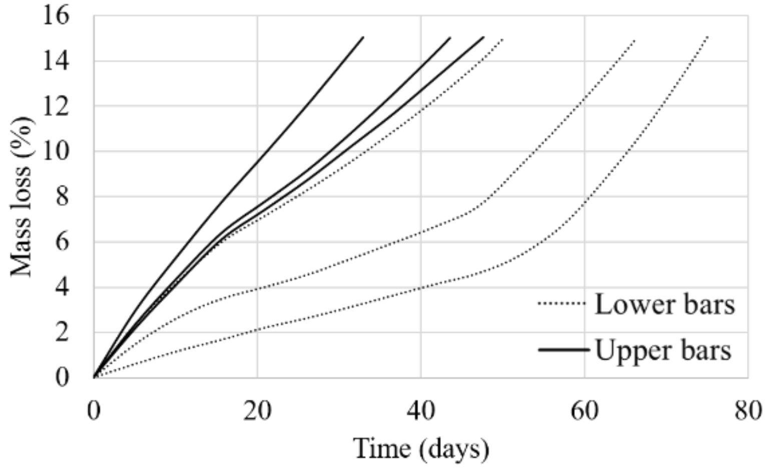

a. Mild corrosion level - S15-D1

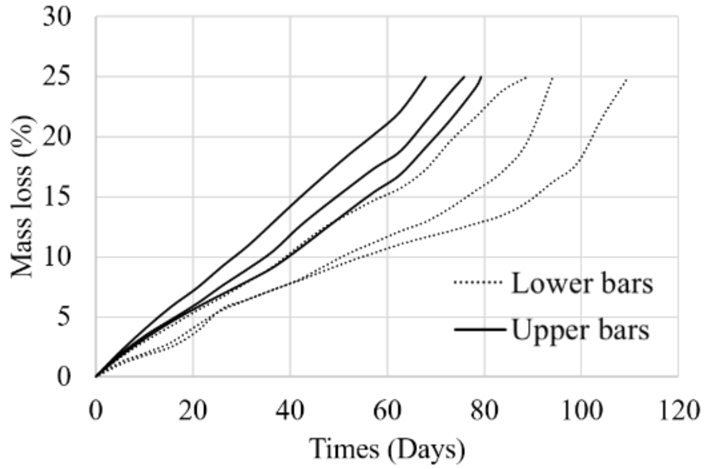

b. Moderate corrosion level - S25-D1

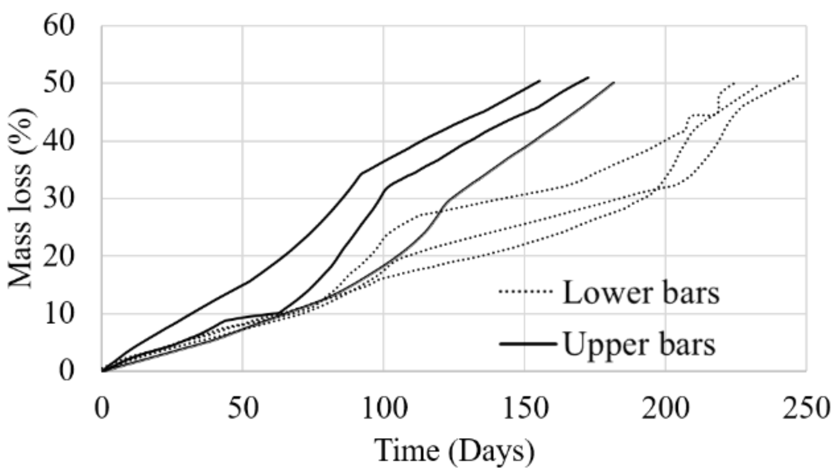

c. Severe corrosion level - S50-D1

Figure 3-11 Mass loss rate for the tested slabs.

3.5.4. Half-cell Potential Measurement

Figure 3.12 demonstrates the average half-cell reading versus the level of corrosion. While Fig. 3.13 displays the average half-cell reading versus time of accelerated corrosion of the tested slab. From Figs. 3.12 and 3.13 it has been concluded that the potential readings for upper layer of flexural reinforcement mesh had more negative value comparing with lower layer of the flexural reinforcement mesh at the same corrosion level and the same time. This could be attributed to the concrete cover for upper layer was less than the concrete cover for the lower layer. This behaviour matched with previous studies that increasing concrete cover has a significant effect on decreasing the half-cell potential negative values (Klinghoffer 1995). The results were presented in an equipotential contour map to illustrate the graphical delineation for the corrosion activity on the tested slabs under investigation.

Figures 3.14, 3.15, and 3.16 show the equipotential contour maps for S15-D1, S25-D1, and S50-D1, respectively. The maps drew at four different ages; 3, 9, 36, and 75 days for the all tested slabs. It has been concluded that in all tested slabs that the higher negative contour values produced around the direction of upper layer for the flexural reinforcement. At day 3, no slab had recorded potential value less than -150 mV, which meant that the tested slab may have 10% chance of active corrosion. It has been observed after 9 days S15-D1 and S50-D1 had potential values between -400 mV and -300 mV, which mean that according to ASTM (C876 2015) that the percentage chance of active corrosion was around 90%, while S25-D1 had values around -300 mV and -200 mV which meant that S25-D1 after 9 days may have around 50% chance of active corrosion. This could be attributed to the starting of accelerated corrosion process for S25-D1, which did not start directly after the curing time like S15-D1 and S50-D1. Thus, concrete electrical resistivity increased with gaining the concrete strength for S25-D1. Thus the resistance against chloride ion penetration increased causing restrict in increasing corrosion rate, which delays the initiation of corrosion (Ahmad 2003). After 36 days, it could be noticed that the potential readings for all points for all tested slabs exceeded the -400 mV, which meant that the potential readings at late testing age of corrosion had very closed values to each other. In addition, Figs. 3.12 and 3.13 showed that there was no noticeable variation in the half-cell potential reading at late age of corrosions. Therefore, this test is used only as an indication of the occurrence probability of corrosion for un-corroded members.

3.5.5. General Cracking Observation

The cracks that induced from corrosion were monitored during the test period. A precise microscope, that has 0.02 mm accuracy and 60× focusable eyepiece magnifier, was used to measure the crack propagation. Figure 3.17 shows the maximum crack width measurement versus the corresponding mass loss level in each corroded slab. The crack pattern that was induced in the corroded area for each tested slab is shown in Fig. 3.18. It has been found that the maximum crack width at the end of the period test for S15-D1, S25-D1, and S50-D1 was 0.15, 0.5, and 2.00 mm, respectively. In addition, it has been noticed that the crack widening rate (slope of the curve in Fig. 3.17) increased with the increase of the mass loss level. The increased of the crack width and crack widening rate with the increased of mass loss could be attributed to the increased volume of the corrosive products under concrete cover, in which these products exerted internal tensile pressure that widened the cracks. It has been noticed that at S50-D1 the maximum crack width at the average mass loss of 15% and 25% was 0.18, 0.6 mm, respectively. Therefore, the difference between the maximum crack width in S15-D1 and S25-D1 versus the corresponding average mass loss in S50-D1 was 6.7% and 20%, respectively. While the maximum crack width at the average mass loss of 15% in S25-D1 was 0.08 mm; therefore, the difference between maximum crack width in S15-D1 and the corresponding average mass loss in S25-D1 was 46.6%. These difference in the crack width could be attributed to the measurement of the crack width at the corresponding average mass loss, in which all the corroded bars did not reach the same mass loss compared with the measurement of the final maximum crack width that occurred when all corroded bars reached the same mass loss level. This difference also could be attributed to the random and unexpected behaviour of the corrosion.

3.5.6. Natural Frequency Measurements

The purpose of measuring natural frequency was to investigate the possibility of using it as a non-destructive test to help in detecting the structural response of corroded elements based on the change of dynamic properties. It has been found that the natural frequency for the control slab equal to 134 Hz, which has a close agreement with the analytical value that calculated before by Ahmed & Mohammad (2014). Figure 3.19 shows the natural frequency values for the tested slabs. It has been noticed that the natural frequency for S15-D1, S25-D1, and S50-D1 equal to 104, 64, and 41 Hz, respectively. It has appeared that increasing the mass loss, decreasing the natural frequency. The decrease in natural frequency was by 22.4%, 52.2%, and 69.4% for S15-D1, S25-D1, and S50-D1, respectively compared to S0. This decreased could be attributed to the decrease of the stiffness with the increase in mass loss, which has an effect on the natural frequency. In addition, loss of bond between corroded bars and concrete cover also has an effect on reducing the natural frequency. The decrease in natural frequency related also to the maximum crack widths and the cracks distribution. While the corrosion is a random process and produces unexpected cracks distribution, more corroded samples are required to be tested to improve the reliability of measured natural frequency and do a good correlation between the mass loss level and loss in the natural frequency.

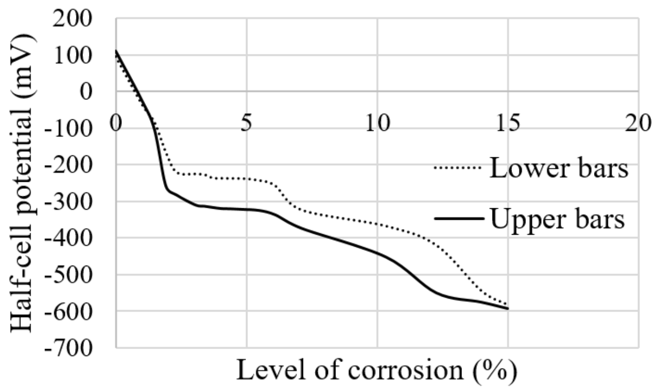

a. S15-D1

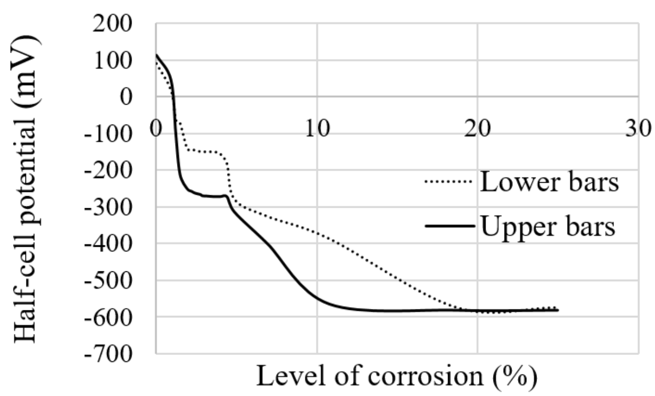

b. S25-D1

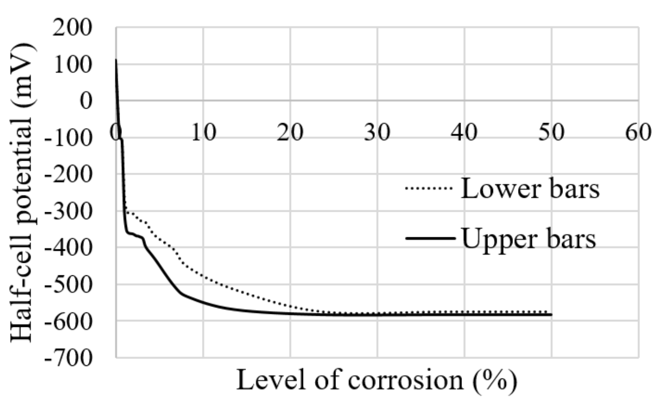

c. S50-D1

Figure 3-12 Average half-cell potential reading versus corrosion level.

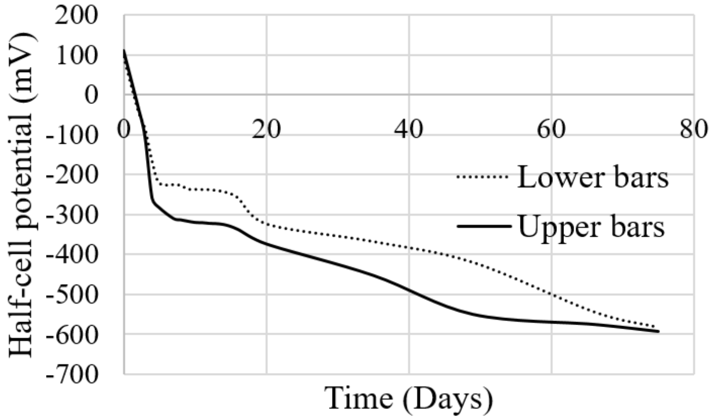

a. S15-D1

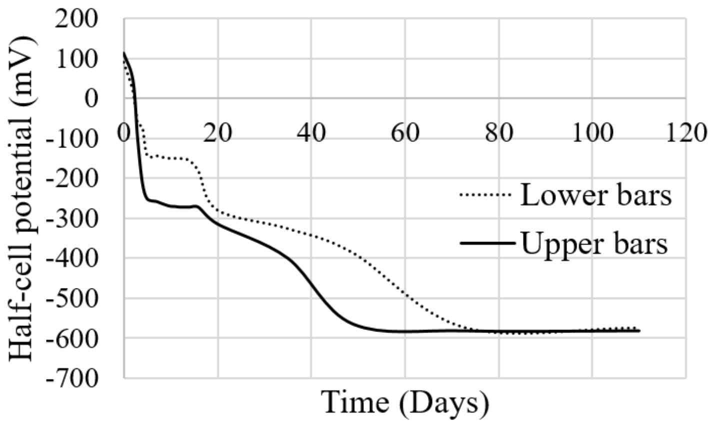

b. S25-D1

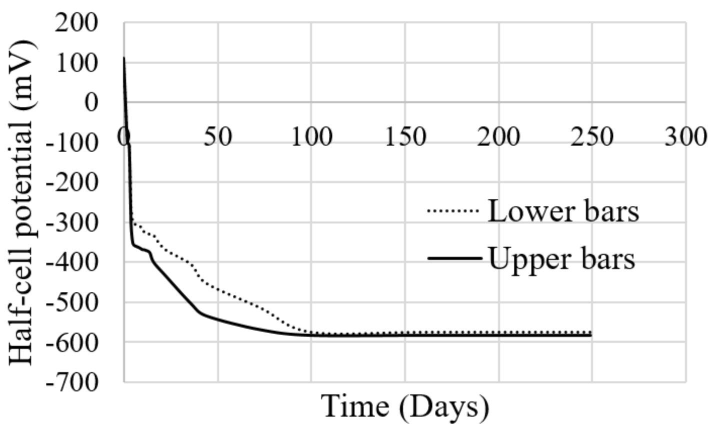

c. S50-D1

Figure 3-13 Average half-cell potential reading versus accelerated corrosion time.

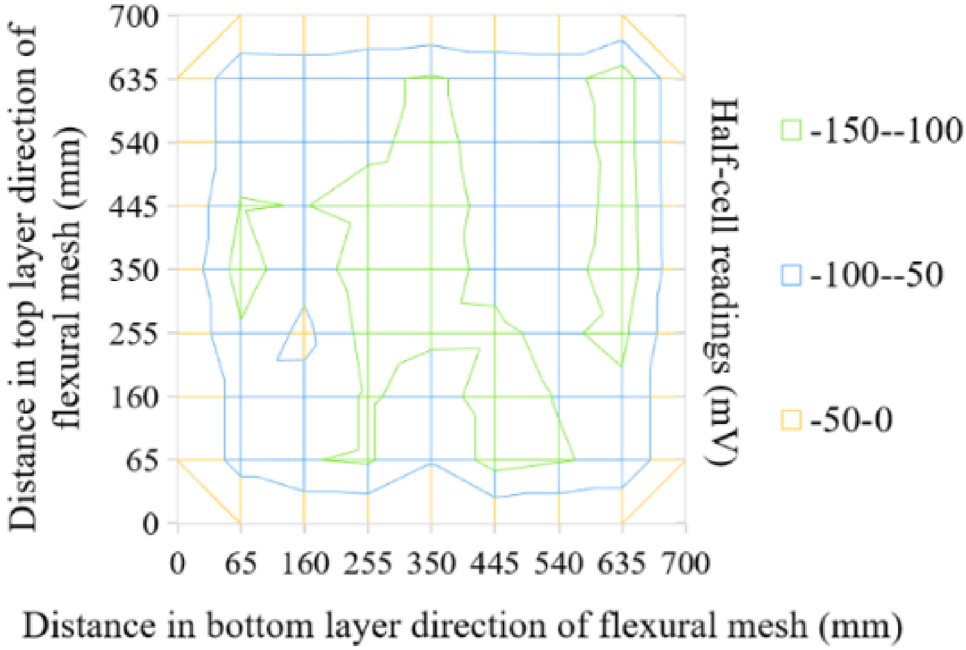

a. 3 days

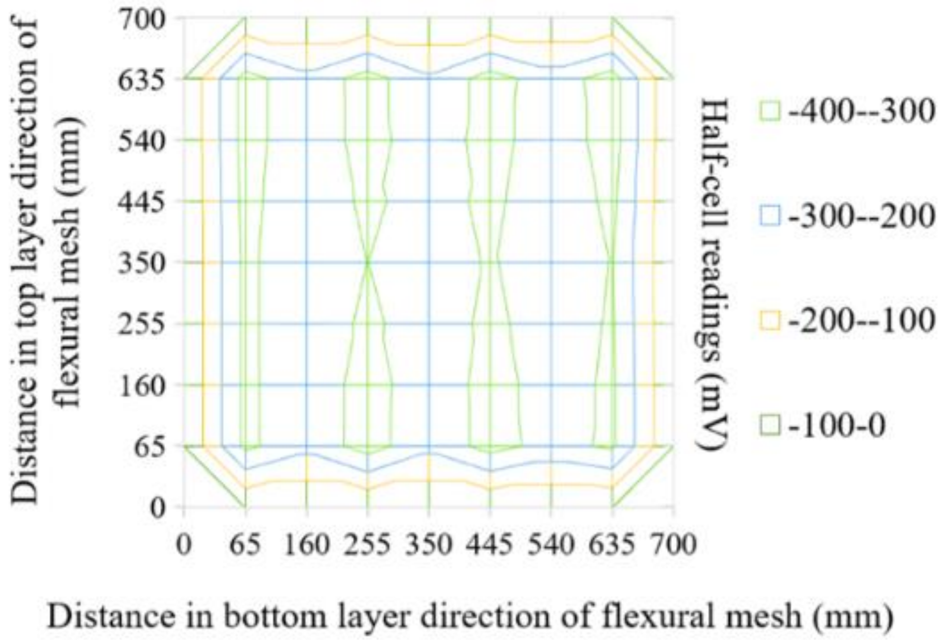

b. 9 days

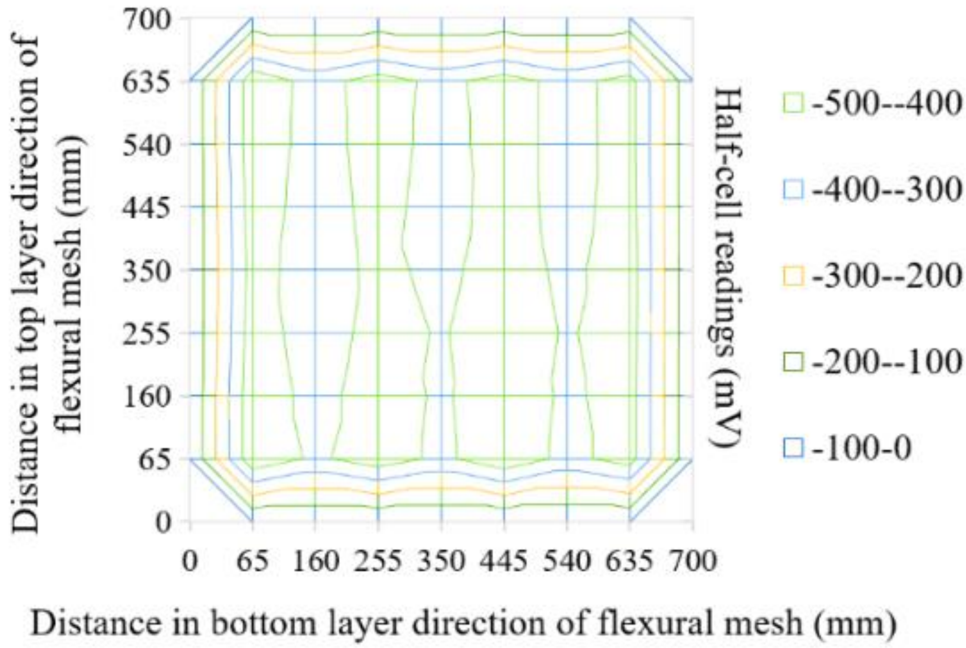

c. 36 days

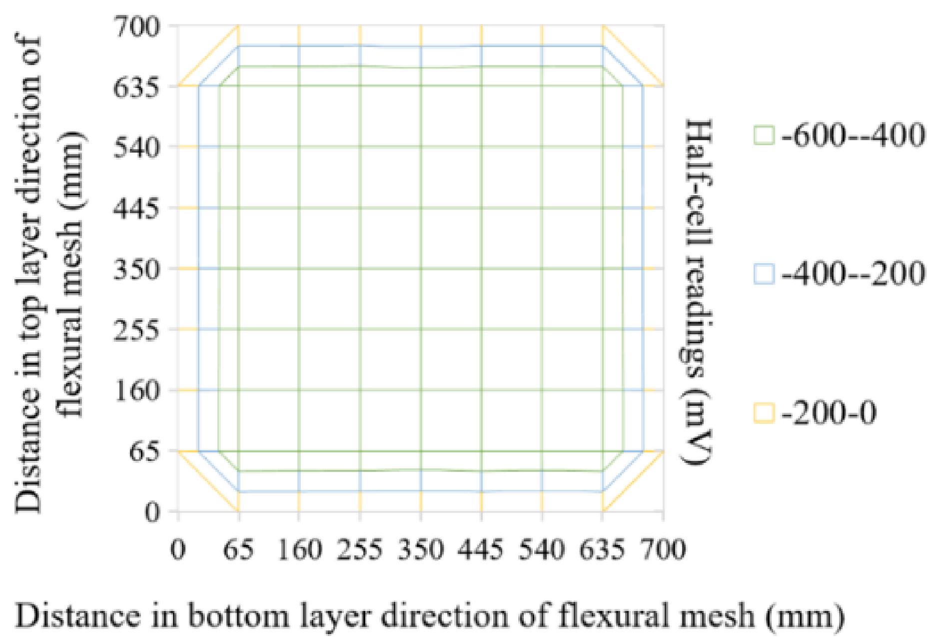

d. 75 days

Figure 3-14 Equipotential contour map for S15-D1.

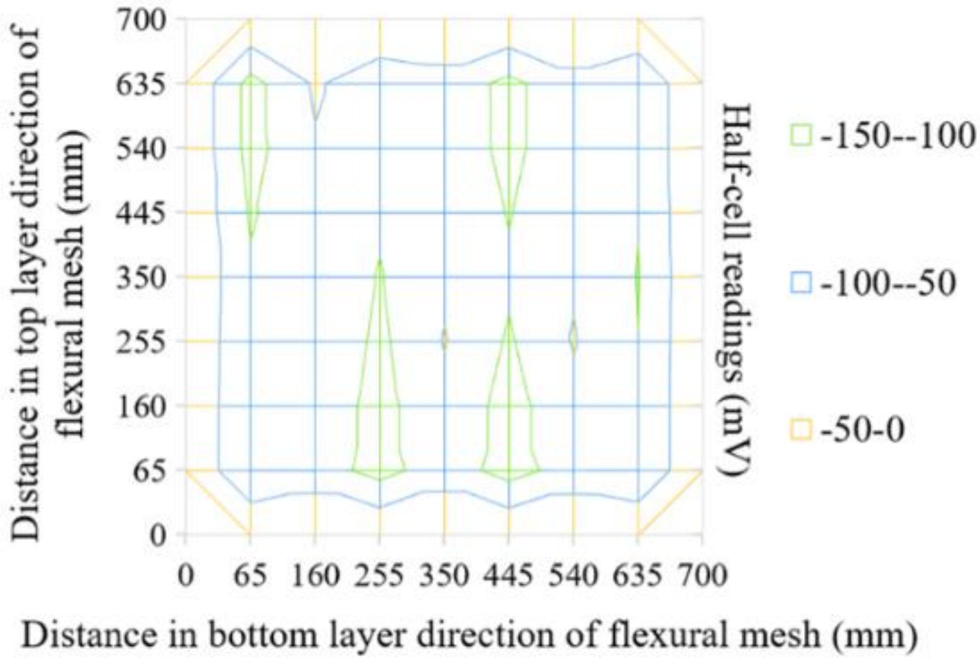

a. 3 days

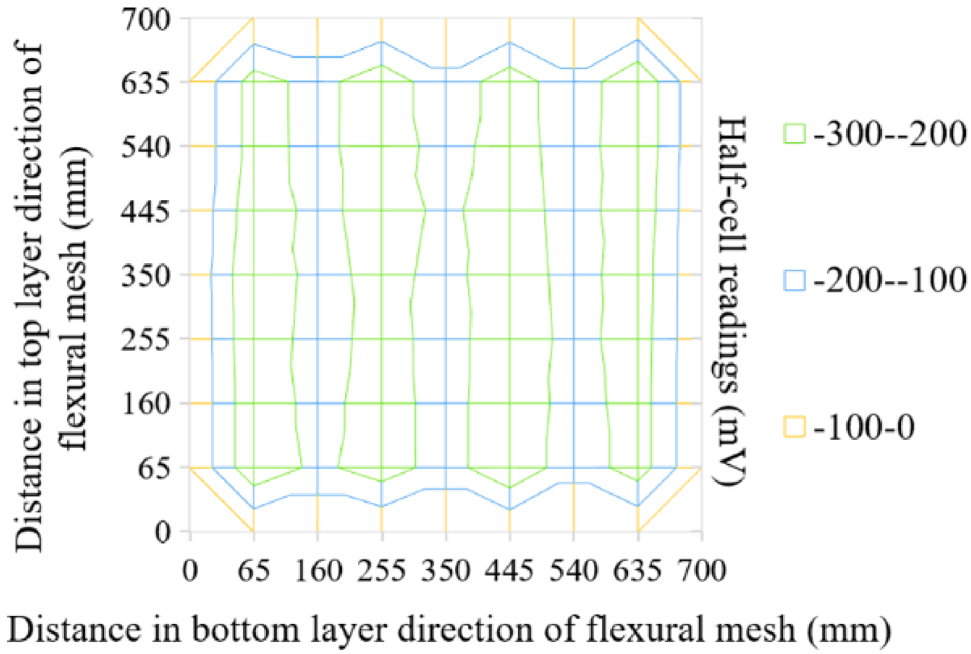

b. 9 days

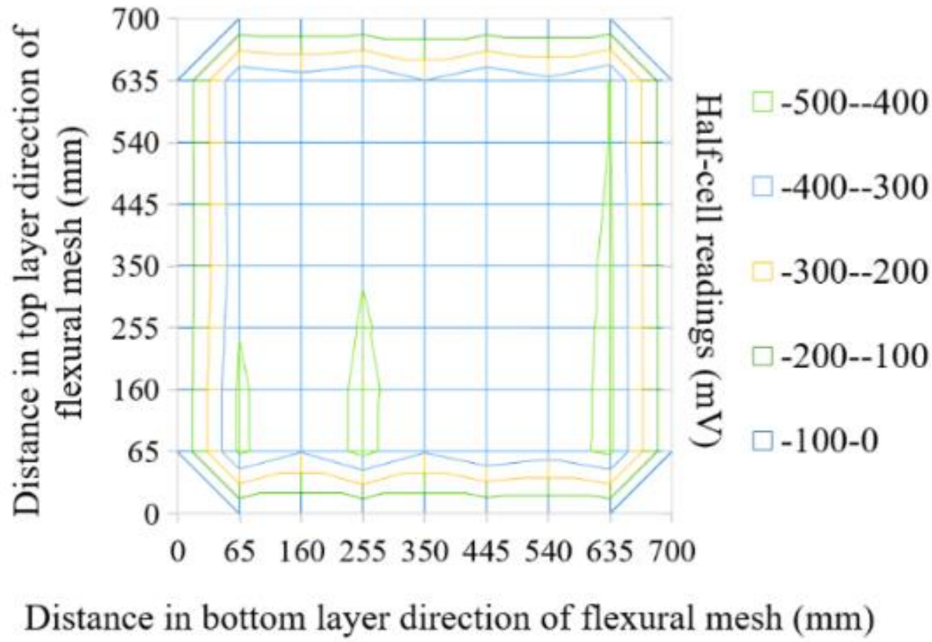

c. 36 days

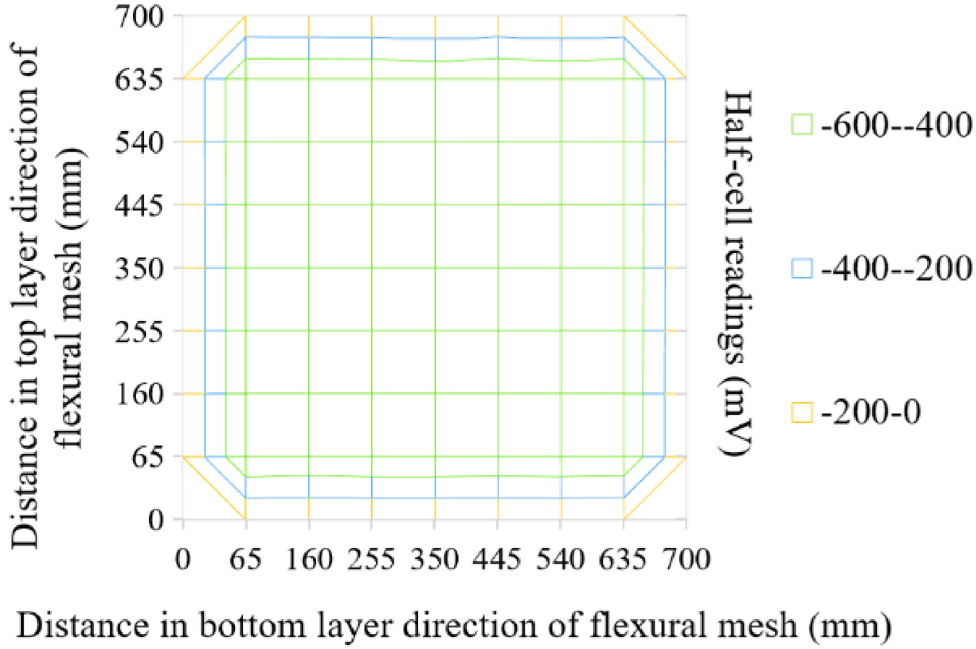

d. 75 days

Figure 3-15 Equipotential contour map for S25-D1.

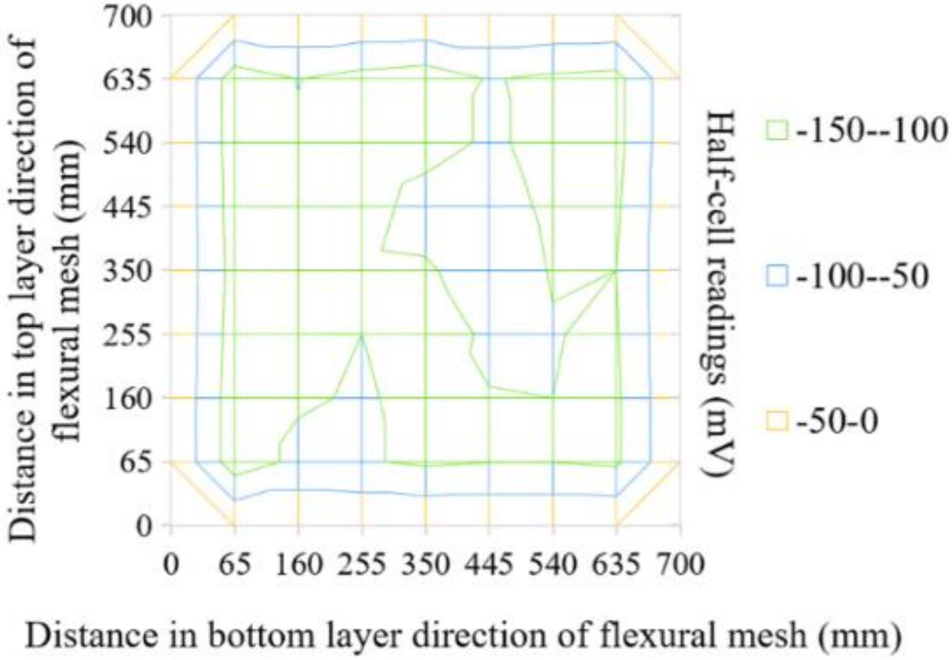

a. 3 days

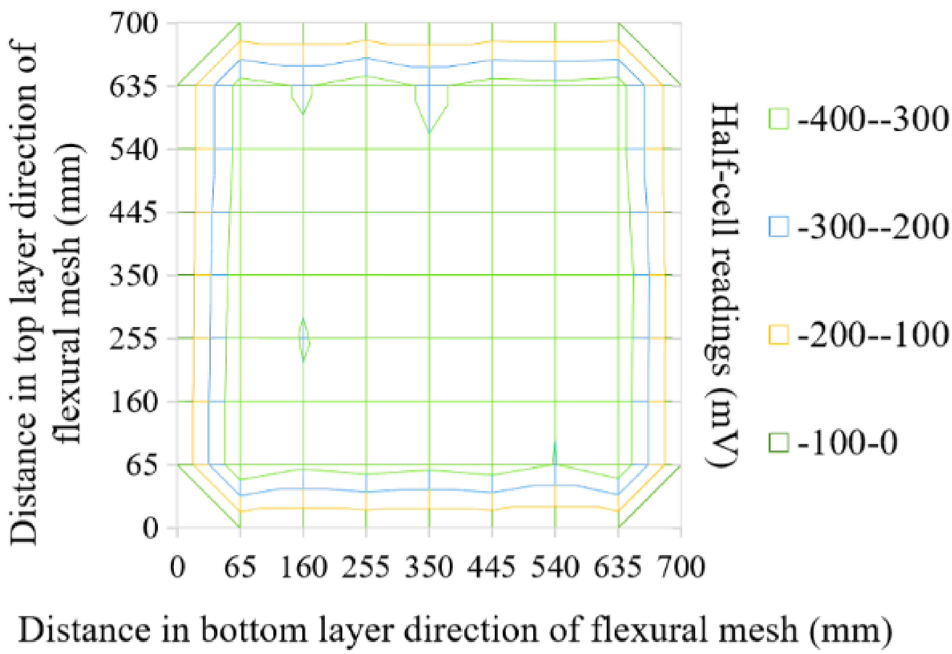

b. 9 days

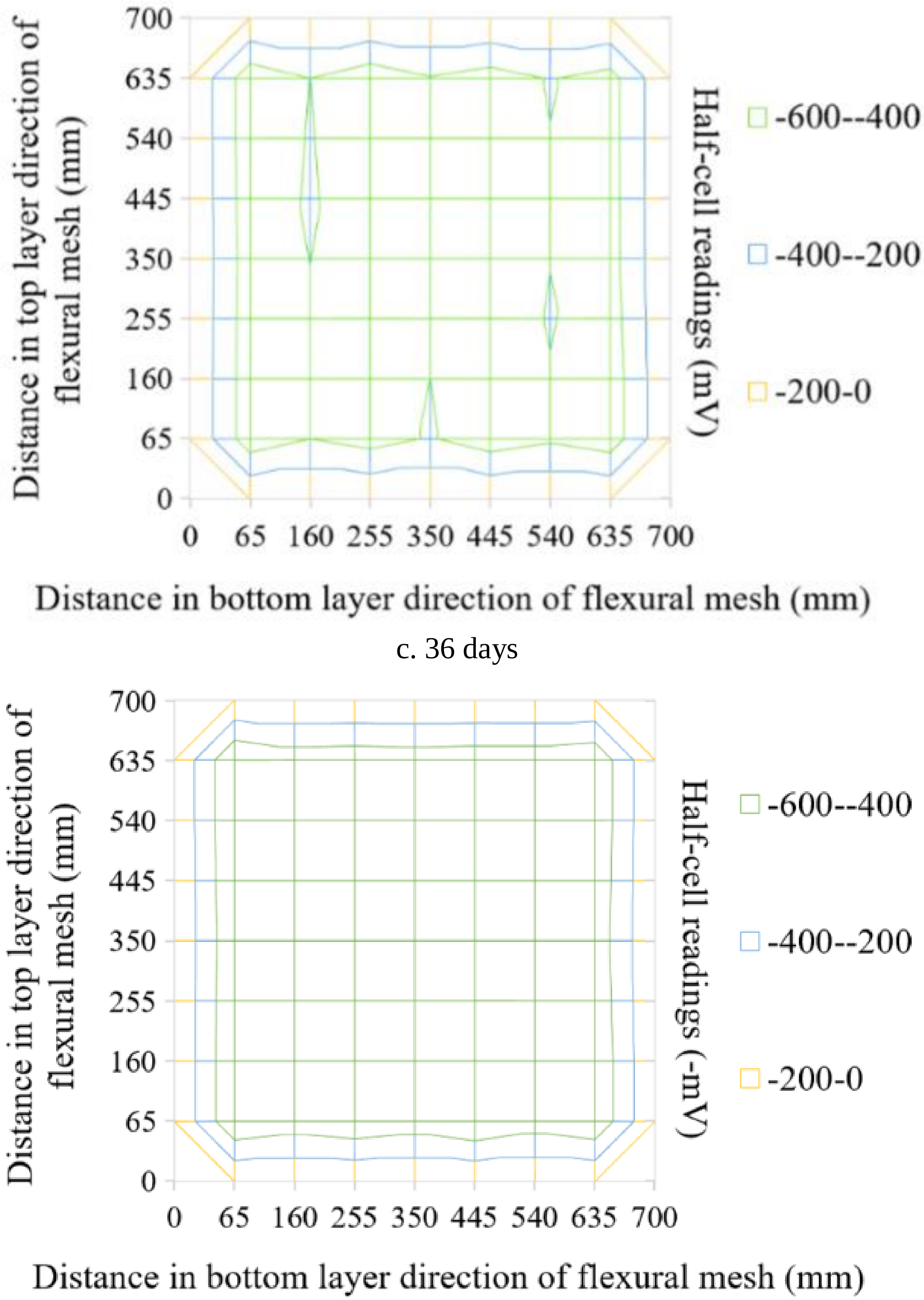

c. 36 days

d. 75 days

Figure 3-16 Equipotential contour map for S50-D1.

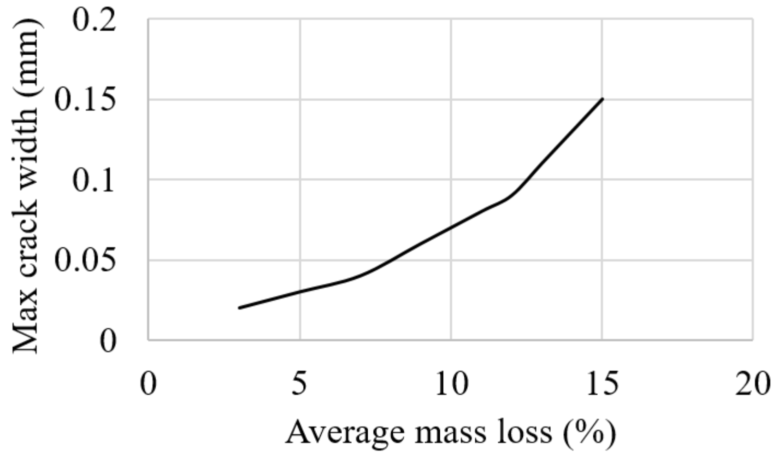

a. S15-D1

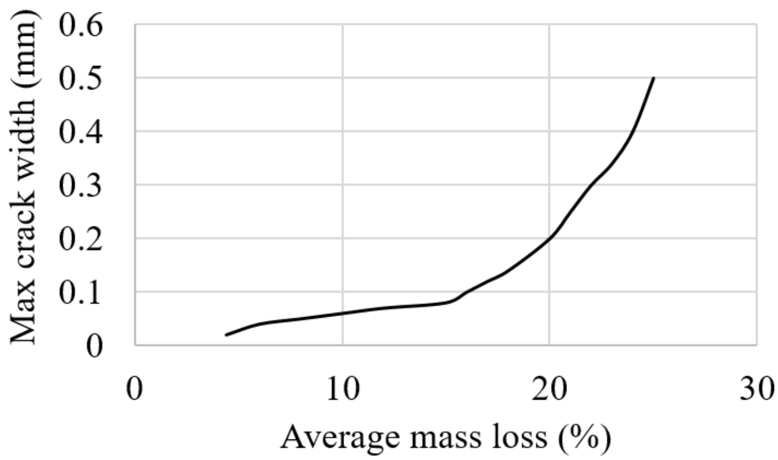

b. S25-D1

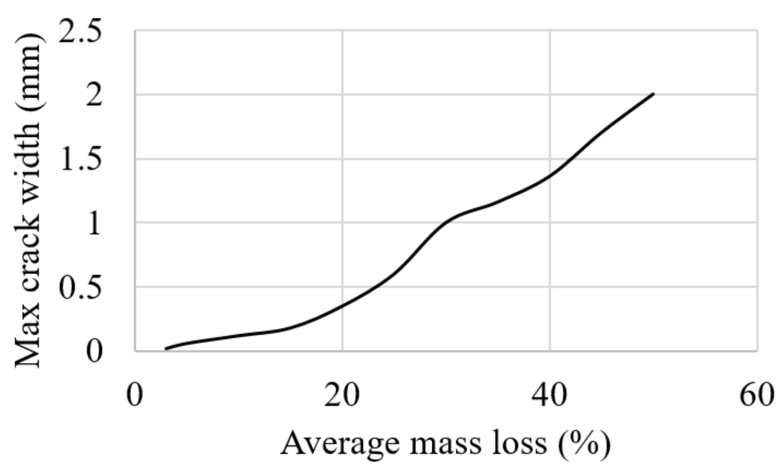

c. S50-D1

Figure 3-17 Maximum crack width propagation versus the corresponding mass oss.

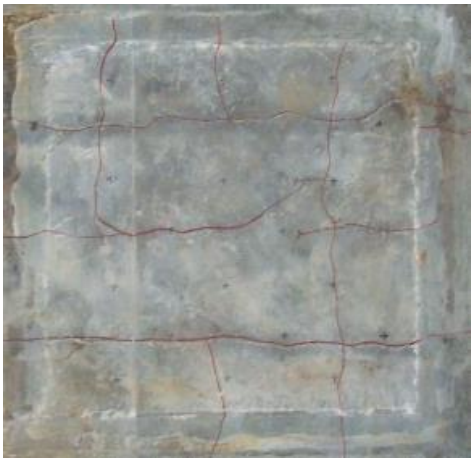

a. S15-D1 b. S25-D1

c. S50-D1

Figure 3-18 Cracks patterns due to corrosion over the corroded area.

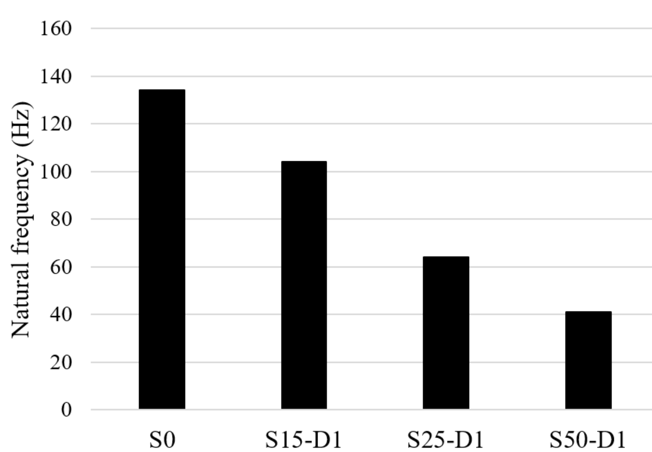

Figure 3-19 Natural frequency values for the tested slabs.

3.5.7. Chloride Content Measurements

Figure 3.20 presents the results of the chloride ion content in all tested slabs in both upper and lower layers of the flexural mesh. The average value of the chloride ion content at the top layer of the flexural mesh for S5, S25-D1, and S50-D1 was 0.79%, 1.222%, and 1.591%, respectively. This results indicated that the chloride content increased with the increased mass loss. This result confirms other researchers' results (Rasheeduzzafar 1990; Amleh & Mirza 1999), that the increases in the mass loss, increases chloride ion contents.

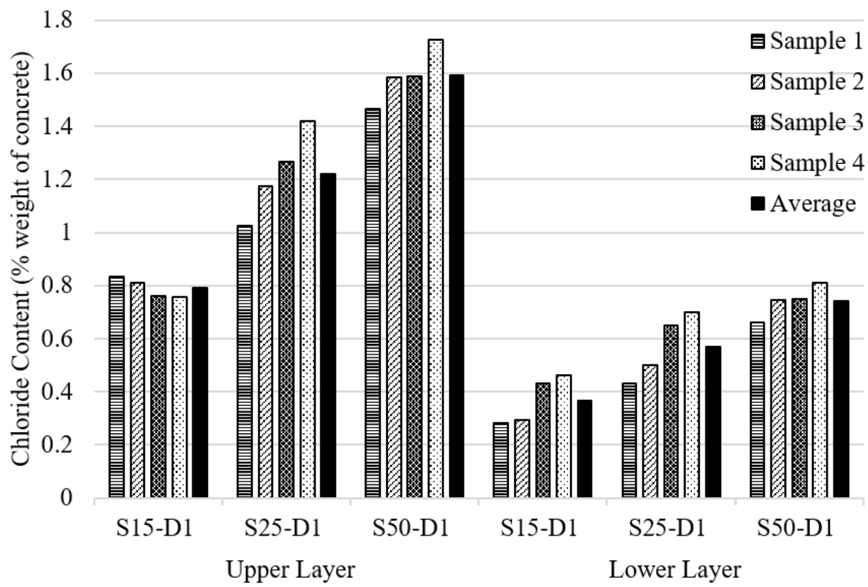

Figure 3-20 Chloride ion content values at upper and lower reinforcement mesh.

It has been found that the average value for chloride content at the lower layer of flexural mesh for S15-D1, S25-D1, and S50-D1 was 0.368%, 0.57%, 0.742%, respectively. Therefore, it has been concluded that the chloride content at the contact surface with the top layer of flexural mesh was higher than that at the contact surface with the lower layer of the flexural mesh for the tested slab. This could be attributed to the effect of concrete cover thickness, in which the top layer had a concrete cover thickness less than the lower layer; therefore, the chloride content had higher values in top layer than lower lone. This conclusion is similar to that found by other researchers (Amleh & Mirza 1999; Montemor et al. 2002), that the chloride content decreased with increasing of concrete cover thickness.

3.5.8. Mass Loss Measurements

Figure 3.21 shows the extracted corroded reinforcement for the tested slabs after removing the concrete cover. The corroded bars cleaned according to ASTM G1-03 (2003). Then the corroded bars weighted. Figure 3.22 shows a sample of corroded bars after extracting and cleaning them from corrosion products. Figure 3.23 shows the actual mass loss for each corroded bar in each tested slab. It has been noticed that the actual mass loss for all corroded bars did not exceed the targeted theoretical mass loss. This finding is similar to the finding that reached by other researchers on corrosion of concrete beams (Spainhour & Wootton 2008; YuBun Auyeung et al. 2000). Not all current used to causing ionization to the iron at the anode but there are some current passed through the water causing decomposition to the water particles into cations and anions. This decomposition released oxygen which appear as bubbles on the electrolyte solution surface (Chen & Luckham 1994). Hence, the current used to cause actual mass loss is less than that used to calculate the theoretical mass loss. Figure 3.24 shows the error between the actual mass loss for each corroded bar and the corresponding theoretical value. It has been concluded that the error between the actual and theoretical mass loss increased with the increase in mass loss. The average error was found equal to 1.1%, 24%, and 4.3% for S15-D1, S25-D1, and S50-D1, respectively. The maximum error value in S15-D1, S25-D1, and S50-D1 was 1.52%, 4.27%, and 5.32%, respectively. The increase of error could be attributed to the loss of current to overcome any corrosive products surrounded the bar under investigation, in which these corrosive products increase with the increase of the mass loss. However, the relation between the predicated and the actual mass loss is still perfect with a severe level of corrosion, which showed the efficiency of Faraday’s equation.

S15-D1

S25-D1

S50-D1

Figure 3-21 The corroded bars for each tested slab.

Figure 3-22 Samples of corroded reinforcement after the demolition of concrete cover.

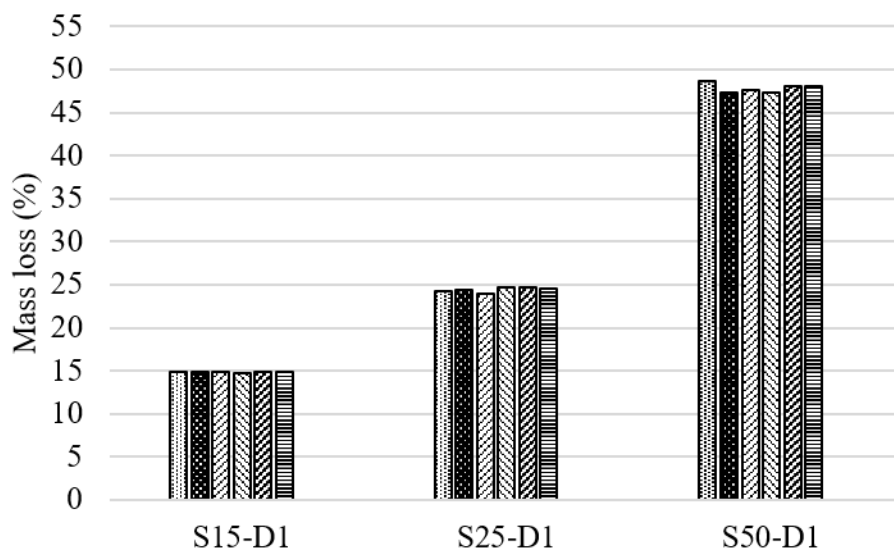

Figure 3-23 Mass loss % for all corroded bars in each slab.

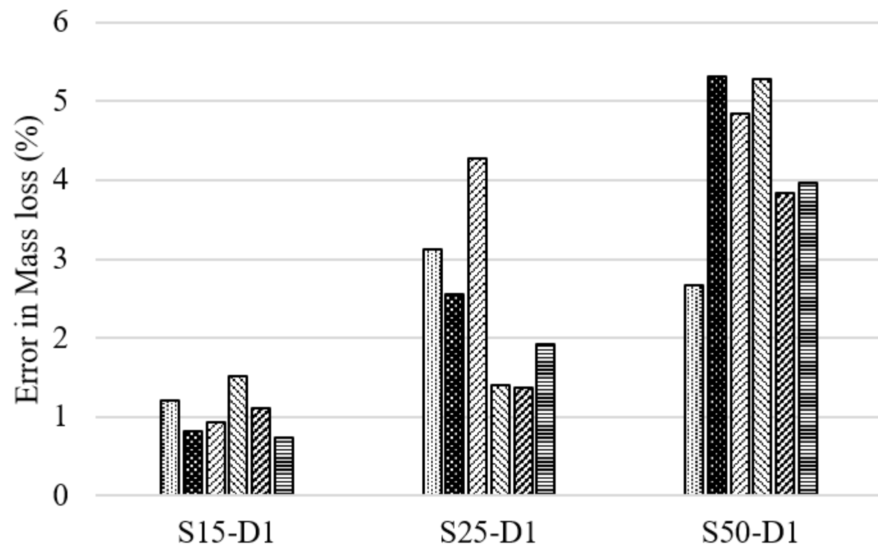

Figure 3-24 The error in mass loss % for all corroded bars in each slab.

3.6. Conclusion

The corrosion performance of RC two-way slabs was monitored. The following conclusions can be drawn:

- The performance of current to reach severe corrosion was monitored, which provided a complete view of this performance. In general, the current decreased in the initiation of test period formerly at a certain moment the current started to slightly increased. The first sag point from changing the current from decreasing to increasing rate considered the initiation of the corrosion. During the corrosion period, the current would suffer from sudden jumps and sudden drops on its value. The first sudden jump could be attributed to the induced cracks and the widening of their widths, which facilitated the conductivity of current to the embedded corroded bar especially with keeping the applied voltage constant without changing. Then followed by the first drop that was attributed to the excessive corrosive products that could lock the cracks widths, which affect the conductivity of the current. Any previous jump occurred on the current could be due to any widening in the cracks or any opening through the corrosive products enclosed inside cracks. When the cracks lock again the current dropped down and so on. This behaviour of current through the application of constant voltage technique did not provide any facility to predict the actual period of the corrosion test to reach the targeted corrosion behaviour.

- The equipotential mapping was constructed to monitor the corrosion of the embedded reinforcement. The mapping was drawn at different four ages for all tested specimen. For early periods, it has been noticed that the potential readings for the upper layer of flexural mesh were higher than the reading for the lower layer for the flexural mesh. Accordingly, the upper layer had higher chance to suffer from the probability of corrosion occurrence than the lower layer in the flexural mesh. This could be attributed to the effect of the concrete cover, in which the chloride ingress decreased with the increased of concrete cover. The half-cell readings, after corrosion has taken place, have no significant purpose because half-cell is a non-destructive tool used to give an indication of the occurrence probability of corrosion for un-corroded members.
- The maximum crack width was monitored during the corrosion test periods for all tested slabs. It has been found that the cracks width increased with the increased mass loss. This could be attributed to the corrosive products that were created beneath the concrete cover which created internal tensile pressure. Therefore, the internal tensile pressure would induced the cracks and widened them, and increased

with the increased mass loss. The crack widths could be an indication of the presence of corrosion especially when the half-cell readings have high negative values around the crack area.

- The natural frequency was measured for the tested slabs. It has been noticed that the natural frequency decreased with the increased value of the mass loss. This could be attributed to the bond loss between the corroded bars and the concrete covers due to the excessive corrosive products. This causing loss to the rigidity and weakened the stiffness of the slab, which affected the resonance and the natural performance of the tested slab. The natural frequency test could be considered as a non-destructive technique to be an indication of the presence of corrosion. More tests need to be done with different boundary conditions and more specimens to enhance the reliability of using natural frequency as an indication for the corrosion.
- The chloride content was measured for all tested slabs at the depth of the top and the lower layer for the flexural mesh. It has been found that the chloride content increased with the increased mass loss level, in addition, the chloride content decreased with the depth of measurement be farther from the surface.
- The constant voltage accelerated corrosion technique showed a close agreement between the actual and the theoretical mass loss. The actual mass loss for all corroded bars in any corrosion level was less than the theoretical mass loss. It has been noticed that the error between the actual and theoretical mass loss increased with the increased mass loss level. The maximum error between the two mass did not exceed 5.5%. Thus, Faraday's equation showed the perfect and close prediction for the mass loss in the corrosion tests of RC two-way slabs.

3.7. References

Ahmad, S. (2003) ‘Reinforcement corrosion in concrete structures, its monitoring and service life prediction - A review’, Cement and Concrete Composites, 25(4–5 SPEC), pp. 459–471. doi: 10.1016/S0958-9465(02)00086-0.

Ahmed, M. S. and Mohammad, F. A. (2014) ‘Theoretical modal analysis of freely and simply supported RC slabs’, International Journal of Mechanical, Aerospace, Industrial, Mechatronic and Manufacturing Engineering, 8(12), pp. 2026–2030.

Amleh, L. and Mirza, S. (1999) ‘Corrosion influence on bond between steel and concrete’, ACI Structural Journal, 96(3), pp. 415–423. doi: 10.14359/676.

Andrade, C. (1993) ‘Calculation of chloride diffusion coefficients in concrete from ionic migration measurements’, Cement and concrete research. Elsevier, 23(3), pp. 724–742.

Andrade, C. and Alonso, C. (1996) ‘Corrosion rate monitoring in the laboratory and on-site’, Construction and Building Materials, 10(5 SPEC. ISS.), pp. 315–328. doi: 10.1016/0950-0618(95)00044-5.

Andrade, C. and Alonso, C. (2001) ‘On-site measurements of corrosion rate of reinforcements’, Construction and Building Materials, 15(2–3), pp. 141–145. doi: 10.1016/S0950-0618(00)00063-5.

Aoude, H., Cook, W. D. and Mitchell, D. (2014) 'Effects of simulated corrosion and delamination on response of two-way slabs', Journal of structural Engineering, 140(1), pp. 1–9. doi: 10.1061/(ASCE)ST.1943-541X.0000775.

ASTM C1202-17a (2017) 'Standard Test Method for Electrical Indication of Concrete's Ability to Resist Chloride Ion Penetration', American Society for Testing and Materials., pp. 1–8. doi: 10.1520/C1202-12.2.

ASTM C143/C143M-15a (2015) 'Standard Test Method for Slump of Hydraulic-Cement Concrete'. ASTM International West Conshohocken, PA.

ASTM C150/C150M (2017) 'Standard specification for Portland cement', ASTM International, p. 9.

ASTM C1556-11a (2016) 'Standard Test Method for Determining the Apparent Chloride Diffusion Coefficient of Cementitious Mixtures by Bulk Diffusion', ASTM International, pp. 1–7. doi: 10.1520/C1556-04.2.

ASTM C876 (2015) 'Standard test method for corrosion potentials of uncoated reinforcing steel in concrete', p. 8. doi: 10.1520/C0876-09.2.

ASTM G1 (2003) Standard practice for preparing, cleaning, and evaluation corrosion test specimens.

Auyeung, Y., Balaguru, P. and Chung, L. (2000) 'Bond behavior of corroded reinforcement bars', Materials Journal, 97(2), pp. 214–220.

Bazant, Z. P. (1979) ‘Physical model for steel corrosion in concrete sea structures-theory’, ASCE J Struct Div. American Society of Civil Engineers (ASCE), 105(6), pp. 1137–1153.

Berto, L., Simioni, P. and Saetta, A. (2008) ‘Numerical modelling of bond behaviour in RC structures affected by reinforcement corrosion’, Engineering Structures. Elsevier, 30(5), pp. 1375–1385.

Bertolini, L., Elsener, B., Pedeferri, P., Redaelli, E. and Polder, R. B. (2013) Corrosion of steel in concrete: prevention, diagnosis, repair. John Wiley & Sons.

Broomfield, J. P. (2006) Corrosion of steel in concrete: understanding, investigation and repair, Second Edition. doi: 10.4324/9780203414606.

Cady, P. D. and Weyers, R. E. (1984) ‘Deterioration rates of concrete bridge decks’, Journal of Transportation Engineering. American Society of Civil Engineers, 110(1), pp. 34–44.

Carnot, A., Frateur, I., Zanna, S., Tribollet, B., Dubois-Brugger, I. and Marcus, P. (2003) ‘Corrosion mechanisms of steel concrete moulds in contact with a demoulding agent studied by EIS and XPS’, Corrosion science. Elsevier, 45(11), pp. 2513–2524.

Chen, T. Y. and Luckham, P. F. (1994) ‘A study of the electrical current passing through water-activated electro-rheological fluids’, Jpournal pf Physics D: Applied Physics, 27(7), p. 1556.

Chitty, W.-J., Dillmann, P., L'Hostis, V. and Lombard, C. (2005) 'Long-term corrosion resistance of metallic reinforcements in concrete—a study of corrosion mechanisms based on archaeological artefacts', Corrosion Science. Elsevier, 47(6), pp. 1555–1581.

Cornet, I., Ishikawa, T. and Bresler, B. (1968) 'Mechanism of steel corrosion in concrete structures', Materials Protection, 7(3), p. 45.

Coronelli, D. and Gambarova, P. (2004) 'Structural assessment of corroded reinforced concrete beams: modeling guidelines', Journal of Structural Engineering. American Society of Civil Engineers, 130(8), pp. 1214–1224.

CSA A23.1-14 (2014) Concrete materials and methods of concrete construction/Test methods and standard practices for concrete, CSA Group, Mississauga, Ontario, Canada.

CSA A23.3-14 (2014) Design of concrete structures. Mississauga, Ont.: Canadian Standard Association.

Dodd, L. L. and Restrepo-Posada, J. I. (1995) 'Model for predicting cyclic behavior of reinforcing steel', Journal of Structural Engineering. American Society of Civil Engineers, 121(3), pp. 433–445.

El-Maaddawy, T. and Soudki, K. (2003) 'Effectiveness of impressed current technique to simulate corrosion of steel reinforcement in concrete', Journal of Materials in Civil Engineering. American Society of Civil Engineers, 15(1), pp. 41–47. doi: 10.1061/(ASCE)0899-1561(2003)15:1(41).

Fedrizzi, L., Azzolini, F. and Bonora, P. L. (2005) 'The use of migrating corrosion inhibitors to repair motorways' concrete structures contaminated by chlorides', Cement and concrete research. Elsevier, 35(3), pp. 551–561.

Gerhardus H. Koch, M. P. H. B. (2002) Corrosion costs and preventive strategies in the United States, Nace International.

Klinghoffer, O. (1995) 'In situ monitoring of reinforcement corrosion by means of electrochemical methods', Nordic Concrete Research, 95(1), pp. 1–13. Available at: http://www.germann.org/Publications/GalvaPulse/2. Klinghofer, O., In Situ Monitoring of Reinforcement Corrosion by means of Electrochemical Methods, Nordic Concrete Research 95 1.pdf.

Konecný, P. (2007) Reliability of reinforced Concrete bridge decks with respect To ingress of chlorides, Department of Structural Mechanics\Faculty of Civil Engineering\ University of Ostrava. doi: 10.13140/RG.2.1.3729.4165.

Lachemi, M., Al-Bayati, N., Sahmaran, M. and Anil, O. (2014) 'The effect of corrosion on shear behavior of reinforced self-consolidating concrete beams', Engineering Structures. Elsevier Ltd, 79, pp. 1–12. doi: 10.1016/j.engstruct.2014.07.044.

Litvan, G. G. (1982) 'Evaluation and repair of deteriorated garage floors', Canadian Building Digest, Division of Building Research, p. 4.

Miyagawa, T. (1991) ‘Durability design and repair of concrete structures: chloride corrosion of reinforcing steel and alkali–aggregate reaction’, Magazine of Concrete Research. Thomas Telford Ltd, 43(156), pp. 155–170.

Montemor, M. F., Cunha, M. P., Ferreira, M. G. and Simões, A. M. (2002) ‘Corrosion behaviour of rebars in fly ash mortar exposed to carbon dioxide and chlorides’, Cement and Concrete Composites, 24(1), pp. 45–53. doi: 10.1016/S0958-9465(01)00025-7.

Moreno, E. I., Solís-Carcaño, R. G., Varela-Rivera, J., Pacho-Monforte, J. C. and Cua-Cuevas, R. A. (2015) ‘Diffusion of chlorides in pozzolanic concrete made with high-absorption aggregates exposed under tropical marine environment’, International Journal of Electrochemical Science, 10(8), pp. 6444–6453.

Neville, A. M. (2011) Properties of concrete (Fifth Edition), Cement and Concrete Research. doi: 10.1016/0008-8846(96)82366-0.

Park, J. I., Lee, K. M., Kwon, S. O., Bae, S. H., Jung, S. H. and Yoo, S. W. (2016) ‘Diffusion decay coefficient for chloride ions of concrete containing mineral admixtures’, Advances in Materials Science and Engineering, 2016. doi: 10.1155/2016/2042918.

Rasheeduzzafar (1990) ‘Effect of Tricalcium Aluuminate Content of Cement on Corrosion of Reinforced Steel in Concrete’, Cement and Concrete Research, (89), pp. 723–738.

Raupach, M. (1996) ‘Chloride-induced macrocell corrosion of steel in concrete - Theoretical background and practical consequences’, Construction and Building Materials, 10(5 SPEC. ISS.), pp. 329–338. doi: 10.1016/0950-0618(95)00018-6.

Reilly, J. L., Cook, W. D., Bastien, J. and Mitchell, D. (2014) 'Effects of delamination on the performance of two-way reinforced concrete slabs', Journal of Performance of Constructed Facilities, 28(4), pp. 1–8. doi: 10.1061/(ASCE)CF.

Roberge, P. R. and Pierre, R. (1999) Handbook of corrosion engineering library of congress cataloging-in-publication data. doi: 10.1016/S0026-0576(00)83445-5.

Spainhour, L. K. and Wootton, I. A. (2008) 'Corrosion process and abatement in reinforced concrete wrapped by fiber reinforced polymer', Cement and Concrete Composites. Elsevier, 30(6), pp. 535–543.

Chapter 4 Effect of Bandwidth Reinforcement Corrosion on the Response of Two Way Slabs

4.1. Abstract

The present work was conducted to investigate the influence of different levels of mass loss, due to corrosion of reinforcement, on the structural behaviour of two-way reinforced concrete slabs. Four full-size two-way reinforced concrete slabs were cast for this investigation. Four levels of corrosion were reached: 0% of mass loss, control; 15% mass loss, mild corrosion level; 25% mass loss, moderate corrosion level; and 50% mass loss, severe corrosion level. These levels were achieved using an accelerated corrosion technique. The targeted corroded area was chosen to be around the column bandwidth as defined in CSA A23.3-14. The performance of the slabs was evaluated in terms of cracking behaviour, deflection profiles, slab rotation, energy absorption, ductility, and load carrying capacity. In general, an increase in the corrosion level had a negative impact on the load capacity and stiffness. On the other hand, energy absorption, deflection, and ductility seem to increase with the increase in mass loss. The capacity of each slab is compared with the design values using four codes. By reducing the reinforcement ratio with an amount equivalent to the mass loss, it could conclude that both BS 8110-97 and EC2 can still reasonably predict the actual capacity of the corroded slabs.

Keywords: Accelerated corrosion technique; two-way reinforced concrete slabs; deflection; ductility index

4.2. Introduction

Deterioration of numerous reinforced concrete (RC) structures due to corrosion is a serious worldwide issue (Roberge & Pierre 1999). Corrosion is an old problem facing civil engineers since at the beginning of mining and refinery of metals (Broomfield 2006). The researchers got engaged in studying the corrosion of RC structures when problems started to appear in the North America highways due to the use of de-icing salts. In addition to the flourishing construction in the Arabian Gulf region which is distinguished by their ambient salinity air (Broomfield 2006). The battle against corrosion is also a problem for offshore industry, pipelines, any structures, and equipment widely exposed to seawater, relative humidity, and ambient salty air. The formation of flexural or shrinkage cracks in RC structures exists in corrosive environment. For instance, salt-laden condensation, contaminated rainwater, and carbon dioxide gases. This mixture in the presence of moisture could penetrate the cracks in concrete covers reaching the embedded steel reinforcement which accelerate the corrosion process (Zhang et al. 2004).

Many studies were conducted from different point of views about corrosion. Some studies aimed to provide better explanation and understanding of the corrosion process (Raupach 1996; Carnot et al. 2003; Chitty et al. 2005), while other studies investigated the behaviour of corroded beams compared to un-corroded ones, for example, El Maaddawy & Soudki (2003). Furthermore, others carried out research on monitoring the corrosion of RC elements under both laboratory and field conditions (Andrade & Alonso 1996; Andrade & Alonso 2001; Ahmad 2003; Gowda et al. 2017; Andrade & C. Alonso 2004). In addition, other studies were involved with the development of numerical models to predict the behaviour of corroded beams (Dodd & Restrepo-Posada 1995; Berto et al. 2008; Coronelli & Gambarova 2004). Moreover, some researchers studied the repairing techniques and rehabilitation methods for corroded beams (Bertolini et al. 2013; Miyagawa 1991; Fedrizzi et al. 2005; Broomfield 2006). Nonetheless, there is a lack of studies about the corrosion of slab-column connections which is considered the most vulnerable element in two-way slabs systems (Aoude et al. 2014). Many parking garages and bridge decks suffered from corrosion especially in North America due to the excessive use of de-icing salts (Donnelly et al. 2006). To eliminate the corrosion problems in structures that are exposed to any corroding agents such as de-icing slats, Glass Fiber-Reinforced Polymer (GFRP) has been successfully used instead of conventional reinforcement (El-Gamal et al. 2009).

Constant volt accelerated corrosion technique has been used to study the effect of corrosion on beams (Pellegrini-Cervantes et al. 2013; Al-Swaidani & Aliyan 2015; Kumar et al. 2012; Lee et al. 2000; Deb & Pradhan 2013; Amleh 2000; Ahwazi 2001). In this technique, an electrochemical potential is applied to the reinforcement steel that works as an anode and an internal or external cathode. A constant voltage is applied to the corroded specimen. The constant volt for several studies varied from 5V to 30V (Ahwazi 2001; Yoon et al. 2001; Xia et al. 2012). The corrosion is monitored by measuring the current using a computer-controlled data acquisition system to measure the theoretical mass loss according to Faraday's equation.

Rahman (1992) examined the effect of corrosion on the structural behaviour of two-way slab-column connection. Twelve slabs with reinforcement and post-tension tendons were tested. The corrosion of the reinforcement was simulated by using fewer top reinforcement.

This was done to reflect the mass loss of the reinforcement due to corrosion. The corrosion of post-tension slabs was simulated by reducing the tendons numbers and replacing some with empty sheathes to act as broken tendons. The author concluded that reducing reinforcement and tendons mass reduces the strength of the corroded slabs. He found that 50% of mass loss in reinforcement and tendons caused 30% drop in the punching shear capacity. The author also studied the effect of loss of bond and effect on delamination on the punching capacity by wrapping the reinforcement with adhesive plastic tape. Whereas the delamination was simulated by placing polyethylene sheets between the flexural reinforcement top and bottom layers. It was concluded that loss of bond and delamination cause more deflections and cracks; however, they had a small effect on the punching capacity. This finding was unexpected. Aoude et al. (2014) investigated the effect of both corrosion and delamination. Again, the authors simulated the corrosion of reinforcement by using smaller bar diameters and the delamination by placing a plastic sheet under the flexural reinforcement mesh. One level of corrosion, 50% of the mass loss was investigated. The effect of three different delaminated areas was examined; the area around the column bandwidth, the area around development length, and the area when the reinforcement only had half of its development length. The authors concluded that small delaminated area did not have a significant effect on the punching shear capacity. When the delaminated area was increased, the punching shear capacity decreased. As well, the reduced bar area caused a loss of the punching capacity. The effect of reducing the bar area and delamination on the slabs caused more cracks and large widths. The research team, Reilly et al. (2014), also studied the effect of different delaminated areas on the structural behaviour of two-way slabs. The delamination area was mimed by placing a plastic sheet beneath the reinforcement. It was concluded that the increase of delamination area caused a decrease in both post-punching stiffness and punching capacity.

The previous experimental work to simulate corrosion in two-way slabs has several flaws. Firstly, reducing the bar diameter or numbers to simulate the mass loss caused a change in the reinforcement ratio of the whole slab and not only for the targeted corroded area which could affect the slab capacity. Secondly, the change in bar diameter does not give a realistic representation of the effect of corrosion on the loss of bond. Furthermore, the bars wrapped with plastic tape still have bond between the bar and concrete cover which misrepresent the loss of bond due to corrosion.

Nevertheless, until now there is no corrosion on two-way RC slabs by using accelerated corrosion techniques. Such research would provide actual simulation of the behaviour of the bond, the change of steel mechanical properties, and the cracking of the concrete cover under corrosion. Thus, a better understanding of the behaviour of corroded two-way RC slabs would be developed.

4.3. Research Significance

The behaviour of two-way RC slabs under realistic corrosion conditions is not yet examined. The available literature lacks information about the behaviour of two-way slabs with corroded reinforcement. The purpose of this research is to evaluate the performance and durability of two-way RC slabs under realistic corrosion conditions. The investigation covers the evaluation of the structural performance under different levels of corrosion (mild, moderate, and severe). The corrosion conditions considered in this paper is a true representation of the bond deterioration between the reinforcement and concrete cover.

Moreover, this experiment gives better simulation of both the crack growth in concrete cover and steel mechanical properties deterioration due to corrosion. The investigation will provide engineers with a better understanding that guides them in assessing the performance and integrity of deteriorated slabs.

4.4. Experimental Program

4.4.1. Details of Test Specimen

Four RC slabs with identical dimension (1900 mm × 1900 mm × 150 mm) were constructed. The details are shown in Fig. 4.1. The tension reinforcement ratio (ρ) was kept constant at 1% and consisted of 15M bars with bar spacing of 190 mm. The compression reinforcement consisted of 10M with a spacing of 300 mm. The tension and compression reinforcement were placed with a clear concrete cover of 30 mm. The tension reinforcement bars were subjected to corrosion. Therefore, the intersection points between bars were insulated, to avoid any conductivity between them, using electrical tape between the contact surfaces. Also, plastic ties were used instead of steel ties. This insulation helped to control the corrosion level for each bar separately and to ensure uniform corrosion within the targeted corroded area. The reinforcement was placed inside the formwork as shown in Fig. 4.2. The concrete was placed in the formwork and a mechanical vibration was used to compact the concrete during the pouring process. After 24 hours from casting the slabs, the column stub was poured. After a day from casting column stub, the formwork was de-moulded. A water-curing process started till the fourth day of casting the slab followed by air curing until the end of 28 days. The details of the test specimens are shown in Table 4.1.

The control slab (S0) was used as a reference and was considered to be subjected to 0% mass loss. The other three slabs were subjected to three different levels of corrosion, mild, moderate, and severe. S15-D1 was mild corroded slab that was corroded to 15% mass loss. S25-D1 was corroded till 25% mass loss as the moderate one. The last was the severe by corroded slab, S50-D1, which reached 50% mass loss. The corroded area was chosen as the reinforcement bandwidth of c + 3h (700 mm × 700 mm), where c is the column dimension and h is the slab thickness, as defined in CSA A23.3-14 (2014) as shown in Fig. 4.3.

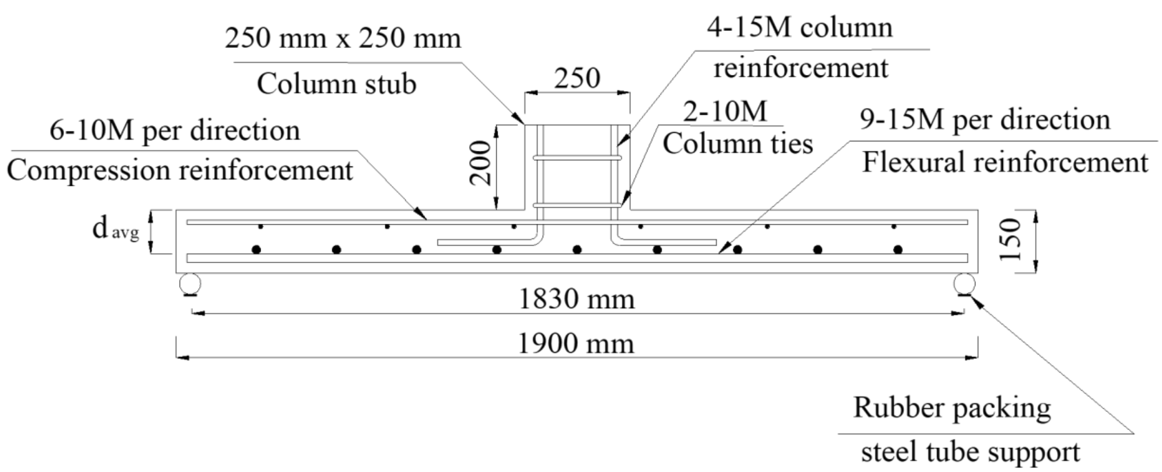

Figure 4-1 Details of a typical slab.

Table 4-1 Detailed of Slab Specimens

Side dimensions (mm × mm)	h (mm)	c (mm)	d (mm)	f'_c (MPa)	Main reinforcement
1900 × 1900	150	250	104	41.1	Two layers-15M bars (ρ = 1%)

*h is the height; c is column width; d is the effective slab depth; ρ is the reinforcement ratio; and f'_c is the concrete compressive strength.

Figure 4-2 Formwork and reinforcement mesh.

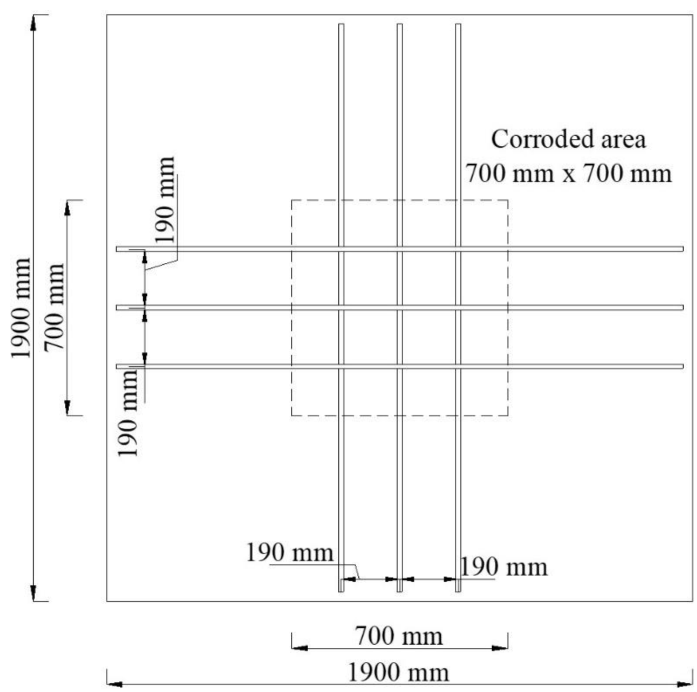

Figure 4-3 The targeted corroded area.

4.4.2. Material Properties

The concrete used in pouring the slabs was supplied by a local batch plant. The cement was a Normal Portland cement similar to Type I (ASTM C150/C150M 2017), with a specific gravity of 3.15. A maximum aggregate size of 10 mm and natural sand, both had a specific gravity of 2.6, were used. Class F3 exposure as specified in ACI 318 was considered in determining the desired water to cement ratio (w/c) and the minimum compressive strength. This class takes into consideration concrete that is exposed to freezing-thawing cycles and to the accumulation of snow and ice with de-icing chemicals (ACI 318-14 2014). Therefore, w/c used was 0.4 and the compressive strength was 40 MPa. The mix composition is shown in Table 4.2. The measured properties of the reinforcement and mechanical properties of the concrete are shown in Table 4.3.

Table 4-2 Mix Composition of One Meter Cube of Concrete

Cement (kg)	w/c	Water (l)	C/F	C.A. (kg)	F.A. (kg)	Aggregate size (mm)	Fresh density (kg/m^3)
350	0.4	140	1.3	1083	833	10	2407

* w/c is the water to cement ratio, C/F is the coarse to fine ratio, C.A. is the coarse aggregate, and F.A. is the fine aggregate

Table 4-3 Steel and Concrete Properties

Designation	Steel properties			Concrete Properties	
	Area (mm^2)	f_y (MPa)	ε_y ($\mu\varepsilon$)	f'_c (MPa)	f_r (MPa)
15M	200	475	2200	41.1	3.82

* f_y is the yield strength, ε_y is the yield strain, f'_c is the compressive strength, and is f_r the modulus of rupture.

4.4.3. Accelerated Corrosion Setup

The setup of the accelerated corrosion technique consisted of: A source of direct current (power supply), electrolyte solution, a cathode as steel mesh, computer, data acquisition system, a current transducer, electrical board, hose, valve, and foam sheets. Figure 4.4 shows a schematic diagram for the constant voltage accelerated corrosion technique setup used in this study. First, each slab was placed in an upside-down levelled position. The foam sheets were used to construct a dike above the targeted corroded area. A hose with a valve was attached to the lowest level point of the dike to facilitate the emptying of the dike from the electrolyte solution. The steel mesh that acted as a cathode was placed inside the dike above the targeted corroded area then connected to the ground of the power supply. The dike was then filled with the electrolyte solution. The solution consisted of 5% sodium Chloride by weight of water. The solution was replaced every week to keep a constant concentration of the sodium chloride. The positive charge of the power supply was connected to the targeted corroded bars which worked as an anode. The power supply was adjusted to maintain the condition of a constant voltage of 15 V.

The theoretical mass loss is calculated based on Faraday's equation as shown in Eq. 4.1:

$$\text{Mass loss} = \frac{t\,I\,M}{z\,F} \qquad 4.1$$

where t is the time passed in seconds, I is the current passed in Amperes, M is the atomic weight (for iron M=55.847 g/mol), z is the ion charge (two moles of electrons), and F is Faraday's constant which is the amount of electrical charge in one mole of electron. The constant F was assumed as 96,487 coulombs per mole (C/mol) (Lachemi et al. 2014).

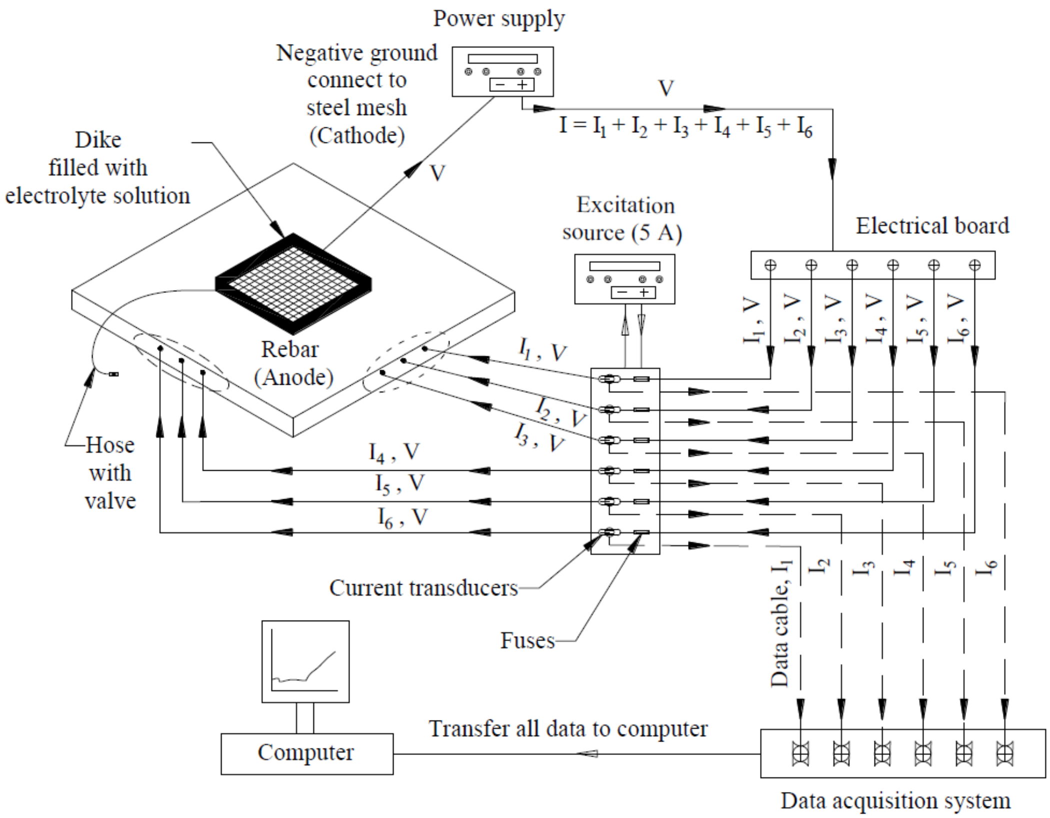

Figure 4-4 A Schematic diagram for the accelerated corrosion setup.

The theoretical mass loss has the current as a parameter. Therefore, the input current had to be measured for each targeted bar. The test was stopped when the bar reached the targeted mass loss based on the measured current. Most of the data acquisition system available at laboratories are equipped to measure voltage only. Consequently, current transducers were used to convert the input current reading to a voltage reading and sent it to the data acquisition system. After that, the recorded voltage was converted into current readings using a calibration equation for each current transducer. Each slab had six bars that needed to be corroded within the targeted area. An electrical distribution board, connected in parallel, was used to split the current with a constant volt of 15 V from the power supply to six outlets. Each outlet had the same voltage value but different current readings. It took 75, 112, and 249 days to reach the targeted level of corrosion for slabs S15-D1, S25-D1, and S50-D1, respectively.

4.4.4. Test Setup and Instrumentation

The slabs were tested in a vertical position by applying a concreated load through the column stub as shown in Fig. 4.5. The supports represented the lines of contra-flexure; therefore, the slabs were simply supported along all four edges. The applied load was monitored and recorded using a pressure gauge connected to the hydraulic jack. The load was applied in small increments. During the loading, the deflection and the crack widths were monitored and recorded using the data acquisition system. Five linear variable differential transformers (LVDT) were used to measure the deflection profile. Four LVDTs were placed in the front of the slab and one LVDT was placed on the back side of the slab as shown in Fig. 4.6. Five crack gauges with a capacity of $\pm$ 5 mm were used to measure the crack widths during the loading test. The initial crack widths before the start of the test were measured using a crack measuring microscope with an accuracy of 0.02 mm and 60× focusable eyepiece magnifier. The control slab, S0, has no cracks before the loading test; therefore, a pre-cracking load was applied to induce cracks in order to be able to setup the crack gauges to measure the crack widths during the loading. The intial pre-crack widths were measured using the microscope

a. Back view

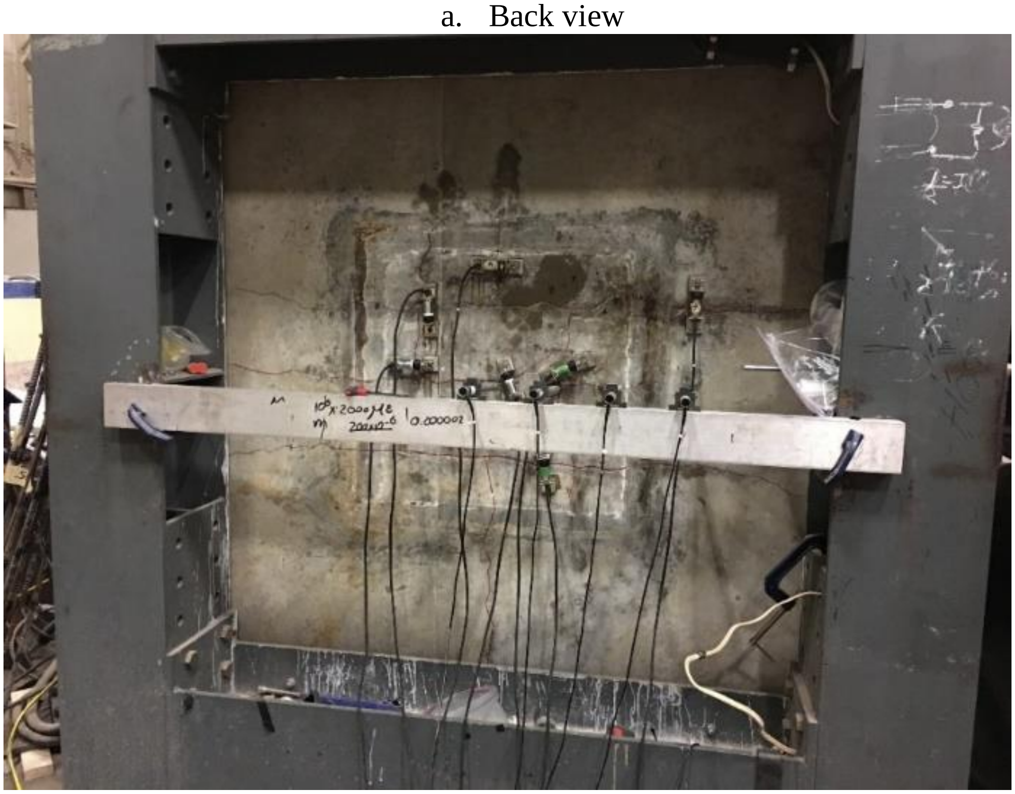

b. Front view

Figure 4-5 A slab in the loading frame and instrumentation used.

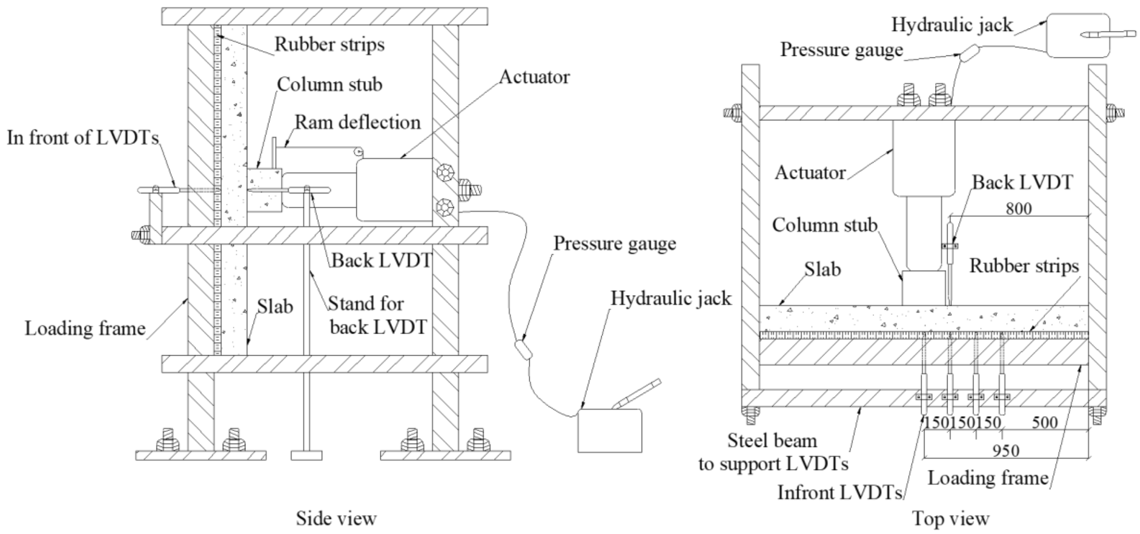

Figure 4-6 Plan view sketch for the loading test setup.

4.5. Test Results and Discussion

4.5.1. Load Carrying Capacity

The load versus central deflection plots for all slabs are shown in Fig. 4.7. It can be noticed that the failure load of all corroded slabs were above the service load for the reference specimen by 44.7%, 36.2%, and 14.5% for slabs S15-D1, S25-D1, and S50-D1, respectively. The service load is assumed as 60% of the ultimate load of the control slab which is equal to 235 kN (Aoude et al. 2014). The serviceability load was attained even for severe levels of corrosion. The ultimate capacity was 391 kN, 340 kN, 320 kN, and 269 kN for slabs S0, S15-D1, S25-D1, and S50-D1, respectively. Compared to the control specimen, the punching shear capacity was reduced by 13.1%, 19.5%, and 31.2% for slabs S15-D1, S25-D1, and S50-D1, respectively.

Table 4.4 shows a summary of the test results. There was a close agreement between S50-D1 and a previous study by Aoude et al. (2014). Aoude et al. simulated the mass loss by decreasing the reinforcement bars from 15M to 10M which was considered as 50% mass loss. Moreover, the delamination was mimed by placing steel sheet under the concrete cover. The study found that the punching capacity was reduced by 24%. There is around 7% difference in the reduction of the punching shear capacity with 50% mass loss between Aoude and the current test results. This could be attributed to two reasons: first, simulating corrosion by reducing bar diameter would cause a reduction of the reinforcement ratio of the slab. Several studies concluded that the punching shear capacity of two-way slabs is reduced as a result of the reduction in the flexural reinforcement ratio (Marzouk & Hussein 1991; Dilger et al. 2005). Second, the study by Aoude (2014) failed to simulate the loss in bond between the corroded bars and the concrete cover, whereas the current study used an accelerated technique that caused realistic corrosion and; consequently, loss of bond.

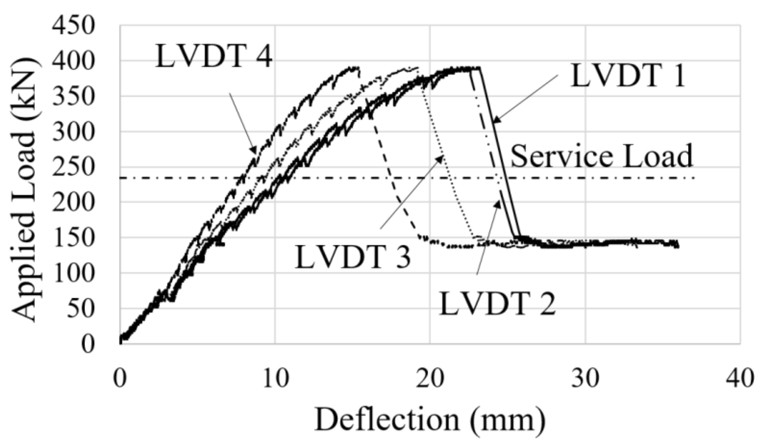

a. S0

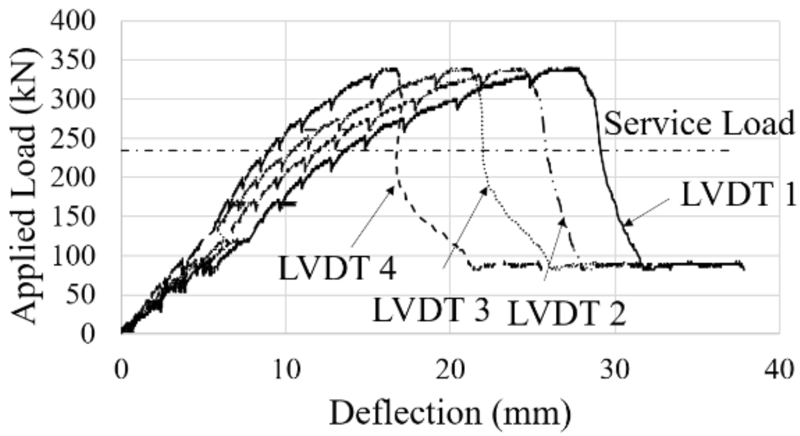

b. S15-D1

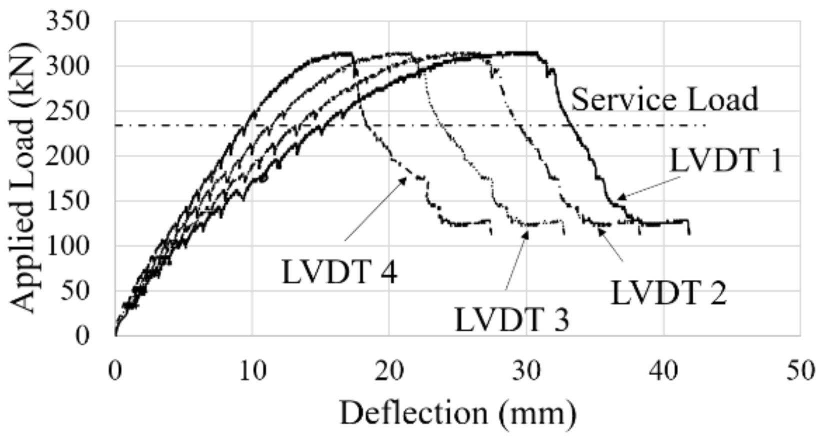

c. S25-D1

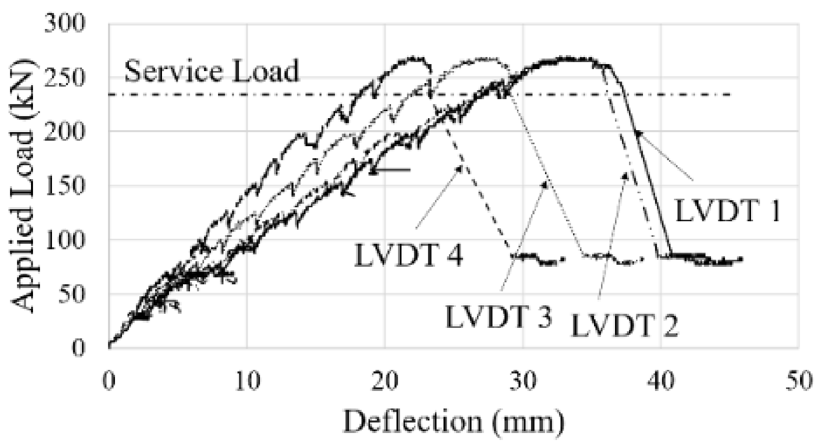

d. S50-D1

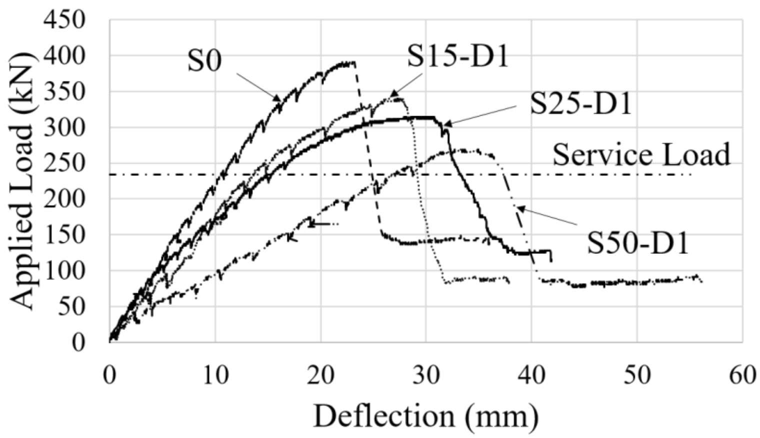

e. Applied load vs. mid-span deflection for each slab
Figure 4-7 Applied load vs. deflection.

Table 4-4 Summary of Test Results

Specimen	w_c (mm)	Service Load P_{SL} (kN)	Service Load Δ_{SL} (mm)	Service Load w_{SL} (mm)	Ultimate P_u (kN)	Ultimate Δ_u (mm)	Ultimate w_{max} (mm)
S0	0.00	235	10.6	0.71	391	21.8	2.49
S15-D1	0.15	235	13.6	2.00	340	26.0	3.86
S25-D1	0.50	235	15.3	5.00	315	28.5	7.62
S50-D1	2.00	235	27.0	6.60	269	32.7	8.33

w_c is the maximum corrosion crack width, P_{SL} is the service load for the un-corroded slab S0, Δ_{SL} is the deflection corresponding to the service load, w_{SL} is the maximum crack width at the service load, P_u is the ultimate load, Δ_u is the corresponding deflection, and w_{max} is the maximum crack width at ultimate load.

4.5.2. Stiffness

The stiffness is defined as the slope of the load-deflection curve. The stiffness values were found to be 17.8 kN/mm, 16.4 kN/mm, 13.2 kN/mm, and 9.1 kN/mm for S0, S15-D1, S25-D1, and S50-D1, respectively. From Fig. 4.7, it can be seen that increasing the percentage of mass loss appeared to decrease the stiffness of the corroded slabs. The mild level of corrosion reduced the stiffness by 7.9%, while the moderate level of corrosion S25-D1 dropped the stiffness by 25.8%, and the severe level of corrosion S50-D1 caused a 48.8% reduction in the stiffness. The lower slopes of the load-deflection curves could be attributed to the mass loss that resulted in a reduction in the load that caused yielding of the reinforcement and the loss of the bond between reinforcement and concrete cover. Moreover, as moss loss increased, the crack width due to corrosion became wider which also diminished the overall stiffness of the slab. In contrast, the reference slab S0 had the steepest slope of the load-deflection curve. The slope was highest till reaching the cracking load 58 kN. The slope then decreased gently with the increase in the numbers of the developed crack till reaching the yielding of reinforcement. Hereafter, a significant decrease in the slope was observed till the load reached the ultimate value and; subsequently, a sudden drop occurred in the load.

4.5.3. Slab Rotation and Energy Absorption

The energy absorption is calculated as the area under the load versus the central deflection curve up to failure (Fig. 4.7-e). The energy absorption values for slabs S0, S15-D1, S25-D1, and S50-D1 are 6157, 6601, 7540, and 6529 kN.mm, respectively. The results indicated the trend that the energy absorption capacity increased as the mass loss increased till the corrosion level reach 25% (S25-D1). After that, it began to decrease when the level was 50% (S50-D1). Nonetheless, slab S50-D1 still had energy absorption higher than the reference un-corroded slab (S0) by 6%. The results indicate that the ability of corroded slab to absorb energy decreased after reaching a mass loss of 25%. The significant reduction in the capacity of the slab at 25% mass loss led to the reduction in the energy absorption capacity despite the increase in the deflection at ultimate load. Although the ultimate load decreased as the corrosion levels were increased, the deflection at ultimate load was increased. Hence, the energy absorption seemed to increase with the increase in the corrosion levels. Figure 4.8 shows the slab rotation versus load for the slabs. The slab rotation was measured for the portion outside the shear crack which rotates as a rigid body (Marzouk & Hussein 1991; Hussein 1990). The results revealed that the slab rotation increased with the increase in the mass loss. This could also be attributed to the decrease in the stiffness that was associated with the increase in mass loss.

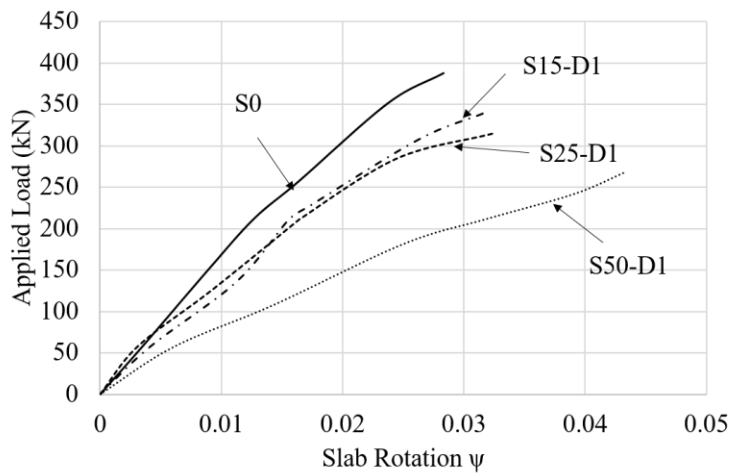

Figure 4-8 Applied load vs. slab rotation.

4.5.4. Deflection Profiles and Deflection Capacities

Figure 4.9 shows the deflection profiles for the slabs at the ultimate load. The deflection capacity, which is defined as the deflection value at failure (El-Maaddawy et al. 2005b), increased with the increase in mass loss as shown in Table 4.4. S50-D1 has the maximum deflection capacity among all specimens, it exceeded the control slab S0 by 50%. Regarding S12 and S25-D1, both exceeded the deflection capacity of S0 by 19.3% and 30.7%, respectively. This could be attributed to the decrease of the stiffness of the corroded slabs. Moreover, the crack widths and numbers increased with the increase in mass loss will subsequently cause a deterioration of the cracked stiffness. Consequently, the slab deflection increased under the same load level. In addition, the loss of bond between the corroded bars and concrete covers increase the deflection capacities (El-Maaddawy et al. 2005b). Slab S50-D1 showed the most ductile punching failure, where it had a gradual drop of the load-deflection curve after the ultimate load was reached, as shown in Fig. 4.7-e, followed by S25-D1, S15-D1, and then S0.

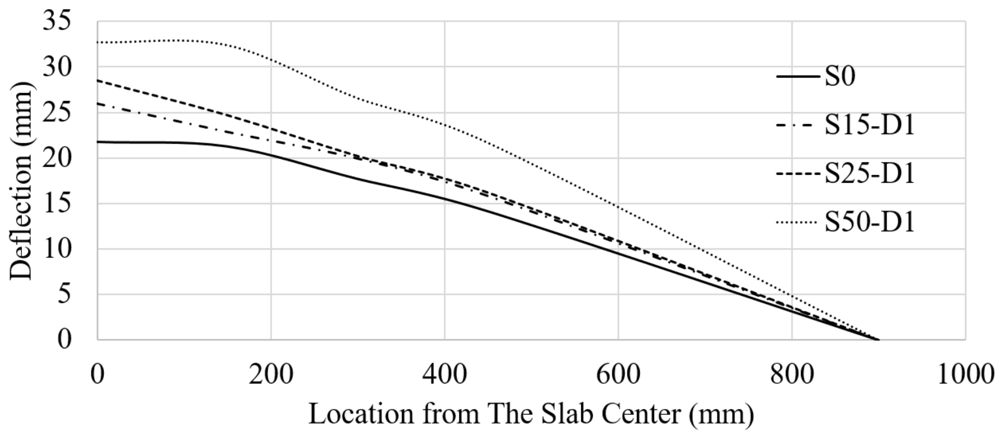

Figure 4-9 Deflection profile at ultimate load.

Figure 4.10 shows the deflection for compression and tension sides at the same location. It can notice that there is no significant differential deflection between both sides. The difference between the readings could be as a result of the formation of the internal inclined shear crack. Also before the loading was applied, the corroded slabs from the tension side showed some swelling compares to S0. For the decreasing portion of the curves, a snap-back in the load-deflection curve occurred for the back LVDT. This is an indication of the separation of the tension reinforcement mesh after the peak load was reached.

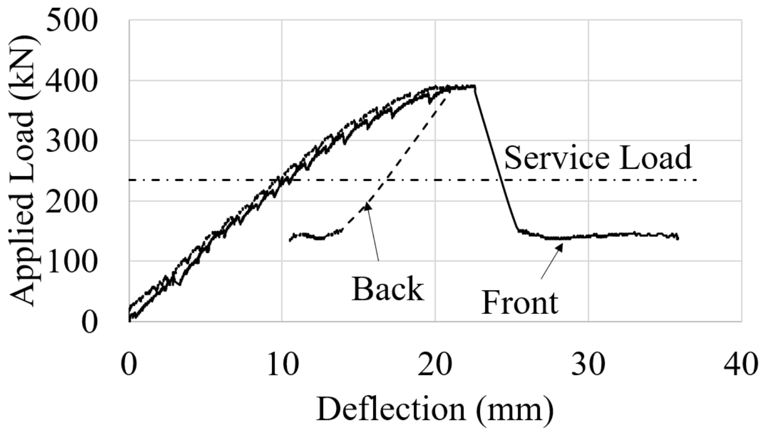

500
400
300
200
100
0
Applied Load (kN)
Service Load
Back
Front
0
10
20
30
40
Deflection (mm)

a. S0

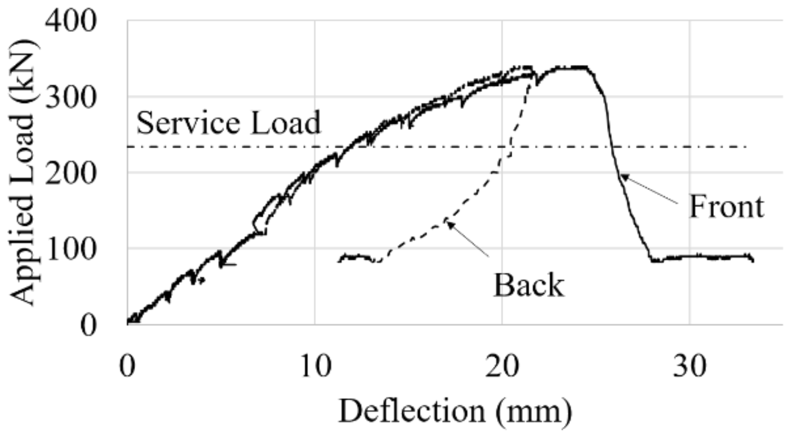

400
300
200
100
0
Applied Load (kN)
Service Load
Front
Back
0
10
20
30
Deflection (mm)

b. S0

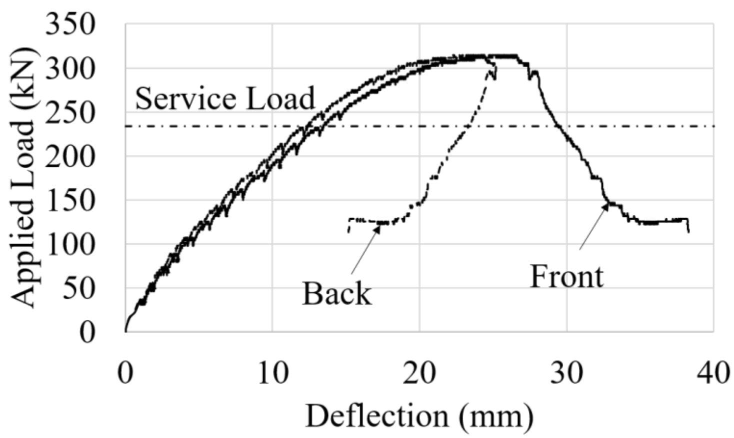

350
300
250
200
150
100
50
0
Applied Load (kN)
Service Load
Back
Front
0
10
20
30
40
Deflection (mm)

c. S0

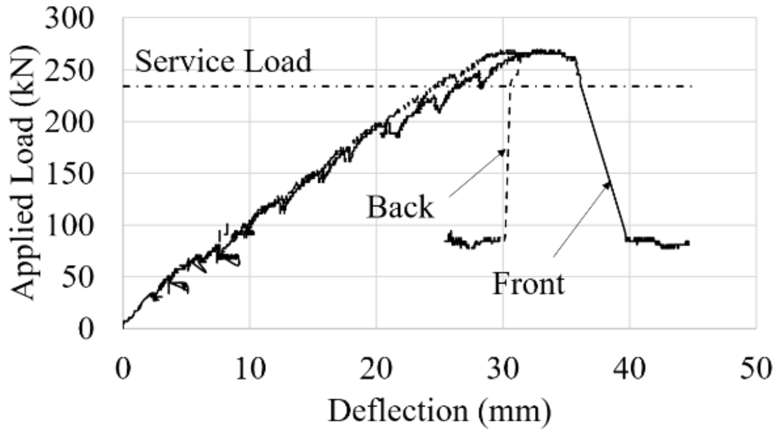

d. S0

Figure 4-10 Difference between front and back deflection.

4.5.5. Ductility

Ductility is determined as the ratio between the deflection at the ultimate failure load (Δ_u) and the deflection at the first yielding of the flexural reinforcement (Marzouk & Hussein 1991). This definition of ductility requires the measurement of the yield stress in the reinforcement during loading. During the corrosion process, there is a direct current passing through the reinforcement that is being corroded, which destroys the electric strain gauge itself. Moreover, the corrosion products will destroy the adhesion between the strain gauge and steel bar. Therefore, using this definition for ductility cannot be applied in the current study. Ductility represents the deformation capacity of the slab until failure. A modified definition for ductility for corroded elements has been proposed by some researchers. It is referred to as ductility index (Dang & François 2014). Ductility index is defined as the ratio between the deflection capacity for corroded and the reference un-corroded element. Hence, ductility index with value equal 1 refers to the un-corroded reference specimen, and more than one means that corrosion has been induced. The ductility indices for S0, S15-D1, S25-D1, and S50-D1 were 1, 1.19, 1.31, and 1.5, respectively.

4.5.6. Cracking Response

The corroded crack pattern for the all corroded specimens is shown in Fig. 4.11. It has been noticed that the number of the cracks in the corroded slabs increased with the increasing the mass loss. Moreover, the crack widths also increased with the increase in mass loss. Table 4.4 shows that the maximum crack widths for S15-D1, S25-D1, and S50-D1 which was 0.15 mm, 0.5 mm, and 2.0 mm, respectively due to corrosion and prior to the application of load. This increase in crack widths was expected. More mass loss causes more corrosion products under the concrete cover. These products cause internal pressure that leads to induce more cracks and assist to increase their widths.

The crack pattern after the loading test was completed shown in Fig. 4.12 for all slabs. The relation between the applied load and the maximum crack width are shown in Fig. 4.13. The cracks pattern distribution in the reference slab S0 was an orthogonal pattern with high intensity that is a large number of cracks. Regarding the corroded slabs, new cracks were formed outside the corroded area. In addition, these cracks were the extension of the cracks due to corrosion. A few number of cracks occurred inside the corroded area during loading. Some cracks were initially formed due to corrosion, but their widths were small and could not be detected by the naked eye. After starting loading, these cracks become wider. It was noticed that the corroded slabs showed a radial flexural cracks pattern. On the other hand, orthogonal cracks pattern were dominated in S0. This could be attributed to the reduction in the reinforcement ratio that occurred with increasing mass loss. For slabs with low reinforcement ratio, radial flexural cracks are formed, but for slabs with high reinforcement ratio, orthogonal cracks dominate the crack behaviour (Rashid 2004).

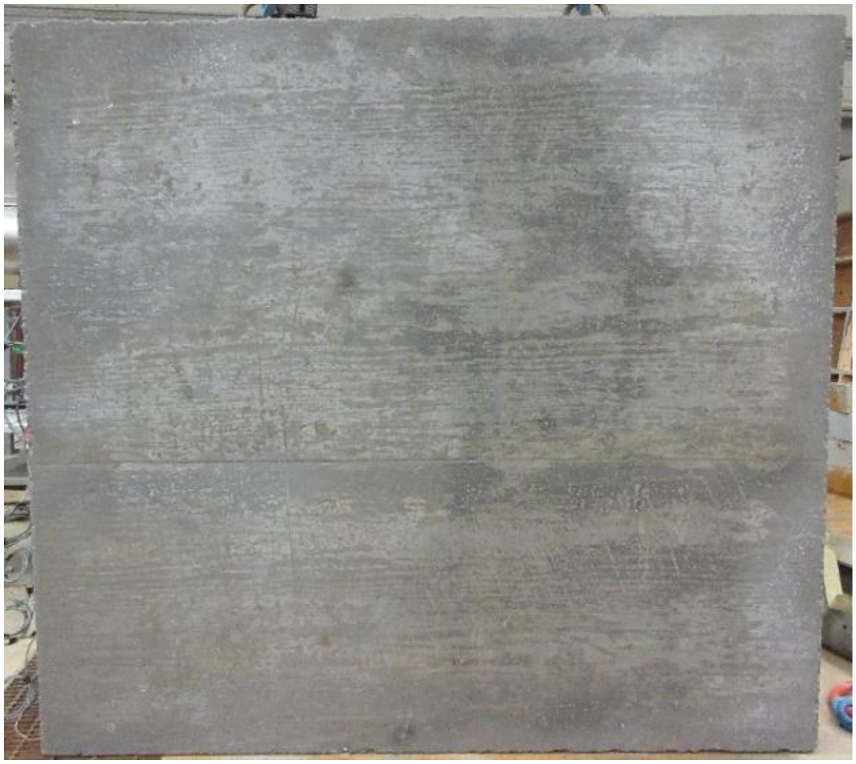
a. S0

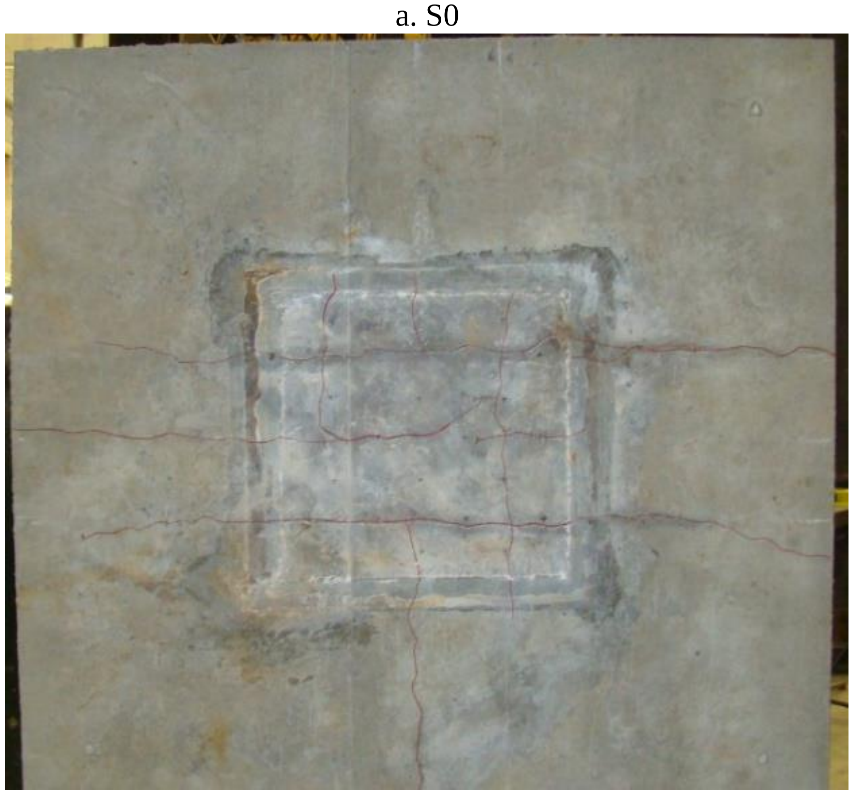
b. S15-D1

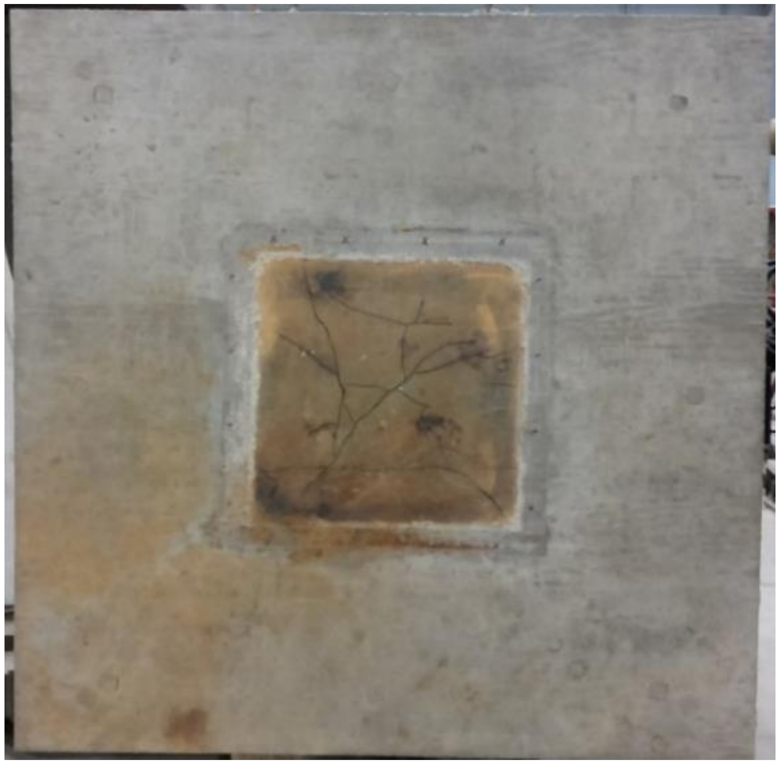

c. S0

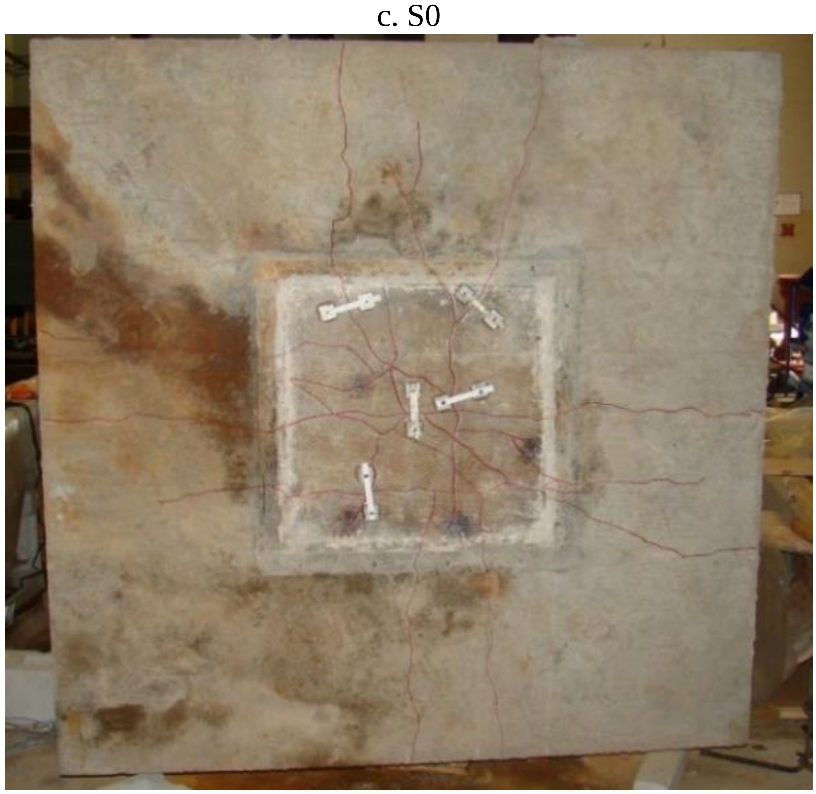

d. S0

Figure 4-11 Cracks patterns due to corrosion before loading test.

a. S0

b. S15-D1

c. S0

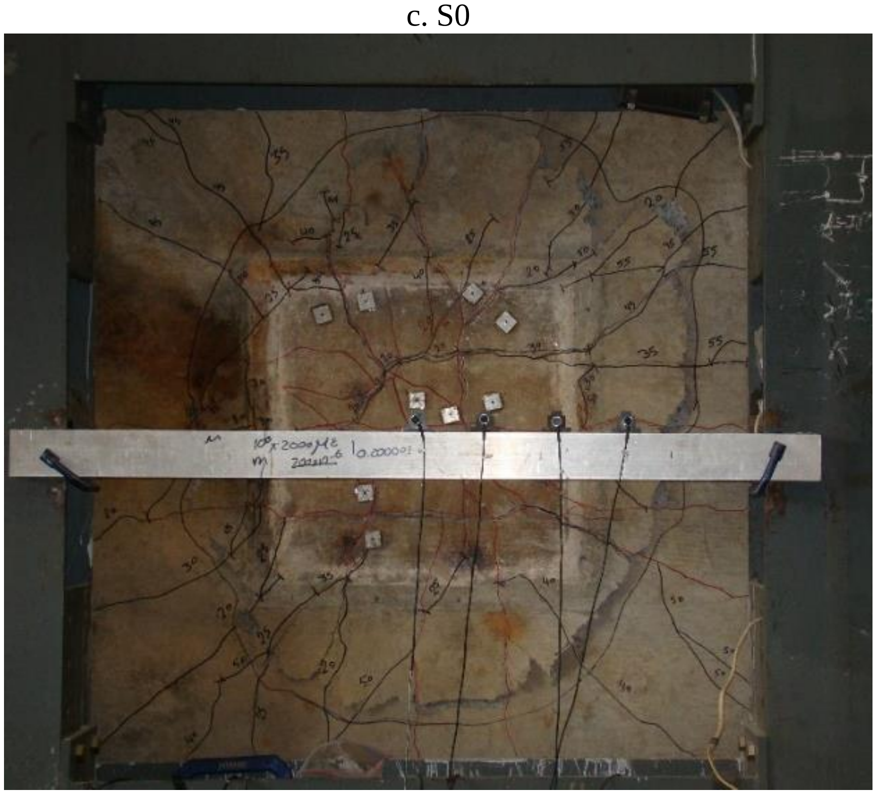

d. S0

Figure 4-12 Crack patterns after loading test.

The maximum recorded crack widths after failure, due to loading test, for S0, S15-D1, S25-D1, and S50-D1 were 2.49 mm, 3.86 mm, 7.62 mm, and 8.33 mm, respectively. The wider crack widths could have resulted from the pre-formation of cracks in the corroded specimen before loading test. Severely corroded specimen had wider cracks than mild specimens. Therefore, during loading, those cracks became wider and the formation of new cracks was reduced. That explains why S0 had more cracks intensity than corroded slabs. It has been noticed also in Fig. 4.12 that S50-D1 had lower cracking intensity comparing with the other corroded slabs.

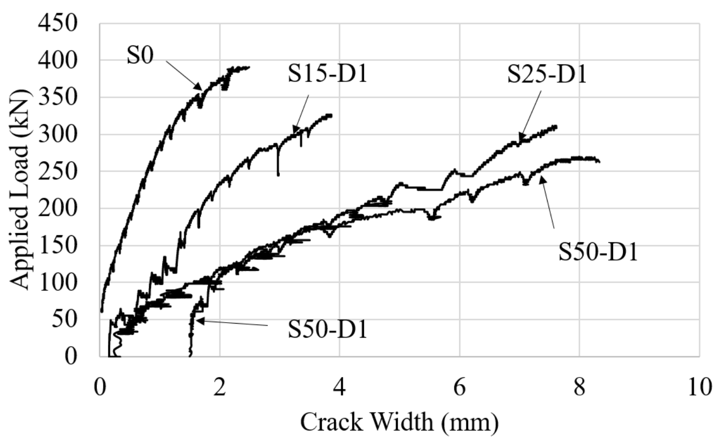

Figure 4-13 Crack width vs. applied load.

4.6. Comparison with Code Predictions

4.6.1. Yield Line Theory

Table 4.5 shows the recorded ultimate load (P_u) from the experiments and the flexural capacity based on yield line theory $(P_{flexural})$. The yield line theory is used to determine an upper bound solution for the flexural capacity $(P_{flexural})$ of conventional slab-column connections. The flexural capacity is calculated as follows (Marzouk & Hussein 1991):

$$P_{flexural} = 8\left(s / (a\text{-}c) - 0.172\right) M_n \qquad 4.2$$

where s is the side dimension of the slab (1900 mm), a is the side dimension between supports of a square slab (1830 mm), c is the side dimension of the square column stub (250 mm), M_n is the nominal flexure capacity for the slab section per meter (The resistance factors are taken as unity, $\varphi_c = \varphi_s = 1$). According to A23.3-14, M_n is calculated as:

$$M_n = \rho\, f_y\, d^2 \left(1 - \left(\alpha_1\, \rho\, f_y\right) / f_c'\right) \qquad 4.3$$

$$\alpha_1 = 0.85 - 0.0015\, f_c' \qquad 4.4$$

where ρ is the reinforcement ratio, d is the slab depth (112 mm), f_y is the reinforcement yield stress (475 MPa), and f_c' is the concrete compressive strength (41.1 MPa).

Hence, the term $P_u/P_{flexural}$ is traditionally used as an indication to determine the failure made wether it is shear failure or flexural. If $P_u/P_{flexural} > 1$ that means failure is due to flexural, and if $P_u/P_{flexural} \leq 1$ then failure is due to shear. From the values shown in Table 4.5 it can be seen that $P_u/P_{flexural}$ are lower than one for all slabs which indicates punching failure. In fact, $P_u/P_{flexural}$ for S0 is equal to 0.88 which could be considered as a ductile punching failure. On the other hand, the $P_u/P_{flexural}$ values are 0.76, 0.71, and 0.60 for S15-D1, S25-D1, and S50-D1, respectively, which indicate that the failure was due to punching. The yield line theory calculates the flexural capacity using the nominal resistance of the slab. Hence, it has the reinforcement ratio as a parameter. Therefore, if the reinforcement ratio is reduced by the same percentage as mass loss, the flexural capacity can be recalculated on this basis. This value could be used as an indication of the failure mode rather than using the un-coroded reinforcement ratio. Table 4.6 shows the calculated flexural capacity based on the reduced bar area. From the table, it can be seen that the ratio $P_u/P_{flexural}$ is equal to 0.88, 0.92, and 1.15 for S15-D1, S25-D1, and S50-D1, respectively. The ratios show that S15-D1 and S25-D1 failed in shear, while S50-D1 failed in flexural where the $P_u/P_{flexural}$ is more than one. However, all corroded slabs actually failed in ductile or secondary punching. It should be noted that the use of the yield line theory itself is based on reinforcement ratio that is assumed uniform for the whole slab, while the corroded area was only bounded by the bandwidth.

4.6.2. Canadian Code [CSA 23.3-14] Provisions

The punching shear strength (ν_c) in CSA 23.3-14 depends on the concrete compressive strength, the effective depth, and the perimeter of the critical section as shown in Eq. 4.5. The resistance factors are taken as unity, $\varphi_c = \varphi_s = 1$. The resistance (ν_r) is only based on the concrete (ν_c) in the absence of shear reinforcement. It should also be noted that the loss of bond can not be accounted for calculating the nominal moments used by the yield line theory.

$$\nu_r = \nu_c = \text{smallest of} \begin{cases} 0.38\,\lambda\,\varphi_c\,\sqrt{f'_c} \\ 0.19\,\lambda\,\varphi_c\,\sqrt{f'_c}\left(1+\dfrac{2}{\beta_c}\right) \\ \left(\dfrac{\alpha_s}{b_o/d}+0.19\right)\lambda\,\varphi_c\,\sqrt{f'_c} \end{cases} \tag{4.5}$$

where, β_c is the ratio of long side to short side of the column $(\beta_c = 1)$, α_s is the adjusting factor ($\alpha_s = 4$ for interior column, $\alpha_s = 3$ for edge column, or $\alpha_s = 2$ for corner column), λ is the concrete density factor ($\lambda = 1$ for normal concrete, $\lambda = 0.85$ for semi-low density concrete, $\lambda = 0.75$ for low density concrete), φ_c is the resistance factor for concrete (φ_c has taken as unity to calculate the nominal shear resistance), $f_c^{'}$ is the concrete compressive strength, d is the slab effective depth, b_o is the perimeter of the critical section.

The critical section perimeter in the Canadian code is at $d/2$ from the face of the column (CSA A23.3-14 2014); $b_o = 4(c + d)$, where c is the side dimension of the square column.

The shear capacity based on CSA 23.3-14 code expression is then calculated as:

$$P_{code\ |_{CSA}} = \nu_r b_o d \tag{4.6}$$

The actual capacities of the corroded slabs are less than the designed values according to CSA 23.3-14 code. This means that the code predictions are unsafe. Table 4.5 shows that the actual capacity of S15-D1, S25-D1, and S50-D1 are below the CSA 23.3-14 predictions by 5%, 12%, and 25%, respectively. It should be noted that CSA 23.3-14 does not take into consideration the effect of the reinforcement ratio on the punching shear strength. Hence, CSA 23.3-14 does not have the ability to account for the reduced reinforcement ratio based on equivalent mass loss.

4.6.3. American Code [ACI 318-14] Provisions

Similar to the CSA 23.3-14, the American code (ACI 318-14) considers the location of the critical punching shear perimeter at $d/2$ from the column face. The shear strength (ν_c) is the smallest of the values in Eq. 4.7. The shear capacity based is calculated using Eq. 4.8.

$$\nu_c = \text{smallest of} \begin{cases} 0.33\,\lambda\,\sqrt{f'_c} \\ 0.17\,\lambda\left(1+\dfrac{2}{\beta_c}\right)\sqrt{f'_c} \\ 0.083\left(\dfrac{\alpha_s d}{b_o}+0.2\right)\lambda\,\sqrt{f'_c} \end{cases} \tag{4.7}$$

$$P_{code}\big|_{ACI} = \nu_c b_o d \tag{4.8}$$

where, β_c is the ratio of long to short sides of the column $(\beta_c=1)$, α_s is a factor used for column location ($\alpha_s=40$ for interior column, $\alpha_s=30$ for edge column, or $\alpha_s=20$ for corner column), λ is the concrete density factor ($\lambda=1$ for normal concrete, $\lambda=0.85$ for semi-lightweight concrete), f'_c is the concrete compressive strength, d is the slab effective depth, b_o is the perimeter of the critical section.

Table 4.5 shows the design capacities using ACI 318-14 and the comparison with the experimental ultimate loads for the corroded slabs P_u/P_{code}. The results indicate that the actual capacity for S50-D1 is below the design value by 14%. Whereas the actual capacity of S15-D1 and S-25-D1 are slightly higher than the ACI 318-14 predictions by 9% and 1%, respectively. The American code does not take the effect of the reinforcement ratio in calculating the punching shear capacity (ACI 318-14 2014). Consequently, and similar to CSA 23.3-14, a reduced reinforcement ratio as an equivalent to mass loss cannot be used.

4.6.4. British Code [BS8110-97] Provision

The British Code (BS8110-97) specifies the critical punching shear perimeter at a distance of $1.5d$ from the column face (BS 8110 1997). Therefore, the perimeter of the critical section is $b_o = 4(c + 3d)$, where c is the side dimension of the square column. The punching shear design capacity takes into consideration the concrete strength $\left(f_c^{'}\right)$, the flexural reinforcement ratio (ρ), the effective slab depth (d), and a size effect factor as follows:

$$P_{code}\big|_{BS} = 0.79\left(100\,\rho\,\frac{f_c^{'}/0.78}{25}\right)^{1/3}(400/d)^{1/4}\,b_o\,d \qquad 4.9$$

Based on the reinforcement ratio of the un-corroded slab, the results in Table 4.5 reveal that the experimental loads are below the design capacity according to BS8110-97 by 5%, and 19% for S25-D1 and S50-D1, respectively. Slab S15-D1 has a margin of safety of 2% above the design capacity. The reinforcement ratio is considered as one of the parameters in the BS8110-97 code equation. Hence, the reinforcement ratio could be reduced by the same percentage as mass loss. This could provide a better approximation of the capacity of the corroded slabs. It should be noted; however, that the loss of bond cannot be considered in the BS8110-97 expression. Table 4.6 shows the ratio of P_u/P_{code} using a reduced reinforcement ratio as the mass loss. The results revealed that the capacities of S15-D1, S25-D1, and S50-D1 are higher than the code predictions by 8%, 5%, and 2%, respectively.

This is a close agreement. Hence, BS8110-97 could be used to predict the capacity of two-way slabs with small corroded area around the column.

4.6.5. European Code [EC2] Provision

The European Code (EC2) specify the critical punching shear perimeter at a distance of $2\,d$ from the column face (British Standards Institution 2004). Therefore, the perimeter of the critical section considering the rounded corners is $b_o = 4\,c + 4\,\pi\,d$, where c is the side dimension of the square column. The shear punching capacity based on EC2 takes into account the characteristic concrete compressive strength (f_c), the flexural reinforcement ratio (ρ), the effective slab depth (d), and a size effect (k). The punching capacity is calculated using Eq. 4.10.

$$P_{code}\,\big|_{EC2} = \text{smallest of } \begin{cases} 0.18\,k\,(100\,\rho_l\,f_c)^{1/3}\,b_o\,d \\ 0.035\,k^{3/2}\,f_c^{1/2}\,b_o\,d \end{cases} \qquad 4.10$$

$$k = 1 + \sqrt{200/d} \le 2.0 \qquad 4.11$$

$$\rho_l = \sqrt{\rho_{ly} \times \rho_{lz}} \le 0.02 \qquad 4.12$$

where ρ_{ly} and ρ_{lz} are the reinforcement ratio in y and z direction, respectively, taking into consideration the effect of depth in each direction.

The results shown in Table 4.5 reveal that the experimental results of all corroded slabs are below the design capacity of EC2 similar to BS8110-97 predictions. The capacities of S15-D1 and S25-D1 are higher than the EC2 predictions by 13%, and 5%, respectively. On the other hand, S50-D1 is 10% lower than the EC2 design value. Although the reinforcement ratio used in EC2 predictions are those of a virgin slab, the difference between the actual and design values is the lowest compared to other codes. Similar to BS8110-97, EC2 considers the reinforcement ratio as a parameter in calculating the punching design capacity. Table 4.6 shows that the experimental loads of S15-D1, S25-D1, and S50-D1 are higher than the design EC2 predictions by 20%, 16% and 13%, respectively.

Thus, BS8110-97 gives the closest agreement with the test results; where the difference did not exceed 8%. None the less, EC2 also provides safe and reasonable predictions.

Table 4-5 Test Results versus Code Predictions

Slab	P_u kN	$P_{flexural}$ kN	$\frac{P_u}{P_{flexural}}$	CSA 23.3-14		BS 8110-97		ACI 318-14		EC2	
				P_{code} kN	$\frac{P_u}{P_{code}}$	P_{code} kN	$\frac{P_u}{P_{code}}$	P_{code} kN	$\frac{P_u}{P_{code}}$	P_{code} kN	$\frac{P_u}{P_{code}}$
S0	391	447	0.88	359	1.09	332	1.18	312	1.25	300	1.30
S15-D1	340		0.76		0.95		1.02		1.09		1.13
S25-D1	315		0.71		0.88		0.95		1.01		1.05
S50-D1	269		0.60		0.75		0.81		0.86		0.90

* P_u is the experimental punching shear capacity, $P_{flexural}$ is the flexural slab capacity based on un-corroded reinforcement ratio, and P_{code} is the code predicted punching shear resistance.

Table 4-6 Test Results versus Code Predictions with reduced reinforcement ratio

Slab	P_u kN	$P_{flexural}$ kN	$\frac{P_u}{P_{flexural}}$	BS 8110-97		EC2	
				P_{code}	$\frac{P_u}{P_{code}}$	P_{code}	$\frac{P_u}{P_{code}}$
S15-D1	340	385	0.88	314	1.08	284	1.20
S25-D1	315	343	0.92	301	1.05	272	1.16
S50-D1	269	234	1.15	263	1.02	238	1.13

* P_u is the experimental punching shear capacity, $P_{flexural}$ is the flexural slab capacity based on modified reinforcement ratio, and P_{code} is the code predicted punching shear resistance.

4.7. Conclusion

The assessment of the structural behaviour of corroded two-way slabs was performed in the current paper. A total of four full-scale two-way slabs were investigated; a control slab (0% mass loss), and three other slabs with mild corrosion level (15% mass loss), moderate corrosion level (25% mass loss), and severe corrosion level (50% mass loss). The reinforcement was subjected to accelerated corrosion within an area equal to a bandwidth as defined by CSA 23.3-14. The ultimate loads, stiffness, slab rotation, energy absorption, deflections, and cracking behaviour were investigated. From the results described in this paper, the following conclusion can be drawn:

- Increasing the corrosion level causes a reduction in the punching shear capacity and stiffness. The punching capacity was reduced by 13.1%, 19.5%, and 31.2% and the reduction of the stiffness was 7.9%, 25.8%, and 48.8% for the slabs with 15%, 25%, and 50% mass loss, respectively. This reduction could be attributed to the mass loss that occurred to the flexural reinforcement due to corrosion, and the corresponding reduction in the reinforcement area. This also led to a reduction in the load that causes the first yield of the reinforcement, which reduced the capacity and the stiffness. Moreover, the bond loss between the corroded reinforcement and concrete cover and the wider crack widths also played a role in diminishing the overall stiffness and capacity of the slab.
- The service load for the reference specimen was above the failure load of all corroded slabs. The ultimate capacities for S15-D1, S25-D1, and S50-D1 were above the service load of S0 by 44.7%, 36.2%, and 14.5%, respectively. The

serviceability limits show acceptable ranges for severe levels of corrosion within a concentrated corroded area equivalent to the reinforcement bandwidth defined in CSA A23.3-14 (2014).

- Increasing the level of corrosion appeared to increase the slab rotation and deflection capacity. These increases could be attributed to the reduction in the area of the flexural reinforcement and the deterioration of bond which weakens the stiffness of the corroded slabs.
- A revised term for ductility index was adopted to represent the ductility. The term was used in previous studies (Dang & François 2014) on beams. Ductility index is defined as the ratio between the deflection capacity of a corroded element to its value with no corrosion occurring. It has been found that the ductility indices were 1.19, 1.31, and 1.5, for 15, 25, and 50% mass loss, respectively. The ductility index increased with increasing mass lass as expected as the deflection capacity increased with increasing the mass loss.
- The width and number of cracks in the corroded slabs increased with increasing mass loss. This could be attributed to the excessive corrosion products that enlarged the undercover with increasing mass loss. These products cause tensile stress under the concrete cover which induces cracks in the surface.
- The capacity of all corroded slab fell below the design values according to CSA A23.3-14. It has been found that by reducing the reinforcement ratio proportional to the mass loss in the corroded slabs, that EC2 and BS8110-97 predicting punching capacities have a reasonable agreement with actual ones with all mass loss levels. In general, the North American codes for the punching shear do not take into

consideration the effect of reinforcement ratio. Therefore, these codes cannot be used to predict the capacity of deteriorated slabs.

4.8. References

ACI 318-14 (2014) Building code requirement for structural concrete (ACI 318M-14) and commentary (ACI 318RM-14), Building Code Requirements for Structural Concrete.

Ahmad, S. (2003) 'Reinforcement corrosion in concrete structures, its monitoring and service life prediction - A review', Cement and Concrete Composites, 25(4–5 SPEC), pp. 459–471. doi: 10.1016/S0958-9465(02)00086-0.

Ahwazi, B. B. N. (2001) A comparative study of deterioration of bond due to corrosion in different concretes. McGill University.

Al-Swaidani, A. M. and Aliyan, S. D. (2015) 'Effect of adding scoria as cement replacement on durability-related properties', International Journal of Concrete Structures and Materials. Korea Concrete Institute, 9(2), pp. 241–254. doi: 10.1007/s40069-015-0101-z.

Amleh, L. (2000) Bond deterioration of reinforcing steel in concrete due to corrosion. McGill University.

Andrade, C. and Alonso, C. (1996) 'Corrosion rate monitoring in the laboratory and on-site', Construction and Building Materials, 10(5 SPEC. ISS.), pp. 315–328. doi: 10.1016/0950-0618(95)00044-5.

Andrade, C. and Alonso, C. (2001) ‘On-site measurements of corrosion rate of reinforcements’, Construction and Building Materials, 15(2–3), pp. 141–145. doi: 10.1016/S0950-0618(00)00063-5.

Andrade, C. and C. Alonso (2004) ‘“Electrochemical techniques for measuring metallic corrosion”: test methods for on-site corrosion rate measurement of steel reinforcement in concrete by means of the polarization resistance method’, Materials and Structures, 37(9), pp. 623–643. doi: 10.1007/BF02483292.

Aoude, H., Cook, W. D. and Mitchell, D. (2014) ‘Effects of simulated corrosion and delamination on response of two-way slabs’, Journal of structural Engineering, 140(1), pp. 1–9. doi: 10.1061/(ASCE)ST.1943-541X.0000775.

ASTM C150/C150M (2017) ‘Standard specification for Portland cement’, ASTM International, p. 9.

Berto, L., Simioni, P. and Saetta, A. (2008) ‘Numerical modelling of bond behaviour in RC structures affected by reinforcement corrosion’, Engineering Structures. Elsevier, 30(5), pp. 1375–1385.

Bertolini, L., Elsener, B., Pedeferri, P., Redaelli, E. and Polder, R. B. (2013) Corrosion of steel in concrete: prevention, diagnosis, repair. John Wiley & Sons.

British Standards Institution (2004) Eurocode 2: design of concrete structures: part 1-1: general rules and rules for buildings. British Standards Institution.

Broomfield, J. P. (2006) Corrosion of steel in concrete: understanding, investigation and repair, Second Edition. doi: 10.4324/9780203414606.

BS 8110 (1997) 'Structural use of concrete. Part I: Code of practice for design and construction', British Standards Institution, UK.

Carnot, A., Frateur, I., Zanna, S., Tribollet, B., Dubois-Brugger, I. and Marcus, P. (2003) 'Corrosion mechanisms of steel concrete moulds in contact with a demoulding agent studied by EIS and XPS', Corrosion science. Elsevier, 45(11), pp. 2513–2524.

Chitty, W.-J., Dillmann, P., L'Hostis, V. and Lombard, C. (2005) 'Long-term corrosion resistance of metallic reinforcements in concrete—a study of corrosion mechanisms based on archaeological artefacts', Corrosion Science. Elsevier, 47(6), pp. 1555–1581.

Coronelli, D. and Gambarova, P. (2004) 'Structural assessment of corroded reinforced concrete beams: modeling guidelines', Journal of Structural Engineering. American Society of Civil Engineers, 130(8), pp. 1214–1224.

CSA A23.3-14 (2014) Design of concrete structures. Mississauga, Ont.: Canadian Standard Association.

Dang, V. H. and François, R. (2014) 'Prediction of Ductility Factor of Corroded Reinforced Concrete Beams Exposed to Long Term Aging in Chloride Environment', Cement and Concrete Composites, 53(October 2014), pp. 136–147. doi: 10.1016/j.cemconcomp.2014.06.002.

Deb, S. and Pradhan, B. (2013) 'A study on corrosion performance of steel in concrete under accelerated condition', in Proceedings of the International Conference on Structural Engineering Construction and Management, Kandy, Sri Lanka. Available at: http://dl.lib.mrt.ac.lk/handle/123/9365.

Dilger, W., Birkle, G. and Mitchell, D. (2005) 'Effect of flexural reinforcement on punching shear resistance', ACI Special Publication 232-4, pp. 57–74. doi: 10.1007/s13398-014-0173-7.2.

Dodd, L. L. and Restrepo-Posada, J. I. (1995) 'Model for predicting cyclic behavior of reinforcing steel', Journal of Structural Engineering. American Society of Civil Engineers, 121(3), pp. 433–445.

Donnelly, J. P., Pulver, B. E. and Popovic, P. L. (2006) 'Condition assessment of parking structures', In Structures Congress : Structural Engineering and Public Safety ASCE., p. 10.

El-Gamal, S., Benmokrane, B., El-Salakawy, E., Wiseman, A. and Chaallal, O. (2009) 'Monitoring of an innovative concrete parking garage reinforced with GFRP composite bars', in 4th International Conference on Structural Health Monitoring of Intelligent Infrastructure (SHMII-4) 22-24 July 2009, Zurich, Switzerland.

El-Maaddawy, T. and Soudki, K. (2003) 'Effectiveness of impressed current technique to simulate corrosion of steel reinforcement in concrete', Journal of Materials in Civil

Engineering. American Society of Civil Engineers, 15(1), pp. 41–47. doi: 10.1061/(ASCE)0899-1561(2003)15:1(41).

El-Maaddawy, T., Soudki, K. and Topper, T. (2005b) 'Long-term performance of corrosion-damaged reinforced concrete beams', ACI Stractural Journal, 102(5), pp. 649–656.

Fedrizzi, L., Azzolini, F. and Bonora, P. L. (2005) 'The use of migrating corrosion inhibitors to repair motorways' concrete structures contaminated by chlorides', Cement and concrete research. Elsevier, 35(3), pp. 551–561.

Gowda, M. R., R, K. M. and Vijin Xavier (2017) 'Corrosion rate analysis in reinforced slab elements', International Journal for Scientific Research & Development|, 4(11).

Hussein, A. A. (1990) Behaviour of reinforced concrete slabs made with high-strength concrete. Memorial University of Newfoundland.

Kumar, M. K., Rao, P. S., Swamy, B. L. P. and Chandra Mouli, C. (2012) 'Corrosion resistance performance of fly ash blended cement concrete', Internatioanl Journal of Research in Engineering and Technologi, 1(3), pp. 448–454. doi: 10.1016/0140-6701(95)93047-7.

Lachemi, M., Al-Bayati, N., Sahmaran, M. and Anil, O. (2014) 'The effect of corrosion on shear behavior of reinforced self-consolidating concrete beams', Engineering Structures. Elsevier Ltd, 79, pp. 1–12. doi: 10.1016/j.engstruct.2014.07.044.

Lee, C., Bonacci, J. F., Thomas, M. D. a., Maalej, M., Khajehpour, S., Hearn, N., Pantazopoulou, S. and Sheikh, S. (2000) ‘Accelerated corrosion and repair of reinforced concrete columns using carbon fibre reinforced polymer sheets’, Canadian Journal of Civil Engineering, 27(5), pp. 941–948. doi: 10.1139/cjce-27-5-941.

Marzouk, H. and Hussein, A. (1991) ‘Experimental investigation on the behavior of high-strength concrete slabs’, ACI Structural Journal, 88(6), pp. 701–713. doi: 10.1139/l91-118.

Miyagawa, T. (1991) ‘Durability design and repair of concrete structures: chloride corrosion of reinforcing steel and alkali–aggregate reaction’, Magazine of Concrete Research. Thomas Telford Ltd, 43(156), pp. 155–170.

Pellegrini-Cervantes, M. J., Almeraya-Calderon, F., Borunda-Terrazas, A., Bautista-Margulis, R. G., Chacón-Nava, J. G., Fajardo-San-Miguel, G., Almaral-Sanchez, J. L., Barrios-Durstewitz, C. P. and Martinez-Villafañe, A. (2013) ‘Corrosion resistance, porosity and strength of blended portland cement mortar containing rice husk ash and nano-SiO2’, International Journal of Electrochemical Science, 8(8), pp. 10697–10710.

Rahman, A. H. (1992) ‘Effect of steel corrosion on the strength of slab-column connections’, National Research Council Canada, Institute for Research in Construction.

Rashid, M. I. (2004) Concrete Slabs Reinforced with GFRP Bars. Memorial University of Newfoundland.

Raupach, M. (1996) 'Chloride-induced macrocell corrosion of steel in concrete - Theoretical background and practical consequences', Construction and Building Materials, 10(5 SPEC. ISS.), pp. 329–338. doi: 10.1016/0950-0618(95)00018-6.

Reilly, J. L., Cook, W. D., Bastien, J. and Mitchell, D. (2014) 'Effects of delamination on the performance of two-way reinforced concrete slabs', Journal of Performance of Constructed Facilities, 28(4), pp. 1–8. doi: 10.1061/(ASCE)CF.

Roberge, P. R. and Pierre, R. (1999) Handbook of corrosion engineering library of congress cataloging-in-publication data. doi: 10.1016/S0026-0576(00)83445-5.

Xia, J., Jin, W.-L. and Li, L.-Y. (2012) 'Effect of chloride-induced reinforcing steel corrosion on the flexural strength of reinforced concrete beams', Magazine of Concrete Research. Thomas Telford, 64(6), pp. 471–485.

Yoon, S., Wang, K., Weiss, W. and Shah, S. (2001) 'Interaction of reinforced between loading, corrosion, and serviceability of reinforced concrete', ACI Materials Journal, 97(6), pp. 637–644.

Zhang, B., Masmoudi, R. and Benmokrane, B. (2004) 'Behaviour of one-way concrete slabs reinforced with CFRP grid reinforcements', Construction and Building Materials, 18(8), pp. 625–635. doi: 10.1016/j.conbuildmat.2004.04.007.

Chapter 5 The Response of Two-Way Slabs due to Corrosion of Large Reinforcement Area

5.1. Abstract

This investigation was conducted to study the effect of different corrosion levels, within a large area around the column, on the structural performance of two-way reinforced concrete slabs. A total of four slabs were subjected to four level of corrosion; control (0% mass loss), mild corrosion (15% mass loss), moderate corrosion (25% mass loss), and severe corrosion (50% mass loss). An accelerated corrosion technique was used through the application of constant current, $200\,\mu A/cm^2$ to the flexural reinforcement. The full length of the reinforcement was corroded except for a distance equal to the development length at each end of a corroded bar. Therefore, a large corroded area was under investigation. The test results revealed that there is a degradation of capacity and stiffness with increased corrosion levels. The capacity of slabs with severe corrosion fell below its service load. Moreover, the increase in corrosion levels caused an increase in deflection capacity, slab rotation and ductility. The actual capacity was compared to the predictions of four codes. The BS 8110-97 and EC2 are able to safely predict the capacity when the reinforcement ratio is reduced by a value equivalent to the mass loss.

Keywords: Two-way reinforced concrete slabs; severe corrosion; constant current; deflection; ductility index

5.2. Introduction

North America spends large amounts of federal infrastructure funding on roads, bridges, municipals, and marine structures (Roberge & Pierre 1999). Structures in North America, especially marine, offshore, and Arctic, are more vulnerable to deterioration due to corrosion. This is due to harsh climatically conditions such as temperature fluctuation around freezing point, relative humidity, ambient salinity, and extreme use of salts for dicing purposes. All these reasons provide a reasonable environment to cause corrosion in reinforced concrete (RC) structures. This leads to the deterioration of the structures, reduction in the serviceability, and possible collapse (Zhang et al. 2004). Corrosion causes a major headache to civil engineers who are responsible to maintain the ageing structures that suffer from corrosion. This area of study has attracted researchers to build and strengthen their expertise and to carry out an innovative solution to deal with this problem (Broomfield 2006).

Many efforts have been exerted in studying the corrosion from different points of views. Some researcher focused on the understanding of the corrosion process (Raupach 1996; Carnot et al. 2003; Chitty et al. 2005), while other investigated the effect of corrosion on the structural behaviour (El-Maaddawy & Soudki 2003). Other research was sought to monitor the performance of RC beams under corrosion in both laboratory and field conditions (Andrade & Alonso 1996; Andrade & Alonso 2001; Ahmad 2003). Moreover, some researchers tried to develop numerical models to simulate the structural behavior of corroded beams (Dodd & Restrepo-Posada 1995; Berto et al. 2008; Coronelli & Gambarova 2004). In addition, others proposed repair and rehabilitation schemes for corroded beams

(Bertolini et al. 2013; Miyagawa 1991; Fedrizzi et al. 2005; Broomfield 2006). Nonetheless, there is very limited research on the effect of corrosion on the most vulnerable connection in some RC structures; the slab-column connection (Aoude et al. 2014). This connection is the most critical in structures such as parking garages and bridge decks (Donnelly et al. 2006).

Rahman (1992) investigated the effect of corrosion on slab-column connections. The author attempted to simulate the corrosion, loss of bond, and delamination. The corrosion was simulated by changing the number of reinforcing bars at the flexural side. It was concluded that the punching shear capacity was reduced by 30% when the reinforcement loss was 50% by mass. The bond was simulated by wrapping the embedded reinforcement with adhesive plastic sheets. The delamination was mimicked by placing polyethylene sheets between the top and bottom layers of the flexural reinforcement. The experimental results revealed that the loss of bond and delamination had little effect on the punching capacity. However, the slabs with simulation corrosion showed more deflections and cracks. Aoude et al. (2014) studied the effect of corrosion and delamination on the structural response of two-way slabs. The researchers simulated the corrosion by reducing the flexural reinforcement bar diameter and the delamination by placing a plastic sheet under the flexural reinforcement mat. The authors concluded that the mass loss due to corrosion caused a reduction in the punching shear capacity. In addition, when the delamination area increased, the capacity decreased. However, the effect of small delaminated area had a negligible effect on the punching shear capacity. In an extension to the research program, Reilly et al. (2014) investigated the effect of delamination on the structural response of two-way slabs. The delamination was simulated in the same manner as Aoude et al. (2014). The results revealed that increasing the delamination area caused a decrease in the capacity of the slab. The effect of the integrity bars was also investigated. It was found that integrity bars increased the post-punching shear resistance and ultimate load capacity.

Hence, there is no investigation in the literature that addressed the real reinforcement corrosion of two-way RC slabs using accelerated corrosion techniques. On the other hand, accelerated techniques were used to study the effect of corrosion on the structural behaviour of beams (El-Maaddawy & Soudki 2003; El-Maaddawy et al. 2005a; Kashani et al. 2013; Pritzl et al. 2014; Talakokula et al. 2014; Altoubat et al. 2016). Impressed current techniques need a direct source of current, electrolyte solution, reinforcement bars that are considered as an anode, and external bar considered as a cathode. The range of current densities used in several studies ranged from $45\,\mu A/cm^2$ to $10400\,\mu A/cm^2$ (Almusallam et al. 1996; Bonacci et al. 1998). El Maaddawy & Soudki (2003) recommended that the current density should not exceed $200\,\mu A/cm^2$. The authors noticed that using current density above $200\,\mu A/cm^2$ could cause a significant increase in crack width and strain response due to corrosion. The impressed current technique allows that targeted corrosion level be reached within a reasonable amount of time (El-Maaddawy & Soudki 2003). There is no published studies in the literature on two-way slabs under accelerated corrosion technique. This research would provide better simulation of the behaviour of the bond, the change of steel mechanical properties, and the cracking of the concrete cover under realistic corrosion condition. Thus, a better understanding of the behaviour of corroded two-way RC slabs could be developed.

5.3. Research Significance

To predict the serviceability of corroded two-way slabs, it is important to investigate the behaviour with the development of corrosion. This paper reports the results of three different levels of corrosion (mild, moderate, and severe) under realistic conditions for two-way slabs. These levels were reached by using an accelerated technique, which provided more realistic simulation for both bond deterioration and cracks growth due to corrosion. Moreover, the remaining capacity of the corroded two-way RC slabs was also approximately checked. The available literature has a complete lacked of information about the two-way slabs due to corrosion conditions. Therefore, the authors believe that this study has an important contribution in providing a better understanding of the behaviour such elements. The results will aid practicing engineers in assessing the condition of existing corroded two-way slabs and/or estimate the residual capacity of those corroded two-way slabs.

5.4. Experimental Program

5.4.1. Details of Test Specimen

Figure 5.1 shows the dimension and the typical cross section of a typical test slab. All test slabs have identical dimensions with a length of 1900 mm, a width of 1900 mm, and height of 150 mm. The concrete clear cover was 30 mm. The slab dimensions flexural reinforcement were chosen to ensure a ductile punching behaviour. The flexural reinforcement ratio (ρ) was kept constant at 1% for all slabs, and it consisted of 15M bars spaced at 190 mm. In addition, the compression reinforcement consisted of 10M bars spaced at 300 mm. The details of the test specimens are shown in Table 5.1.

Table 5-1 Detailed of Slab Specimens

Side dimensions (mm × mm)	h (mm)	c (mm)	f'_c (MPa)	Main reinforcement
1900 × 1900	150	250	41.1	Two layers-15M bars

*h is the height; c is column width; and f'_c is the concrete compressive strength.

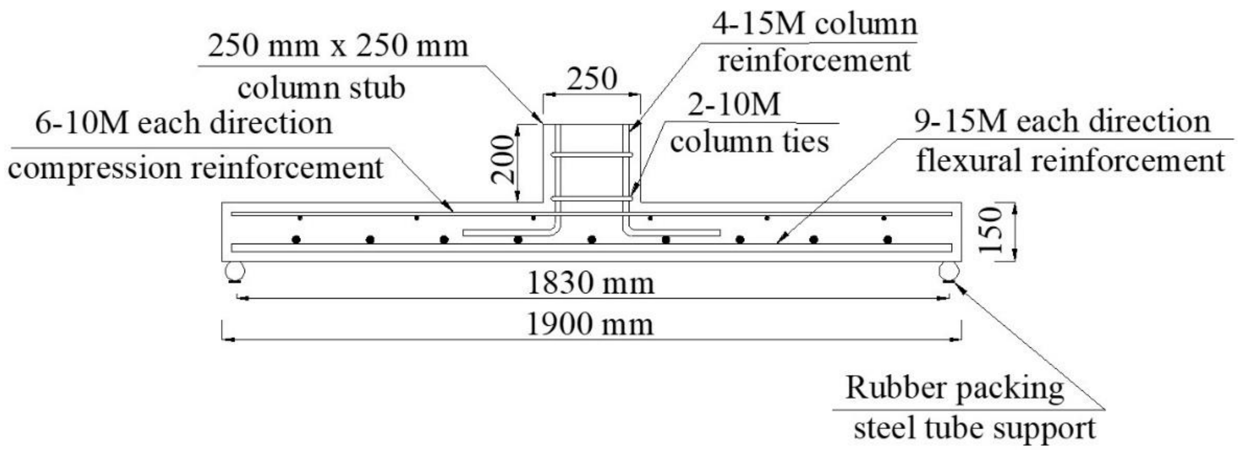

Figure 5-1 Details of a typical slab.

In order to prepare the flexural reinforcement for the accelerated corrosion tests, the following procedure was followed. First, the bars were insulated from each other by avoiding direct contact between them at the intersection points using electrical tape and plastic ties. Secondly, two wires was connected to the targeted bars from each end. At one end, the wire was used to connect the direct current from the power supply to the bar. At the other end, two wires were connected, one of them was a spare in case of any problems happening to the wires during casting. Wooden formwork was used as shown in Fig. 5.2. The main reinforcement was placed at the bottom of the formwork and the wires were extended out from the formwork. All cast slabs were compacted using a mechanical vibration. The column stub was cast after 24 hrs from pouring the slab. The slabs were de-moulded after 24 hrs from pouring the column stub and then water-cured for four days followed by air-curing under laboratory conditions till the rest of the 28 days.

Figure 5-2 Formwork and reinforcement mesh.

Four slabs were tested. Slab S0 was the control slab with no corrosion. The other three slabs S15-D2, S25-D2, and S50-D2 were subjected to three different levels of corrosion: mild – 15% mass loss, moderate – 25% mass loss, and severe – 50% mass loss, respectively. The targeted bars were corroded leaving each end with sufficient un-corroded development length. That is, the selected area extended over the slab leaving a development length (L_d) without corrosion at each side of the slab as shown in Fig. 5.3.

The development length (L_d) was calculated using the CSA A23.3-14 (2014) simplified equation:

$$L_d = 0.45\,k_1\,k_2\,k_3\,k_4\,\frac{f_y}{\sqrt{f_c'}}\,d_b \qquad 5.1$$

where f_y, f_c', and d_b are the yield stress of the reinforcement, the compressive strength of the concrete, and the nominal diameter of the reinforcing bars, respectively. The factors k_1, k_2, k_3, and k_4 are bond location, coating, concrete density factor, and bar size factor, respectively. The first three factors can be taken as 1; while the fourth one is taken as 0.8 for 20M or smaller bars.

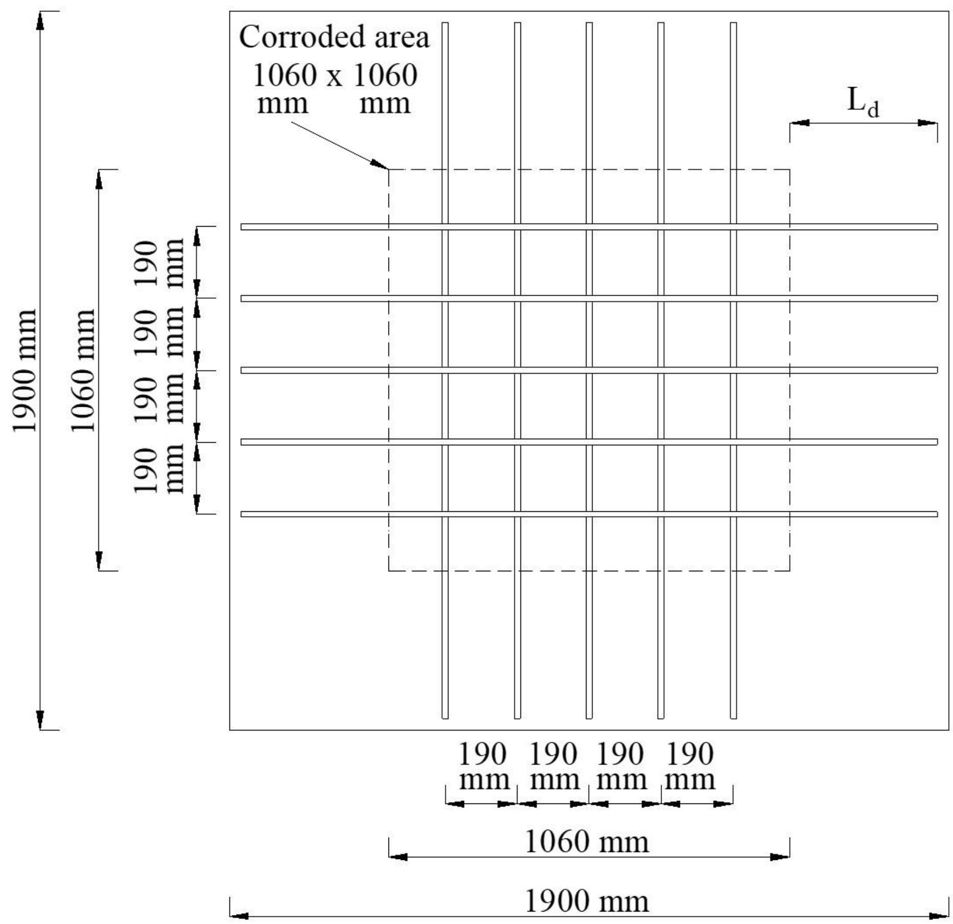

Figure 5-3 The targeted corroded area.

5.4.2. Material Properties

Type I Portland cement (ASTM C150/C150M 2017) was used. Crushed granite with a 10-mm maximum size was used as the coarse aggregate. The sand was of the same material. Both had a specific gravity of 2.6. A local concrete batch plant delivered the concrete to the laboratory. Table 5.2 shows the mixture composition used. The water to cement (w/c) ratio was 0.4 and the targeted compressive strength was 40 MPa. These values were chosen based on the recommendation of the ACI specification for Class F3 exposure (ACI 318-14 2014). This class is used for concrete elements in parking garages, foundations, and basement walls extending above grade that are exposed to freezing-thawing cycles, and possibility to the cumulative amount of snow with de-icing chemicals. Table 5.3 shows the measured properties of the reinforcement and the mechanical properties of the concrete.

Table 5-2 Composition of Concrete Mixtures

Cement (kg)	w/c	Water (l)	C/F	C.A. (kg)	F.A. (kg)	Aggregate size (mm)	Fresh density $(\mathrm{kg/m^3})$
350	0.4	140	1.3	1083	833	10	2407

* w/c is the water to cement ratio, C/F is the coarse to fine ratio, C.A. is the coarse aggregate, and F.A. is the fine aggregate

Table 5-3 Reinforcement and Concrete Properties

Designation	Steel properties			Concrete Properties	
	Area $(\mathrm{mm^2})$	f_y (MPa)	ε_y ($\mu\varepsilon$)	f_c' (MPa)	f_r (MPa)
15M	200	475	2200	41.1	3.82

* f_y is the yield strength, ε_y is the yield strain, f_c' is the compressive strength, and is f_r the modulus of rupture.

5.4.3. Accelerated Corrosion Setup

The accelerated corrosion technique was based on the application of constant current to induce corrosion in the reinforcement. The setup consisted of power supplies, electrolyte solution, and steel mesh. Figure 5.4 shows a schematic diagram for constant current accelerated corrosion setup. Each slab had ten bars within the targeted corroded area. Each bar required a power supply. Hence, each slab needed ten power supplies to reach the same targeted corroded level simultaneously. Each power supply was adjusted to provide $200\,\mu A/cm^2$ of the bar area based on El Maaddawy & Soudki (2003) recommendation that the current density not to exceed $200\,\mu A/cm^2$ to avoid any significant increase in crack width and strain response due to the induced corrosion. The bar diameter was 16 mm and targeted length was 1060 mm. The current density is equal to the current in Amperes divided by the surface area of the bar.

The theoretical mass loss is calculated based on Faraday's equation as following:

$$\text{Mass loss} = \frac{t\,I\,M}{z\,F} \qquad 5.2$$

where t is the time passed in seconds, I is the current in Amperes, M is the atomic weight and is equal to 55.847g/mol for iron, z is the ion charge (two moles of electrons), and F is Faraday's constant which is the amount of electrical charge in one mole of electron and is equal to 96,487 coulombs per mole (Lachemi et al. 2014).

The corrosion time started to be measured after ensuring that the current overcame the concrete resistance. The overcoming of concrete resistance was assumed when the half-cell potential read more than -350 mV indicating that the corrosion occurrence probability is more than 90% (ASTM C876 2015). The relatively high electrical current was applied in order to reach the severe targeted mass loss in a reasonable period of time. The slabs took 87, 145, and 290 days to reach their targeted level of corrosion for S15-D2, S25-D2, and S50-D2, respectively.

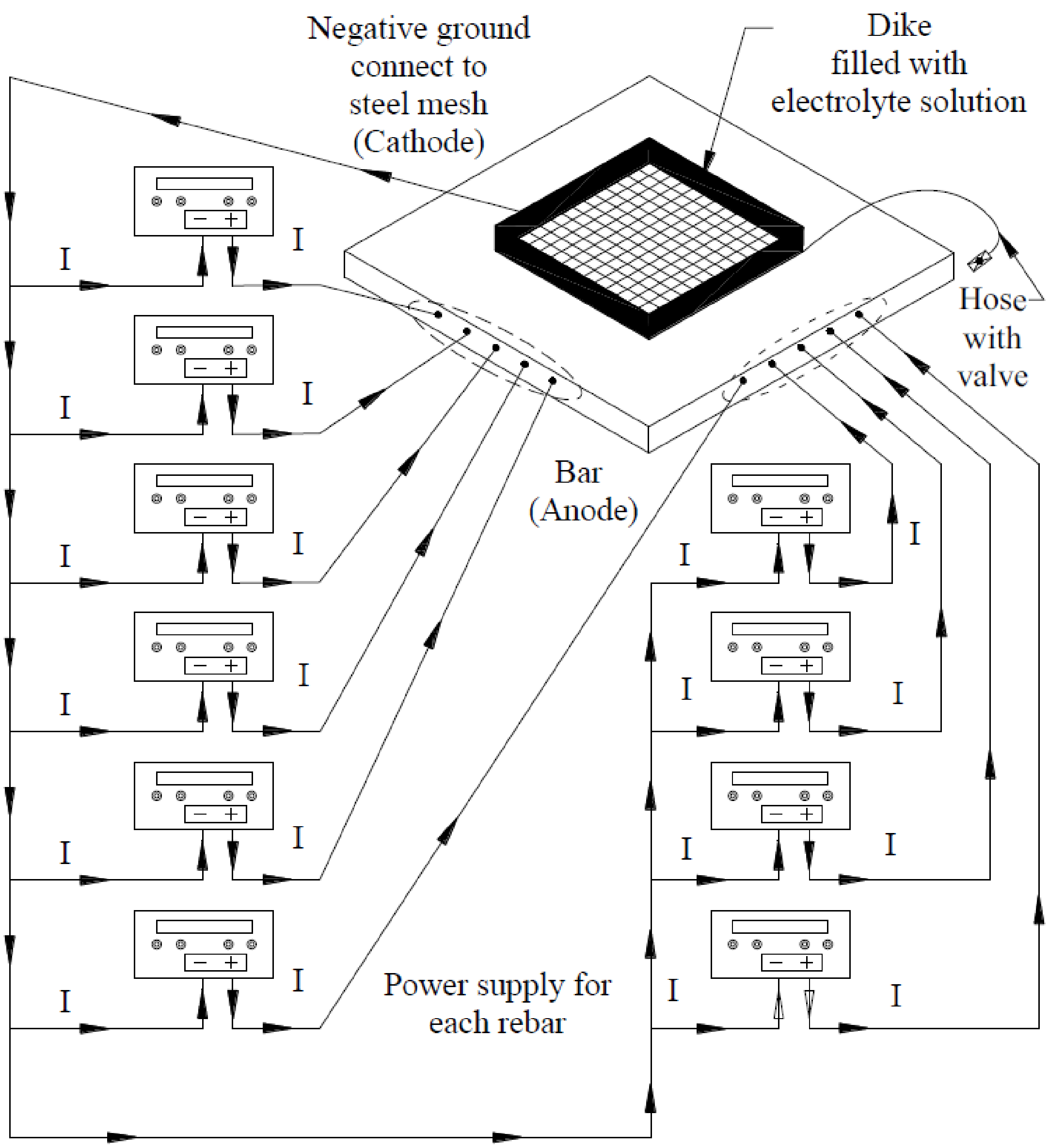

Figure 5-4 Schematic diagram for constant current accelerated corrosion setup.

5.4.4. Test Setup and Instrumentation

A hydraulic jack with a capacity of 1000 kN was used to apply a concentrated load to the slab through the column stub as shown in Fig. 5.5. All tested slabs were simply supported along all the four edges with corner free to lift. These conditions represent the portion of the slab-column connection within the lines of contra-flexure.

The mid-span deflection was measured by using a linear variable differential transformer (LVDT) placed at mid-point of the tension side of the tested slab. The deflection profile was obtained using four LVDTs also placed at the tension side as shown in Fig. 5.6-a. In addition, the difference in the deflections between the front and back side of the slabs was measured using another LVDT at the compression side. Electric stain gauges were used to monitor the concrete compression strains as shown in Fig. 5.6-b. All crack widths in the slabs during the induced corrosion process were measured using a microscope with an accuracy of 0.02 mm and with 60× focusable eyepiece magnifier. The crack widths were measured using crack gauges with a capacity of ± 5 mm at five locations during the loading test. The crack development was detected and monitored by the naked eye. The cracks were marked at the end of each load step. The control slab S0 had no cracks before the loading test. Therefore, a pre-load was applied first to initiate the cracks that was measured using the microscope. The crack gauges were then installed to measure and record the crack widths during the loading test. Figure 5.7 shows a schematic diagram for the loading test setup

a. Back-view (compression side)

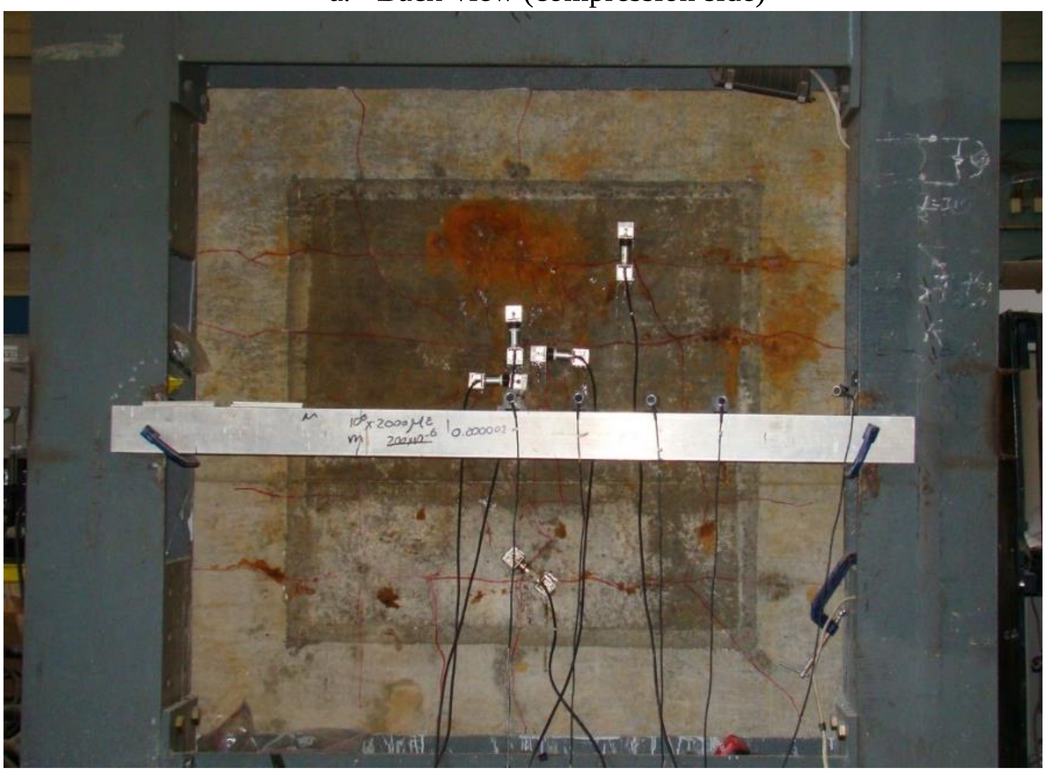

b. Front-view (tension side)

Figure 5-5 Photograph of a typical slab instrumentation on a test frame.

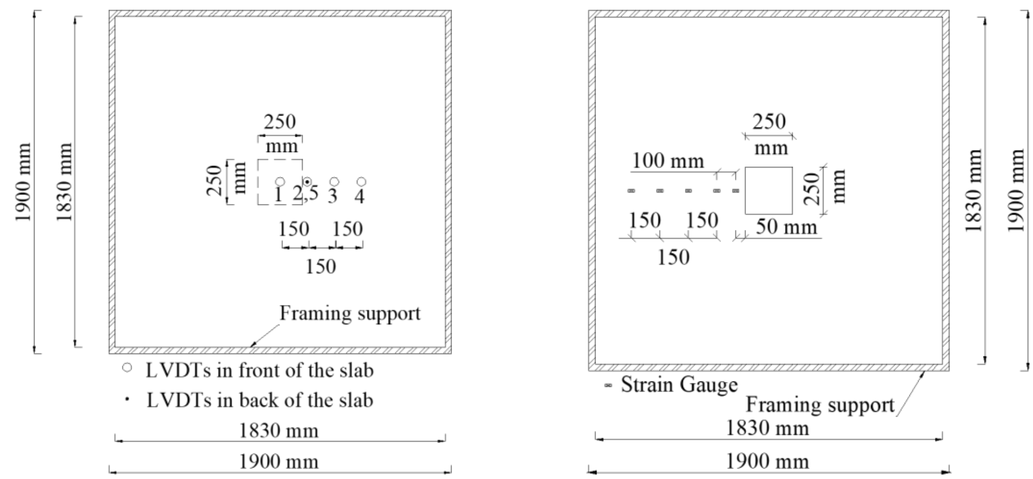

a. LVDTs b. Concrete strain

Figure 5-6 LVDTs and concrete strain gauges arrangements.

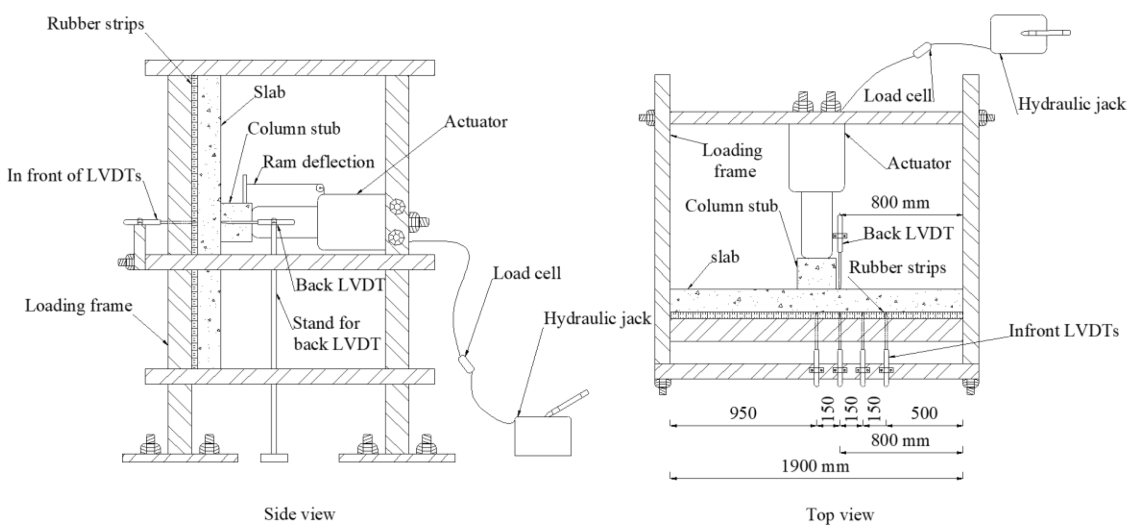

Figure 5-7 Schematic for the loading test setup.

5.5. Test Results and Discussion

5.5.1. Load Carrying Capacity

Figures 5.8-a to 5.8-d show the load-deflection curves for the test slabs S0, S15-D2, S25-D2, and S50-D2, respectively. Each figure shows the load-deflection of the four LVDTs that were placed in front of the slab as mentioned previously. Figure 5.8-e shows the load versus mid-deflection for all slab.

The shear capacity of the un-corroded slab S0 was 391 kN. Whereas the capacity of the corroded slabs S15-D2, S25-D2, and S50-D2 were 320 kN, 286 kN, and 183 kN, respectively. Consequently, the capacity of corroded slabs were reduced by 18.2%, 26.9%, and 53.1% for S15-D2, S25-D2, and S50-D2, respectively. Hence, the 50% mass loss in the flexural reinforcement within the targeted corroded area caused significant reduction in the peak punching capacity compared to S0. Aoude et al. (2014) simulated 50% mass loss in the full length of the flexural reinforcement. The results revealed that the punching capacity was reduced by 28% compared to the control specimen. The mass loss was simulated by reducing the bar diameter. In another study by Rahman (1992), it was found that 50% mass loss caused a reduction in punching capacity by 34% and 35% for uncoated bars and coated bars, respectively. In that study the mass loss was simulated by reducing the number of bars, the delamination by placing a polyethylene sheet between the two layers of the flexural reinforcement mesh, and the loss of bond by wrapping each bar by plastic adhesive tape. There was no agreement between the reduction in slab S50-D2 capacity and the previous two studies mentioned above. This could be attributed to several factors; firstly, changing the bar diameter or reducing the number of bars to simulate the mass loss would cause a change in the reinforcement ratio of the whole slab. That would cause a reduction of the punching shear capacities due to the lower reinforcement ratio (Marzouk & Hussein 1991; Dilger et al. 2005). The corrosion of the flexural reinforcement in the current study did not cover the full slab length. Consequently, the reduction in capacity was more pronounced than in the previous studies. Secondly, some bond between the bars and the concrete cover will still exist even after wrapping the bars with a plastic adhesive tape which would only cause a slight reduction in the bond. Thirdly, there were no corrosion cracks induced in the test slabs before the loading test. On the other hand, in the current study, an accelerated corrosion technique was applied to corrode the specimen under realistic simulation of the corrosion conditions. This would create more suitable environment to obtain better simulation of the behavior reflecting of the bond and mass loss. Moreover, the current slabs contained corrosion cracks before the loading test. As a result of these factors, a higher reduction in the capacity for severe corrosion were observed compared to those obtained by Aoude et al. (2014) and Rahman (1992). Table 5.4 shows a summary of the test results. The results show that S50-D2 failed before reaching the service load by 22.1%. Thus, S50-D2 would be unsafe as it cannot resist the acceptable serviceability limits. The service load was assumed as 60% of the capacity of the reference slab S0 which is around 235 kN (Aoude et al. 2014). On the other hand, the capacity of slabs S15-D2 and S25-D2 were above the service load by 38.2% and 21.7% respectively.

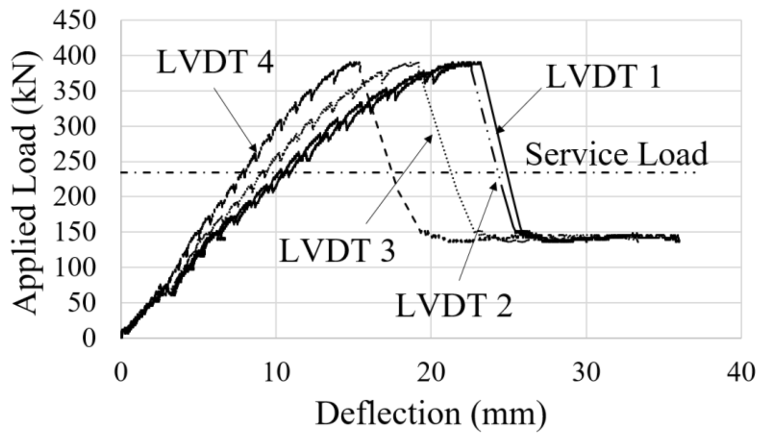

a. S0

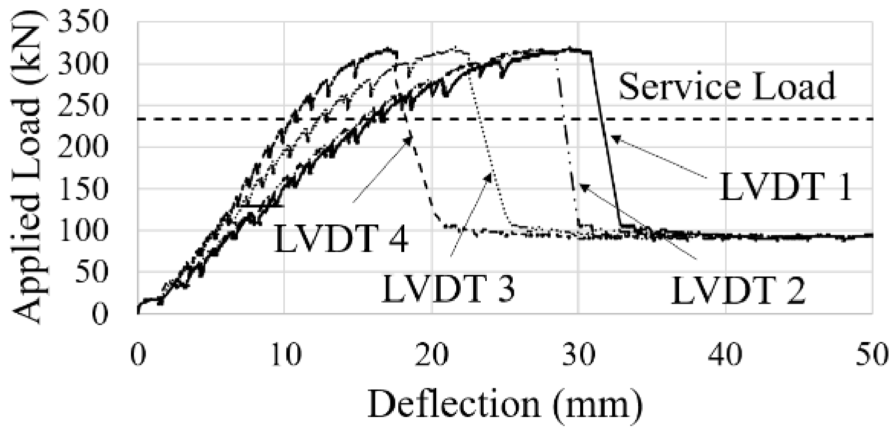

b. S15-D2

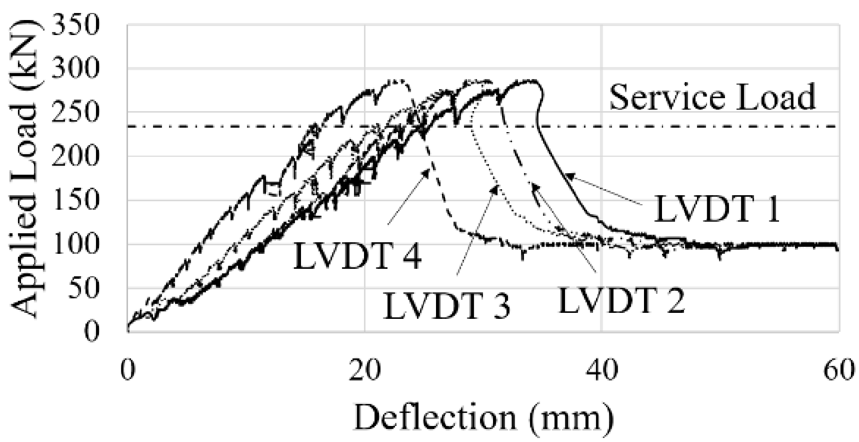

c. S25-D2

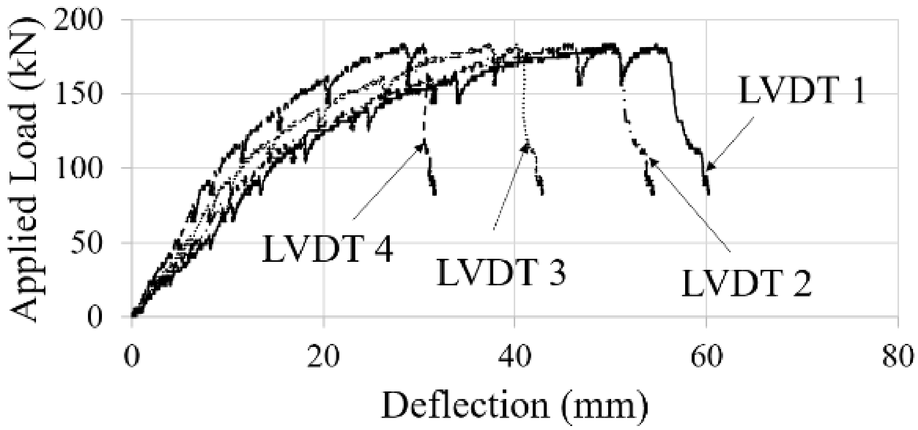

d. S50-D2

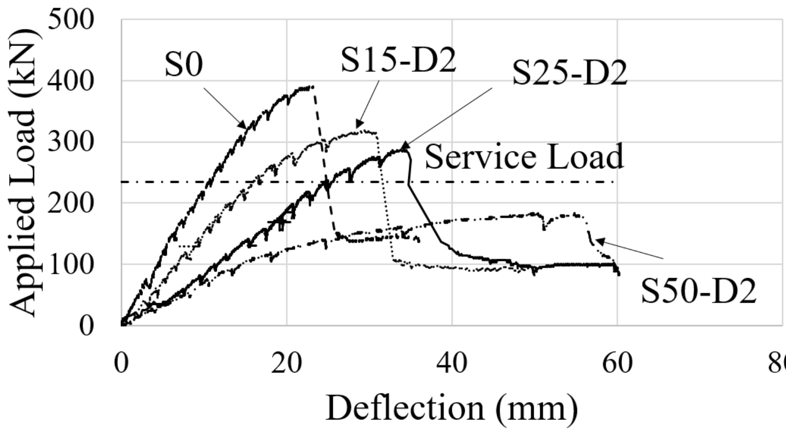

e. Applied load vs. mid-span deflection for all slabs

Figure 5-8 Applied load vs. deflection.

Table 5-4 Summary of Test Results

Specimen	w_c (mm)	Service Load P_{SL} (kN)	Service Load Δ_{SL} (mm)	Service Load w_{SL} (mm)	Capacity P_u (kN)	Capacity Δ_u (mm)	Capacity w_{max} (mm)
S0	0.00	235	10.6	0.71	391	21.8	2.49
S15-D2	0.40	235	16.0	2.01	320	29.4	4.72
S25-D2	0.80	235	24.5	5.25	286	32.8	8.10
S50-D2	2.90	-	-	-	183	49.2	9.39

w_c is the maximum crack width due to corrosion, P_{SL} is the service load for the un-corroded slab S0, Δ_{SL} is the deflection corresponding to the service load, w_{SL} is the maximum crack width at the service load, P_u is the experimental punching shear capacity, and Δ_u and w_{max} are the corresponding deflection and crack width at the ultimate load, respectively.

5.5.2. Stiffness

Figure 5.8 shows the load-deflection curves for slabs S0, S15-D2, S25-D2, and S50-D2. The figures show that the stiffness (slope of the load-deflection curve) decreased with increasing the percentage of mass loss. This observation is in agreement with previous studies (Aoude et al. 2014; Rahman 1992b). The stiffness for S0, S15-D2, S25-D2, and S50-D2 were 17.8 kN/mm, 11.6 kN/mm, 9.7 kN/mm, and 5.9 kN/mm, respectively. The reduction in the stiffness of slabs S15-D2, S25-D2, and S50-D2 was found to be 34.8%, 45.5%, and 66.9%, respectively. The slope of the reference slab was S0 the steepest one amongst all test slabs. The slab had no existing cracks due to corrosion before the loading test and hence it had its full stiffness. As the load was applied to S0, the first crack was observed at a load of 58 kN. As the load was increased, the slope gradually decreased until the reinforcement yielding, the slope decreased till ultimate load was reached. Finally, the load suddenly dropped and a horizontal load-deflection plateau was reached. There are two reasons that contributed to reducing the overall stiffness of the corroded slabs in addition to the corrosion cracks. The mass loss for the corroded bars reduces its cross-section and hence caused the yield of the reinforcement. In addition, the corrosion products between the corroded bar and concrete cover reduced the bond between them.

5.5.3. Slab Rotation and Energy Absorption

The energy absorption was calculated from the load-deflection plots shown in Fig. 5.8-e. Energy absorption is defined as the area under the load-deflection curve up to failure. The energy absorption values for slabs S0, S15-D2, S25-D2, and S50-D2 are 6157, 6594, 7556, and 6545 kN.mm, respectively. The energy absorption showed an increasing trend with the increase in mass for all test slabs except slab S50-D2. At such a high mass loss, the energy absorption for slab S50-D2 decreased. The energy absorption for the reference slab S0 was the lowest value. During the loading, the slabs absorbed the energy and the stresses were redistributed, and these formed plastic deformations without fracturing. This explains the increase of energy absorption with increasing mass loss till 25% mass loss. Nevertheless, when the mass loss exceeded 25%, the reduction of the flexural capacity increased to a high level, which as a consequence reduced the energy absorption value of the corroded slab. The slab with flexural failure tends to have higher energy absorption than those in failure in shear (Marzouk & Hussein 1991; Hussein 1990).

The slab rotations versus the applied loads are plotted in Fig. 5.9 for all test slabs. The slab rotation was measured for the slab portion outside the shear crack which rotates as a rigid body (Hussein 1990). The results indicated an increase in slab rotation with the increase in mass loss. This could be attributed to the loss of the stiffness due to the increase in mass loss.

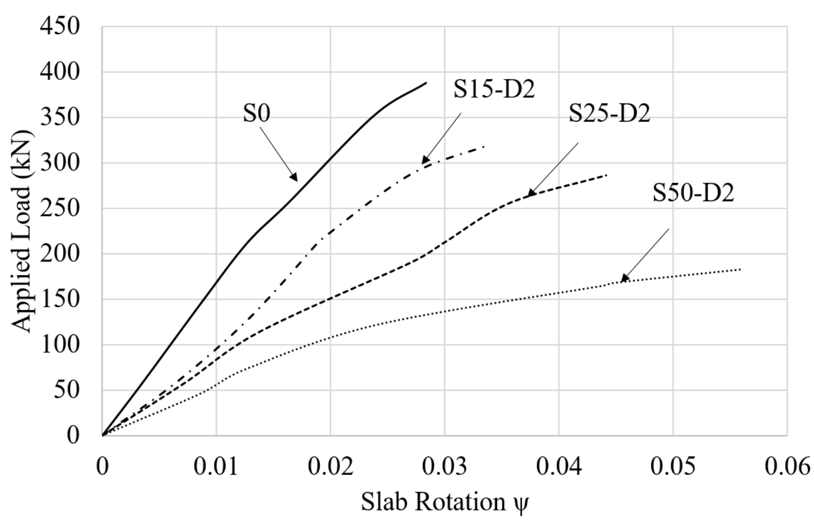

Figure 5-9 Applied load vs. slab rotation for test slabs.

5.5.4. Deflection Profiles

The deflection profiles for all slabs, at the ultimate load, are shown in Fig. 5.10. The deflection capacity is defined as the maximum deflection at failure load according to Maaddawy et al. (2006). The slab deflection capacity increased with the increase in mass loss as shown in Table 5.4. For slabs S15-D2, S25-D2, and S50-D2 the deflection capacity exceeded the control slab S0 by 34.9%, 50.4%, and 125.7%, respectively. This implies that S50-D2 had the highest value, where the deflection capacity increased with increasing the mass loss. This could be attributed to the reduction of the reinforcement area with increasing mass loss. In addition, the presence of the cracks due to corrosion reduced the stiffness. The crack widths increased with increasing mass loss, which caused a deterioration in the stiffness that led to increase the deflection capacities.

5.5.5. Ductility

Ductility is defined as the ratio between the deflections at ultimate load and first yielding of the reinforcement (Marzouk & Hussein 1991). This definition could not be used for the corroded slabs as it requires to measure the first yielding of reinforcement. It is not possible to use a normal electrical strain gauge to measure the strains in reinforcement for several reasons: first, the corrosion products would destroy the adhesion between the bar and the strain gauge. Second, if the strain gauge is well insulated to avoid the corrosion at this part, the remainder of the bar is subjected to corrosion which reduces its cross-sectional area of the bar and consequently affects the bar elongation. Consequently, the uninsulated portion will reach the yield strain before the insulated portion; as a result, the strain gauge would not read the real strains in the bar. Third, a direct current is used to induce corrosion in the bar; therefore, this could damage the strain gauge. Hence, the idea of using electrical strain gauges that are commonly used is not suitable. A revised ductility index was introduced by some researchers to refer to the deformation capacity of corroded beams until failure (Dang & François 2014). This ductility index is defined as the ratio of the deflection capacity of the corroded slab to the reference un-corroded one. Hence, if the index is equal to one, that means there is no corrosion in the slab. If the index value was more than one that means corrosion has taken place. Although this revised ductility index was proposed for corroded beams, it is adopted in the current paper for corroded slabs. Accordingly, the ductility indices for S0, S15-D2, S25-D2, and S50-D2 were 1, 1.34, 1.51, and 2.26, respectively. Hence, the ductility index increases with the increase in mass loss and that could be attributed to the increase in the deflection capacity.

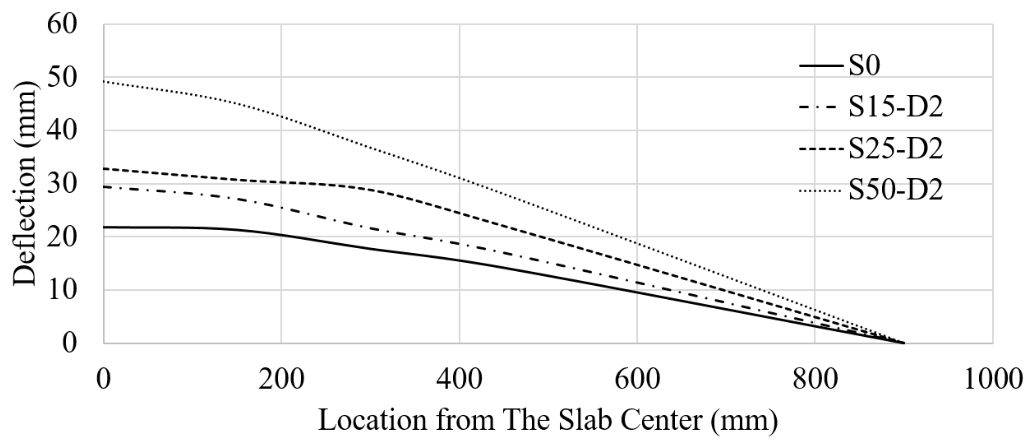

Figure 5-10 Deflection profile at ultimate load.

5.5.6. Cracking Response

Figure 5.11 shows the crack patterns in the specimen after the end of the corrosion process. The cracks occurred due to the corrosion products under the concrete cover. The corrosion products caused excessive internal pressure on the concrete cover, which caused it to crack. It was noticed that the crack numbers and widths increased with the increase of mass loss, which caused more internal pressure that led to more cracks with larger widths. The maximum crack widths in the corroded slabs were 0.40 mm, 0.80 mm, and 2.90 mm for S15-D2, S25-D2, and S50-D2, respectively, as listed in Table 5.4.

Figure 5.12 show the relationship between the crack widths and the applied load. The crack patterns at failure for all slabs are shown in Fig. 5.13. The maximum crack widths, at failure, were 2.49 mm, 4.72 mm, 8.1 mm, and 9.39 mm for S0, S15-D2, S25-D2, and S50-D2, respectively, as listed in Table 5.4. It could be seen that the maximum crack width increased with the increase in mass loss. This could be attributed to the preformation of cracks in the corroded slabs. In general, the reference slab S0 had the most crack intensity and the cracks were formed in an orthogonal pattern. Whereas few new cracks occurred in the corroded slabs during loading. Few new cracks were formed in slab S50-D2, and thus it had the lowest crack intensity compared with other slabs. In fact, the formation of new cracks decreased with the increase of mass loss. This could be attributed to the pre-existing cracks due to corrosion before the loading test. The width of cracks increased with higher mass loss and hence they became wider during loading test which led to the decrease in the formation of new cracks. After loading, the cracks in the corroded slabs formed in a radial flexural pattern in contrast to the reference slab S0. This could be attributed to the effect of reinforcement ratio. When the reinforcement ratio increases, the cracks tend to form in an orthogonal pattern, and if it decreases, the cracks starts to form in a radial pattern (Rashid 2004). Since the corrosion of the bars reduces the reinforcement ratio, the cracks in the corroded slabs tends to form in a radial pattern.

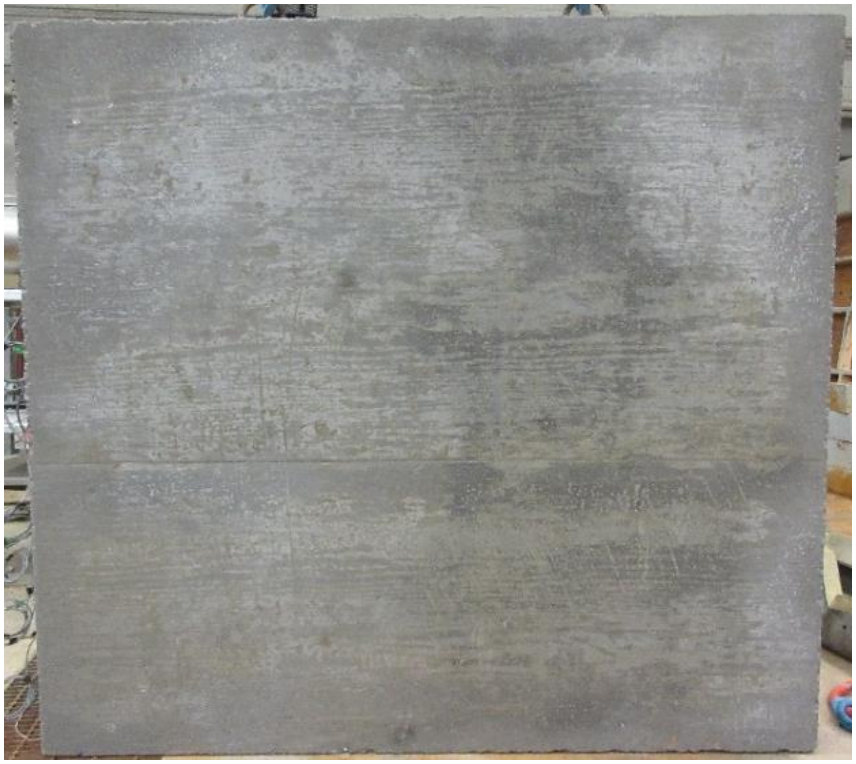

a. S0

b. S15-D2

c. S25-D2

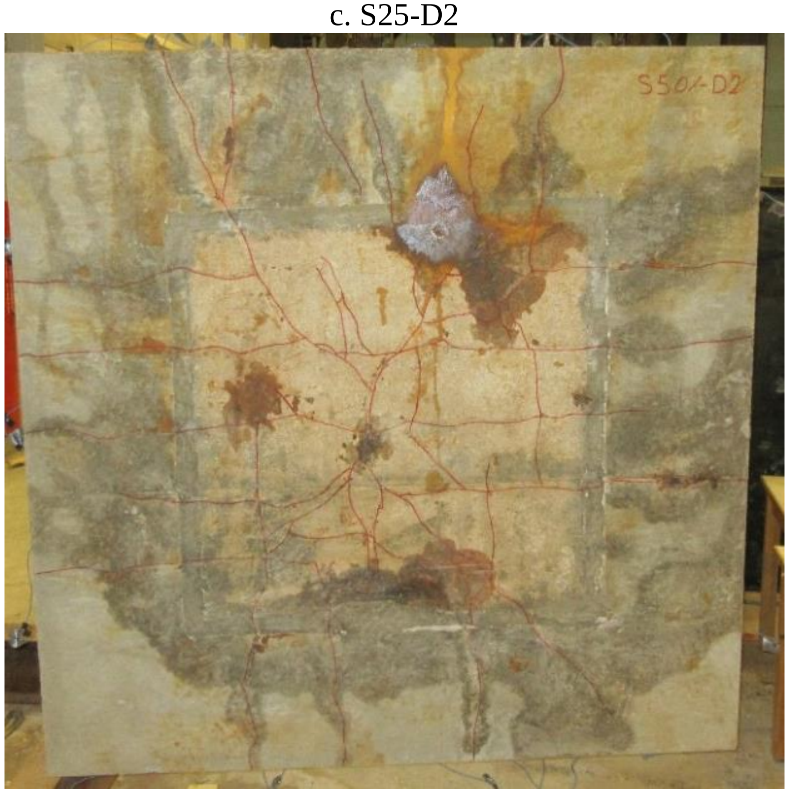

d. S50-D2

Figure 5-11 Cracks patterns due to corrosion before loading test.

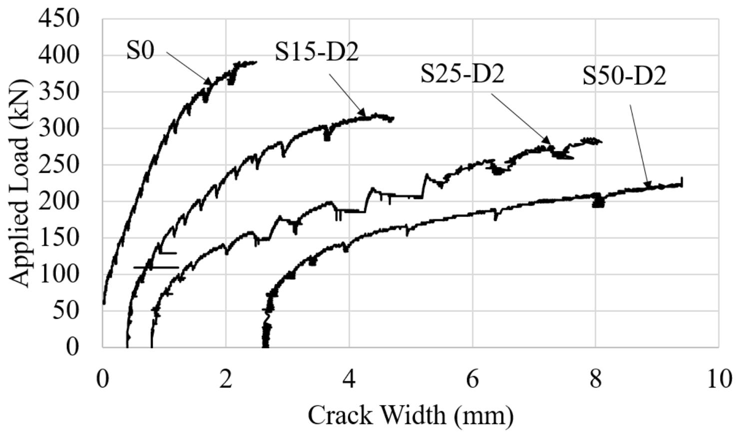

Figure 5-12 Crack width vs. applied load.

a. S0

b. S15-D2

c. S25-D2

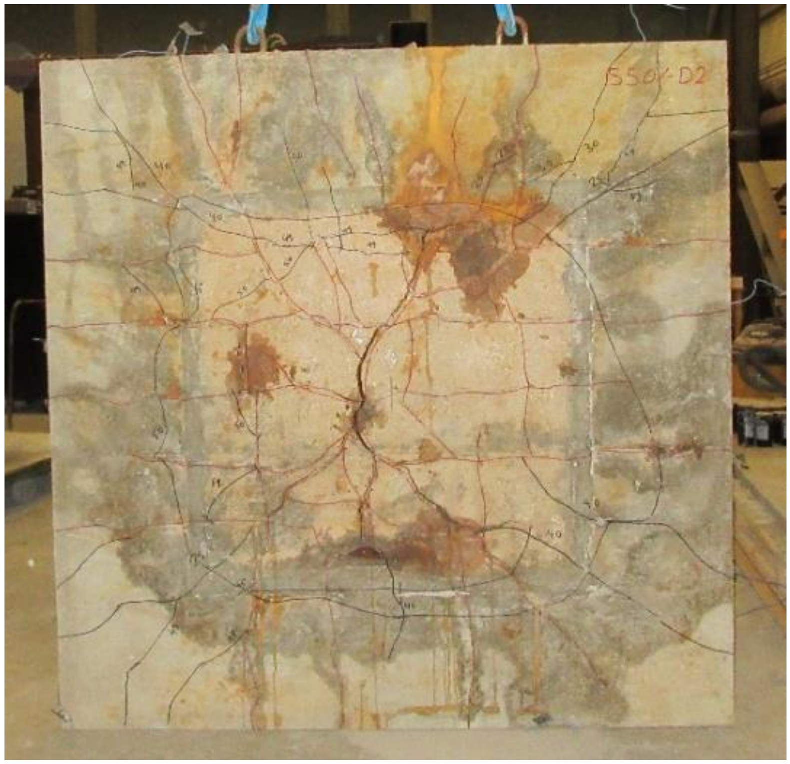

d. S50-D2

Figure 5-13 Crack patterns after loading test.

5.6. Comparison with Different Codes

Table 5.5 shows the experimental ultimate loads (P_u), the flexural capacity based on yield line theory $(P_{flexural})$, and the predictions of four codes (P_{code}); the Canadian Code (CSA A23.3-14 2014); the American Code (ACI 318-14 2014); the British Standard (BS 8110-97); and the European Code (EC2). The yield line theory has been used to differentiate if the failure occurred due to shear or flexural. For conventional slab-column connection test specimen (Marzouk & Hussein 1991). In Table 5.5, the flexural capacity is calculated using yield line theory and assuming that the area of reinforcement remains the same even for corroded slabs. $P_u/P_{flexural}$ are less than one for all slabs, which mean that they failed due to punching. For the reference slab S0, $P_u/P_{flexural}$ is equal to 0.88 which could be considered as a ductile punching (Marzouk & Hussein 1991). The $P_u / P_{flexural}$ values for slabs S15-D2, S25-D2 are 0.72, 0.64, and 0.41, respectively. This would indicate that the failures were due to punching. The ultimate capacity was reduced by 18.2%, 26.9%, and 53.1% for mild corrosion slab 15%, moderate corrosion 25%, and severe corrosion 50%, respectively. For mild corrosion (S15-D2), the actual capacity of the slab is above the design capacity according to ACI 318-14 and EC2 by 3% and 7%, respectively. According to CSA A23.3-14 and BS8110-97, the actual capacities for all corroded slabs are below the design capacities. The slabs with moderate to severe corrosion, S25-D2 and S50-D2, have no margin of safety according to all design codes. The actual capacity of S50-D2 is lower than the design values calculated by CSA A23.3-14, BS8110-97, ACI 318-14, and EC2 by 49%, 45%, 41%, and 39%, respectively. Slab S25-D2 with moderate corrosion has a capacity that is lower by 20%, 14%, 8%, and 5% according to CSA A23.3-14, BS8110-97, ACI 318-14, and EC2, respectively. It should be noted that the North American Codes (CSA and ACI) do not take the effect of the reinforcement ratio into consideration in calculating the punching shear capacity of slabs. Whereas the British standard and the European code consider the effect of the flexure reinforcement ratio (British Standards Institution 2004; BS 8110 1997). The resistance factors in the code equations are taken as unity when comparing the prediction of the code equations to the test results and the reinforcement area was assumed to be un-affected by corrosion.

Table 5.6 shows the capacity based on yield line theory, EC2, and BS8110-97 by reducing the reinforcement ratio in proportion to the mass loss. The design capacity was not recalculated based on North American Codes as it is not included in these codes as a parameter. Based on BS8110-97, the design capacity of the corroded slabs with a reduction in the reinforcement area by 15%, 25%, and 50% give prediction values that are less than the actual ones by 2%. On the other hand, the code overestimate the capacity of the corroded slabs S25-D2 and S50-D2 by 5% and 30%, respectively. In a similar fashion the EC2 code predictions, for 15% and 25% reduction in reinforcement ratio, are lower than the actual capacity by 13% and 5%, respectively. Whereas the reduction of 50% in mass led to an overestimation of the capacity by 23%. Regarding the yield line theory, the values of $P_u / P_{flexural}$ are 0.83, 0.83, and 0.78 for S15-D2, S25-D2, and S50-D2, respectively. This indicates that all corroded slabs failed in shear. It should be noted that the length of the bars within the targeted area only was subjected to corrosion. Outside that area, the development length remained intact. This would have an effect on the reinforcement ratio on the slab that is used in the calculations. In addition, the reduction in the reinforcement area alone does not necessarily reflect the reduction in bond due to corrosion.

Table 5-5 Test Results versus Code Predictions Assuming No Reduction in the Reinforcement Area

Slab	P_u kN	$P_{flexural}$ kN	$\frac{P_u}{P_{flexural}}$	CSA 23.3-14		BS 8110-97		ACI 318-14		EC2	
				P_{code} kN	$\frac{P_u}{P_{code}}$	P_{code} kN	$\frac{P_u}{P_{code}}$	P_{code} kN	$\frac{P_u}{P_{code}}$	P_{code} kN	$\frac{P_u}{P_{code}}$
S0	391	447	0.88	359	1.09	332	1.18	312	1.25	300	1.30
S15-D2	320		0.72		0.89		0.96		1.03		1.07
S25-D2	286		0.64		0.80		0.86		0.92		0.95
S50-D2	183		0.41		0.51		0.55		0.59		0.61

***** P_u is the experimental punching shear capacity, $P_{flexural}$ is the flexural slab capacity, and P_{code} is the code predicted punching shear resistance.

Table 5-6 Test Results versus Code Predictions Using Reduced Reinforcement Ratio

Slab	P_u kN	$P_{flexural}$ kN	$\frac{P_u}{P_{flexural}}$	**BS 8110-97** P_{code}	**BS 8110-97** $\frac{P_u}{P_{code}}$	**EC2** P_{code}	**EC2** $\frac{P_u}{P_{code}}$
S15-D2	320	385	0.83	314	1.02	284	1.13
S25-D2	286	343	0.83	301	0.95	272	1.05
S50-D2	183	234	0.78	263	0.70	238	0.77

***** P_u is the experimental punching shear capacity, $P_{flexural}$ is the flexural slab capacity, and P_{code} is the code predicted punching shear resistance.

5.7. Conclusions

The following conclusions can be drawn from the experimental investigation on two-way slabs that are subjected to different levels of corrosion within a large area but with sufficient intact development length. The levels of corrosion are 0% (control), 15% (mild), 25% (moderate), 50% (severe) mass loss.

- Increasing the corrosion level causes a reduction in the punching shear capacity that could be considered as significant. The capacity decreases by 18.2%, 26.9%, and 53.1% for mild, moderate, and severe corrosion level, respectively.
- The ultimate load for the slabs with mild and moderate corrosion, S15-D2 and S25-D2, were above the service load. However, the capacity of the slab with severe corrosion, S50-D2, felt below the service load of the reference. Hence, 50% of mass loss for large corroded even with adequate development length could lead to collapse.

- The corrosion of the flexural reinforcement also causes a significant decrease in the stiffness by 34.8%, 45.5%, and 66.9% for 15%, 25%, and 50% mass loss, respectively.
- A ductility index term was introduced in this study. This term was previously prepared for corroded beams by Dang & François (2014). Ductility index is defined as the ratio between the deflection capacity of a corroded slab to that without corrosion. The ductility indices were 1.34, 1.51, and 2.26 for mild, moderate, and severe corrosion, respectively.
- The energy absorption increases with increasing the level of corrosion for mild and moderate corrosion levels. However, it tends to decrease at severe level. Energy absorption for S0 still the lowest value.
- The slab rotation and deflection capacity increase with the increase in the mass loss due to the decrease in stiffness and deterioration of bond.
- The crack numbers and crack widths due to corrosion increased with the increase in mass loss. The corrosion products that were formed caused a larger tensile pressure under the concrete cover that led to larger cracks on the concrete surface.
- The cracks formed in a radial pattern in the corroded slabs as opposed to an orthogonal pattern at the control slab. The reduction in the area of reinforcement due to corrosion reaches the flexural cracking more predominated.
- The capacity of all corroded slabs fell below the design values according to CSA A23.3-14, BS8110-97, EC2, and ACI A318-14. The slab with mild corrosion has a margin of safety of 3% and 7% according to ACI A318-14 and EC2, respectively. By reducing the reinforcement ratio with a proportion similar to the mass loss in the

corroded slabs, to calculate the code design capacities, BS8110-97 and EC2 gave a safe estimate for slabs with mild corrosion. This procedure could not be used with CSA A23.3-14 and ACI A318-14 as codes do not take into consideration the effect of reinforcement ratio on the calculation of the punching capacities.

5.8. References

ACI 318-14 (2014) Building code requirement for structural concrete (ACI 318M-14) and commentary (ACI 318RM-14), Building Code Requirements for Structural Concrete.

Ahmad, S. (2003) 'Reinforcement corrosion in concrete structures, its monitoring and service life prediction - A review', Cement and Concrete Composites, 25(4–5 SPEC), pp. 459–471. doi: 10.1016/S0958-9465(02)00086-0.

Almusallam, A., Al-Gahtani, A. S., Aziz, A. R. and Rasheeduzzafar, A. (1996) 'Effects of reinforcement corrosion on bond strength', Construction and Building Materials, 10(2), pp. 123–129.

Altoubat, S., Maalej, M. and Shaikh, F. U. A. (2016) 'Laboratory simulation of corrosion damage in reinforced concrete', International Journal of Concrete Structures and Materials. Korea Concrete Institute, 10(3), pp. 383–391. doi: 10.1007/s40069-016-0138-7.

Andrade, C. and Alonso, C. (1996) 'Corrosion rate monitoring in the laboratory and on-site', Construction and Building Materials, 10(5 SPEC. ISS.), pp. 315–328. doi: 10.1016/0950-0618(95)00044-5.

Andrade, C. and Alonso, C. (2001) 'On-site measurements of corrosion rate of reinforcements', Construction and Building Materials, 15(2–3), pp. 141–145. doi: 10.1016/S0950-0618(00)00063-5.

Aoude, H., Cook, W. D. and Mitchell, D. (2014) 'Effects of simulated corrosion and delamination on response of two-way slabs', Journal of structural Engineering, 140(1), pp. 1–9. doi: 10.1061/(ASCE)ST.1943-541X.0000775.

ASTM C150/C150M (2017) 'Standard specification for Portland cement', ASTM International, p. 9.

ASTM C876 (2015) 'Standard test method for corrosion potentials of uncoated reinforcing steel in concrete', p. 8. doi: 10.1520/C0876-09.2.

Berto, L., Simioni, P. and Saetta, A. (2008) 'Numerical modelling of bond behaviour in RC structures affected by reinforcement corrosion', Engineering Structures. Elsevier, 30(5), pp. 1375–1385.

Bertolini, L., Elsener, B., Pedeferri, P., Redaelli, E. and Polder, R. B. (2013) Corrosion of steel in concrete: prevention, diagnosis, repair. John Wiley & Sons.

Bonacci, J., Thomas, M., Hearn, N., Lee, C. and Maalej, M. (1998) 'Laboratory simulation of corrosion in reinforced concrete and repair with CFRP wraps', in Annual Conference of the Canadian Society of Civil Engineering, pp. 653–662.

British Standards Institution (2004) Eurocode 2: design of concrete structures: part 1-1: general rules and rules for buildings. British Standards Institution.

Broomfield, J. P. (2006) Corrosion of steel in concrete: understanding, investigation and repair, Second Edition. doi: 10.4324/9780203414606.

BS 8110 (1997) 'Structural use of concrete. Part I: Code of practice for design and construction', British Standards Institution, UK.

Carnot, A., Frateur, I., Zanna, S., Tribollet, B., Dubois-Brugger, I. and Marcus, P. (2003) 'Corrosion mechanisms of steel concrete moulds in contact with a demoulding agent studied by EIS and XPS', Corrosion science. Elsevier, 45(11), pp. 2513–2524.

Chitty, W.-J., Dillmann, P., L'Hostis, V. and Lombard, C. (2005) 'Long-term corrosion resistance of metallic reinforcements in concrete—a study of corrosion mechanisms based on archaeological artefacts', Corrosion Science. Elsevier, 47(6), pp. 1555–1581.

Coronelli, D. and Gambarova, P. (2004) 'Structural assessment of corroded reinforced concrete beams: modeling guidelines', Journal of Structural Engineering. American Society of Civil Engineers, 130(8), pp. 1214–1224.

CSA A23.3-14 (2014) Design of concrete structures. Mississauga, Ont.: Canadian Standard Association.

Dang, V. H. and François, R. (2014) 'Prediction of Ductility Factor of Corroded Reinforced Concrete Beams Exposed to Long Term Aging in Chloride Environment', Cement and

Concrete Composites, 53(October 2014), pp. 136–147. doi: 10.1016/j.cemconcomp.2014.06.002.

Dilger, W., Birkle, G. and Mitchell, D. (2005) 'Effect of flexural reinforcement on punching shear resistance', ACI Special Publication 232-4, pp. 57–74. doi: 10.1007/s13398-014-0173-7.2.

Dodd, L. L. and Restrepo-Posada, J. I. (1995) 'Model for predicting cyclic behavior of reinforcing steel', Journal of Structural Engineering. American Society of Civil Engineers, 121(3), pp. 433–445.

Donnelly, J. P., Pulver, B. E. and Popovic, P. L. (2006) 'Condition assessment of parking structures', In Structures Congress : Structural Engineering and Public Safety ASCE., p. 10.

El-Maaddawy, T. and Soudki, K. (2003) 'Effectiveness of impressed current technique to simulate corrosion of steel reinforcement in concrete', Journal of Materials in Civil Engineering. American Society of Civil Engineers, 15(1), pp. 41–47. doi: 10.1061/(ASCE)0899-1561(2003)15:1(41).

El-Maaddawy, T., Soudki, K. and Topper, T. (2005a) 'Analytical model to predict nonlinear flexural behavior of corroded reinforced concrete beams', ACI Structural Journal, 102(4), pp. 550–559.

El-Maaddawy, T., Soudki, K. and Topper, T. (2005b) ‘Long-term performance of corrosion-damaged reinforced concrete beams’, ACI Stractural Journal, 102(5), pp. 649–656.

Fedrizzi, L., Azzolini, F. and Bonora, P. L. (2005) ‘The use of migrating corrosion inhibitors to repair motorways’ concrete structures contaminated by chlorides’, Cement and concrete research. Elsevier, 35(3), pp. 551–561.

Hussein, A. A. (1990) Behaviour of reinforced concrete slabs made with high-strength concrete. Memorial University of Newfoundland.

Kashani, M. M., Crewe, A. J. and Alexander, N. A. (2013) ‘Nonlinear stress-strain behaviour of corrosion-damaged reinforcing bars including inelastic buckling’, Engineering Structures, 48, pp. 417–429. doi: 10.1016/j.engstruct.2012.09.034.

Lachemi, M., Al-Bayati, N., Sahmaran, M. and Anil, O. (2014) ‘The effect of corrosion on shear behavior of reinforced self-consolidating concrete beams’, Engineering Structures. Elsevier Ltd, 79, pp. 1–12. doi: 10.1016/j.engstruct.2014.07.044.

Marzouk, H. and Hussein, A. (1991) ‘Experimental investigation on the behavior of high-strength concrete slabs’, ACI Structural Journal, 88(6), pp. 701–713. doi: 10.1139/l91-118.

Miyagawa, T. (1991) ‘Durability design and repair of concrete structures: chloride corrosion of reinforcing steel and alkali–aggregate reaction’, Magazine of Concrete Research. Thomas Telford Ltd, 43(156), pp. 155–170.

Pritzl, M. D., Tabatabai, H. and Ghorbanpoor, A. (2014) 'Laboratory evaluation of select methods of corrosion prevention in reinforced concrete bridges', International Journal of Concrete Structures and Materials, 8(3), pp. 201–212. doi: 10.1007/s40069-014-0074-3.

Rahman, A. H. (1992) 'Effect of steel corrosion on the strength of slab-column connections', National Research Council Canada, Institute for Research in Construction.

Rashid, M. I. (2004) Concrete Slabs Reinforced with GFRP Bars. Memorial University of Newfoundland.

Raupach, M. (1996) 'Chloride-induced macrocell corrosion of steel in concrete - Theoretical background and practical consequences', Construction and Building Materials, 10(5 SPEC. ISS.), pp. 329–338. doi: 10.1016/0950-0618(95)00018-6.

Reilly, J. L., Cook, W. D., Bastien, J. and Mitchell, D. (2014) 'Effects of delamination on the performance of two-way reinforced concrete slabs', Journal of Performance of Constructed Facilities, 28(4), pp. 1–8. doi: 10.1061/(ASCE)CF.

Roberge, P. R. and Pierre, R. (1999) Handbook of corrosion engineering library of congress cataloging-in-publication data. doi: 10.1016/S0026-0576(00)83445-5.

Talakokula, V., Bhalla, S. and Gupta, A. (2014) 'Corrosion assessment of reinforced concrete structures based on equivalent structural parameters using electro-mechanical impedance technique', Journal of Intelligent Material Systems and Structures, 0(0), pp. 1–16. doi: 10.1177/1045389X13498317.

Zhang, B., Masmoudi, R. and Benmokrane, B. (2004) ‘Behaviour of one-way concrete slabs reinforced with CFRP grid reinforcements’, Construction and Building Materials, 18(8), pp. 625–635. doi: 10.1016/j.conbuildmat.2004.04.007.

Chapter 6 Corroded Two-way Slabs with Insufficient Development Length

6.1. Abstract

The experimental work presented in this paper investigated the effect of large corroded area of the flexural reinforcement on the structural response of two-way reinforced concrete slabs. Four typical full-size two-way reinforced concrete slabs were fabricated and tested for this study. The slab dimensions were 1900 mm × 1900 mm × 150 mm. The reinforcement of the slabs were totally corroded except for one-half of the development length at the end of the reinforcement. The corroded area was 1480 mm × 1480 mm. A uniform level of corrosion was induced by using an accelerated corrosion technique through applying constant current density of $200 \mu A/cm^2$ through the reinforcement. Four different levels of corrosion were reached 0%, 15%, 25%, and 50% of the mass loss. The results are obtained in terms of load versus deflection curves, load versus crack width curves, crack patterns, deflection profiles, slab rotations, energy absorption, and ductility index. The results showed that the increase in mass loss, led to a reduction in the slab capacity and stiffness. Whereas the deflection capacities, slab rotations, and crack widths increased with increased mass loss. The experimental failure loads were compared with the predictions of four different codes. None of codes gave safe predictions for the slabs with 25% and 50% mass loss.

Keywords: Accelerated corrosion technique; development length; deflection; ductility index

6.2. Introduction

One of the serious degradation problems in any reinforced concrete (RC) structure is the corrosion of the embedded reinforcement (Broomfield 2006). Concrete structures nowadays are the most widely used in the construction of infrastructure (Chung et al. 2008). Some countries have harsh environmental conditions that could cause corrosion to the embedded reinforcement in the concrete elements. For instance, offshore structures are constructed in the North Atlantic and in Arctic regions. In addition, parking garages and bridges are exposed to de-icing salts in the snowfall seasons. Moreover, the structures in the Persian Gulf are surrounded by ambient salinity atmosphere that distinguishes this region (Broomfield 2006). Flexural or shrinkage cracks exist in RC structures in corrosive environment such as salt-laden condensation and contaminated rainwater with carbon dioxide. In the presence of moisture, this corrosive mixture could ingress through the cracks and reach the reinforcement which may induce corrosion process and accelerates it (Zhang et al. 2004).

Many efforts were made to study the corrosion from various aspects. Some of the investigations were conducted to have a better understanding of the corrosion process (for example, Raupach 1996; Carnot et al. 2003; Chitty et al. 2005). Others were carried out to examine the effect of corrosion on RC beams (for example, El-Maaddawy & Soudki 2003). In addition, monitoring the corrosion rate was also investigated (Andrade & Alonso 1996; Andrade & Alonso 2001; Ahmad 2003). Some researchers developed models to predict the structural behaviour of corroded beams. The models were verified using experimental results (Dodd & Restrepo-Posada 1995; Berto et al. 2008; Coronelli & Gambarova 2004).

Repair and rehabilitation of corroded beams were also investigated (Bertolini et al. 2013; Miyagawa 1991; Fedrizzi et al. 2005; Broomfield 2006). Nonetheless, there are very limited investigations on the effect of corrosion when it comes to two-way RC slabs. Therefore, the objective of the current study is to focus on developing a better understanding of the behaviour of corroded two-way RC slabs that are widely used in partaking garages and bridge decks. They are mostly subjected to deterioration due to corrosion that occurs because of the use of de-icing salts in winter seasons (Donnelly et al. 2006).

Rahman (1992) simulated the corrosion of the reinforcement in slab-column connections by decreasing the number of flexural reinforcement bars and wrapping the reinforcement with an adhesive plastic tape to simulate the loss of bond. Moreover, a polyethylene sheets were placed between the top and lower layers of the flexural reinforcement to simulate the delamination. The author concluded that 30% of the punching shear capacity was reduced due to a simulated 50% mass loss of the bars. The simulated loss of bond and delamination led to the formation of more cracks and increased deflection; however, they did not have significant effect on the punching capacity. Aoude et al. (2014) examined the effect of corrosion on two-way slab-column connection. The corrosion was simulated by using smaller bar diameter. The authors also examined the effect of delamination by placing a plastic sheet under the top reinforcement. The effect of different delaminated areas was investigated. It was concluded that small delaminated areas had small effect on the punching capacity. However, when the delaminated area increased the capacity decreased. Moreover, corrosion and delamination increased the crack widths. Reilly et al. (2014)

examined the effect of simulated delamination and presence of structural integrity bars on the structural behavior of two-way slabs. The authors simulated the delamination using the same technique that was followed by Aoude et al. (2014). It was concluded that delamination caused deterioration of the punching shear capacity and post-punching stiffness of the slabs. They also concluded that the presence of integrity bars increased both the capacity and the post-punching resistance.

Nevertheless, two-way slabs with actual corroded bars in the literature. Accelerated corrosion techniques were used in several investigations to study the structural behaviour of corroded beams (El-Maaddawy & Soudki 2003; El-Maaddawy et al. 2005a; Kashani et al. 2013; Pritzl et al. 2014; Talakokula et al. 2014; Altoubat et al. 2016). Said & Hussein (2019) investigated the use of two accelerated corrosion techniques for two-way slabs. The authors concluded that using constant current could lead to some benefits over constant voltage regarding time management and cost. However, both techniques showed a close agreement between actual and theoretical mass loss. On the other hand, the current could not be controlled in constant voltage technique and could reach high values. That could lead to more damage in the specimen. Hence, a constant current technique was used in the current study. There is need to investigate two-way slabs with corroded bars such research would provide better simulation of the behaviour of the bond, the change of steel mechanical properties, and the cracks of the concrete cover due to corrosion. Thus, a better understanding of the behaviour of corroded two-way RC slabs could be developed.

6.3. Research Significance

The present work aims to investigate the effect of different levels of corrosion that cause the flexural reinforcement in two-way slabs to have inadequate development length. The review of the literature on this subject indicates that most of the available research has been carried out under non-realistic conditions and there is no data available when it comes to testing of slabs with corroded reinforcement. Therefore, this work is conducted to investigate the corrosion effects on two-way slabs using an accelerated corrosion technique. This technique is used to ensure more realistic representation for both the bond deterioration and crack growth due to corrosion of reinforcement. The study evaluates the structural performance under different levels of corrosion. The authors believe that this study will effectively contribute to enhancing the understanding of the performance of two-way RC slabs with corroded reinforcement. Moreover, the results of the investigation would provide guidance to practicing engineers to evaluate the performance and residual capacity of corroded slabs.

6.4. Experimental Program

This paper used an accelerated corrosion technique to investigate the effect of three different corrosion levels on the structural behaviour of two-way slabs. The corroded reinforcement exceeded the development length of the embedded bars. The test results are presented in terms of load vs. deflection response, load vs. crack width curves, crack patterns, deflection profiles, slab rotations, and ultimate loads.

6.4.1. Details of Test Specimen

Each slab specimen was reinforced at the tension side with 15M bars spaced at 190 mm, and in the compression side with 10M bars spaced at 300 mm. The bars conform to CAN/CSA-G30. 18-09 (2009). The 10M bars have a diameter of 11.3 mm and cross sections area of 100 mm^2, and the 15M bars have a diameter of 16 mm and cross sections area of 200 mm^2. All test slabs had a span of 1900 mm × 1900 mm and a thickness of 150 mm. The concrete clear cover was 30 mm and the effective depth (d) was 104 mm. The configuration and dimensions of all slabs are shown in Fig. 6.1. In order to prepare the slabs for the accelerated corrosion before casting, two wires were connected to each bar from its end and eventually they were connected to a power source. In addition, all intersection points of the reinforcement were insulated to avoid any electrical conductivity between the bars using electrical tape and plastic ties. A wooden formwork was constructed and the reinforcement was placed inside it as shown in Fig. 6.2. Then the concrete was poured and compacted using a mechanical vibrator. The column stub was cast separately. After 24 hrs from casting the column stub, the formwork was removed and the specimen was water-cured for four days then air-cured the remaining 28 days. Table 6.1 shows the details of the test specimens.

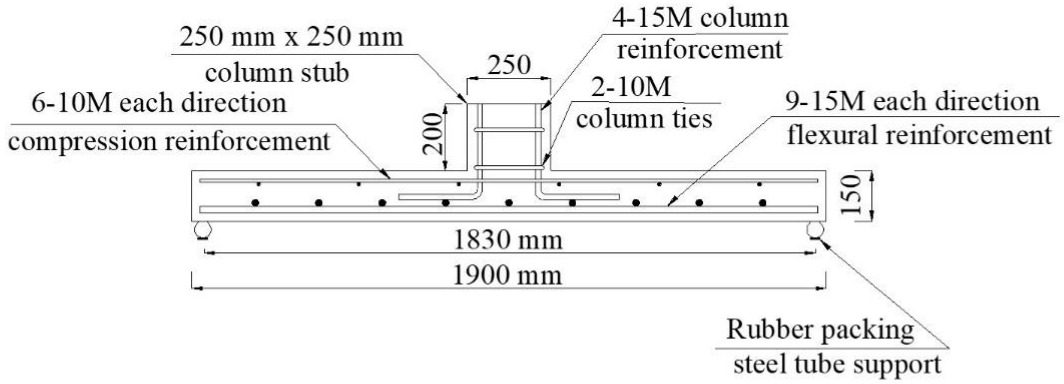

Figure 6-1 Details of typical slab.

Figure 6-2 Formwork and reinforcement mesh.

Four different levels of corrosion were targeted; 0%, 15%, 25%, and 50% mass loss. In the absence of a universally agreed-upon definition, the lowest level of corrosion, 15% mass loss, is referred to as “mild”, while the middle level, with 25% mass loss, as “moderate”, and the highest level, with 50% mass loss as “severe. The letter S is added before each level of corrosion as an indication for each slab. For example, slab S15-D3 refers to the slab with 15% mass loss. The corroded area was 1480 mm × 1480 mm. Hence, the reinforcement did not have enough development length and the corroded area extended all over the slab leaving only $0.5L_d$ intact at the ends of each bar as shown in Fig. 6.3. The development length, L_d, is calculated using the simplified version of CSA A23.3-14 (2014):

$$L_d = 0.45\, k_1\, k_2\, k_3\, k_4 \frac{f_y}{\sqrt{f'_c}}\, d_b \tag{6.1}$$

where f_y, f'_c, and d_b are the yield stress of the reinforcement, the compressive strength of the concrete, and the nominal diameter of the reinforcing bars, respectively. The factors k_1, k_2, k_3, and k_4 are bond location factor, coating factor, concrete density factor, and bar size factor, respectively. The first three factors can be taken as 1; while the fourth one is taken as 0.8 for 20M or smaller bars.

Table 6-1 Details of Slab Specimens

Side dimensions (mm × mm)	h (mm)	c (mm)	d (mm)	f'_c (MPa)	Main reinforcement
1900 × 1900	150	250	104	41.1	Two layers-15M bars

*h is the height; c is the column width; d is the effective slab depth; and f'_c is the concrete compressive strength.

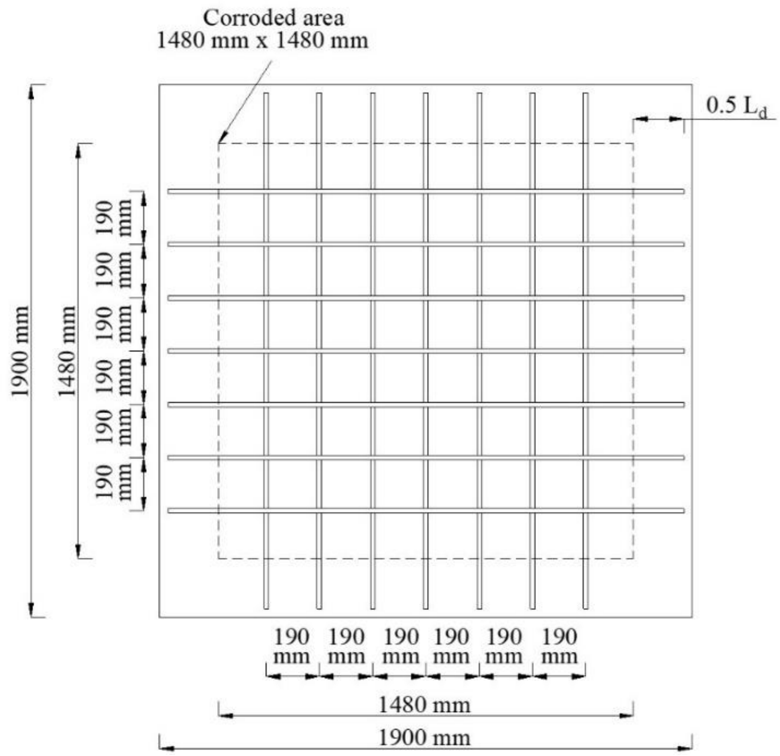

Figure 6-3 The targeted corroded area.

6.4.2. Material Properties

Table 6.2 shows the composition used for one cubic meter of concrete. The cement used was general use (GU) Canadian Portland cement with a specific gravity of 3.15, similar to American Society for Testing and Materials (ASTM) Type I (ASTM C150/C150M 2017). Crushed granite with 10 mm maximum size and sand of the same composition were used as coarse and fine aggregates, respectively. Both aggregates had a specific gravity of 2.6. The targeted compressive strength at 28 days was 40 MPa using Water to Cement ratio (w/c) equal to 0.4. The compressive strength and w/c were chosen to meet the requirements for Class F3 exposure (ACI 318-14 2014). This exposure class is assigned for horizontal concrete elements exposed to de-icing chemicals, freeze-thaw cycles, parking garages, foundations, and basement walls. The concrete used was batched at a local batch plant. The measured properties of the reinforcement and the mechanical properties of the concrete are showed in Table 6.3.

Table 6-2 Mix Composition of Concrete Mixture

Cement (kg)	w/c	Water (l)	C/F	C.A. (kg)	F.A. (kg)	Aggregate size (mm)	Fresh density (kg/m^3)
350	0.4	140	1.3	1083	833	10	2407

* w/c is the water to cement ratio, C/F is the coarse to fine ratio, C.A. is the coarse aggregate, and F.A. is the fine aggregate

Table 6-3 Steel and Concrete Properties

Designation	Steel properties			Concrete Properties	
	Area (mm^2)	f_y (MPa)	ε_y $(\mu\varepsilon)$	f_c' (MPa)	f_r (MPa)
15M	200	475	2200	41.1	3.82

* f_y is the yield strength, ε_y is the yield strain, f_c' is the compressive strength, and f_r is the modulus of rupture.

6.4.3. Accelerated Corrosion Setup

An accelerated corrosion technique was used through applying a constant current of 0.15 A to induce the different percentages of mass loss in the reinforcement. This current value corresponds to a current density of $200\mu A/cm^2$, which is the maximum as recommended by El Maaddawy & Soudki (2003) to avoid any significant increase in crack width and strain response due to the corrosion. The current density is defined as the current in Amperes divided by the surface area of the bar. Hence, the power supply was adjusted to provide a constant current 0.15 A for a bar diameter of 16 mm and targeted length of 1480 mm. This relatively high electrical current was applied in order to reach the targeted mass loss in a reasonable time period. Slabs S15-D3, S25-D3, and S50-D3 took 87, 145, and 290 days, respectively to reach their targeted level of corrosion. At the end of the corrosion period, the crack widths were measured using a crack measuring microscope with an accuracy of 0.02 mm. The theoretical mass loss was calculated based on Faraday's equation as:

$$\text{Mass loss} = \frac{t\,I\,M}{z\,F} \qquad 6.2$$

where t is the time passed in seconds, I is the current in Amperes, M is the atomic weight (for iron $M = 55.847$ g/mol), z is the ion charge (two moles of electrons), and F is Faraday's constant which is the amount of electrical charge (Coulombs) in one mole of electron ($F = 96{,}487$ C/mol) as recommended by Lachemi et al. (2014).

The test setup consisted of fourteen power supplies, a steel mesh that served as cathode, electrolyte solution, and foam sheets. Figure 6.4 shows the different components used. The slab was placed upside down and a dike was constructed above the targeted corroded area using foam sheets. Then, the dike was filled with the electrolyte solution that consisted of 5% Sodium Chloride by weight. The solution was changed every week to ensure a constant concentration of salinity. A steel mesh was placed in the dike that covered all the targeted area. It was then connected to the ground of each power supply as it served as the cathode. Each power supply was connected to one of the bars that served as an anode. The time for corrosion started to be counted after the half-cell potential read more than -350 mV to ensure that the current overcame the concrete resistant and that the occurrence probability of corrosion be more than 90% (ASTM C876 2015).

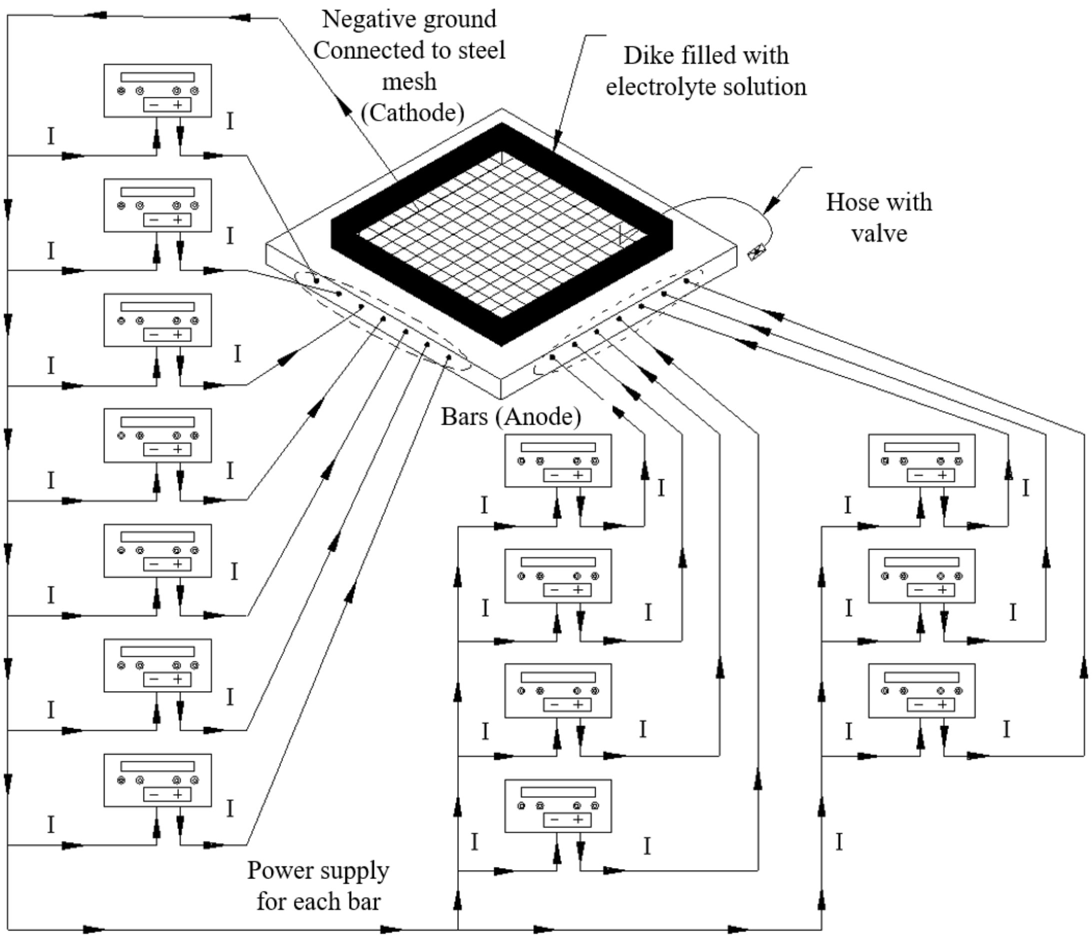

Figure 6-4 Schematic for Constant current accelerated corrosion technique setup.

6.4.4. Test Setup and Instrumentation

All slabs were tested under concentrated load to evaluate their structural performance as shown in Fig. 6.5. The load was applied using a hydraulic jack with a capacity of 1000 kN through the column stub. The dimensions of the test specimen represented the flexural line of contra-flexure. Therefore, all four edges of a slab were simply supported on the loading frame.

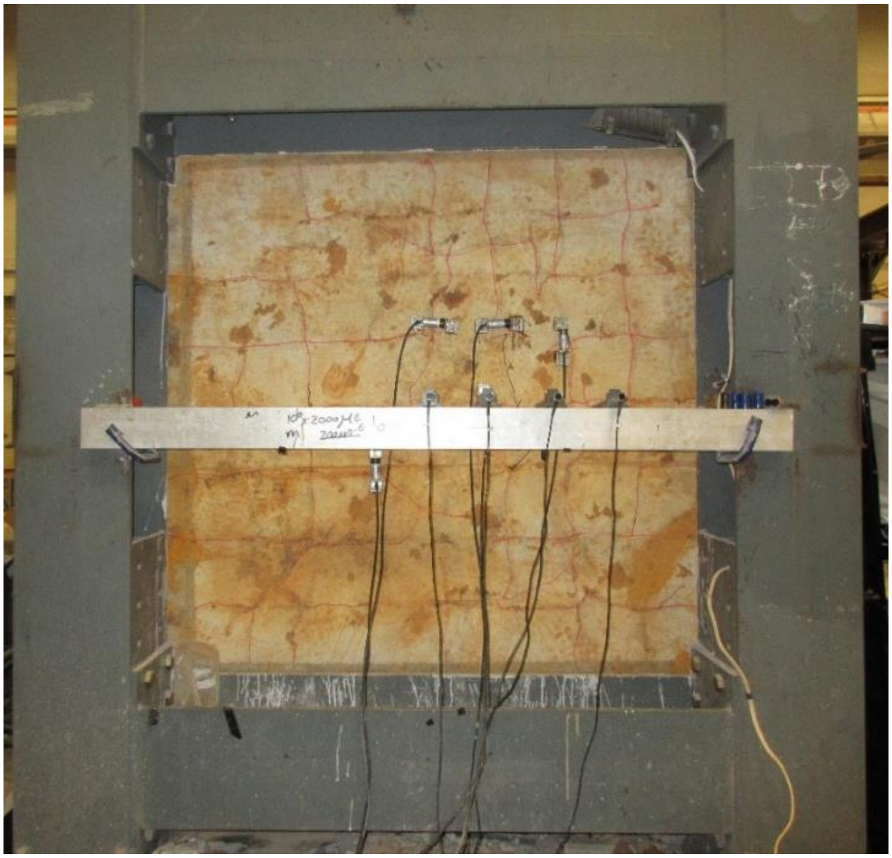

a. LVDTs and crack gauge

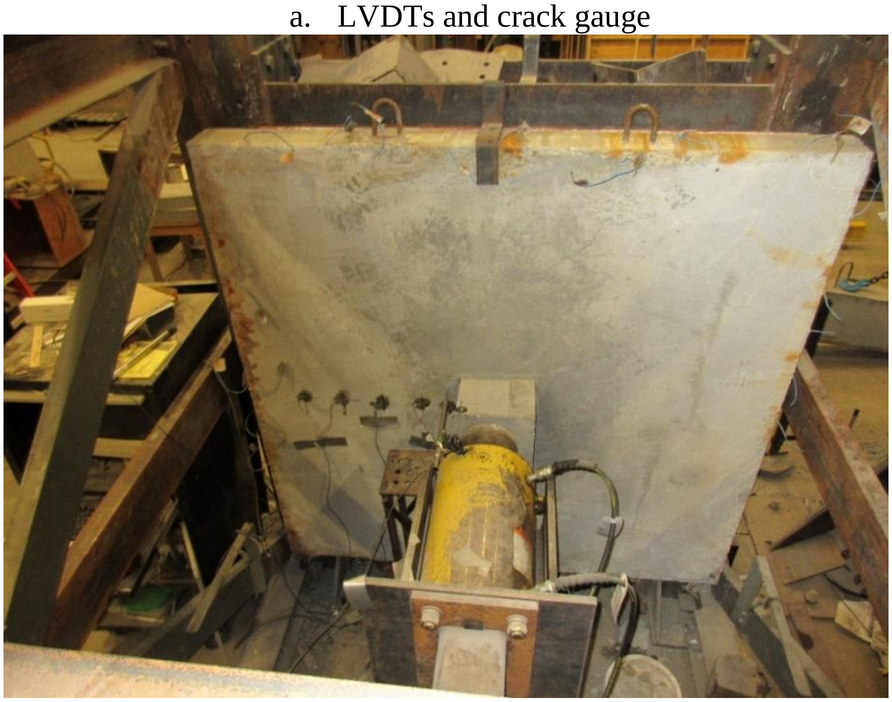

b. Actuator, back LVDT, and concrete strain gauges

Figure 6-5 Tested slab inside the loading frame.

The load was monitored and recorded using a pressure transducer connected to the hydraulic jack. The load was applied monotonically in small load increments of 2 kN. The deflection, crack widths, and concrete strains were recorded at each load increment. The deflections were measured using four linear variable differential transformer (LVDTs); four LVDT were placed on the front as shown in Fig. 6.6. Five crack gauges were used to measure the crack widths during loading. The crack widths, before loading, and at the end of the corrosion stage were measured using a crack measuring microscope with the focusable eyepiece of 60× and an accuracy of 0.02 mm. A small load was applied on the control slab S0 to induce initial cracks that was measured using the microscope, then three crack gauges with a capacity of ± 5 mm were mounted to trace the crack widths during loading. The cracks at the end of each load increment was detected by naked eye and marked. Figure 6.6 show a schematic diagram of the test setup.

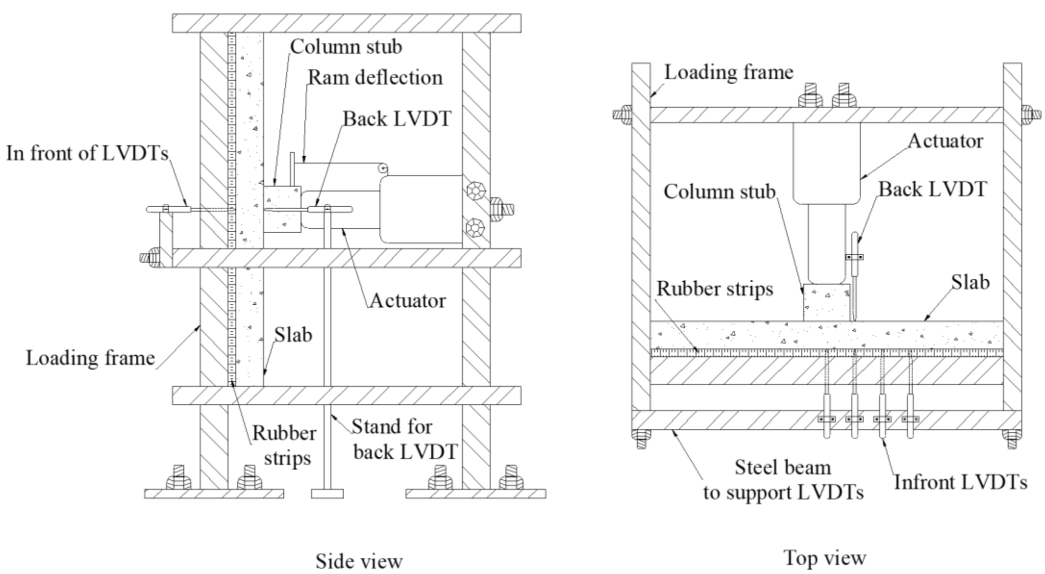

Figure 6-6 A sketch of the loading test setup.

6.5. Test Results and Discussion

6.5.1. Load Carrying Capacity

Table 6.4 shows a summary of the test results. Plots of the deflections along the centre line versus the load are shown in Fig. 6.7 for all slabs. Figure 6.7-e shows the load versus the mid-deflection for each test slab. The ultimate load was 391 kN, 289 kN, 225 kN, and 113 kN for slabs S0, S15-D3, S25-D3, and S50-D3, respectively. The capacity of both slabs S25-D3 and S50-D3 did not reach the service load for the control slab S0. The service load was determined as 60% of the capacity of the control slab as recommended by Aoude et al. (2014). S25-D3 had 4.3% lower capacity than the service load of the control slab. On the other hand, the ultimate load of S50-D3 was below the service load by 51.9%. Whereas, the ultimate load for S15-D3 exceeded the service load by 23%. The capacity of S15-D3, S25-D3, and S50-D3 were reduced by 26.1%, 42.5%, and 71.1%, respectively compared to the reference slab S0. In a previous study by Aoude et al. (2014), the authors simulated 50% mass loss in the full slab area by reducing the bar diameter. It was found that the punching capacity for 50% mass loss was reduced by 28%. In another investigation by Rahman (1992), it was concluded that the reduction in punching capacity for 50% mass loss was 34% for uncoated bars and 35% for coated bars. Rahman simulated the loss in bond by wrapping the bars with plastic adhesive tape. Moreover, the mass loss was simulated by using less number of bars. Furthermore, the delamination was simulated by placing a sheet between the upper and lower layers of the flexural mesh. Hence, the reduction in capacity for 50% mass loss reported in the previous studies were lower than there in the current investigation. This could be attributed to the use of accelerated corrosion which provided more realistic conditions. The corrosion technique followed in this study caused a loss to bond as the loss of mass is fairly similar to what would occur in nature. The corrosion products produced from the mass loss of the corroded bars weakened and loosened the bond between the reinforcement and the concrete cover. Moreover, these products caused internal pressure on the cover which led to the formation of cracks. The cracks widened with the increase in corrosion level which caused a negative effect on the capacity. Thus, the technique used provided better simulation of the corroded element than the previous studies. Moreover, the previous studies used a reduction in the diameter or number of bars to simulate the mass loss which caused a reduction in the reinforcement ratio. Consequently, the reinforcement ratio led to a reduction in the punching capacity (Marzouk & Hussein 1991; Dilger et al. 2005). Hence, the slabs did not have any cracks due to corrosion before the loading test. Accordingly, the reduction in capacity in the current study is more representative than that reported by Aoude et al. (2014) and Rahman (1992).

Table 6-4 Summary of Test Results

Specimen	w_c (mm)	Service Load			Ultimate Load		
		P_{SL} (kN)	Δ_{SL} (mm)	w_{SL} (mm)	P_u (kN)	Δ_u (mm)	w_{max} (mm)
S0	0.00	235	10.6	0.71	391	21.8	2.49
S15-D3	0.50	235	25.7	2.28	289	43.9	5.03
S25-D3	1.00	-	-	-	225	48.2	9.00
S50-D3	3.20	-	-	-	113	56.9	9.97

w_c is the maximum crack width due to corrosion, P_{SL} is the service load for the reference slab S0, Δ_{SL} is the deflection corresponding to the service load, w_{SL} is the maximum crack width at service load, P_u is the ultimate load, and Δ_u is the corresponding deflection, and w_{max} is the maximum crack width at ultimate load.

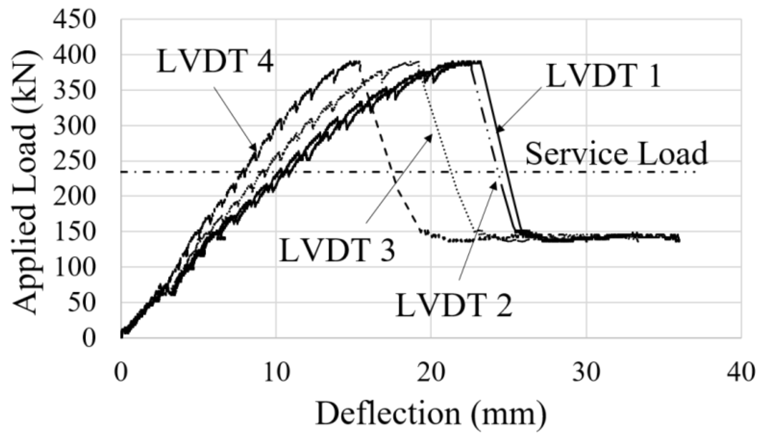

Fig a. S0

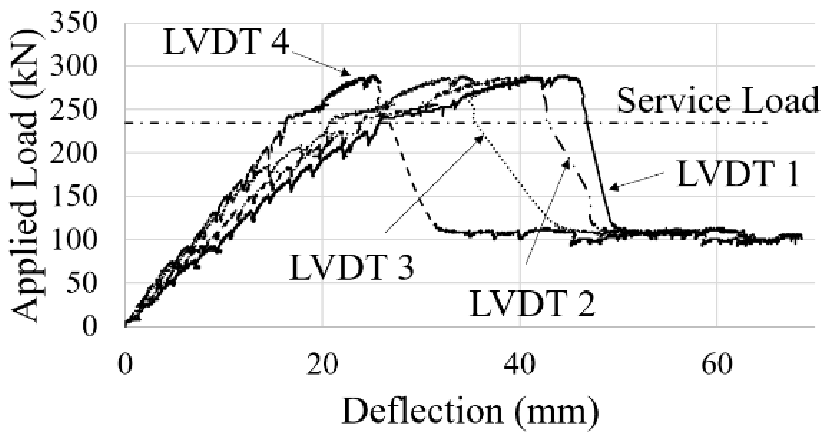

b. S15-D3

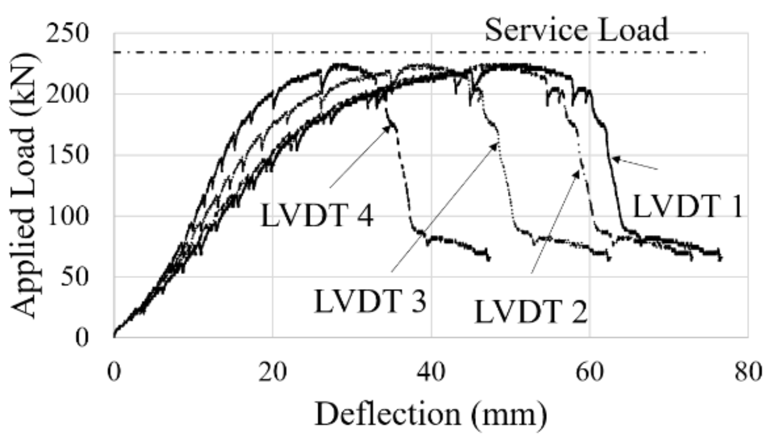

c. S25-D3

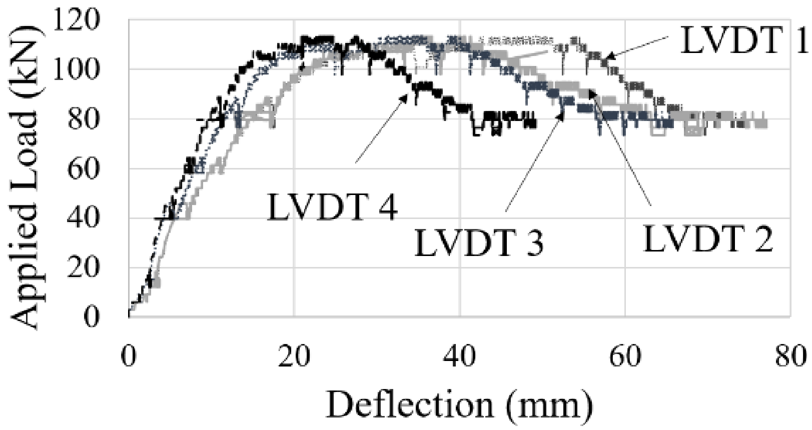

d. S50-D3

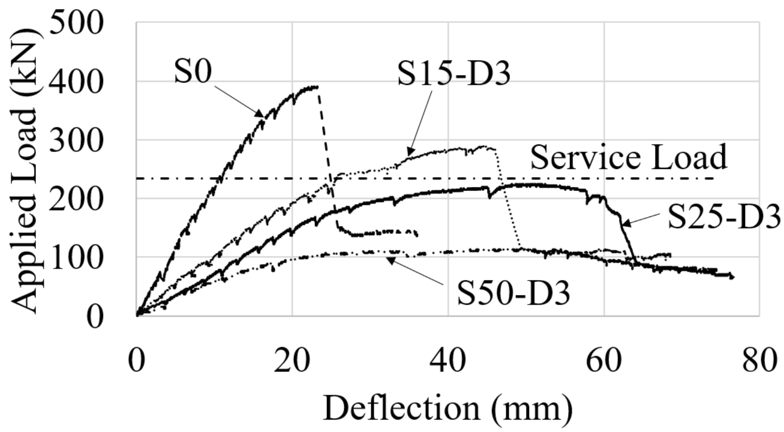

e. All test specimen

Figure 6-7 Applied load vs. Deflection.

6.5.2. Stiffness

The stiffness is defined as the slope of the load-deflection curves shown in Fig. 7. The stiffness of S0, S15-D3, S25-D3, and S50-D3 are 17.8 kN/mm, 7.7 kN/mm, 7.0 kN/mm, and 4.4 kN/mm, respectively. The 50% mass loss causes a significant loss in stiffness by 75.3% which is three-quarter of the overall stiffness of the reference slab. In a previous study by Aoude et al. (2014), it was found that the loss in stiffness for 50% simulated mass loss was 66.7%. The difference between the experimental results could be attributed to the use of induced corrosion which provided more realistic conditions and gave better simulation of the loss in bond in addition to the loss of rebar mass. Meanwhile, 25% mass loss of reinforcement in S25-D3 lead to a loss in stiffness by 60.7%, and 15% mass loss causes a drop in the overall stiffness by 56.7%. The reduction in stiffness that increase with the increase in mass loss could be attributed to several reasons. First, the mass loss reduces the bar diameter which reduce the load required to cause yielding in bars. Second, the corrosion products from bars destroy the bond strength between them and the concrete. Third, the cracks due to corrosion are wider with the increase in mass loss. On the other hand, the reference slab S0 has no existing cracks due to corrosion before starting the loading test. Therefore, the initial slope of the load-deflection curve for S0 is the steepest, among all slabs. For the reference slab, the slope started to gradually decrease when the first crack occurred and then started to decrease after the reinforcement started to yield. Finally, the load suddenly dropped when the ultimate capacity was reached.

6.5.3. Slab Rotation and Energy Absorption

Figure 6.7-e shows the load-deflection curves at mid-span for all slabs. The energy absorption defined as the area under the curve. The highest energy absorption is 10208 kN.mm for S25-D3 followed by S15-D3 with a value of 9370 kN.mm, and S50-D3 has the lowest value amongst all slabs with a value of 6567 kN.mm. The lowest energy absorption is for the control slab S0; 6157 kN.mm. The increase in energy absorption with the increase in mass loss for mild and moderate corrosion could be attributed to the reduction in the bar areas and consequent by the reinforcement ratio within the corroded area. The energy absorption started to decrease once the corrosion level exceeded 25% mass loss. The slab

rotation was measured for the portion outside the shear crack which rotates as a rigid body (Marzouk & Hussein 1991; Hussein 1990) and plotted in Fig. 6.8 for the test slab. The results reveal that the slab rotation increased with the increase in mass loss which could be attributed to the reduction in the stiffness with the higher mass loss.

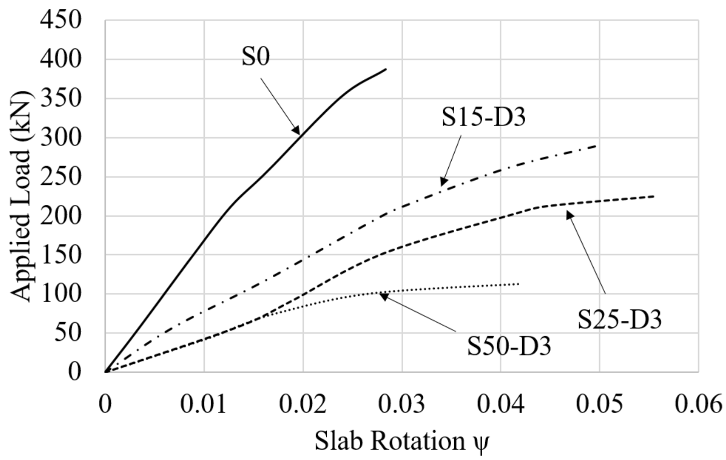

Figure 6-8 Applied load vs. slab rotation.

6.5.4. Deflection and Ductility

Table 6.4 shows the deflection capacity for the test slabs. It is defined as the deflection at ultimate load according to Maaddawy et al. (2006). The deflection profiles for all slabs at the ultimate load are shown in Fig. 6.9. The deflection capacity of the corroded slabs exceeded the control by 101.4%, 121.1%, and 161% for S15-D3, S25-D3, and S50-D3, respectively.

The term ductility index was introduced to represent the ductility of corroded beams by Dang & François (2014). The ductility index is defined as the ratio between the deflection at ultimate load in a corroded element to the reference. In the current investigation, the index is used to represent the ductility in corroded two-way slabs to demonstrate the deformation capacity until failure. If the ductility index is equal to one, then no corrosion took place. If the index value is more than one, corrosion has occurred. Increasing the mass loss cause an increase in the ductility index as the deflection at ultimate load increases with the increase in mass loss. The ductility indices for S0, S15-D3, S25-D3, and S50-D3 were 1, 2.01, 2.21, and 2.61, respectively. Previous ductility definitions (for example (Marzouk & Hussein 1991) could not be used for corroded elements because its defined as the ratio between the ultimate deflection at failure and that at first yielding of the flexural reinforcement. Hence, the yielding of reinforcement has to be determined. Strain gauges that are normally used face many practical problems during the inducing of corrosion. First, the corrosion products between the corroded bar and a strain gauge cause separation between them. Second, the current used to induce corrosion would cause damage to the strain gauge. In a previous study done by Aoude et al. (2014), it was observed that the ductility index for 50% mass loss to be 1.5. The higher value of 2.61 that was recorded reflects that without proper simulation of loss of bond and rebar mass loss, the degree of degradation in the slab performance may not be properly reflected.

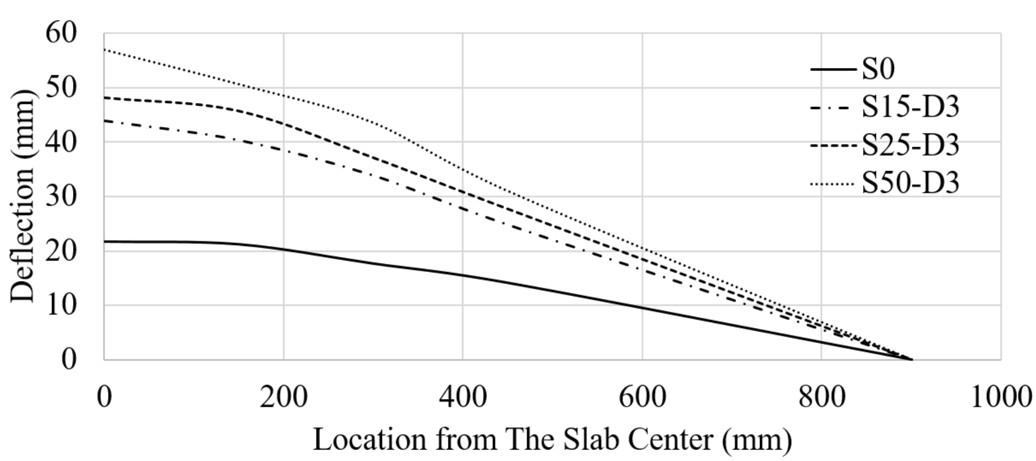

Figure 6-9 Deflection profile at ultimate load.

6.5.5. Cracking Response

Table 6.4 shows that the maximum crack widths due to corrosion for S15-D3, S25-D3, and S50-D3 were equal to 0.5 mm, 1.00 mm, and 3.20 mm, respectively. Figure 6.10 shows the crack patterns in the slabs at the end of the induced corrosion process and before the loading test. It can be noticed that the crack numbers and widths increased with the increase of mass loss and the corresponding increase of the corrosion products. This led to an increase in the internal pressure under the concrete cover. As the corrosion products increase, the cracks become wider.

a. S15-D3

b. S25-D3

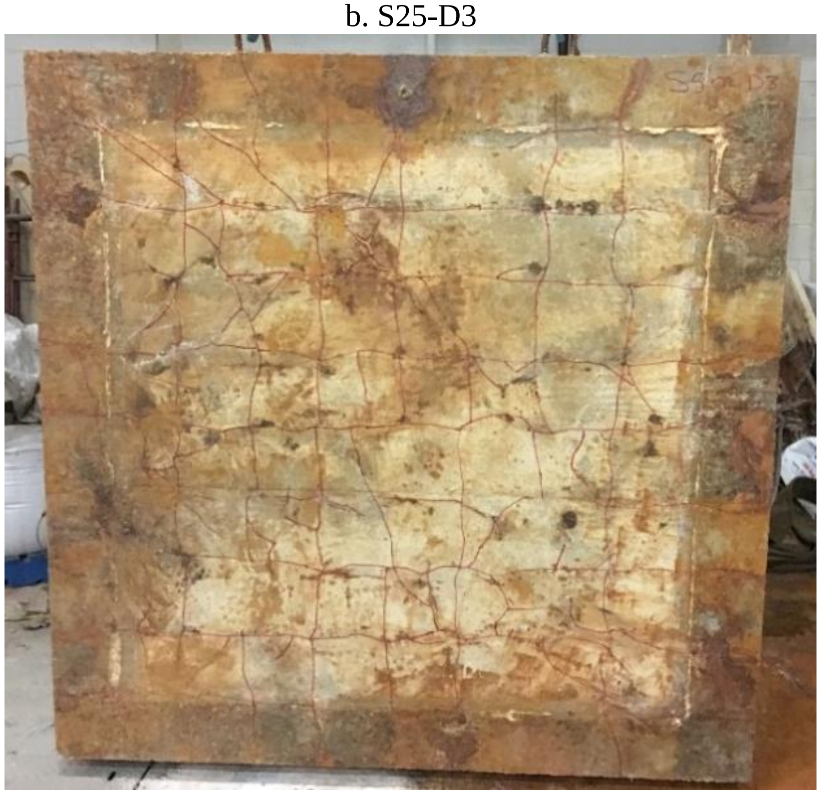

c. S50-D3

Figure 6-10 Cracks patterns due to corrosion before loading test.

After the load tests, the maximum crack widths at failure for S0, S15-D3, S25-D3, and S50-D3 were 2.49 mm, 5.03 mm, 9.00 mm, and 9.97 mm, respectively, as given in Table 6.4. The maximum crack width at failure occurred in S50-D3, the slab with severe level of corrosion. The crack width at failure was smaller for lower mass loss and the smallest crack width was observed in the un-corroded slab S0. The wider crack widths could be attributed to the presence of corroded cracks before the load test.

Figure 6.11 shows the Crack width vs. the applied load. Figure 6.12 shows the crack patterns for the test slabs at failure. Slab S0 had the maximum crack intensity after the load test was completed. The cracks formed in a typical manner for two-way slab load tests (Marzouk & Hussein 1991). The cracks were first formed in a radial direction extending from the column. As the load was increased, tangential cracks started to form that were roughly concentric with the circumference of the stub column. The slab failed with the final shear crack coinciding with, or located outside these cracks before the flexure yield lines were well developed.

Before the load test was performed, slabs S15-D3, S25-D3 and S50-D3 had cracks that were formed due to the corrosion of the reinforcement. Those cracks were formed in an orthogonal manner and were almost parallel to the reinforcing bars. As the load test was performed, slab S15-D3 showed few new radial cracks. On the other hand, slabs S25-D3 and S50-D3 did not show any new cracks due to the applied load. This could be attributed to the pre-formed corrosion cracks before the load test. These cracks become wider during loading and no new cracks were formed. In addition, the loss of bond due to the large corroded area inhibited the formation of any yield-line like flexural cracks.

a. S0

b. S15-D3

b. S25-D3

d. S50-D3

Figure 6-11 Crack patterns after loading test.

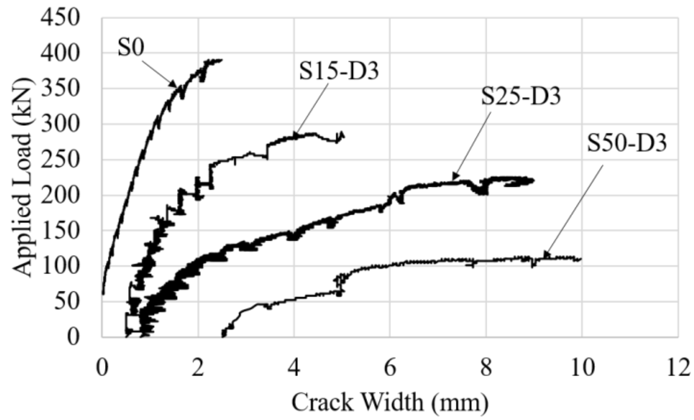

Figure 6-12 Crack width vs. applied load.

6.5.6. Failure Modes

A ductile failure occurs when the slab flexural capacity is reached, i.e., $P_u / P_{flexural}$ = 1.0, where P_u is the experimental ultimate load and $P_{flexural}$ is the flexural capacity of the slab based on the yield line theory. In this case, the load deflection curve shows a horizontal plateau once the yielding is spread in all the reinforcement. On the other hand, pure punching failure takes place without yielding occurring at any point in the reinforcement and the slab does not reach its flexural capacity; $P_u / P_{flexural}$ < 1.0. In that case, the load deflection curve could be approximated with two straight lines; the slope of the first line is the un-cracked stiffness of the slab and the second line is the cracked stiffness. Ductile punching could be classified as a case in-between where the load deflection curve shows signs of flexural behaviour but the slab fails in punching before the flexural capacity is reached (Broms 1991). For the current study, based on the load-deflection curve (Figure 7e), slab S0 showed a ductile punching failure mode. For the corroded slabs, cracks were formed due to corrosion before the load test. Slab S15-D3 showed more ductility behaviour than S0, but nonetheless a ductile punching failure occurred. The load-deflection curves of the corroded slabs S25-D3 and S50-D3 indicate a behaviour that is typical of a flexural failure. This could be attributed to the reduction in the reinforcement ratio due to corrosion and to the degradation of bond.

6.6. Comparison with Code Predictions

Table 6.5 shows the experimental ultimate loads (P_u) for the slabs. The table also provides the flexural capacity of each slab, $P_{flexural}$. The calculation of the flexural capacity $P_{flexural}$ is based on the yield-line theory assuming perfect bond between the reinforcement and concrete. The original cross-section area of the bars is used without any consideration to possible reduction due to corrosion. It can be noticed that ratio $P_u / P_{flexural}$ for S0 is 0.88 and hence the failure of the slab can be classified as ductile punching. For slabs S15-D3, S25-D3, and S50-D3 the ratios $P_u / P_{flexural}$ are 0.65, 0.50, and 0.25, respectively. Hence, the failure of the corroded slabs could be classified as punching shear mode based on the previous yield-line calculation that assumes no reduction in the area of reinforcement. This is contrary to the mode of failure observed from the experiments. The capacity of the slabs was also calculated according to four different codes; the Canadian Code (CSA 23.3-14), the American Code (ACI 318-14), the British Standard (BS 8110-97), and the European Code (EC2). The British standard and the European code take into consideration the effect of the reinforcement ratio on the punching shear capacity, while the North American Codes (CSA and ACI) do not consider it (British Standards Institution 2004; BS 8110 1997; CSA A23.3-14 2014; ACI 318-14 2014). The resistance factors in the code equations are taken as unity when calculating the moment capacity. As mentioned earlier, the corrosion of the flexural reinforcement reduced the punching capacity by 26.1%, 42.5%, and 71.1% for slabs S15-D3, S25-D3, and S50-D3, respectively. It can be noted from Table 6.5 that the ultimate experimental loads of the corroded slab fell below the design capacities according to all codes.

Table 6-5 Test Results versus Code Predictions

Slab	P_u kN	$P_{flexural}$ kN	$\frac{P_u}{P_{flexural}}$	CSA 23.3-14		BS 8110-97		ACI 318-14		EC2	
				P_{code} kN	$\frac{P_u}{P_{code}}$	P_{code} kN	$\frac{P_u}{P_{code}}$	P_{code} kN	$\frac{P_u}{P_{code}}$	P_{code} kN	$\frac{P_u}{P_{code}}$
S0	391	447	0.88	359	1.09	332	1.18	312	1.25	300	1.30
S15-D3	289		0.65		0.81		0.87		0.93		0.96
S25-D3	225		0.50		0.63		0.68		0.72		0.75
S50-D3	113		0.25		0.31		0.34		0.36		0.38

***** P_u is the experimental punching shear capacity, $P_{flexural}$ is the flexural slab capacity, and P_{code} is the code predicted punching shear resistance.

The previous expressions could be re-evaluated by considering the reduction in reinforcement ratio to the proportional to the mass loss. The predictions of the North American codes were not re-evaluated as they do not consider the reinforcement ratio as a parameter in their equations.

It can be seen from Table 6.6 that all experimental ultimate loads fell below the modified predictions according to the yield line theory, EC2, and BS8110-97. The ultimate load of S15-D3 was 8% below and 2% above the predicted capacity according to BS8110-97 and EC2, respectively. The ultimate load of S25-D3 is fell below the predictions of BS8110-97, and EC2 by 25%, and 17%, respectively. While S50-D3 fell also below the predictions by 57% and 53%, respectively. The yield line theory predictions are based on the assumption that the corrosion only lead to a reduction in the bar area. On the other hand, the corrosion also has a negative effect on the bond. Moreover, the development length that was left intact was not sufficient. Hence, the yield line predictions could be unrealistically high.

Table 6-6 Test Results versus Code Predictions Considering the Reduction in the Reinforcement Ratio

Slab	P_u kN	$P_{flexural}$ kN	$\frac{P_u}{P_{flexural}}$	BS 8110-97		EC2	
				P_{code}	$\frac{P_u}{P_{code}}$	P_{code}	$\frac{P_u}{P_{code}}$
S15-D3	289	385	0.75	314	0.92	284	1.02
S25-D3	225	343	0.66	301	0.75	272	0.83
S50-D3	113	234	0.48	263	0.43	238	0.47

***** P_u is the experimental ultimate load, $P_{flexural}$ is the flexural capacity, and P_{code} is the code predicted values.

6.7. Conclusions

This experimental investigation evaluates the behaviour of slabs with different levels of corrosion of the flexural reinforcement. A total of four full-scale two-way slabs were tested. The slabs suffered from mild corrosion level (15% mass loss), moderate corrosion level (25% mass loss), severe corrosion level (50% mass loss), and the control slab (0% mass loss). All slabs had a large corroded area. The area covered all the reinforcement length leaving only one half of the development length intact without corrosion. The ultimate loads, stiffness, slab rotation, energy absorption, deflections, and cracking behaviour were studied. From the results described in this paper, the following conclusions can be drawn:

- The increase in mass loss caused degradation in stiffness that consequently had an adverse effect on deflections and caused an increase in the slab rotation.

- The increase in the mass loss led to an increase in the crack intensity and widths due to the formation of the corrosion products under the concrete cover.
- The punching shear capacity was reduced with the increase in mass loss. The capacity was reduced by 26.1% and 42.5% for 15% and 25% mass loss, respectively.
- The test results revealed that the reduction in slab capacity for 50% mass loss was more severe that those reported using simulated conditions by other authors. The current test results revealed that the slab lost 71% of its capacity for 50% mass loss compared to 28% reduction reported by Aoude et al. (2014), and 34 % reported by Rahman (1992). This significant difference between the current results and previous ones shows the importance of realistic simulation of mass loss and bond degradation using accelerated corrosion techniques.
- The capacity of slabs with 15% mass loss, and despite a large corroded area that caused an inadequate development length, exceeded the service load of the reference slab by 23%. Hence, the serviceability limit state for the slabs is significantly reduced but the slab remains safe from collapse under service loads.
- A 25% and 50% mass loss and a large corroded area that leaves the reinforcement with inadequate development length will cause the slab to collapse at loads below the service load levels.
- For slabs with corrosion levels up to 15%, the BS8110-97 and EC2 codes could be used, with modifications, to predict an approximate value for the capacity of the corroded slabs. The authors suggest using the equations with reduced reinforcement ratio that is proportional to the mass loss.

- The North American codes gave unsafe predictions and should not be used to predict the reduced capacity of corroded slabs. The codes in its current format can not be modified as they do not consider the effect of the reinforcement ratio the on capacity of two-way slabs.

6.8. References

ACI 318-14 (2014) Building code requirement for structural concrete (ACI 318M-14) and commentary (ACI 318RM-14), Building Code Requirements for Structural Concrete.

Ahmad, S. (2003) ‘Reinforcement corrosion in concrete structures, its monitoring and service life prediction - A review’, Cement and Concrete Composites, 25(4–5 SPEC), pp. 459–471. doi: 10.1016/S0958-9465(02)00086-0.

Altoubat, S., Maalej, M. and Shaikh, F. U. A. (2016) ‘Laboratory simulation of corrosion damage in reinforced concrete’, International Journal of Concrete Structures and Materials. Korea Concrete Institute, 10(3), pp. 383–391. doi: 10.1007/s40069-016-0138-7.

Andrade, C. and Alonso, C. (1996) ‘Corrosion rate monitoring in the laboratory and on-site’, Construction and Building Materials, 10(5 SPEC. ISS.), pp. 315–328. doi: 10.1016/0950-0618(95)00044-5.

Andrade, C. and Alonso, C. (2001) ‘On-site measurements of corrosion rate of reinforcements’, Construction and Building Materials, 15(2–3), pp. 141–145. doi: 10.1016/S0950-0618(00)00063-5.

Aoude, H., Cook, W. D. and Mitchell, D. (2014) ‘Effects of simulated corrosion and delamination on response of two-way slabs’, Journal of structural Engineering, 140(1), pp. 1–9. doi: 10.1061/(ASCE)ST.1943-541X.0000775.

ASTM C150/C150M (2017) ‘Standard specification for Portland cement’, ASTM International, p. 9.

ASTM C876 (2015) ‘Standard test method for corrosion potentials of uncoated reinforcing steel in concrete’, p. 8. doi: 10.1520/C0876-09.2.

Berto, L., Simioni, P. and Saetta, A. (2008) ‘Numerical modelling of bond behaviour in RC structures affected by reinforcement corrosion’, Engineering Structures. Elsevier, 30(5), pp. 1375–1385.

Bertolini, L., Elsener, B., Pedeferri, P., Redaelli, E. and Polder, R. B. (2013) Corrosion of steel in concrete: prevention, diagnosis, repair. John Wiley & Sons.

British Standards Institution (2004) Eurocode 2: design of concrete structures: part 1-1: general rules and rules for buildings. British Standards Institution.

Broms, E. (1991) ‘Punching of flat plates - a question of concrete properties in biaxial compression and size effect’, ACI Structural Journal, (87), pp. 292–304.

Broomfield, J. P. (2006) Corrosion of steel in concrete: understanding, investigation and repair, Second Edition. doi: 10.4324/9780203414606.

BS 8110 (1997) 'Structural use of concrete. Part I: Code of practice for design and construction', British Standards Institution, UK.

CSA-G30. 18-09 (2009) Carbon steel bars for concrete reinforcement, Mississauga, Ontario, Canada.

Carnot, A., Frateur, I., Zanna, S., Tribollet, B., Dubois-Brugger, I. and Marcus, P. (2003) 'Corrosion mechanisms of steel concrete moulds in contact with a demoulding agent studied by EIS and XPS', Corrosion science. Elsevier, 45(11), pp. 2513–2524.

Chitty, W.-J., Dillmann, P., L'Hostis, V. and Lombard, C. (2005) 'Long-term corrosion resistance of metallic reinforcements in concrete—a study of corrosion mechanisms based on archaeological artefacts', Corrosion Science. Elsevier, 47(6), pp. 1555–1581.

Chung, L., Najm, H. and Balaguru, P. (2008) 'Flexural behavior of concrete slabs with corroded bars', Cement and Concrete Composites, 30(3), pp. 184–193. doi: 10.1016/j.cemconcomp.2007.08.005.

Coronelli, D. and Gambarova, P. (2004) 'Structural assessment of corroded reinforced concrete beams: modeling guidelines', Journal of Structural Engineering. American Society of Civil Engineers, 130(8), pp. 1214–1224.

CSA A23.3-14 (2014) Design of concrete structures. Mississauga, Ont.: Canadian Standard Association.

Dang, V. H. and François, R. (2014) ‘Prediction of Ductility Factor of Corroded Reinforced Concrete Beams Exposed to Long Term Aging in Chloride Environment’, Cement and Concrete Composites, 53(October 2014), pp. 136–147. doi: 10.1016/j.cemconcomp.2014.06.002.

Dilger, W., Birkle, G. and Mitchell, D. (2005) ‘Effect of flexural reinforcement on punching shear resistance’, ACI Special Publication 232-4, pp. 57–74. doi: 10.1007/s13398-014-0173-7.2.

Dodd, L. L. and Restrepo-Posada, J. I. (1995) ‘Model for predicting cyclic behavior of reinforcing steel’, Journal of Structural Engineering. American Society of Civil Engineers, 121(3), pp. 433–445.

Donnelly, J. P., Pulver, B. E. and Popovic, P. L. (2006) ‘Condition assessment of parking structures’, In Structures Congress : Structural Engineering and Public Safety ASCE., p. 10.

El-Maaddawy, T. and Soudki, K. (2003) ‘Effectiveness of impressed current technique to simulate corrosion of steel reinforcement in concrete’, Journal of Materials in Civil Engineering. American Society of Civil Engineers, 15(1), pp. 41–47. doi: 10.1061/(ASCE)0899-1561(2003)15:1(41).

El-Maaddawy, T., Soudki, K. and Topper, T. (2005a) ‘Analytical model to predict nonlinear flexural behavior of corroded reinforced concrete beams’, ACI Structural Journal, 102(4), pp. 550–559.

El-Maaddawy, T., Soudki, K. and Topper, T. (2005b) 'Long-term performance of corrosion-damaged reinforced concrete beams', ACI Stractural Journal, 102(5), pp. 649–656.

Fedrizzi, L., Azzolini, F. and Bonora, P. L. (2005) 'The use of migrating corrosion inhibitors to repair motorways' concrete structures contaminated by chlorides', Cement and concrete research. Elsevier, 35(3), pp. 551–561.

Hussein, A. A. (1990) Behaviour of reinforced concrete slabs made with high-strength concrete. Memorial University of Newfoundland.

Kashani, M. M., Crewe, A. J. and Alexander, N. A. (2013) 'Nonlinear stress-strain behaviour of corrosion-damaged reinforcing bars including inelastic buckling', Engineering Structures, 48, pp. 417–429. doi: 10.1016/j.engstruct.2012.09.034.

Lachemi, M., Al-Bayati, N., Sahmaran, M. and Anil, O. (2014) 'The effect of corrosion on shear behavior of reinforced self-consolidating concrete beams', Engineering Structures. Elsevier Ltd, 79, pp. 1–12. doi: 10.1016/j.engstruct.2014.07.044.

Marzouk, H. and Hussein, A. (1991) 'Experimental investigation on the behavior of high-strength concrete slabs', ACI Structural Journal, 88(6), pp. 701–713. doi: 10.1139/l91-118.

Miyagawa, T. (1991) 'Durability design and repair of concrete structures: chloride corrosion of reinforcing steel and alkali–aggregate reaction', Magazine of Concrete Research. Thomas Telford Ltd, 43(156), pp. 155–170.

Pritzl, M. D., Tabatabai, H. and Ghorbanpoor, A. (2014) 'Laboratory evaluation of select methods of corrosion prevention in reinforced concrete bridges', International Journal of Concrete Structures and Materials, 8(3), pp. 201–212. doi: 10.1007/s40069-014-0074-3.

Rahman, A. H. (1992) 'Effect of steel corrosion on the strength of slab-column connections', National Research Council Canada, Institute for Research in Construction.

Raupach, M. (1996) 'Chloride-induced macrocell corrosion of steel in concrete - Theoretical background and practical consequences', Construction and Building Materials, 10(5 SPEC. ISS.), pp. 329–338. doi: 10.1016/0950-0618(95)00018-6.

Reilly, J. L., Cook, W. D., Bastien, J. and Mitchell, D. (2014) 'Effects of delamination on the performance of two-way reinforced concrete slabs', Journal of Performance of Constructed Facilities, 28(4), pp. 1–8. doi: 10.1061/(ASCE)CF.

Said, M. E. and Hussein, A. A. (2019) 'Induced corrosion techniques for two-way slabs', Journal of performance of constructed Facility, 33(3). doi: 10.1061/(ASCE)CF.1943-5509.0001299.

Talakokula, V., Bhalla, S. and Gupta, A. (2014) 'Corrosion assessment of reinforced concrete structures based on equivalent structural parameters using electro-mechanical impedance technique', Journal of Intelligent Material Systems and Structures, 0(0), pp. 1–16. doi: 10.1177/1045389X13498317.

Zhang, B., Masmoudi, R. and Benmokrane, B. (2004) ‘Behaviour of one-way concrete slabs reinforced with CFRP grid reinforcements’, Construction and Building Materials, 18(8), pp. 625–635. doi: 10.1016/j.conbuildmat.2004.04.007.

Chapter 7 Probabilistic Analysis of Strength Degradation for Corroded Two-Way Slabs

7.1. Abstract

A reliability assessment on deteriorated structures elements is needed to determine their serviceability is either safe or not. This study proposed an equation based on response service methodology to determine the strength degradation for existing corroded two-way reinforced concrete slabs. An experimental program was designed to collect enough results to construct an equation that could be used as a guide to practicing engineers. Ten full-scale slabs were cast for this purpose. Three different levels of corrosion were reached, and three different corroded areas occurred. The equation was constructed on three phases to give more feasibility to use the equation regarding the measurable data availability in filed. The first phase predicts the residual slab capacity based on chloride ion content and corroded area. The second phase added another parameter; maximum crack width, while the third phase added the natural frequency. The equation showed a close agreement with the verified experimental test which shows its applicability to be used in the field.

Keywords: Reliability assessment; deteriorated structures; two-way slabs; corrosion; natural frequency

7.2. Introduction

Safety and reliability consider one of the important assessment process aspects of any current existing structures. Reliable assessment for any structure ensures that its serviceability lies in acceptable level during its service life and assures its safety against structural collapse (Šomodíková et al. 2016). Deterioration of reinforced concrete (RC) structures could lead to loss of structural integrity and serviceability. Corrosion is one of the main reasons that is causing deterioration in RC structures. RC is commonly used in North America in the construction of residential buildings, bridges, tunnels, parking garages, and offshore structures. North America has harsh environmental weather that generates dire conditions, which lead to an increase in the probability of corrosion occurrence (Aoude et al. 2014). Corrosion is a worldwide problem, which also occurs in many structures in industrialized countries in Europe and Asia, and also in developing countries (Chung et al. 2008).

Many efforts carried out on studying corrosion from various aspects. Some investigations were conducted to develop a better understanding of the corrosion process (Raupach 1996; Carnot et al. 2003; Chitty et al. 2005), and to examine the effect of corrosion on the RC structural elements (El-Maaddawy & Soudki 2003). Other investigations monitored the corrosion process (Andrade & Alonso 1996; Andrade & Alonso 2001; Ahmad 2003).In addition, some researchers developed numerical models to predict the structural behaviour of the corroded elements (Dodd & Restrepo-Posada 1995; Berto et al. 2008; Coronelli & Gambarova 2004). Repair and rehabilitation of corroded structures were explored in some investigations (Bertolini et al. 2013; Miyagawa 1991; Fedrizzi et al. 2005; Broomfield 2002). Most of the studies were conducted on RC beams while there are very limited investigations on the effect of corrosion on RC slabs. The previous studies on corrosion of two-way slabs simulated it by reducing bar numbers or diameter (Rahman 1992b; Reilly et al. 2014; Aoude et al. 2014).

The statistical design of experimental methodology is an efficient tool for providing appropriate statistical models. These models help many researchers in understanding the interactions between the statistical parameters (Ghezal & Khayat 2002). Response surface method (RSM) is a compilation of mathematical and statistical techniques that carried out for the purpose of developing, refining, and optimizing processes. RSM is an integration between the variations of the simple linear regression with the second order effects of non-linear relationships. RSM is one of the most common optimization techniques that determine the superlative potential combinations of factors to specify the optimized response. RSM techniques have the ability to evaluate the factors and their relative significance even for complex interactions. In addition, the ability to determine the change of the response behaviour with the change of the factors levels. Moreover, the ability to exchange the complex models into simpler second order regression models to be used within a limited range, such as the replacement of finite element models with a simple regression model. Thus, RSM provides the researchers with a deep understanding that guide them to predict the response behaviour over a certain insensitive spot condition (Montgomery 2012). RSM depends on analysis of variance (ANOVA), a method that picks a few points out of the full factorial set that can represent adequate information about the response space. RSM techniques were applied in several civil engineering applications (Bayramov et al. 2004; Wong et al. 2005; Kang et al. 2010; Chen et al. 2010). It also used in industries (Rajan 2018). RSM distinguished from other traditional statistical methods, such as one factor at one time (OFAT) and changing one single thing (COST), that it avoids misguiding the computation of the optimum, which it takes into consideration the effect of interaction between factors.

To the best of the authors' knowledge, there is no previous statistical analysis carried out to develop models to predict the residual carrying loading capacity for corroded RC two-way slabs. The objective of this investigation was focused on developing a prediction model for the residual capacity for the corroded RC two-way slabs. The models incorporated the effect of four variables: corrosion level, corroded area, maximum crack width, and natural frequency. The second objective was purposing the natural frequency as a non-destructive test for the corrosion elements.

7.3. Research Significance

The research outcome proposed equations that could enable, with low costs, the evaluation of the deterioration of two-way RC slabs in existing structures. The research outcome will contribute to helping the decision makers to assess the structural integrity of the existing structures at the end of their service life. Decisions could be made in extending the lifespan of the project, in case of need, or in decommissioning of the structure especially offshore. Ultimately, this research provides a tool to engineers for assessing the corroded two-way RC slabs and determining the corresponding residual strength to make the right decision about their safety.

7.4. Experimental Program

7.4.1. Statistical Design of Experimental Methodology

The experimental program was designed to get enough results that could be sufficient to create an effective statistical model. The objective of the statistical design of experiment was to predict the residual capacity of corroded RC two-way slabs. There were two main factors for this model. The first factor was the corrosion level, in order to cover a wide range of corrosion level four levels were reached: no corrosion (0% mass loss), mild (15% mass loss), moderate (25% mass loss), and severe (50% mass loss). The second factor depended on the corroded area. The choice of the corroded area based on the effective punching perimeter and the effective bonded length of the un-corroded part of the corroded bar. There was three corroded area; around the reinforcement bandwidth, and large corroded area with and without enough development length. There were other two factors dependent on the first two factors; the maximum crack width due to corrosion and the natural frequency. These two factors were measured for each corroded slab and used to enhance the prediction of the residual strength. Three models were created in three stages: one model contained all four factors, another one contained all factors except the natural frequency, and the last one contained only corrosion levels and corroded areas. The model without natural frequency was created because it is hard sometimes to measure the natural frequency on site. Therefore, the authors sought to provide more flexibility to the specialist engineer to predict the residual strength with enough measurable data in site. A total number of ten slabs were tested; nine of them used to create the models and one used as a verification for the model.

7.4.2. Material Properties

Normal weight concrete was used to cast all slabs using Ordinary Portland Cement of Type I (ASTM C150/C150M 2017), with a specific gravity of 3.15. The concrete mixture contained natural sand as a fine aggregate and aggregate with a maximum size of 10 mm as coarse aggregate; both have a specific gravity of 2.6. Table 7.1 shows the mixture composition used in casting the tested slabs. The targeted compressive strength (40 MPa) and the water to cement (w/c) ratio (0.4) were selected based on the exposure requirement of class F3 according to ACI specification. Class F3 considered for the horizontal elements such as parking garages that exposed to snow and ice mixed up with de-icing chemicals (ACI 318-14 2014). Table 7.2 shows the mechanical properties of the tested concrete after 28 days after casting the specimen. A Grade 400 MPa (15M) was used as a flexural reinforcement, and the properties of the reinforcement were measured as shown in Table 7.2.

Table 7-1 Mix Composition of Concrete Mixture

Cement (kg)	w/c	Water (l)	C/F	C.A. (kg)	F.A. (kg)	Aggregate size (mm)	Fresh density (kg/m^3)
350	0.4	140	1.3	1083	833	10	2407

* w/c is the water to cement ratio, C/F is the coarse to fine ratio, C.A. is the coarse aggregate, and F.A. is the fine aggregate

Table 7-2 Steel and Concrete Properties

Designation	Steel properties			Concrete Properties	
	Area (mm^2)	f_y (MPa)	ε_y ($\mu\varepsilon$)	f'_c (MPa)	f_r (MPa)
15M	200	475	2200	41.1	3.82

* f_y is the yield strength, ε_y is the yield strain, f'_c is the compressive strength, and f_r is the modulus of rupture.

7.4.3. Details of Test Specimen

Table 7.3 shows the test specimen details. Ten identical full-scale RC two-way slab was cast for this study. Each slab had dimensions 1900 × 1900 × 150 mm and a concrete cover of 30 mm. A column stub with dimensions 250 mm × 250 mm × 200 mm was attached to each slab from one side as shown in Fig. 7.1. The flexural reinforcement ratio was 1%, 15M distributed every 190 mm. The compression reinforcement used 10M that distributed every 300 mm. Some precautions had been taken during the assembly of the flexural reinforcement mesh before pouring concrete. First an electrical tape used to isolate the bars from each other at the intersection points; in addition, the assembly of bars done by using plastic ties instead of steel ties to avoid any conductivity between them as shown in Fig. 7.2. Avoid conductivity between bars provided an opportunity to control the mass loss level separately for each bar. Finally, before pouring, an electrical wire was connected from both sides of each bar to be used in the accelerated corrosion process as shown in Fig. 7.3.

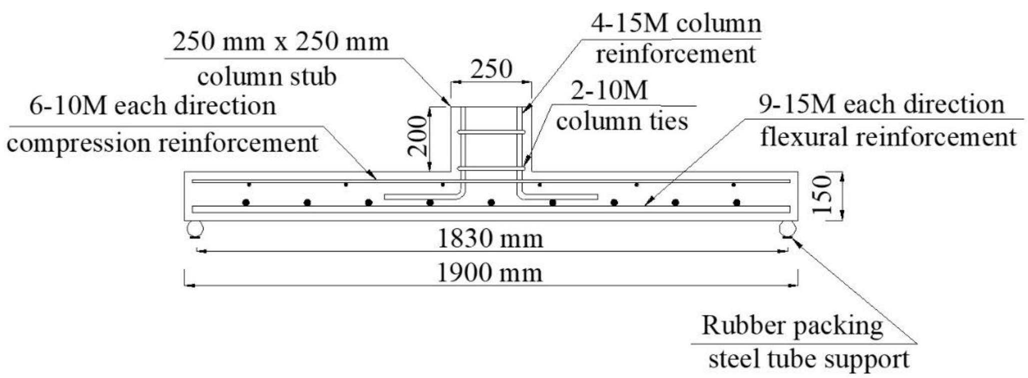

Figure 7-1 Details of a typical slab.

Table 7-3 Details of Slab Specimens

Side dimensions (mm × mm)	h (mm)	c (mm)	d (mm)	f_c' (MPa)	Main reinforcement
1900 × 1900	150	250	104	41.1	Two layers-15M bars (ρ = 1%)

*h is the height; c is column width; d is the effective slab depth; ρ is the reinforcement ratio; and f_c' is the concrete compressive strength.

a.

b.

Figure 7-2The isolation precautions for the assembly of flexural reinforcement.

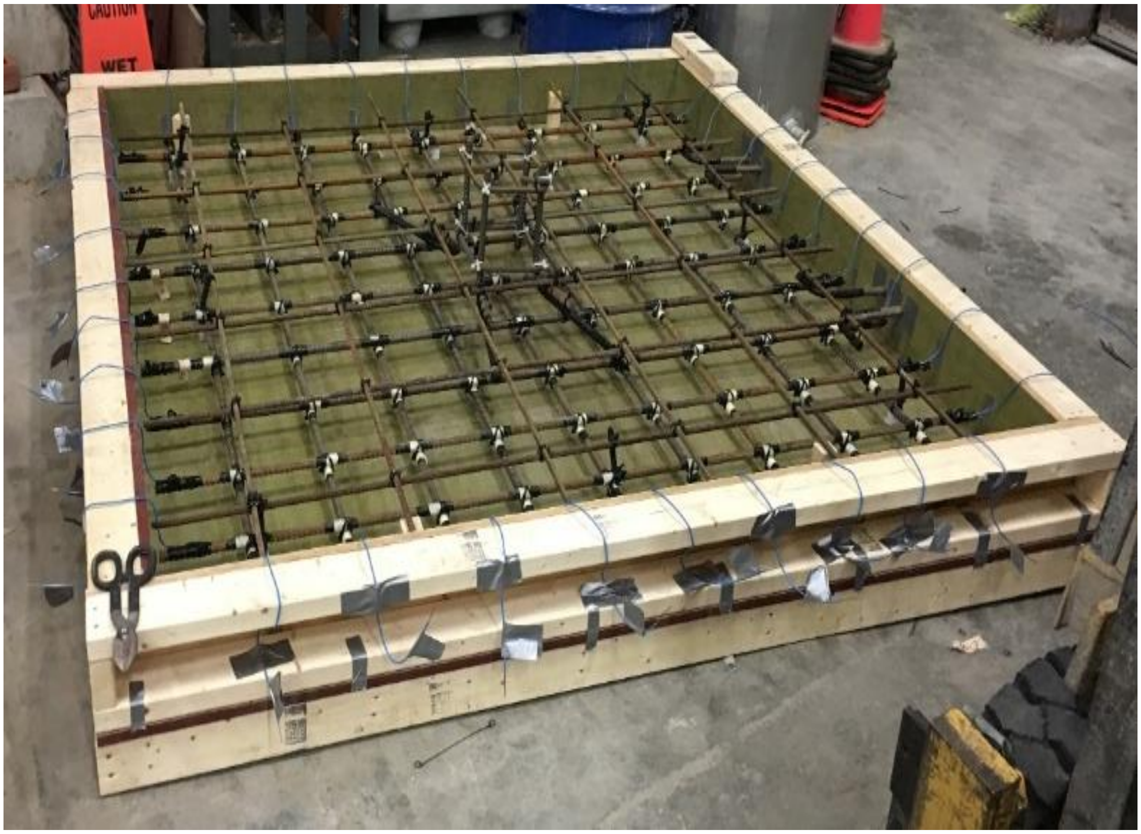

Figure 7-3 The wires that connected to the bars under corrosion.

Table 7.4 summarized the corrosion details for each tested slab. The symbols for each tasted slab were created as “S” referred to the slab and the number following it represented mass loss percentage. There were four mass loss levels, 0%, 15%, 25%, and 50%. The letter D referred to the delaminated corroded area. There was three corroded area chosen for this study. D1 had corroded area equal to the reinforcement bandwidth, c + 3h (700 mm × 700 mm), where c is the column dimension, and h is the slab thickness, as defined in CSA A23.3-14 (2014). D2 and D3 referred to the corroded area with and without enough development length, respectively. In other words, the embedded bar corroded except the development length from both far sides of each bar in D2 slabs, and the embedded bar corroded except the one-half of the development length from both far sides of each bar for

D3 slabs. i.e. S25-D2 was referred to the moderate level of corrosion, 25% mass loss, over a large area with keeping the development length without corrosion. The targeted corroded area for each corroded slab was shown in Figs. 7.4.

Table 7-4 The corrosion details for each tested slabs

Slab Symbol	Mass loss (%)	Corroded area (mm × mm)
S0	0	-
S15-D1	15	700 × 700
S25-D1	25	700 × 700
S50-D1	50	700 × 700
S15-D2	15	1060 × 1060
S25-D2	25	1060 × 1060
S50-D2	50	1060 × 1060
S15-D3	15	1480 × 1480
S25-D3	25	1480 × 1480
S50-D3	50	1480 × 1480

The development length (L_d) was calculated using the simplified version of CSA A23.3-14 (2014):

$$L_d = 0.45\, k_1\, k_2\, k_3\, k_4\, \frac{f_y}{\sqrt{f_c'}}\, d_b \qquad 7.1$$

Where f_y, f_c' and d_b are the yield stress of the reinforcement, the compressive strength of the concrete, and the nominal diameter of the reinforcing bars, respectively. The factors k_1, k_2, k_3, and k_4 are bond location, coating, concrete density factor, and bar size factor, respectively. The first three factors can be taken as 1; while the fourth one is taken as 0.8 for 20M or smaller bars.

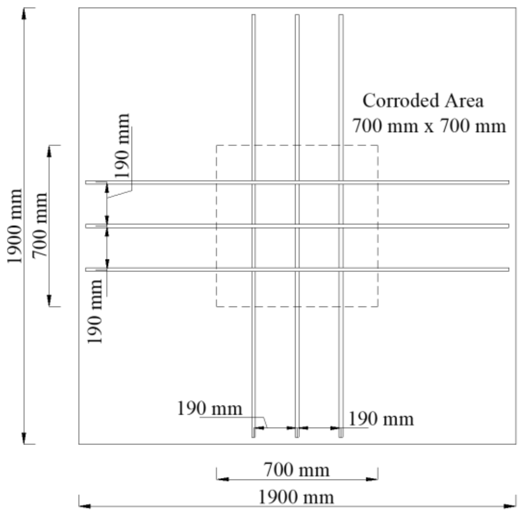

a. S-D1

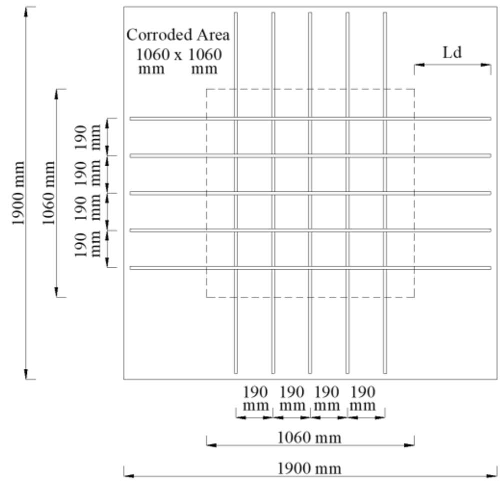

b. S-D2

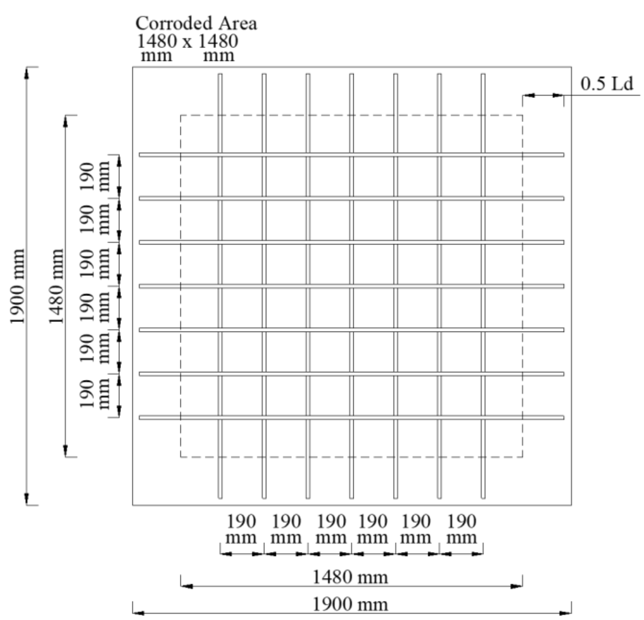

c. S-D3

Figure 7-4 The targeted corroded area for each corroded slab.

7.4.4. Accelerated Corrosion Setup

The corrosion process for all test slabs was subjected to an accelerated corrosion technique. Each slab was placed upside down and a dike constructed around the targeted corroded area and filled with an electrolyte solution (5% Sodium Chloride by weight of water). A steel mesh immersed inside the electrolyte solution and covered all targeted area as shown in Fig. 7.5. A source of direct current used where positive terminal feeder connected to the bars which considered an anode, and the negative terminal connected to the steel mesh which considered as a cathode.

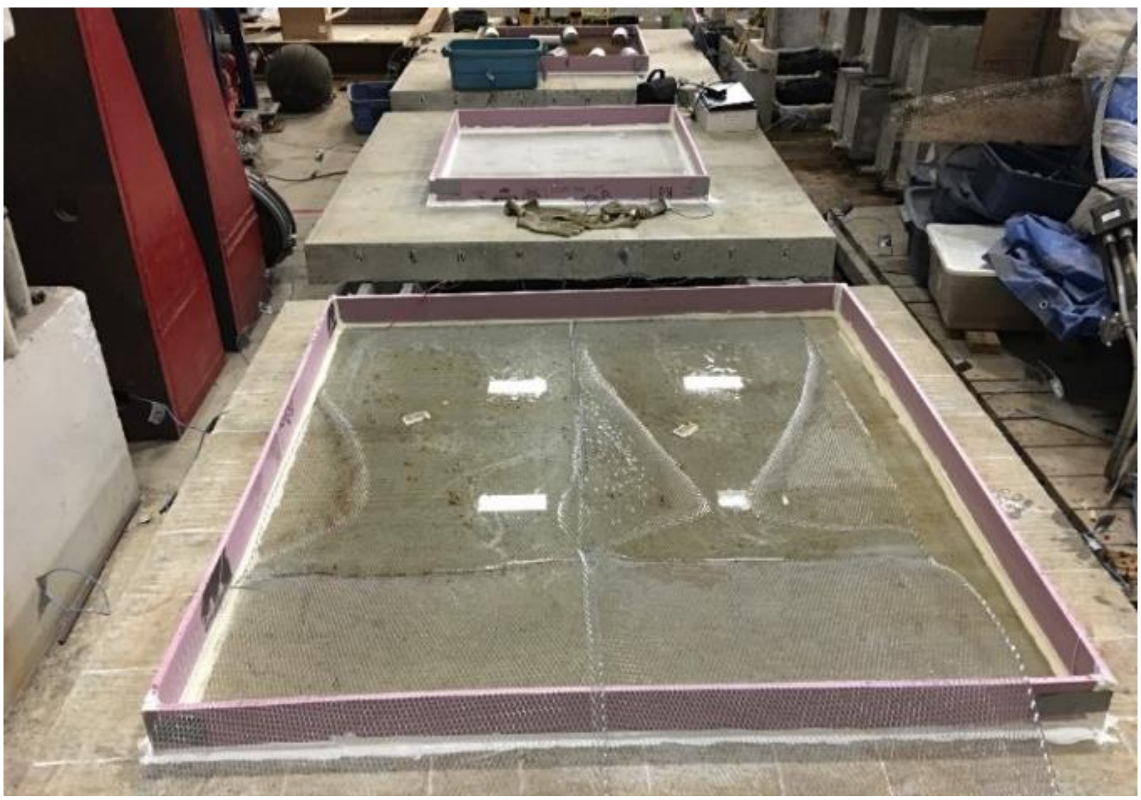

Figure 7-5 Dike constructed around the corroded area.

The theoretical mass loss is calculated based on Faraday's equation as

$$\text{Mass loss} = \frac{t\,I\,M}{z\,F} \qquad 7.2$$

where t is the time passed in seconds, I is the current passed in Amperes, M is atomic weight (for iron $M = 55.847$ g/mol), Z is the ion charge (two moles of electrons), and F is Faraday's constant which is the amount of electrical charge in one mole of electron ($F = 96{,}487$ Coulombs per mole (C/mol)) (Lachemi et al. 2014).

7.5. Test Results and Discussion

7.5.1. Cracks Widths due to Corrosion

The maximum crack width at the end of the corrosion period for each slab was recorded. An accurate crack width microscope that has 60× focusable eyepiece magnifier and has an accuracy of 0.02 mm was used to measure the cracks. In addition, a crack width meter was used to measure large cracks that exceeded the measuring range of the field microscope (2 mm). Table 7.5 shows the maximum crack width for each corroded slab after finishing the test period. It has been noticed from the table that the maximum crack width increased with the increase of both the mass loss and the corroded area. This could be attributed to the effect of corrosive products of the embedded bars that increased with the increase of mass loss and the increase of the corroded portion of the embedded bar under concrete cover.

7.5.2. Natural Frequency Measurements

The corrosion process is a random process, which provides unexpected behaviour such as maximum crack widths and cracks distributions. Therefore, to enhance the predicated equation for the residual strength, the natural frequency measured experimentally for each slab. The experimental measurement of the natural frequency was under free-free boundary condition (FFC), which is more precise than measuring it under simply supported boundary condition (SSC). That is because the rigidity of supports has a significant effect on the dynamic behaviour of the structure.

Table 7-5 Maximum crack widths and natural frequencies measurements

Slab	w_c (mm)	ω_f (Hz)	Difference between S0 and others (%)
S0	0.00	134	0%
S15-D1	0.15	104	22.4%
S25-D1	0.50	64	52.2%
S50-D1	2.00	41	69.4%
S15-D2	0.40	55	60.0%
S25-D2	0.80	35	73.9%
S50-D2	2.90	24	82.1%
S15-D3	0.50	51	61.9%
S25-D3	1.00	23	82.8%
S50-D3	3.20	19	85.8%

* w_c is the maximum corrosion crack width, ω_f Natural frequency – free-free condition.

The natural frequency was measured experimentally by causing a known impact excitation using a special hammer containing a load cell on its face. Three Accelerometers placed at certain locations of the slab to measure the vibration response, two accelerometers placed in top two coroner sides and the last one placed on the middle point of the test slab. A data acquisition system collected the analog signals from hammer and accelerometers, then transferred them to a digital signal to proceed in a computer software to get the natural frequency value. Figure 7.6 illustrates the frequency measurement setup for a test slab.

Table 7.5 represented the experimental measurement of the natural frequencies in case of free-free boundary condition. It has been concluded that the natural frequencies decreased with the increased of corrosion level. This could be attributed to the stiffness loss that occurred with the increase of corrosion level, which affects the rigidity of the slabs and the natural frequency values. In addition, the corrosive products that accumulated under the concrete cover, causing damping which decrease the natural frequency. This decrease does not depend only on corrosion level but also on maximum crack widths and crack distributions. Therefore, the ability to measure natural frequency in situ as a non-destructive test could enhance the capability to predict the capacity for the slabs.

Figure 7-6 Natural frequency measurement setup for a tested slab.

7.5.3. Load Carrying Capacity

The slab capacity is the response that is needed to be predicted at the end of the statistical analysis. The capacity for each slab was determined by applying a concentric load on the column stub using a hydraulic jack. Each slab was tested on a vertical position and was simply supported along all four edges of the loading frame as shown on the schematic Fig. 7.7. The load was applied in small increments that were recorded using a load cell. It has been found that the failure load for the control slab S0 was 391 kN. The load failure capacity for small corroded area slabs S15-D1, S25-D1, and S15-D1 were 340 kN, 315 kN, and 269 kN, respectively. For the large corroded area S15-D2, S25-D2, S50-D2, S15-D3, S25-D3, and S15-D3 were 320 kN, 286 kN, 183 kN, 289 kN, 225 kN, and 113 kN, respectively. It could be concluded from this results that the capacity decreased with the increase of both corrosion level and corroded area. It has been found that 50% of mass loss caused a drop in capacity by 31.2%, 53.1%, and 71.1% for S50-D1, S50-D2, and S50-D3, respectively.

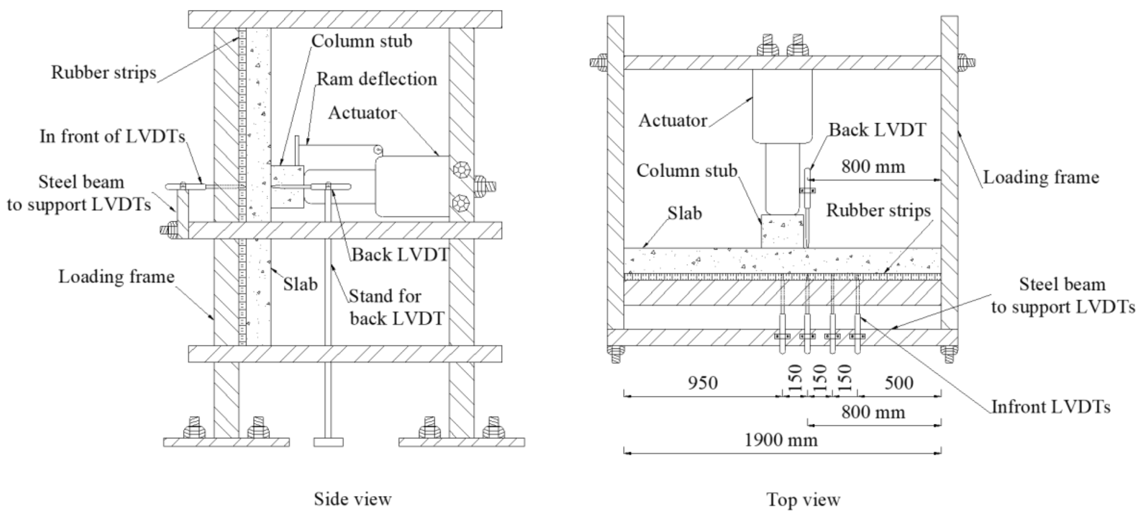

Figure 7-7 Schematic for the loading test setup.

Aoude et al. (2014) simulated the mass loss by decreasing the bar diameter from 15M to 10M which was considered as 50% mass loss. Aoude et al. found that a uniform 50% mass loss in full slab area decreased the load carrying capacity by 28%. Other study did by Rahman (1992), which simulated the corrosion by reducing the bar numbers and using polyethylene sheet that placed between the upper and lower bars of the top reinforcement mesh to simulate the delaminated area. In addition to wrapping the bar with plastic adhesive tape to simulate the bond loss. Rahman concluded that 50% of mass loss decreased the loading capacity by 34% and 35% for uncoated and coated bars, respectively. A further study was done by Aoude et al. (2014) on the effect of 50% mass loss on a small corroded area, reinforcement bandwidth. They found that the loss in capacity was 24%. It has been concluded that for the small corroded area the drop on the capacity in this current study was a little bit more than that measured by Aoude. However, there was a significant change between the drop in capacity for the large corroded area in this current study and the previous studies done by Aoude and Rahman. This could be attributed to several reasons, first, simulating corrosion by reducing bar diameter or numbers causing a decline in the reinforcement ratio for the whole slab not only the targeted corroded area. Several studies concluded that reducing reinforcement ratio is one of the factors that reduced the punching carrying capacity (Hussein 1990; Marzouk & Hussein 1991; Dilger et al. 2005). The current study investigated the reduction of mass loss in a portion of bar length, not the whole length; however, the reduction in capacity was more than that done by Aoude or Rahman. Second, they failed to simulate the real behaviour of losing the bond between the concrete cover and the corroded bars. On the contrary, this current study did realistic corrosion by using accelerated techniques that lead to producing corrosion products that weakened the bond between the concrete cover and corroded bar. Thirdly, in this current study, all the corroded slabs had cracks due to corrosion, which had more effect in reducing the loading capacity of the slabs more than the previous studies. The previous reasons illustrated that using accelerated corrosion technique provided better simulation to corrosion more than the assumption that used by Aoude et al. (2014) or Rahman (1992).

7.5.4. Chloride Content Measurements

The chloride content was measured to be an indication for the corrosion level. It was measured at the contact surface between the concrete cover and the flexural mesh. Eight samples were extracted from each slab from different locations on the same one-quarter of the corroded area. Four samples extracted from the contact surface between the top layer of flexural mesh and the concrete cover, and other four samples extracted from the contact surface between the lower layer of flexural mesh and the concrete cover. Tables 7.6 and 7.7 present the chloride content value for each slab and the chloride content at both depths; top and lower layer of flexural mesh, respectively. It has been concluded from the table that the chloride content values near the top layer have higher values than that near the lower one. This difference also shown in Figs. 7.8 and 7.9. This could be attributed to the effect of concrete cover thickness, where when concrete cover thickness increased, the chloride content value decreased. The results also confirm other researchers results (Amleh & Mirza 1999; Montemor et al. 2002), that the chloride content decreases when it gets far from the concrete surface in the direction of embedded reinforcement. In this study, the chloride concentration at the contact surface between the concrete cover and the top layer was only considered in the statistical analysis. It has been found from Table 7.6 that 15%, 25%, and 50% mass loss have 0.807%, 1.298%, and 1.632% of chloride content.

Table 7-6 Chloride content at depth 30 mm, the upper layer of flexural mesh

Slab	**Specimen 1**	**Specimen 2**	**Specimen 3**	**Specimen 4**	**Average**	**Average** Cl^-_c (%)	
S15-D1	0.834	0.81	0.76	0.756	0.79	15% mass loss	0.807
S15-D2	0.828	0.826	0.808	0.786	0.812		
S15-D3	0.882	0.832	0.81	0.748	0.82		
S25-D1	1.025	1.176	1.268	1.419	1.222	25% mass loss	1.298
S25-D2	1.157	1.249	1.381	1.453	1.31		
S25-D3	1.245	1.265	1.449	1.489	1.362		
S50-D1	1.466	1.584	1.588	1.726	1.591	50% mass loss	1.632
S50-D2	1.491	1.598	1.666	1.793	1.637		
S50-D3	1.494	1.594	1.732	1.852	1.668		

* Cl^-_c Chloride content (%)

Table 7-7 Chloride content at depth 46 mm, the lower layer of flexural mesh

Slab	Specimen 1	Specimen 2	Specimen 3	Specimen 4	Average	Average	Cl^-_c(%)
S15-D1	0.282	0.295	0.431	0.464	0.368	15% mass loss	0.3763
S15-D2	0.291	0.362	0.384	0.475	0.378		
S15-D3	0.315	0.322	0.441	0.454	0.383		
S25-D1	0.432	0.501	0.649	0.698	0.57	25% mass loss	0.6057
S25-D2	0.497	0.583	0.649	0.715	0.611		
S25-D3	0.547	0.605	0.677	0.715	0.636		
S50-D1	0.662	0.744	0.75	0.812	0.742	50% mass loss	0.7613
S50-D2	0.659	0.759	0.779	0.859	0.764		
S50-D3	0.711	0.782	0.784	0.835	0.778		

* Cl^-_c Chloride content (%)

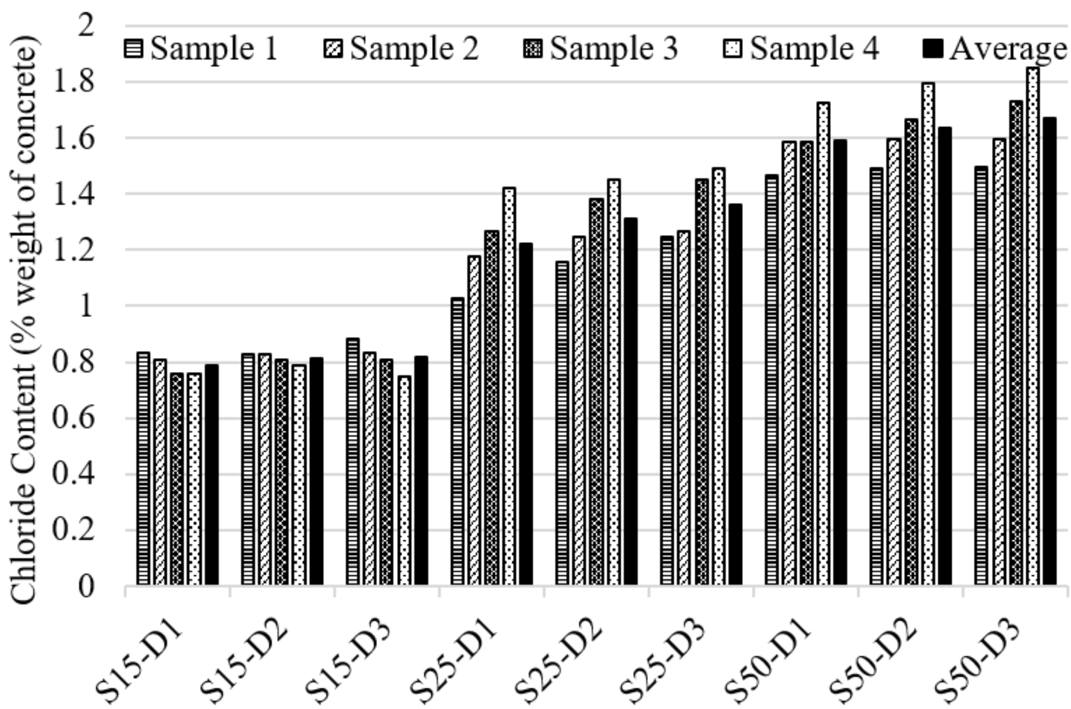

Figure 7-8 Chloride content % above the upper layer of flexural mesh for each slab.

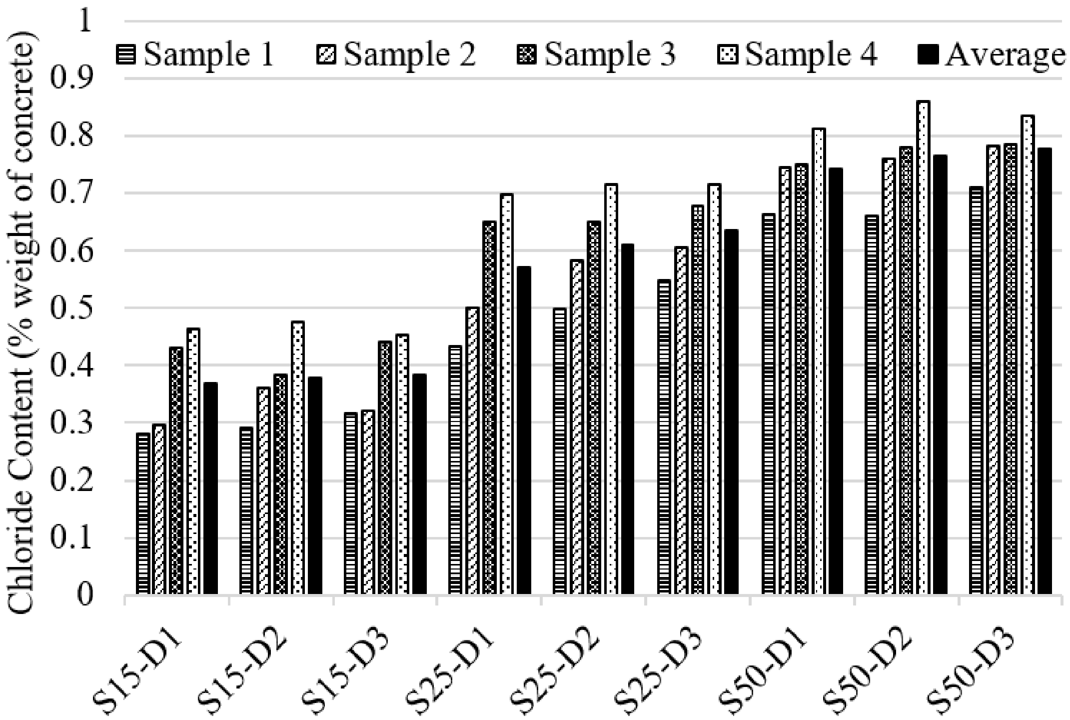

Figure 7-9 Chloride content % above lower layer of flexural mesh for each slab.

7.5.5. Mass Loss Measurements

When the targeted mass loss was reached based on the theoretical calculations of Faraday's equation, the accelerated corrosion process stopped, all requirement measurement recorded, and the slab tested. After finishing all measurements, the concrete cover in each corroded slab was demolished to extract the corroded bars using a demolition hammer as shown in Fig. 7.10. Figs. 7.11, 7.12, and 7.13 show the extracted corroded reinforcement after removing the concrete cover for the tested slabs S-D1, S-D2, and S-D3, respectively. The corrosion products were removed from the corroded bars following the standard instruction of the American Society for Testing and Materials (ASTM G1 2003). The cleaned corroded bars were weighed and then the actual mass loss for each corroded bar was calculated according to the following equation:

$$\% \text{ mass loss} = \frac{\text{initial weight} - \text{final weight}}{\text{initial weight}} \qquad 7.3$$

a. During demolition b. After demolition

Figure 7-10 The extraction process of corroded bars.

a. S15-D1 b. S25-D1 c. S50-D1

Figure 7-11 The corroded bars for each tested slab.

a. S15-D2 b. S25-D2 c. S50-D2

Figure 7-12 The corroded bars for each tested slab.

a. S15-D3 b. S25-D3 c. S50-D3

Figure 7-13 The corroded bars for each tested slab.

Figure 7.14 shows the actual mass loss for each corroded bar in each test slab. The number of bars under corrosion was 6, 10, and 14 bars for S-D1, S-D2, and S-D3 slabs, respectively. It has been noticed in all slabs that the actual mass loss did not exceed the theoretical mass loss. This finding is similar to that fining of previous studies on corrosion of concrete beams (Spainhour & Wootton 2008; YuBun Auyeung et al. 2000). This could be attributed to that some current leakage to electrolyte solution causing dissociating to the water particles into cations and anions. The passing current through water over time releases gases (oxygen and hydrogen) that appear during the test in small bubbles on water surface (Chen & Luckham 1994). Therefore, some current from that used to calculate the theoretical mass loss was used in other process rather than the ionization of iron.

Figure 7.15 shows the error between the actual mass loss for each bar and the corresponding theoretical value. It has been noticed that the error in mass loss calculation increased with the increase of corrosion level. The average error in each slab S15-D1, S15-D1, S15-D1, S25-D1, S25-D1, S25-D1, S50-D1, S50-D1, and S50-D1 is 1.06%, 1.55%, 1.57%, 2.44%, 2.65%, 3.11%, 4.32%, 4.42%, and 4.77%, respectively. Figure 7.16 shows a sample of corroded bars after extracting and cleaning them from corrosion products.

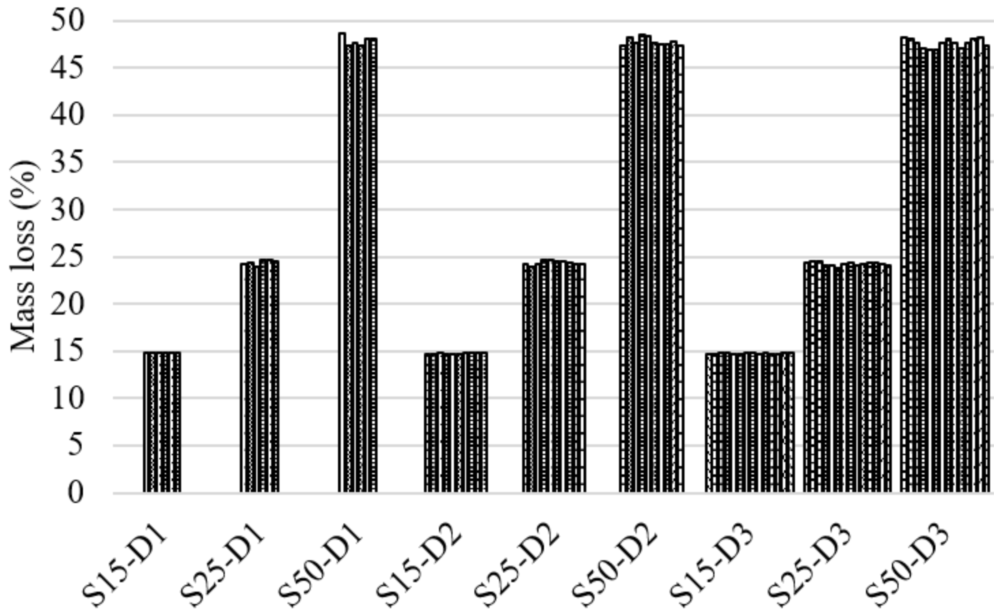

Figure 7-14 Mass loss % for all corroded bars in each slab.

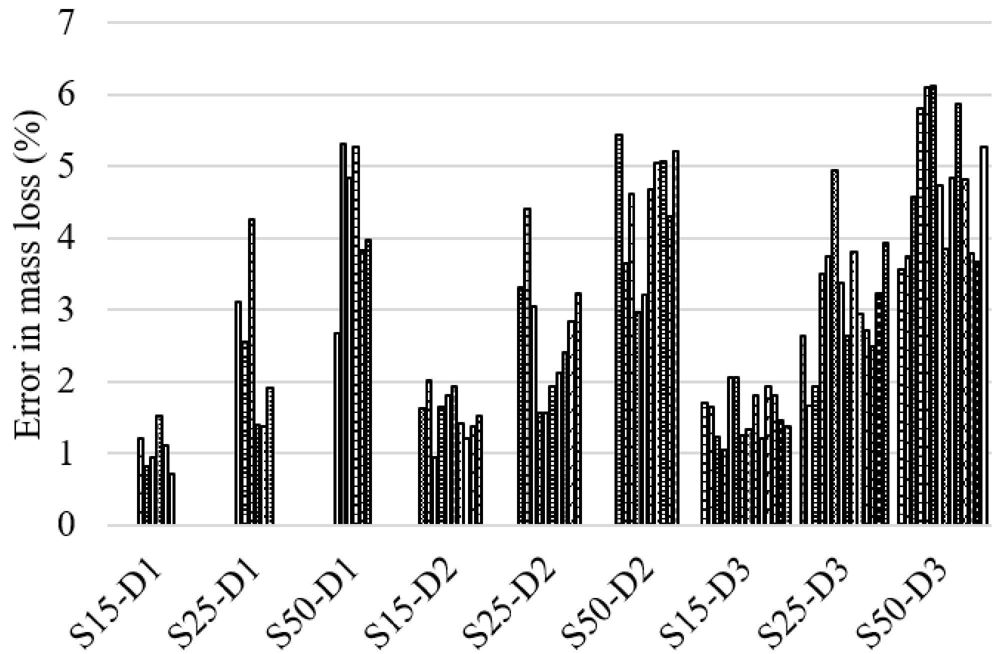

Figure 7-15 The error in mass loss % for all corroded bars in each slab.

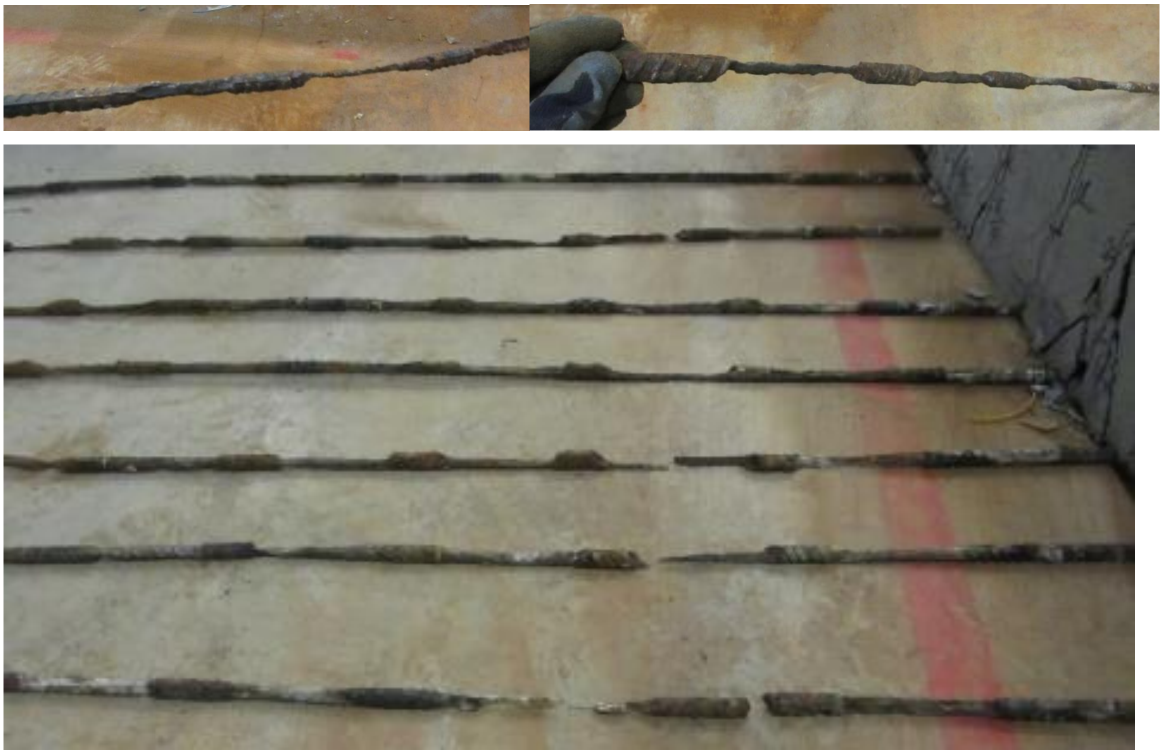

Figure 7-16 Samples of corroded reinforcement after the demolition of concrete cover.

7.6. Statistical Analysis for the Experimental results

A statistical design of experimental tool was used to determine the relationship between constraint parameters that are affecting the response. There were four parameters on this study: parameter A: mass loss level, parameter B: corroded area, parameter C: maximum crack width, and parameter D: normalized natural frequency. There was one response to this study: residual slab capacity. The mass loss was represented by the corresponding chloride content, and the corroded area was represented as the ratio between the corroded area (CA) and the total area (TA). Table 7.8 shows the run parameters of ten models of design variables. Nine slabs were run for the design of the experiment, while one slab (S15-D3) was chosen to be the validation for the prediction equations. Only one equation was chosen because the test consumes a very long time to be finished, it was difficult to do more corrosion tests to increase the validation points. RSM design was established to assess the effect of the four parameters and their interactions on the residual slab capacity. RSM design was divided into three stages: the first stage studied the interaction between the mass loss and corroded area and their effect on the residual capacity. The second stage added the effect of the maximum crack width and their interaction with the parameters on stage one. The final stage studied the natural frequency parameter and its interaction with the parameters of stage two. The natural frequency was represented in a normalized form where its equal to the ratio between the natural frequency in corroded and reference slabs. A regression prediction model was then developed to create prediction equations which can predict the residual corroded slab capacity value for any other existing slab. A Validation of the prediction equations was performed with the experimental test for the S15-D3 slab. Hence, this regression equations is convenient to determine the residual slab capacity for any exiting corroded slab.

Table 7-8 Run parameters of models design variables

Run	A: Cl^{-}_{c} (%)	B: CA/TA	C: w_c (mm)	D: ω_c/ω_r (Hz)	P_u (kN)
S0	0.067	0	0	1.00	391
S15-D1	0.807	0.136	0.15	0.78	340
S25-D1	1.298	0.136	0.5	0.48	315
S50-D1	1.632	0.136	2.0	0.31	269
S15-D2	0.807	0.311	0.4	0.41	320
S25-D2	1.298	0.311	0.8	0.26	286
S50-D2	1.632	0.311	2.9	0.18	183
S15-D3	0.807	0.607	0.5	0.38	289
S25-D3	1.298	0.607	1.0	0.17	225
S50-D3	1.632	0.607	3.2	0.14	113

Cl^{-}_{c} Chloride content, CA is the corroded area, TA is the total slab area, w_c is the maximum corrosion crack width, ω_r is the natural frequency for the reference slab, ω_c is the natural frequency for the corroded slab, and P_u is the experimental slab capacity.

7.6.1. Analysis of Variance

The results showed the model F-value of 37.63, 153.26, and 197.80 for stages 1, 2, and 3, respectively, which implied that the three models were significant. There was only a 0.07% chance that could occur due to noise in stage 1 while it was a 0.01% chance that could occur due to noise in both stages 2 and 3. In the tables 7.9 to 7.11, the values of "Probability > F" less than 0.05 indicated that model terms were significant, while the values greater than 0.1 indicated that the model terms were not significant. In both stages 1 and 2, all factors were significant. Whereas in stage 3 the A, B, and C were the significant model terms, and term D has F value less than 0.1 but more than the significant value 0.05. Indeed, the model required to add insignificant model terms to support the hierarchy.

Table 7-9 ANOVA for RSM for stage 1

Source	Sum of Squares	df	Mean Square	F - Value	P - Value Prob > F	
Model	56066.55	3	18688.85	37.63	0.0007	Significant
A	17052.62	1	17052.62	34.33	0.0021	
B	63.85	1	63.85	0.13	0.0473	
AB	6355.01	1	6355.01	12.79	0.0159	
Residual	2483.45	5	496.69			
Cor Total	58550.00	8				

*df is the degree of freedom, and Prob is the Probability

Table 7-10 ANOVA for RSM for stage 2

Source	Sum of Squares	df	Mean Square	F - Value	P - Value Prob > F	
Model	57920.12	3	19306.71	153.26	<0.0001	Significant
A	164.85	1	164.85	1.31	0.0304	
B	7370.82	1	7370.82	58.54	0.0006	
C	8208.58	1	8208.58	65.16	0.0005	
Residual	629.88	5	125.98			
Cor Total	58550.00	8				

*df is the degree of freedom, and Prob is the Probability

Table 7-11 ANOVA for RSM for stage 3

Source	Sum of Squares	df	Mean Square	F - Value	P - Value Prob > F	
Model	58255.48	4	14563.87	197.80	<0.0001	Significant
A	499.52	1	499.52	6.78	0.0498	
B	4505.80	1	4505.80	61.20	0.0014	
C	7598.37	1	7598.37	103.20	0.0005	
D	335.36	1	335.36	4.55	0.0997	
Residual	294.52	4	73.63			
Cor Total	58550.00	8				

*df is the degree of freedom, and Prob is the Probability

Table 7.12 shows the model summary statistics. The models had a sample standard deviation equal to 22.29, 11.22, and 8.58 for stages 1, 2, and 3, respectively. While the mean for the three stages equals 271.33 kN. It has been observed that the standard deviation decreased with the increase of the studied parameter from stage 1 to stage 3. Thus, those parameters affect the response where the deviation within the data set gets closer to the mean value. However, the F value for the term D (natural frequency) lied out of the significant range.

The adequacy of the model validated by calculating three model summary statistics: R-squared (R^2), adjusted R-squared (R^2_{adj}), and predicted R-squared (R^2_{Pred}). R^2 is the coefficient of determination for regression that considers as a statistical measure that shows the fitting of the data to the regression line. Higher R^2, better the model fits the data. Lower R^2, worse the model fits of the response data around the mean. There is a drawback of using R^2 alone as a measure for best fitting of data to the regression line. In fact, the R^2 increases when the number of factors increases regardless it is significant or not, which considers as a misguidance. Another modified term was introduced as a measure for the variation about the mean expressed by the model, this term is Adjusted R-squared (R^2_{adj}) and it's always less than R^2. R^2_{adj} distinguishes that its only increases or decreases when the added factor would improve the model by more or less than the expected by chance, respectively. The predicted R-squared (R^2_{Pred}) term expresses the ability for the regression model to predict responses for new observation. Higher values of R^2_{Pred}, better model (Montgomery 2012).

Table 7.12 shows the statistics of model summery, where R^2, R^2_{adj}, and R^2_{Pred} increased from stage 1 to stage 3, and they were in reasonable agreement. The high value of R^2_{Pred} meant that each model had a good chance of making a reasonable prediction. This prediction enhanced from stage 1 to stage 3 with increasing the studied parameters. The increase in

R^2_{adj} meant that the added parameters in each stage improved the model by more than the expected by chance; therefore, stage 3 considered the best.

Table 7-12 Model summary statistics

Stage	Standard Deviation	R-squared (R^2)	Adjusted R^2 (R^2_{adj})	Predicted R^2 (R^2_{Pred})	Source
1	22.29	0.96	0.93	0.85	2 FI
2	11.22	0.989	0.982	0.968	Linear
3	8.58	0.995	0.989	0.982	Linear

*FI is factor interaction

The residuals were examined to investigate the model adequacy and the basis assumption of the ANOVA. The residuals represented the deviation between the observed data and the predicted values, which considered as error estimation in the model. The residuals were assumed in the model to be normally distributed with a mean zero and constant standard deviation. There were three checks for the model assumption: check for the normality assumption, checks for the homogeneous variance assumption, and checks for independence assumption. Figure 7.17 shows the plot of the normal probability of the residuals for each stage. The values were well distributed around the mean for all stages. It has been indicated that the plot in each stage was a straight line, which meant that the distribution of the underlying error was normal for each stage. Therefore, normality assumption check considered satisfactory as ANOVA's first assumption.

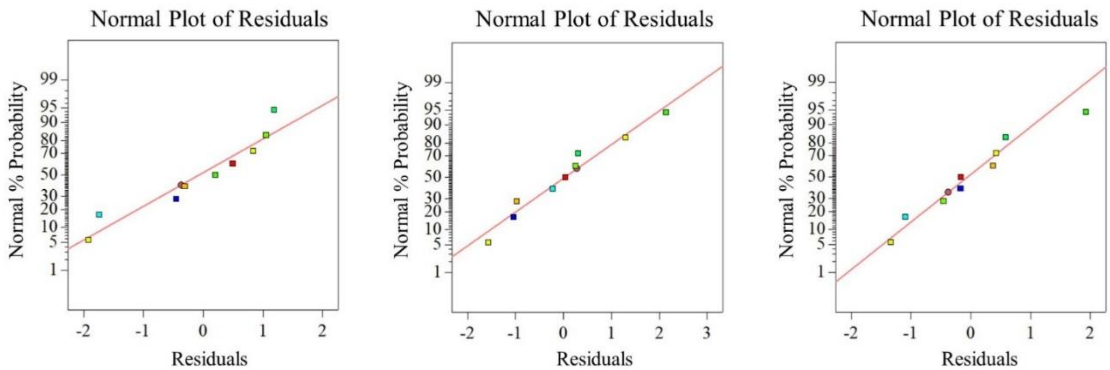

Stage 1 Stage 2 Stage 3

Figure 7-17 Normal Probability Plot of Residuals.

Figure 7.18 shows the distribution of residuals versus predicted values for each stage. It has been noticed that the distribution for each stage was random with no obvious pattern. This behaviour indicated that residuals were independent and had constant variance, which satisfied the ANOVA's second assumption. Figure 7.19 shows the relation between the residuals and the running order. It has been concluded that there was no tendency for positive or negative residuals, which implied that there was no independence among the treatments. In addition, the treatments were randomized. The ANOVA's third assumption was satisfied for all stages. Therefore, the model in each stage provided an adequate fit to the observed data, where the all assumptions were valid.

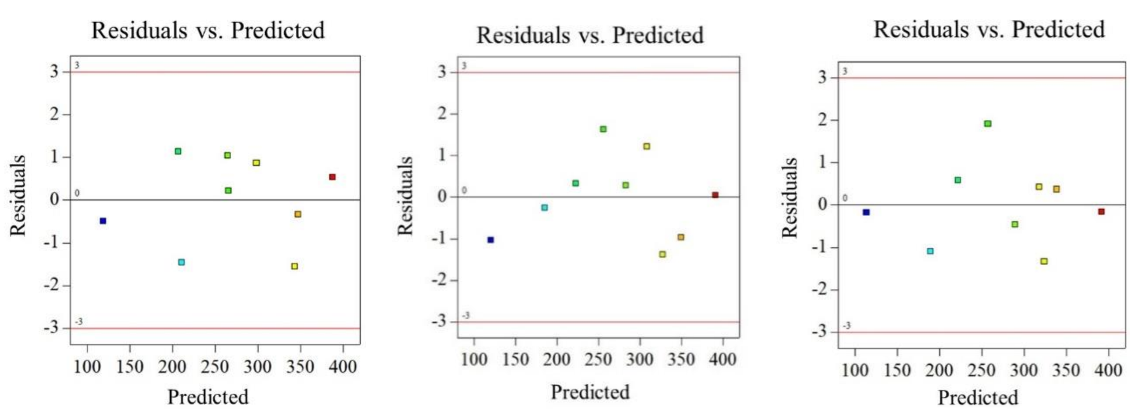

Stage 1 Stage 2 Stage 3

Figure 7-18 Plot between Residuals and Predicted.

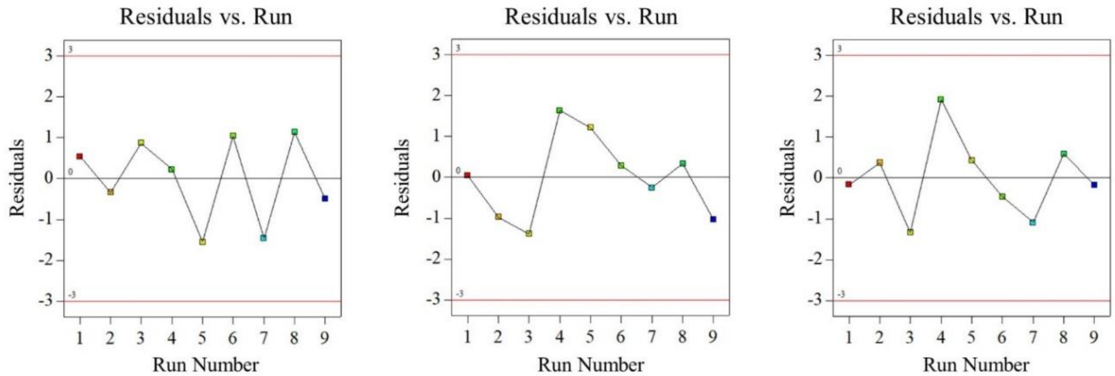

Stage 1 Stage 2 Stage 3

Figure 7-19 Plot between Residuals and Run.

Figure 7.20 shows the contour graph obtained from the statistical analysis from stage one, the relation between A: mass loss levels (represented by chloride content) and B: corroded area (represented by corroding area over the total area of the slab). Stage one contained only two factors; therefore, there was only one contour graph between the mass loss level and corroded area. The figure showed that the residual slab capacity was decreasing with the increase of A: mass loss and B: corroded area.

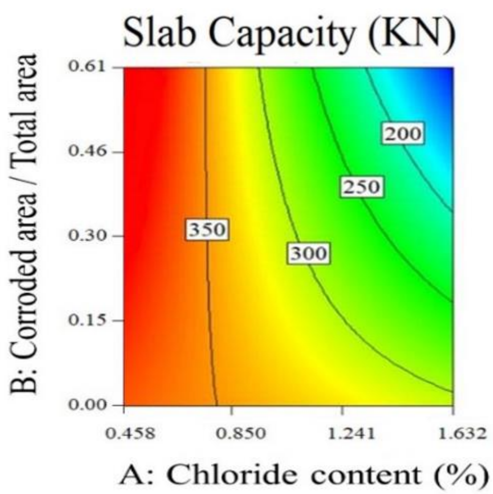

Figure 7-20 Contour shows Interaction between A and B.

7.6.2. Proposed Equations and Verification for the Statistical Model

The purpose of this study is to find an empirical equation based on the regression analysis to predict the residual slab capacity. The predicted equation would guide the engineers to take appropriate decision in a reasonable time which would also save in costs.

The empirical equation from stage one is as follow:

$$\text{Slab capacity} = 396 - 52 * Cl_c^- + 134 * \frac{CA}{TA} - 273 * Cl_c^- * \frac{CA}{TA} \qquad 7.4$$

where Cl_c^- is the chloride content (%), CA is the corroded area, TA is the total slab area. A verification was occurred by using the data of S15-D3 to check the predicted residual slab capacity with the actual one. The actual slab capacity was equal to 289 kN while the predicted one was equal to 302 kN. This result reveals that there was 95.8% agreement between the two values which appear the efficiency of the predicted equation of stage one.

The empirical equation from stage two is as follow:

$$\text{Slab capacity} = 395 - 22 * Cl_c^- - 141 * \frac{CA}{TA} - 47 * w_c \qquad 7.5$$

where w_c is the maximum crack width. This equation at S15-D3 had a value of 269 kN, which had a tolerance of 6.9% and agreement of 93.1%, which still show the efficiency of the equation. Adding the maximum crack width did a significant difference in the empirical equation, where the value of stage one and two had a difference of 11.1%. It has appeared that the maximum crack width had a significant effect on the prediction of the residual slab capacity; however, stage two had predicated value farther from the exact compared to the predicted value from stage one. While the empirical equation for stage three is as follow:

$$\text{Slab capacity} = 474 - 47 * Cl_c^- - 222 * \frac{CA}{TA} - 43 * w_c - 80 * \omega_r / \omega_c \qquad 7.6$$

The verification of this equation at S15-D3 had a value of 249 kN, which had a tolerance of 13.7% and agreement of 86.3%.

One verification was not enough to provide a good judgement for the predicted equations. But this is due to the corrosion test that consumes a long period; therefore, more tests are needed to enhance and validate these equations. As a consequence, the raw data used to establish these equations were used to calculate the tolerance and the agreement between the actual slab capacity and the predicted ones in each stage as shown in Table 7.13. The verified slab was added to the table. It has been found that the maximum tolerance is 14.6%, 11.1% and 13.7% for stages one, two, and three, respectively. While the minimum tolerance is 0.1%, 0.1% and 0.0% for stages one, two, and three, respectively. Therefore, it is recommended to use the three equations to choose the lowest predicted value to be on the safe side.

Table 7-13 Residual slab capacity of the predicted equations and the actual values

Run	P_u	Stage 1			Stage 2			Stage 3		
		P_p	A_{u-p}	T_{u-p}	P_p	A_{u-p}	T_{u-p}	P_p	A_{u-p}	T_{u-p}
	(kN)	(kN)	(%)	(%)	(kN)	(%)	(%)	(kN)	(%)	(%)
S0	391	393	99.6	0.4	394	99.4	0.6	391	100	0.0
S15-D1	340	342	99.3	0.7	352	96.7	3.3	337	99.1	0.9
S25-D1	315	299	94.8	5.2	325	97.0	3.0	323	97.6	2.4
S50-D1	269	269	99.9	0.1	249	92.4	7.6	256	95.3	4.7
S15-D2	320	327	97.8	2.2	315	98.6	1.4	317	99.1	0.9
S25-D2	286	260	90.9	9.1	286	99.9	0.1	289	99.0	1.0
S50-D2	183	214	85.4	14.6	183	99.8	0.2	189	96.7	3.3
S15-D3	289	302	95.8	4.2	269	93.1	6.9	249	86.3	13.7
S25-D3	225	195	86.6	13.4	235	95.6	4.4	222	98.5	1.5
S50-D3	113	122	92.6	7.4	127	88.9	11.1	114	99.3	0.7

* P_u is the experimental slab capacity, P_p is the predicted slab capacity, A_{u-p} and T_{u-p} are the agreement and tolerance between the experimental and the predicted slab capacity, respectively.

7.7. Conclusion

The following conclusions were drawn from studying different mass loss levels and corroded areas on two-way RC slabs:

- The maximum corroded cracks were monitored for each tested slab. It has been found that the crack widths increased with the increase of mass loss levels or the increase of the corroded area. This could be attributed to the corrosive products that increase with increasing the mass loss level or the corroded area. Thus, an internal tensile pressure initiated and increased under the concrete cover causing cracks on its surface and causing also widened to those cracks. The cracks have been taken as a parameter in the regression analysis to study their effect on reducing the slab capacity.
- The natural frequency was measured for the all tested slabs. The natural frequency decreased with the increased of both the mass loss level and the corroded area. This could be attributed to the decreasing of the stiffness of the slab due to the decrease in the loading carrying capacity. In addition to the loss of the bond between the corroded bar and the concrete cover, in which the corrosive products that produced from the corroded bar weakened the bond. The bond loss also causing spalling in the concrete cover which causing a gradually decay and damping for the oscillations; consequently, decreased the natural frequency. Moreover, the increase of mass loss level causing wider crack widths, which affect the rigidity of the slab that consequently weakened the stiffness causing a reduction on the natural

frequency. Indeed, the natural frequency has a reverse relationship with the mass; when mass value decreased, the natural frequency increased. However, the increase in mass loss level (decrease in bar mass) decreased the natural frequency. This could be attributed to the presence of the corrosive products under the concrete cover; consequently, the total slab mass kept the same. The natural frequency could be used as a non-destructive test to detect the corrosion. Nonetheless, more studies need to be done on different boundary condition and more specimens in order to obtain more reliable results that could be guided specialist to detect the corrosion. The natural frequency had considered as a parameter in the prediction of the residual slab capacity.

- It has been found from the loading test that the slab capacity reduced with the increase of both corroded areas and the corroded slab. This result was expected and could be attributed to the loss of the cross-sectional area of the flexural reinforcement; especially this loss increased with the increase of the corroded length or the corrosion level.
- The chloride content was detected in all tested slabs in different two depths: upper and lower layer of the flexural reinforcement mesh. It has been observed that the chloride content value increased with the increase of the mass loss level. In addition, the measured chloride content value in the different corroded area at the same mass level had negligible tolerance. Thus, an average chloride content value was considered for the same mass loss level. It has been also observed that the chloride content for the same mass loss level is higher in the upper layer than that in the lower layer. This could be attributed to the effect of the cover thickness, in which

the chloride content has reversed effect with increasing concrete cover. Therefore, the chloride content for the upper layer was considered in constructing the predictions equations.

- The statistical design of experiment methodology was carried out to construct a simple and cheap approach for predicting the residual slab capacity under corrosion. A response surface method was selected for design three models and the models validated the adequacy and the basic assumption of the ANOVA; thus, the created models considered adequate fit to the observed data.
- It was recommended to calculate the predicted residual capacity from the three different equations and choose the lowest value among them. It has been observed that the maximum tolerance was 14.6%, 11.1% and 13.7% for stages one, two, and three, respectively. While the minimum tolerance is 0.1%, 0.1% and 0.0% for stages one, two, and three, respectively.
- A contour graph was constructed based on two-factor interaction statistics design type. The contour elaborated that increasing the corroded area caused a decrease in the residual slab capacity. In addition, the increase in the mass loss appeared to decrease the residual slab capacity. This decrease could be attributed to the loss of the cross-sectional flexural reinforcement that directly affected the slab capacity.
- The actual mass loss for all tested slabs had a close agreement with the theoretical mass loss that was calculated based on the Faraday's equation. In addition, it has been noticed that the tolerance between the actual and theoretical mass loss increased with the increase of the mass loss levels.

7.8. References

ACI 318-14 (2014) Building code requirement for structural concrete (ACI 318M-14) and commentary (ACI 318RM-14), Building Code Requirements for Structural Concrete.

Ahmad, S. (2003) 'Reinforcement corrosion in concrete structures, its monitoring and service life prediction - A review', Cement and Concrete Composites, 25(4–5 SPEC), pp. 459–471. doi: 10.1016/S0958-9465(02)00086-0.

Amleh, L. and Mirza, S. (1999) 'Corrosion influence on bond between steel and concrete', ACI Structural Journal, 96(3), pp. 415–423. doi: 10.14359/676.

Andrade, C. and Alonso, C. (1996) 'Corrosion rate monitoring in the laboratory and on-site', Construction and Building Materials, 10(5 SPEC. ISS.), pp. 315–328. doi: 10.1016/0950-0618(95)00044-5.

Andrade, C. and Alonso, C. (2001) 'On-site measurements of corrosion rate of reinforcements', Construction and Building Materials, 15(2–3), pp. 141–145. doi: 10.1016/S0950-0618(00)00063-5.

Aoude, H., Cook, W. D. and Mitchell, D. (2014) 'Effects of simulated corrosion and delamination on response of two-way slabs', Journal of structural Engineering, 140(1), pp. 1–9. doi: 10.1061/(ASCE)ST.1943-541X.0000775.

ASTM C150/C150M (2017) 'Standard specification for Portland cement', ASTM International, p. 9.

ASTM G1 (2003) Standard practice for preparing, cleaning, and evaluation corrosion test specimens.

Auyeung, Y., Balaguru, P. and Chung, L. (2000) ‘Bond behavior of corroded reinforcement bars’, Materials Journal, 97(2), pp. 214–220.

Bayramov, F., Taşdemir, C. and Taşdemir, M. A. (2004) ‘Optimisation of steel fibre reinforced concretes by means of statistical response surface method’, Cement and Concrete Composites. Elsevier, 26(6), pp. 665–675.

Berto, L., Simioni, P. and Saetta, A. (2008) ‘Numerical modelling of bond behaviour in RC structures affected by reinforcement corrosion’, Engineering Structures. Elsevier, 30(5), pp. 1375–1385.

Bertolini, L., Elsener, B., Pedeferri, P., Redaelli, E. and Polder, R. B. (2013) Corrosion of steel in concrete: prevention, diagnosis, repair. John Wiley & Sons.

Broomfield, J. P. (2002) Corrosion of steel in concrete: understanding, investigation and repair. CRC Press.

Carnot, A., Frateur, I., Zanna, S., Tribollet, B., Dubois-Brugger, I. and Marcus, P. (2003) ‘Corrosion mechanisms of steel concrete moulds in contact with a demoulding agent studied by EIS and XPS’, Corrosion science. Elsevier, 45(11), pp. 2513–2524.

Chen, J., Xu, Q., Li, J. and Fan, S. (2010) ‘Improved response surface method for anti-slide reliability analysis of gravity dam based on weighted regression’, Journal of Zhejiang University-SCIENCE A. Springer, 11(6), pp. 432–439.

Chen, T. Y. and Luckham, P. F. (1994) ‘A study of the electrical current passing through water-activated electro-rheological fluids’, Jpournal pf Physics D: Applied Physics, 27(7), p. 1556.

Chitty, W.-J., Dillmann, P., L’Hostis, V. and Lombard, C. (2005) ‘Long-term corrosion resistance of metallic reinforcements in concrete—a study of corrosion mechanisms based on archaeological artefacts’, Corrosion Science. Elsevier, 47(6), pp. 1555–1581.

Chung, L., Najm, H. and Balaguru, P. (2008) ‘Flexural behavior of concrete slabs with corroded bars’, Cement and Concrete Composites, 30(3), pp. 184–193. doi: 10.1016/j.cemconcomp.2007.08.005.

Coronelli, D. and Gambarova, P. (2004) ‘Structural assessment of corroded reinforced concrete beams: modeling guidelines’, Journal of Structural Engineering. American Society of Civil Engineers, 130(8), pp. 1214–1224.

CSA A23.3-14 (2014) Design of concrete structures. Mississauga, Ont.: Canadian Standard Association.

Dilger, W., Birkle, G. and Mitchell, D. (2005) ‘Effect of flexural reinforcement on punching shear resistance’, ACI Special Publication 232-4, pp. 57–74. doi: 10.1007/s13398-014-0173-7.2.

Dodd, L. L. and Restrepo-Posada, J. I. (1995) 'Model for predicting cyclic behavior of reinforcing steel', Journal of Structural Engineering. American Society of Civil Engineers, 121(3), pp. 433–445.

El-Maaddawy, T. and Soudki, K. (2003) 'Effectiveness of impressed current technique to simulate corrosion of steel reinforcement in concrete', Journal of Materials in Civil Engineering. American Society of Civil Engineers, 15(1), pp. 41–47. doi: 10.1061/(ASCE)0899-1561(2003)15:1(41).

Fedrizzi, L., Azzolini, F. and Bonora, P. L. (2005) 'The use of migrating corrosion inhibitors to repair motorways' concrete structures contaminated by chlorides', Cement and concrete research. Elsevier, 35(3), pp. 551–561.

Ghezal, A. and Khayat, K. H. (2002) 'Optimizing self-consolidating concrete with limestone filler by using statistical factorial design methods', Materials Journal, 99(3), pp. 264–272.

Hussein, A. A. (1990) Behaviour of reinforced concrete slabs made with high-strength concrete. Memorial University of Newfoundland.

Kang, S.-C., Koh, H.-M. and Choo, J. F. (2010) 'An efficient response surface method using moving least squares approximation for structural reliability analysis', Probabilistic Engineering Mechanics. Elsevier, 25(4), pp. 365–371.

Lachemi, M., Al-Bayati, N., Sahmaran, M. and Anil, O. (2014) ‘The effect of corrosion on shear behavior of reinforced self-consolidating concrete beams’, Engineering Structures. Elsevier Ltd, 79, pp. 1–12. doi: 10.1016/j.engstruct.2014.07.044.

Marzouk, H. and Hussein, A. (1991) ‘Experimental investigation on the behavior of high-strength concrete slabs’, ACI Structural Journal, 88(6), pp. 701–713. doi: 10.1139/l91-118.

Miyagawa, T. (1991) ‘Durability design and repair of concrete structures: chloride corrosion of reinforcing steel and alkali–aggregate reaction’, Magazine of Concrete Research. Thomas Telford Ltd, 43(156), pp. 155–170.

Montemor, M. F., Cunha, M. P., Ferreira, M. G. and Simões, A. M. (2002) ‘Corrosion behaviour of rebars in fly ash mortar exposed to carbon dioxide and chlorides’, Cement and Concrete Composites, 24(1), pp. 45–53. doi: 10.1016/S0958-9465(01)00025-7.

Montgomery, D. C. (2012) Design and analysis of experiments, Design. doi: 10.1198/tech.2006.s372.

Rahman, A. H. (1992) ‘Effect of steel corrosion on the strength of slab-column connections’, National Research Council Canada, Institute for Research in Construction.

Rajan, S. (2018) ‘Response surface methodology , analysis & interpretation’, pp. 1–10.

Raupach, M. (1996) ‘Chloride-induced macrocell corrosion of steel in concrete - Theoretical background and practical consequences’, Construction and Building Materials, 10(5 SPEC. ISS.), pp. 329–338. doi: 10.1016/0950-0618(95)00018-6.

Reilly, J. L., Cook, W. D., Bastien, J. and Mitchell, D. (2014) 'Effects of delamination on the performance of two-way reinforced concrete slabs', Journal of Performance of Constructed Facilities, 28(4), pp. 1–8. doi: 10.1061/(ASCE)CF.

Šomodíková, M., Lehký, D., Doležel, J. and Novák, D. (2016) 'Modeling of degradation processes in concrete: Probabilistic lifetime and load-bearing capacity assessment of existing reinforced concrete bridges', Engineering Structures, 119, pp. 49–60. doi: 10.1016/j.engstruct.2016.03.065.

Spainhour, L. K. and Wootton, I. A. (2008) 'Corrosion process and abatement in reinforced concrete wrapped by fiber reinforced polymer', Cement and Concrete Composites. Elsevier, 30(6), pp. 535–543.

Wong, S. M., Hobbs, R. E. and Onof, C. (2005) 'An adaptive response surface method for reliability analysis of structures with multiple loading sequences', Structural safety. Elsevier, 27(4), pp. 287–308.

Chapter 8 Conclusion and Recommendations for Future Research

8.1. Conclusion

Ten full-scale slab-column connections were cast and corroded with three different levels of corrosion and three corroded areas. Two accelerated corrosion techniques were developed to corroded slab-column connections. The following summarized conclusions can be drawn from the dissertation:

8.1.1. Induced Corrosion Techniques

- A test set-up was developed and built to induce corrosion in the reinforcement of two-way slabs.
- Using constant current as accelerated corrosion technique is more feasible regarding cost and time.
- For severe levels of corrosion, constant current could be more appropriate to simulate the performance of real corrosion compared to a constant voltage.
- Both techniques show a close agreement between the actual mass loss and the theoretical one.
- The amount of raw data in constant voltage technique was very huge which consumes a lot of time and effort to process them.

- The crack pattern due to corrosion in constant voltage technique created in a random pattern for 25% and 50% mass loss. This pattern could occur due to the high current intensities those slabs reached.

8.1.2. Corrosion montoring

The corrosion was montored through the measurments of half-cell potential readings, corrosion cracks width, natural frequency, and chloride contents

- Equipotential mapping was constructed for slabs under constant voltage technique. The mapping was drawn at different four ages for all tested specimen.
- For early periods, the lowest equipotential conture lines were created around the upper layer of flexural reinforcement. The equipotential contour area extended with time until all corroded area reads the lowest reading which means the probability of active corrosion is above 90%.
- The half-cell readings, after corrosion has taken place, have no significant purpose because half-cell is a non-destructive tool used to give an indication of the occurrence probability of corrosion for un-corroded members.
- The crack widths due to corrosion increased with increasing mass loss and corroded area. This could be attributed to the excessive corrosive products with the increase of the mass loss level or the corroded area.
- The natural frequency decreased with the increase of mass loss or corroded area. This could be attributed to the crack of corrosion and the loss of stiffness and bond that causing spalling in the concrete cover which affected the rigidity of the slab.

Consequently, causing a gradual decay and damping for the oscillations, which decreased the natural frequency.

- Indeed, the natural frequency has a reverse relationship with the mass; when mass value decreased, the natural frequency increased. However, the increase in mass loss level (decrease in bar mass) decreased the natural frequency. This could be attributed to the presence of the corrosive products under the concrete cover; consequently, the total slab mass kept the same.
- The natural frequency could be used as a non-destructive test to detect the corrosion. Nonetheless, more studies need to be done on different boundary condition and more specimens in order to obtain more reliable results that could be guided specialist to detect the corrosion. The natural frequency had considered as a parameter in the prediction of the residual slab capacity.
- The chloride content value increased with the increase of the mass loss level. It has been also observed that the chloride content for the same mass loss level is higher in the upper layer for flexural reinforcement than that in the lower ones. This could be attributed to the effect of the cover thickness.

8.1.3. Structural Behavior

- The increase in mass loss caused degradation in stiffness that consequently had an adverse effect on deflections and caused an increase in the slab rotation.
- A revised term for ductility index was adopted to represent the ductility.
- The increase in the mass loss led to an increase in the crack intensity and widths due to the formation of the corrosion products under the concrete cover.

- The width and number of cracks in the corroded slabs increased with increasing mass loss.
- Increasing the corrosion level causes a reduction in the capacity.
- The capacity of all slabs with 15% mass loss was larger than the service load of the reference slab regardless of the size of the corroded area.
- The capacity of slabs with 25% mass loss was larger than the service load of the reference slab when the corroded area was around the bandwidth and when it had sufficient development length. On the other hand, the capacity fell below the service load when the reinforcement did not have sufficient development length.
- The capacity of slabs with 50% mass loss was larger than the service load of the reference slab when the corroded area was around the bandwidth. However, capacity fell below the service load when the corroded area was lager than that and regardless whether the development length was sufficient or insufficient.

8.1.4. Code Predictions

- The capacity of several corroded slabs fell below the design values according to the CSA A23.3-14, BS8110-97, EC2, and ACI A318-14.
- A reasonable predictions could be obtained using the **BS8110-97 and EC2** codes by adjusting the reinforcement ratio in proportion to the same value of mass loss in the reinforcement.
- The North American codes can not be used to predict the reduced capacity as they do not consider the reinforcement ratio in their equations for punching shear.

8.1.5. Statistical Based Model

- Statistical DOE methodology was adopted to construct a practical design equations for predicting the residual slab capacity under corrosion.
- It was recommended to calculate the predicted residual capacity from the three different equations and choose the lowest value among them.
- A contour graph was constructed based on two-factor interaction statistics design type.
- The maximum tolerance was 14.6%, 11.1% and 13.7% for stages one, two, and three, respectively.
- The minimum tolerance was 0.1%, 0.1% and 0.0% for stages one, two, and three, respectively.

8.2. Recommendations for Future Research

- More specimen with the same parameters could be tested to enhance the reliability of the predicted equations to determine the residual strength of the deteriorated structures.
- The experimental program could be extended to includes more parameter such as concrete strength and slab depth in order to study their effect on the deterioration of slab capacity due to corrosion.
- More corrosion levels and areas need to be studied in order to increase the wide use range of the empirical predicted equations.
- Experimental could be conducted to study the effect of corrosion on the structural integrity of bars and their effect on deterioration the punching capacity.

- More measurments on natural frequency under different boundary conditions and more specimens in order to obtain more reliable results that could be guided specialist to detect the corrosion.
- The data analysis obtained from this thesis could be used to start experimentally rehabilitation of two-way slabs that are damaged from corrosion.
- Apply the empirical equations on real existing corroded slab-column connections to check their efficiency.
- Recommend to use corrosion monitoring probes embedded with reinforcement and external ones on the concrete surface and relate these monitoring to the residual slab capacity. These probes also could enhance the probability to capture corrosion before it spread.
- Effect of high velocity impact and plast loading on the structural behavior of corroded slab-column connections.

Reference

ACI 318-14 (2014) Building code requirement for structural concrete (ACI 318M-14) and commentary (ACI 318RM-14), Building Code Requirements for Structural Concrete.

Ahmad, S. (2003) ‘Reinforcement corrosion in concrete structures, its monitoring and service life prediction - A review’, Cement and Concrete Composites, 25(4–5 SPEC), pp. 459–471. doi: 10.1016/S0958-9465(02)00086-0.

Ahmed, M. S. and Mohammad, F. A. (2014) ‘Theoretical modal analysis of freely and simply supported RC slabs’, International Journal of Mechanical, Aerospace, Industrial, Mechatronic and Manufacturing Engineering, 8(12), pp. 2026–2030.

Ahwazi, B. B. N. (2001) A comparative study of deterioration of bond due to corrosion in different concretes. McGill University.

Al-Sulaimani, G. J., Kaleemullah, M., Basunnul, I. A. and Rasheeduzzafar, A. A.-M. (1990) ‘Influence of corrosion and cracking on bond behavior and strength of reinforced concrete members’, ACI Structural Journal, 87(2), pp. 220–231. Available at: http://www.concrete.org/PUBS/JOURNALS/OLJDetails.asp?Home=SJ&ID=2732.

Al-Swaidani, A. M. and Aliyan, S. D. (2015) ‘Effect of adding scoria as cement replacement on durability-related properties’, International Journal of Concrete Structures and Materials. Korea Concrete Institute, 9(2), pp. 241–254. doi: 10.1007/s40069-015-0101-z.

Almusallam, A., Al-Gahtani, A. S., Aziz, A. R. and Rasheeduzzafar, A. (1996) 'Effects of reinforcement corrosion on bond strength', Construction and Building Materials, 10(2), pp. 123–129.

Altoubat, S., Maalej, M. and Shaikh, F. U. A. (2016) 'Laboratory simulation of corrosion damage in reinforced concrete', International Journal of Concrete Structures and Materials. Korea Concrete Institute, 10(3), pp. 383–391. doi: 10.1007/s40069-016-0138-7.

Amleh, L. (2000) Bond deterioration of reinforcing steel in concrete due to corrosion. McGill University.

Amleh, L. and Mirza, S. (1999) 'Corrosion influence on bond between steel and concrete', ACI Structural Journal, 96(3), pp. 415–423. doi: 10.14359/676.

Andrade, C. (1993) 'Calculation of chloride diffusion coefficients in concrete from ionic migration measurements', Cement and concrete research. Elsevier, 23(3), pp. 724–742.

Andrade, C. and Alonso, C. (1996) 'Corrosion rate monitoring in the laboratory and on-site', Construction and Building Materials, 10(5 SPEC. ISS.), pp. 315–328. doi: 10.1016/0950-0618(95)00044-5.

Andrade, C. and Alonso, C. (2001) 'On-site measurements of corrosion rate of reinforcements', Construction and Building Materials, 15(2–3), pp. 141–145. doi: 10.1016/S0950-0618(00)00063-5.

Andrade, C. and C. Alonso (2004) '"Electrochemical techniques for measuring metallic corrosion": test methods for on-site corrosion rate measurement of steel reinforcement in concrete by means of the polarization resistance method', Materials and Structures, 37(9), pp. 623–643. doi: 10.1007/BF02483292.

Aoude, H., Cook, W. D. and Mitchell, D. (2014) 'Effects of simulated corrosion and delamination on response of two-way slabs', Journal of structural Engineering, 140(1), pp. 1–9. doi: 10.1061/(ASCE)ST.1943-541X.0000775.

ASTM C1202-17a (2017) 'Standard Test Method for Electrical Indication of Concrete's Ability to Resist Chloride Ion Penetration', American Society for Testing and Materials., pp. 1–8. doi: 10.1520/C1202-12.2.

ASTM C143/C143M-15a (2015) 'Standard Test Method for Slump of Hydraulic-Cement Concrete'. ASTM International West Conshohocken, PA.

ASTM C150/C150M (2017) 'Standard specification for Portland cement', ASTM International, p. 9.

ASTM C1556-11a (2016) 'Standard Test Method for Determining the Apparent Chloride Diffusion Coefficient of Cementitious Mixtures by Bulk Diffusion', ASTM International, pp. 1–7. doi: 10.1520/C1556-04.2.

ASTM C876 (2015) 'Standard test method for corrosion potentials of uncoated reinforcing steel in concrete', p. 8. doi: 10.1520/C0876-09.2.

ASTM G1 (2003) Standard practice for preparing, cleaning, and evaluation corrosion test specimens.

Auyeung, Y., Balaguru, P. and Chung, L. (2000) 'Bond behavior of corroded reinforcement bars', ACI Structural Journal, 97(2), pp. 214–220. doi: 10.14359/826.

Auyeung, Y., Balaguru, P. and Chung, L. (2000) 'Bond behavior of corroded reinforcement bars', Materials Journal, 97(2), pp. 214–220.

Azad, A. K., Ahmad, S. and Azher, S. a (2007) 'Residual strength of corrosion-damaged reinforced concrete beams', ACI Materials Journal, 104(1), pp. 40–47.

Azam, R. (2010) Behaviour of shear critical RC beams with corroded longitudinal steel reinforcement. Waterloo.

Ballim, Y. and Reid, J. C. (2003) 'Reinforcement corrosion and the deflection of RC beams - An experimental critique of current test methods', Cement and Concrete Composites, 25(6), pp. 625–632. doi: 10.1016/S0958-9465(02)00076-8.

Ballim, Y., Reid, J. C. and Kemp, A. R. (2001) 'Deflection of RC beams under simultaneous load and steel corrosion', Magazine of Concrete Research. Thomas Telford, 53(3), pp. 171–181.

Bayramov, F., Taşdemir, C. and Taşdemir, M. A. (2004) 'Optimisation of steel fibre reinforced concretes by means of statistical response surface method', Cement and Concrete Composites. Elsevier, 26(6), pp. 665–675.

Bazant, Z. P. (1979) ‘Physical model for steel corrosion in concrete sea structures-theory’, ASCE J Struct Div. American Society of Civil Engineers (ASCE), 105(6), pp. 1137–1153.

Bentz, E. C., Vecchio, F. J. and Collins, M. P. (2006) ‘Simplified modified compression field theory for calculating shear strength of reinforced concrete elements’, ACI Structural Journal, 103(4), pp. 614–624. doi: 10.14359/16438.

Berto, L., Simioni, P. and Saetta, A. (2008) ‘Numerical modelling of bond behaviour in RC structures affected by reinforcement corrosion’, Engineering Structures. Elsevier, 30(5), pp. 1375–1385.

Bertolini, L., Elsener, B., Pedeferri, P., Redaelli, E. and Polder, R. B. (2013) Corrosion of steel in concrete: prevention, diagnosis, repair. John Wiley & Sons.

Bhargava, K., Ghosh, A. K., Mori, Y. and Ramanujam, S. (2007) ‘Models for corrosion-induced bond strength degradation in reinforced concrete’, ACI Materials Journal, 104(6), pp. 594–603. doi: 10.1016/j.nucengdes.2007.01.010.

Bonacci, J., Thomas, M., Hearn, N., Lee, C. and Maalej, M. (1998) ‘Laboratory simulation of corrosion in reinforced concrete and repair with CFRP wraps’, in Annual Conference of the Canadian Society of Civil Engineering, pp. 653–662.

British Standards Institution (2004) Eurocode 2: design of concrete structures: part 1-1: general rules and rules for buildings. British Standards Institution.

Broms, E. (1991) ‘Punching of flat plates - a question of concrete properties in biaxial compression and size effect’, ACI Structural Journal, (87), pp. 292–304.

Broomfield, J. P. (2002) Corrosion of steel in concrete: understanding, investigation and repair. CRC Press.

Broomfield, J. P. (2006) Corrosion of steel in concrete: understanding, investigation and repair, Second Edition. doi: 10.4324/9780203414606.

BS 8110 (1997) ‘Structural use of concrete. Part I: Code of practice for design and construction’, British Standards Institution, UK.

Cabrera, J. G. (1996) ‘Deterioration of concrete due to reinforcement steel corrosion’, Cement and Concrete Composites, 18(1), pp. 47–59. doi: 10.1016/0958-9465(95)00043-7.

Cady, P. D. and Weyers, R. E. (1984) ‘Deterioration rates of concrete bridge decks’, Journal of Transportation Engineering. American Society of Civil Engineers, 110(1), pp. 34–44.

Carnot, A., Frateur, I., Zanna, S., Tribollet, B., Dubois-Brugger, I. and Marcus, P. (2003) ‘Corrosion mechanisms of steel concrete moulds in contact with a demoulding agent studied by EIS and XPS’, Corrosion science. Elsevier, 45(11), pp. 2513–2524.

Castel, A., François, R. and Arliguie, G. (2000) ‘Mechanical behaviour of corroded reinforced concrete beams—Part 1: Experimental study of corroded beams’, Materials and Structures, 33(9), pp. 539–544. doi: 10.1007/BF02480533.

Castel, A., Franfois, R., Arliguie, G. and Mat, L. (2000) ‘Mechanical behaviour of corroded reinforced concrete beams - part 2 : bond and notch effects’, Materials and Structures, 33(9), pp. 545–551.

Chen, J., Xu, Q., Li, J. and Fan, S. (2010) ‘Improved response surface method for anti-slide reliability analysis of gravity dam based on weighted regression’, Journal of Zhejiang University-SCIENCE A. Springer, 11(6), pp. 432–439.

Chen, T. Y. and Luckham, P. F. (1994) ‘A study of the electrical current passing through water-activated electro-rheological fluids’, Jpournal pf Physics D: Applied Physics, 27(7), p. 1556.

Chitty, W.-J., Dillmann, P., L’Hostis, V. and Lombard, C. (2005) ‘Long-term corrosion resistance of metallic reinforcements in concrete—a study of corrosion mechanisms based on archaeological artefacts’, Corrosion Science. Elsevier, 47(6), pp. 1555–1581.

Chung, L., Najm, H. and Balaguru, P. (2008) ‘Flexural behavior of concrete slabs with corroded bars’, Cement and Concrete Composites, 30(3), pp. 184–193. doi: 10.1016/j.cemconcomp.2007.08.005.

Cornet, I., Ishikawa, T. and Bresler, B. (1968) ‘Mechanism of steel corrosion in concrete structures’, Materials Protection, 7(3), p. 45.

Coronelli, D. and Gambarova, P. (2004) ‘Structural assessment of corroded reinforced concrete beams: modeling guidelines’, Journal of Structural Engineering. American Society of Civil Engineers, 130(8), pp. 1214–1224.

CSA-G30. 18-09 (2009) Carbon steel bars for concrete reinforcement, Mississauga, Ontario, Canada.

CSA A23.1-14 (2014) Concrete materials and methods of concrete construction/Test methods and standard practices for concrete, CSA Group, Mississauga, Ontario, Canada.

CSA A23.3-14 (2014) Design of concrete structures. Mississauga, Ont.: Canadian Standard Association.

Dang, V. H. and François, R. (2014) 'Prediction of Ductility Factor of Corroded Reinforced Concrete Beams Exposed to Long Term Aging in Chloride Environment', Cement and Concrete Composites, 53(October 2014), pp. 136–147. doi: 10.1016/j.cemconcomp.2014.06.002.

Davis, J. (2000) Corrosion: understanding the basics. doi: 10.1361/cutb2000p001.

Deb, S. and Pradhan, B. (2013) 'A study on corrosion performance of steel in concrete under accelerated condition', in Proceedings of the International Conference on Structural Engineering Construction and Management, Kandy, Sri Lanka. Available at: http://dl.lib.mrt.ac.lk/handle/123/9365.

Dilger, W., Birkle, G. and Mitchell, D. (2005) 'Effect of flexural reinforcement on punching shear resistance', ACI Special Publication 232-4, pp. 57–74. doi: 10.1007/s13398-014-0173-7.2.

Dodd, L. L. and Restrepo-Posada, J. I. (1995) 'Model for predicting cyclic behavior of reinforcing steel', Journal of Structural Engineering. American Society of Civil Engineers, 121(3), pp. 433–445.

Donnelly, J. P., Pulver, B. E. and Popovic, P. L. (2006) 'Condition assessment of parking structures', In Structures Congress : Structural Engineering and Public Safety ASCE., p. 10.

El-Gamal, S., Benmokrane, B., El-Salakawy, E., Wiseman, A. and Chaallal, O. (2009) 'Monitoring of an innovative concrete parking garage reinforced with GFRP composite bars', in 4th International Conference on Structural Health Monitoring of Intelligent Infrastructure (SHMII-4) 22-24 July 2009, Zurich, Switzerland.

El-Maaddawy, T. and Soudki, K. (2003) 'Effectiveness of impressed current technique to simulate corrosion of steel reinforcement in concrete', Journal of Materials in Civil Engineering. American Society of Civil Engineers, 15(1), pp. 41–47. doi: 10.1061/(ASCE)0899-1561(2003)15:1(41).

El-Maaddawy, T., Soudki, K. and Topper, T. (2005a) 'Analytical model to predict nonlinear flexural behavior of corroded reinforced concrete beams', ACI Structural Journal, 102(4), pp. 550–559.

El-Maaddawy, T., Soudki, K. and Topper, T. (2005b) 'Long-term performance of corrosion-damaged reinforced concrete beams', ACI Stractural Journal, 102(5), pp. 649–656.

El-Maaddawy, T., Soudki, K. and Topper, T. (2006) 'Long-term performance of corrosion damaged reinforced concrete beams', ACI Structural Journal, 102(5), pp. 649–656.

Fang, C., Lundgren, K., Chen, L. and Zhu, C. (2004) 'Corrosion influence on bond in reinforced concrete', Cement and Concrete Research, 34(11), pp. 2159–2167. doi: 10.1016/j.cemconres.2004.04.006.

Fedrizzi, L., Azzolini, F. and Bonora, P. L. (2005) 'The use of migrating corrosion inhibitors to repair motorways' concrete structures contaminated by chlorides', Cement and concrete research. Elsevier, 35(3), pp. 551–561.

Fu, X. D. D. L. and Chung, D. D. L. (1997) 'Effect of corrosion on the bond between concrete and steel rebar', Cement and Concrete Research, 27(12), pp. 1811–1815.

Gerhardus H. Koch, M. P. H. B. (2002) Corrosion costs and preventive strategies in the United States, Nace International.

Ghezal, A. and Khayat, K. H. (2002) 'Optimizing self-consolidating concrete with limestone filler by using statistical factorial design methods', Materials Journal, 99(3), pp. 264–272.

Gowda, M. R., R, K. M. and Vijin Xavier (2017) 'Corrosion rate analysis in reinforced slab elements', International Journal for Scientific Research & Development|, 4(11).

Hussein, A. A. (1990) Behaviour of reinforced concrete slabs made with high-strength concrete. Memorial University of Newfoundland.

Imam, A. and Azad, A. K. (2016) ‘Prediction of residual shear strength of corroded reinforced concrete beams’, International Journal of Advanced Structural Engineering. Springer Berlin Heidelberg, (8), pp. 307–318. doi: 10.1016/j.engstruct.2016.04.018.

Juarez, C. a., Guevara, B., Fajardo, G. and Castro-Borges, P. (2011) ‘Ultimate and nominal shear strength in reinforced concrete beams deteriorated by corrosion’, Engineering Structures. Elsevier Ltd, 33(12), pp. 3189–3196. doi: 10.1016/j.engstruct.2011.08.014.

Kang, S.-C., Koh, H.-M. and Choo, J. F. (2010) ‘An efficient response surface method using moving least squares approximation for structural reliability analysis’, Probabilistic Engineering Mechanics. Elsevier, 25(4), pp. 365–371.

Kashani, M. M., Crewe, A. J. and Alexander, N. A. (2013) ‘Nonlinear stress-strain behaviour of corrosion-damaged reinforcing bars including inelastic buckling’, Engineering Structures, 48, pp. 417–429. doi: 10.1016/j.engstruct.2012.09.034.

Klinghoffer, O. (1995) ‘In situ monitoring of reinforcement corrosion by means of electrochemical methods’, Nordic Concrete Research, 95(1), pp. 1–13. Available at: http://www.germann.org/Publications/GalvaPulse/2. Klinghofer, O., In Situ Monitoring of Reinforcement Corrosion by means of Electrochemical Methods, Nordic Concrete Research 95 1.pdf.

Konecný, P. (2007) Reliability of reinforced Concrete bridge decks with respect To ingress of chlorides, Department of Structural Mechanics\Faculty of Civil Engineering\ University of Ostrava. doi: 10.13140/RG.2.1.3729.4165.

Kumar, M. K., Rao, P. S., Swamy, B. L. P. and Chandra Mouli, C. (2012) 'Corrosion resistance performance of fly ash blended cement concrete', Internatioanl Journal of Research in Engineering and Technologi, 1(3), pp. 448–454. doi: 10.1016/0140-6701(95)93047-7.

Lachemi, M., Al-Bayati, N., Sahmaran, M. and Anil, O. (2014) 'The effect of corrosion on shear behavior of reinforced self-consolidating concrete beams', Engineering Structures. Elsevier Ltd, 79, pp. 1–12. doi: 10.1016/j.engstruct.2014.07.044.

Lee, C., Bonacci, J. F., Thomas, M. D. a., Maalej, M., Khajehpour, S., Hearn, N., Pantazopoulou, S. and Sheikh, S. (2000) 'Accelerated corrosion and repair of reinforced concrete columns using carbon fibre reinforced polymer sheets', Canadian Journal of Civil Engineering, 27(5), pp. 941–948. doi: 10.1139/cjce-27-5-941.

Litvan, G. G. (1982) 'Evaluation and repair of deteriorated garage floors', Canadian Building Digest, Division of Building Research, p. 4.

Macgregor, James G. Wight, J. K. (2009) Reinforced concrete mechanics & design. doi: 10.1017/CBO9781107415324.004.

Makki, R. F. (2014) 'Response of reinforced concrete beams retrofitted by ferrocement', International Journal of Science & Technology Research, 3(9), pp. 27–34.

Mangat, P. S. and Elgarf, M. S. (1999) 'Flexural strength of concrete beams with corroding reinforcement', ACI Structural Journal, (96), pp. 149–158. Available at: http://shura.shu.ac.uk/1042/.

Mangat, P. S. and Elgarf, M. S. (1999) 'Flexural strength of concrete beams with corroding reinforcement', ACI Structural Journal, 96(1), pp. 149–158.

Marzouk, H. and Hussein, A. (1991) 'Experimental investigation on the behavior of high-strength concrete slabs', ACI Structural Journal, 88(6), pp. 701–713. doi: 10.1139/l91-118.

Mirzaei, Y. (2008) 'Post punching behavior of reinforced slab-column connections', in 7th Int. FIB Ph.D. Symp., IWB Universität Stuttgart, Stuttgart., pp. 1–8.

Miyagawa, T. (1991) 'Durability design and repair of concrete structures: chloride corrosion of reinforcing steel and alkali–aggregate reaction', Magazine of Concrete Research. Thomas Telford Ltd, 43(156), pp. 155–170.

Montemor, M. F., Cunha, M. P., Ferreira, M. G. and Simões, A. M. (2002) 'Corrosion behaviour of rebars in fly ash mortar exposed to carbon dioxide and chlorides', Cement and Concrete Composites, 24(1), pp. 45–53. doi: 10.1016/S0958-9465(01)00025-7.

Montgomery, D. C. (2012) Design and analysis of experiments, Design. doi: 10.1198/tech.2006.s372.

Moreno, E. I., Solís-Carcaño, R. G., Varela-Rivera, J., Pacho-Monforte, J. C. and Cua-Cuevas, R. A. (2015) 'Diffusion of chlorides in pozzolanic concrete made with high-absorption aggregates exposed under tropical marine environment', International Journal of Electrochemical Science, 10(8), pp. 6444–6453.

Neville, A. M. (2011) Properties of concrete (Fifth Edition), Cement and Concrete Research. doi: 10.1016/0008-8846(96)82366-0.

Ouglova, A., Berthaud, Y., Foct, F., François, M., Ragueneau, F. and Petre-Lazar, I. (2007) ‘The influence of corrosion on bond properties between concrete and reinforcement in concrete structures’, Materials and Structures, 41(5), pp. 969–980. doi: 10.1617/s11527-007-9298-x.

Park, J. I., Lee, K. M., Kwon, S. O., Bae, S. H., Jung, S. H. and Yoo, S. W. (2016) ‘Diffusion decay coefficient for chloride ions of concrete containing mineral admixtures’, Advances in Materials Science and Engineering, 2016. doi: 10.1155/2016/2042918.

Pellegrini-Cervantes, M. J., Almeraya-Calderon, F., Borunda-Terrazas, A., Bautista-Margulis, R. G., Chacón-Nava, J. G., Fajardo-San-Miguel, G., Almaral-Sanchez, J. L., Barrios-Durstewitz, C. P. and Martinez-Villafañe, A. (2013) ‘Corrosion resistance, porosity and strength of blended portland cement mortar containing rice husk ash and nano-SiO2’, International Journal of Electrochemical Science, 8(8), pp. 10697–10710.

Pritzl, M. D., Tabatabai, H. and Ghorbanpoor, A. (2014) ‘Laboratory evaluation of select methods of corrosion prevention in reinforced concrete bridges’, International Journal of Concrete Structures and Materials, 8(3), pp. 201–212. doi: 10.1007/s40069-014-0074-3.

Rahman, A. H. (1992a) Effect of steel corrosion on the strength of slab-column connections, National Research Council Canada, Institute for Research in Construction. National Research Council Canada, Institute for Research in Construction.

Rahman, A. H. (1992b) ‘Effect of steel corrosion on the strength of slab-column connections’, National Research Council Canada, Institute for Research in Construction.

Rajan, S. (2018) ‘Response surface methodology , analysis & interpretation’, pp. 1–10.

Rasheeduzzafar (1990) ‘Effect of Tricalcium Aluuminate Content of Cement on Corrosion of Reinforced Steel in Concrete’, Cement and Concrete Research, (89), pp. 723–738.

Rashid, M. I. (2004) Concrete Slabs Reinforced with GFRP Bars. Memorial University of Newfoundland.

Raupach, M. (1996) ‘Chloride-induced macrocell corrosion of steel in concrete - Theoretical background and practical consequences’, Construction and Building Materials, 10(5 SPEC. ISS.), pp. 329–338. doi: 10.1016/0950-0618(95)00018-6.

Reilly, J. L., Cook, W. D., Bastien, J. and Mitchell, D. (2014) ‘Effects of delamination on the performance of two-way reinforced concrete slabs’, Journal of Performance of Constructed Facilities, 28(4), pp. 1–8. doi: 10.1061/(ASCE)CF.

Roberge, P. R. and Pierre, R. (1999) Handbook of corrosion engineering library of congress cataloging-in-publication data. doi: 10.1016/S0026-0576(00)83445-5.

Rodriguez, D. J., Ortega, L. and Casal, J. (1997) ‘Load carrying capacity of concrete structures with corroded reinforcement’, Construction and Building Materials, 11(4), pp. 239–248.

Sahmaran, M., Anil, O., Lachemi, M., Yildirim, G., Ashour, A. F. and Acar, F. (2015) ‘Effect of corrosion on shear behavior of reinforced engineered cementitious composite beams’, ACI Structural Journal, 112(6), pp. 771–782. doi: 10.14359/51687749.

Said, M. E. and Hussein, A. A. (2019) ‘Induced corrosion techniques for two-way slabs’, Journal of performance of constructed Facility, 33(3). doi: 10.1061/(ASCE)CF.1943-5509.0001299.

Šomodíková, M., Lehký, D., Doležel, J. and Novák, D. (2016) ‘Modeling of degradation processes in concrete: Probabilistic lifetime and load-bearing capacity assessment of existing reinforced concrete bridges’, Engineering Structures, 119, pp. 49–60. doi: 10.1016/j.engstruct.2016.03.065.

Spainhour, L. K. and Wootton, I. A. (2008) ‘Corrosion process and abatement in reinforced concrete wrapped by fiber reinforced polymer’, Cement and Concrete Composites. Elsevier, 30(6), pp. 535–543.

Talakokula, V., Bhalla, S. and Gupta, A. (2014) ‘Corrosion assessment of reinforced concrete structures based on equivalent structural parameters using electro-mechanical impedance technique’, Journal of Intelligent Material Systems and Structures, 0(0), pp. 1–16. doi: 10.1177/1045389X13498317.

Toongoenthong, K. and Maekawa, K. (2004) ‘Interaction of pre-induced damages along main reinforcement and diagonal shear in RC members’, Journal of Advanced Concrete Technology, 2(3), pp. 431–443. doi: 10.3151/jact.2.431.

Torres-Acosta, A. a., Navarro-Gutierrez, S. and Terán-Guillén, J. (2007) ‘Residual flexure capacity of corroded reinforced concrete beams’, Engineering Structures, 29(6), pp. 1145–1152. doi: 10.1016/j.engstruct.2006.07.018.

Val, D. V. (2007) ‘Deterioration of strength of RC beams due to corrosion and its influence on beam reliability’, Journal of Structural Engineering, 133(9), pp. 1297–1306. doi: 10.1061/(ASCE)0733-9445(2007)133:9(1297).

Wang, L., Zhang, X., Zhang, J., Ma, Y. and Liu, Y. (2015) ‘Effects of stirrup and inclined bar corrosion on shear behavior of RC beams’, Construction and Building Materials. Elsevier Ltd, 98, pp. 537–546. doi: 10.1016/j.conbuildmat.2015.07.077.

Wang, X. and Liu, X. (2006) ‘Bond strength modeling for corroded reinforcements’, Construction and Building Materials, 20(3), pp. 177–186. doi: 10.1016/j.conbuildmat.2005.01.015.

Wei-liang, J. and Yu-xi, Z. (2001) ‘Effect of corrosion on bond behavior and bending strength of reinforced concrete beams’, Journal of Zhejiang University-Science, (3), pp. 298–308. doi: 10.1007/BF02839464.

Wong, S. M., Hobbs, R. E. and Onof, C. (2005) ‘An adaptive response surface method for reliability analysis of structures with multiple loading sequences’, Structural safety. Elsevier, 27(4), pp. 287–308.

Xia, J., Jin, W.-L. and Li, L.-Y. (2012) 'Effect of chloride-induced reinforcing steel corrosion on the flexural strength of reinforced concrete beams', Magazine of Concrete Research. Thomas Telford, 64(6), pp. 471–485.

Xia, J., Jin, W. and Li, L. (2011) 'Shear performance of reinforced concrete beams with corroded stirrups in chloride environment', Corrosion Science. Elsevier Ltd, 53(5), pp. 1794–1805. doi: 10.1016/j.corsci.2011.01.058.

Yoon, S., Wang, K., Weiss, W. and Shah, S. (2001) 'Interaction of reinforced between loading, corrosion, and serviceability of reinforced concrete', ACI Materials Journal, 97(6), pp. 637–644.

Zhang, B., Masmoudi, R. and Benmokrane, B. (2004) 'Behaviour of one-way concrete slabs reinforced with CFRP grid reinforcements', Construction and Building Materials, 18(8), pp. 625–635. doi: 10.1016/j.conbuildmat.2004.04.007.